THE UNIVERSITY *of* EDINBURGH

This thesis has been submitted in fulfilment of the requirements for a postgraduate degree (e.g. PhD, MPhil, DClinPsychol) at the University of Edinburgh. Please note the following terms and conditions of use:

This work is protected by copyright and other intellectual property rights, which are retained by the thesis author, unless otherwise stated.
A copy can be downloaded for personal non-commercial research or study, without prior permission or charge.
This thesis cannot be reproduced or quoted extensively from without first obtaining permission in writing from the author.
The content must not be changed in any way or sold commercially in any format or medium without the formal permission of the author.
When referring to this work, full bibliographic details including the author, title, awarding institution and date of the thesis must be given.

Low dimensional models of the transition to turbulence

James Hitchen

Doctor of Philosophy
The University of Edinburgh
August 2020

Abstract

The transition from a regularly ordered state of fluid motion to chaotic and turbulent regime has been long observed and progressively understood through the discovery and application of theoretical tools and frameworks. One such lens through which the problem can be attacked confines the dynamics of a turbulent system to a set of ordinary differential equations describing the time evolution of velocity modes, allowing for the application of techniques from dynamical systems theory.

In this body of work,this framework shall be applied to develop a series of low dimensional models of the transition to turbulence in plane Couette flow (fluid sheared between two parallel plates of anti-parallel velocity). These models will then be investigated to understand certain features of the transition. Initially, the transition to Newtonian turbulence is investigated, with the results used as a starting point for a study of viscoelastic turbulence.

The first Chapter of this thesis will introduce the required theoretical knowledge and contextualise the research outline. The second Chapter will then detail an algorithm for generating a low order model of the transition to turbulence. This process is demonstrated by using the method to create a hierarchy of models for plane Couette flow. In Chapter 3, the thesis will then detail an investigation as to why the lifetime of the turbulent state increases rapidly with the Reynolds number Re, the dimensionless flow parameter quantifying the ratio of inertial to viscous forces, using the models created in Chapter 2. The findings of Chapter 2 and Chapter 3 are then used together to form the basis of a study into effects of viscoelasticity, described by the Oldroyd-B model, on the the dynamics of turbulent flow in Chapter 4.

Declaration

I declare that this thesis was composed by myself, that the work contained herein is my own except where explicitly stated otherwise in the text, and that this work has not been submitted for any other degree or professional qualification except as specified.

(*James Hitchen, August 2020*)

Acknowledgements

I would like to acknowledge and thank the stimulating support afforded to me by my supervisor Professor Alexander Morozov throughout the course of this PhD.

A similar acknowledgement is made to the thought provoking discussions and academic guidance provided by the late Professor Bruno Eckhardt during our time working together.

In addition, the kind scientific and motivational guidance from friends, family and colleagues to numerous too name is duly noted and greatly appreciated.

This work has been gratefully supported by the Engineering and Physical Sciences Research Council (EPSRC).

Contents

List of Figures

List of Tables

Chapter 1

Introduction

Turbulence can be defined as the state of a fluid in motion in which the dynamical variables that describe it, namely the pressure and fluid velocity, evolve in a chaotic manner. Here, the term 'chaotic' takes the mathematical definition of describing a system in which the dynamic variables are governed by deterministic rules, yet the time evolution of the system is extremely sensitive to changes in the initial conditions. Consequentially, exactly predicting the long-time state of a practical realisation of a chaotic system is impossible, due to the inability to determine the initial conditions exactly [1].

This phenomenon of turbulence is ubiquitous across nature and engineering, from the turbulent blood flow leaving the heart to smoke rising from a fire. The wide variety of instances in which one finds turbulence provides ample cross-discipline interest in finding a general theory that can predict its onset and dynamical properties, hence allowing for the engineering of solutions that can control the occurrence of turbulent flow as desired, e.g. as in [2, 3]. For a comprehensive review of such methods see [4].

Ever since the ground breaking experimental [5] and analytical [6] work of Osborne Reynolds, the study of turbulence in simple shear flows has proven a fruitful endeavour. His work yielded the understanding that in practical situations, the onset of turbulence is well predicted by measure of the dimensionless Reynolds number defined by $Re = \frac{\rho UL}{\mu}$; where Re is the Reynolds number, U is the mean velocity of the fluid, L is a defining length scale associated with the channel (such a pipe diameter), ρ is the density of the fluid and μ is the dynamic viscosity of the fluid. The use of such non-dimensional numbers to characterise

flow is commonplace across the field of fluid dynamics as it allows for the useful comparison of systems with different sizes and shapes and for the construction of general theories and observations of their dynamic properties.

A typical flow geometry used for the study of turbulence is Hagen-Poiseuille flow (flow driven by a pressure difference down a pipe of circular cross-section). In this regime, the region of Re at which fluid flow becomes turbulent has been found experimentally to span very large ranges of critical Re, ranging from as low as $Re_c \sim 2000$ to in excess of $Re_c > 40000$ [7], depending upon the roughness of the walls of the pipe and the isolation from outside interference of the experiment. This poses interesting questions about the nature of the transition to turbulence, which will be explored throughout this Thesis. For an overview of modern experimental methods associated with measuring turbulence, see Darbyshire & Mullin [8].

The Navier-Stokes equations describe the evolution of the velocity and pressure fields of a fluid through time. They may be derived from Newton's laws using conservation of mass and momentum arguments, as shown in [9]. Doing so, one arrives at

$$\rho\left(\frac{\partial \mathbf{v}}{\partial t} + \mathbf{v}\cdot\nabla\mathbf{v}\right) = \mathbf{f} + \nabla\cdot\boldsymbol{\sigma}, \tag{1.1}$$

where $\mathbf{v}$ is the fluid velocity, $\mathbf{f}$ is the density of an external force applied to the fluid, and $\boldsymbol{\sigma}$ is the stress tensor for the fluid. For an incompressible Newtonian fluid, the stress tensor is defined as

$$\boldsymbol{\sigma} = -p\mathbf{I} + \mu\dot{\boldsymbol{\gamma}}, \tag{1.2}$$

where p is the pressure, and μ the viscosity, a measure of the fluid's resistance to deformation under stress. $\dot{\boldsymbol{\gamma}}$ is the rate of strain tensor defined by the symmetric component of the velocity,

$$\dot{\boldsymbol{\gamma}} = \nabla\mathbf{v} + (\nabla\mathbf{v})^T, \tag{1.3}$$

where is $\mathbf{v}$ is the velocity vector, and ^{T} superscript denotes the transpose of a tensor. If we then introduce the scales of length L, time T and velocity $U = L/T$ such that $\mathbf{x} = \hat{\mathbf{x}}/L$, $\mathbf{v} = \hat{\mathbf{v}}/U$, $t = \hat{t}/T$, $p = \frac{L\hat{p}}{\mu U}$ and $\mathbf{F} = \frac{\mathbf{f}L^2}{\mu U}$ and substitute Eq.

1.2 into Eq. 1.1 we arrive at

$$Re\left(\frac{\partial \mathbf{v}}{\partial t} + \mathbf{v}\cdot\nabla\mathbf{v}\right) = \mathbf{F} - \nabla p + \nabla^2\mathbf{v}. \tag{1.4}$$

In addition, the condition that the fluid is incompressible combined with the conservation of mass gives the so called divergence free condition of the velocity,

$$\nabla\cdot\mathbf{v} = 0, \tag{1.5}$$

as shown in [9]. Eq. 1.5, together with Eq. 1.4, form the incompressible Newtonian Navier-Stokes equations. Alternatively, the Navier-Stokes equations may be derived using statistical mechanics techniques from the Boltzmann transport equation, see [10].

Solving these equations in different geometries provides us with the velocity and pressure fields of the fluid as it evolves with time through the chosen system. Despite the apparent simplicity of the equations, locating non-trivial solutions is typically difficult, with no general theory providing a recipe for obtaining solutions to the equations. Approaches vary from very high dimensional and computationally expensive models to low order models that try and reduce the key characteristics of turbulence to a small number of degrees of freedom. The equations are studied by mathematicians, engineers and physicists alike, with the Clay Mathematics Institute setting proving the existence and smoothness of solutions to the Navier-Stokes equations for all initial conditions as one of its famed millennium problems [11].

1.1 The transition to turbulence in parallel shear flows

When investigating the transition to turbulence, a sub-class of flows known as parallel shear flows are often used due to their geometric simplicity, which aids in the ease of simulation and performing experiments. The defining feature of such flows is a trivial state, the so-called laminar profile, characterised by a unidirectional profile that varies as a function of the coordinate in an orthogonal direction. The laminar flow is generally observed at lower Re than the turbulent

state and does not display and chaotic behaviour. The shape of the profile is determined by the geometry of the system, with fluid flowing at a slower speed close to a bounding solid wall and faster further away from it in pressure driven flows. The converse of this is true for wall-driven shear flows. In the laminar regime, the velocity at a fixed position within the system will remain constant in time provided Re remains constant and the system is isolated from external perturbations.

1.1.1 Categorising the transition to turbulence

The laminar-turbulent transition can be categorised into several different types of transition scenario, depending upon the dynamic connection between the laminar and non-laminar states. Here, the term 'non-laminar' is used rather than 'turbulent', as some of these states whilst not being laminar still display some level of regular spatio-temporal structure in which the fluid velocity and pressure fields do not evolve chaotically. In general, the governing equations of the system maybe linearised around the laminar solution with an infinitesimal perturbation introduced. If this perturbation grows exponentially in time the flow is said to be linearly unstable, whilst if it decays the flow is linearly stable.

We can define Re_{sn} as the Re at which the non-laminar state appears via a saddle node bifurcation and Re_{lm} as the Re at which the state dynamically connects to the laminar solution. If the non-laminar state connects dynamically to the laminar state at the Re it appears at, i.e $Re_{sn} = Re_{lm}$ the system is said to bifurcate supercritically. This connection allows the flow to continuously transition to the non-laminar state after an infinitesimal perturbation has been introduced at $Re > Re_{sn}$. In contrast, the non-laminar solution may appear at a $Re_{sn} < Re_{lm}$. A flow of this type may only access the non-laminar state with a perturbation of finite size in the $Re_c < Re_{lm}$ range, and will hop discontinuously to the non-laminar state for $Re > Re_{lam}$. It follows that such transition scenarios are termed subcritical bifurcations. A pictorial representation of this type of transition is shown in Fig. 1.1. For both types of transition, the laminar state is a global attractor for the system at $Re < Re_{sn}$ and a local attractor for $Re > Re_{sn}$.

For certain types of flow, namely fluid bounded by two walls moving antiparallel to each other (plane Couette flow) and fluid driven by a pressure gradient through a circular pipe (Hagen-Poiseuille flow), the laminar profile has no linear instability for which analysis in the manner of [12] can be undertaken. As a

consequence, flows with a linearly unstable laminar profile, such as fluid between two independently rotating cylinders (Taylor-Couette flow) or fluid heated from below (Rayleigh-Bernard flow), have harboured more success in locating non-laminar solutions, as the linear instability analysis can typically be formed as a generalised eigenvalue problem to which the instability eigenvectors give hints as to the form of the non-laminar solutions. Such linearly unstable flows have been found to undergo a series of bifurcations as Re is increased, with the flow pattern increasing in spatial and temporal complexity. A recent review of experimental and numerical results for Taylor-Couette flow can be found in [13].

Despite the absence of a linear instability in the former flows, experimental investigation has shown a power law between the Reynolds number and the size of a perturbation $\epsilon = O(Re^{\lambda})$ required to induce turbulence [14], as shown in Fig. 1.2. The exponent is necessarily negative such that $\epsilon \to 0$ as $Re \to \infty$. This suggests that the transition is subcritical and that the turbulent solutions only connect to the laminar state at infinite Re, which is known as a 'bifurcation from infinity'. These two observations then allow for the question 'when does a linearly stable flow become turbulent?' to be broken down into two parts, namely; when is $Re > Re_c$ and ϵ is greater than the minimum threshold perturbation size, ϵ_c, which itself is a function of Re. As an aside, in the subcritical region of Re, a plot of the length of a turbulent lifetime against Re and the size of perturbation ϵ is of a fractal nature [15], implying that the turbulent state is indeed a long lived transient on a repeller.

A note here is made to the fact that performing linear stability analysis and finding eigenvalues only within the lower half plane does not imply that all perturbations will monotonically decay, as the non-normality of the corresponding linear operators can produce transient growth of the perturbations to many times their original magnitude [16]. In addition, these decaying perturbations may also transfer the system to an unstable state [17].

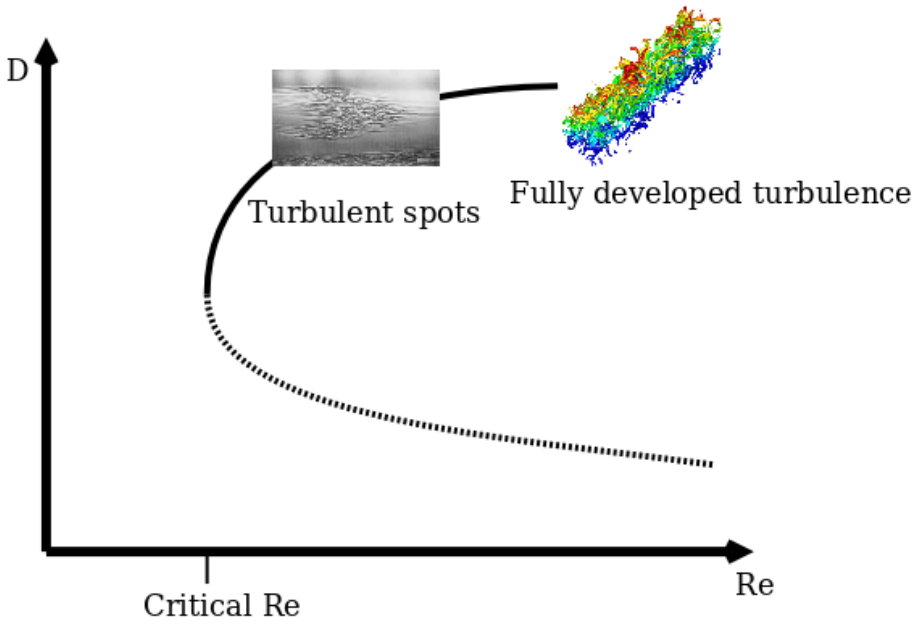

Figure 1.1 *A sketch of the typical bifurcation from infinity scenario for plane Couette flow, plotting some disorder parameter D against Re. The unstable lower branch only connects the laminar $D = 0$ at $Re \to \infty$.*

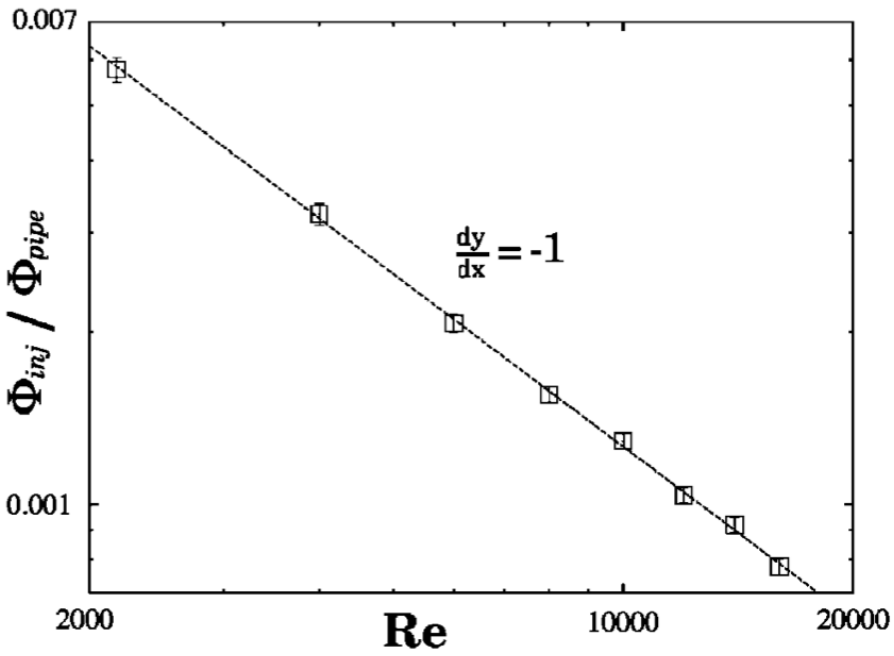

Figure 1.2 *The experimental stability curve for a constant mass flux pipe of circular cross-section. The perturbation size has been non-dimensionalised by the ratio of the perturbation mass flux Φ_{inj} to the flow mass flux Φ_{pipe}. Reproduced with permission from [14]*

1.1.2 Coherent structures

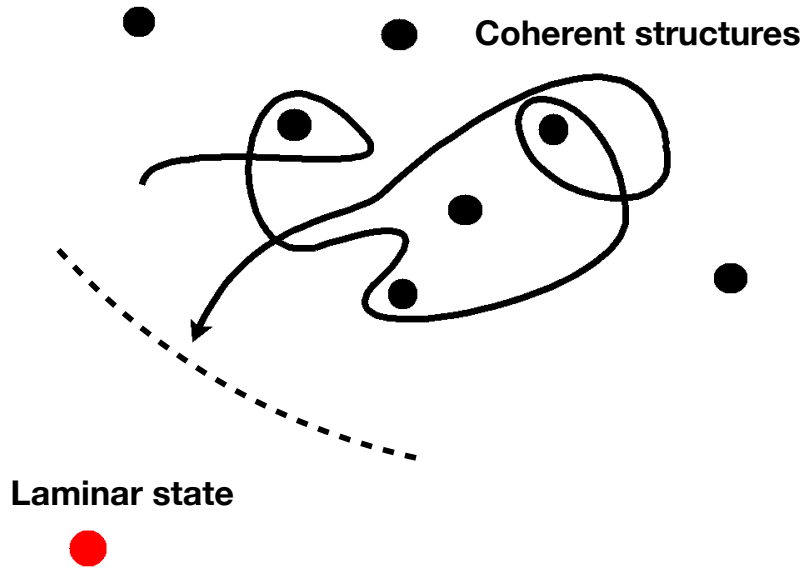

Figure 1.3 *A pictorial representation of a typical turbulent trajectory through phase space, bouncing between the locally attracting saddles of exact coherent structures before eventually relaminarising. In reality, the phase space is a chaotic saddle of infinite dimension [18].*

Pioneering experimental work [19] has shown that in the transition region of Re, the flow field, whilst chaotic, is not completely random and unorganised. Instead, the phase space is organised by 'coherent structures', invariant solutions of the Navier-Stokes equations. Fig. 1.3 shows a pictorial representation a typical path through phase space in the transition region, passing through the locally attracting domains of the coherent structures before eventually relaminarising.

Coherent structures have been defined as 'regions of concentrated vorticity, characteristic and flow-specific organization, recurrence, appreciable lifetime and scale' [20]. They correspond to either steady states (where $\dot{\mathbf{v}}, \dot{p} = f(\mathbf{v}, p) = 0$), or limit cycles and travelling waves. As the system traces out its path through phase space it follows a chaotic path, visiting locally attracting regions of these coherent structures [21]. This is manifested in the lack of pre-indicators that a turbulent trajectory is about to relaminarise [22]. The attractors form chaotic saddles in which there are several dynamic directions the system can leave the region. A good analogy is a gas particle trapped in a box with several small holes in it. The probability that the particle shall leave the box for infinite time

is 1, despite the possibly low escape probability dependent upon the size and number of holes and velocity of the particle. To be termed a coherent structure the flow must remain within the phase domain of the structure for sufficient time such that time-averaged statistics are a valid method of description. As an increase in Re increases the disorder within the system, and hence typically reduces the time that a turbulent trajectory can be caught within the chaotic saddle of a coherent structure domain, coherent structures are usually recorded experimentally within the transition region of Re, where the trajectory through phase spaces persists within their specific domain for the longest times. Recent experiments have however shown evidence of the turbulent flow field visiting the domain of coherent structures in fully developed turbulence at $Re > 30000$ [23]. A comparison between experimentally observed coherent structures and numerically generated structures is shown in Fig. 1.4. Any detected coherent structure is drawn from an infinite family of states, as the continuous symmetries of a flow do not specify a structures location within the flow geometry [24]. For example, any of the coherent structures shown in Fig. 1.4 could be rotated about or shifted along its central longitudinal axis of the pipe and remain dynamically equivalent.

There also exists a subclass of coherent structures known as relative periodic orbits. These are flow structures that repeat periodically in a frame moving along an axis of continuous symmetry for the flow. A numerical method to find such structures is described in [25], and examples of such structures found in plane Couette flow are given in [26].

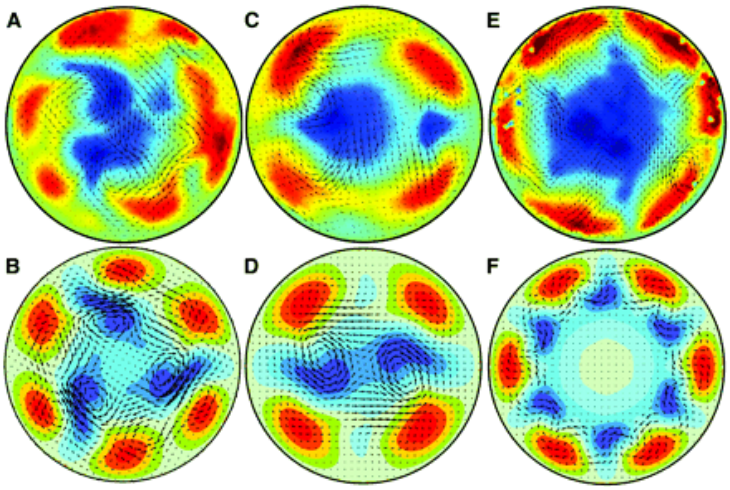

Figure 1.4 *A comparison of coherent structures found experimentally (top) and numerically (bottom) for pressure driven pipe flow. The colour corresponds to the streamwise velocity of the fluid and arrows correspond to its transverse velocity.* ***A*** *- Experimentally observed puffs at* $Re = 2000$. ***B*** *- Streamwise travelling wave found at* $Re = 1250$ *[27, 28].* ***C*** *- Travelling wave observed at* $Re = 2500$. ***D*** *- The corresponding wave found numerically at* $Re = 1360$. ***E*** *- Travelling wave observed at* $Re = 5300$ *in fully turbulent flow.* ***F*** *- The corresponding wave found numerically at* $Re = 2900$. *From [19]. Reproduced with permission from AAAS.*

As coherent structures correspond to distinct regions of phase space, they cannot overlap. This in theory therefore allows the dynamics of turbulent flow to be well represented by a reduced selection of velocity modes in a low dimensional model, especially in the transition region of Re. In fact even in the fully extended system of infinite dimension, for long timed trajectories the dynamics will be confined to a finite-dimensional manifold [29–31]. An interesting new area of research is the use of techniques from machine learning to locate these manifolds, showing some promising signs detailed in [32].

To construct a mathematical description of turbulence, one must first find the coherent structures that correspond to the flow geometry in question. For systems in which there is no linear instability of the laminar state, these solutions are particularly difficult to find as they cannot be located by analysis of the instability eigenvectors generated via linear instability analysis. Several methods exist to locate coherent structures in linearly stable flows, namely the continuation

method, globally convergent Newton-Rapheson methods (see [33]), the forcing approach and direct numerical simulation. The body forcing method introduces an additional forcing term to the Navier-Stokes equations that modifies the laminar profile such that it possesses a linear instability. The solutions are then located and traced back to the unforced case as the magnitude of the forcing is infinitesimally reduced. In a similar fashion the continuation approach locates solutions in an adjacent problem geometrically and then slowly alters the geometry such that the solutions are traced to the desired geometry. This technique was shown to be successful for plane Couette flow in [34] by first locating solutions in Taylor-Couette flow and infinitesimally increasing the radii of both concentric cylinders until the geometry approached the plane Couette geometry, also discussed in [35]. Finally, the direct numerical simulation method involves time iterating a trajectory through phase space and then searching for regions in which the orbit is trapped within a locally attracting domain of phase space or areas of periodic oscillation. This corresponds to the system being in the locality of a coherent structure acting as a chaotic saddle. Realisations of the system sampled from these points may then be used as initial conditions for a numerical solver (e.g. Newton's method [36] or Jacobian-free Newton-Krylov solvers [37]) and are much more successful than random initial conditions in locating the structures, as has been found for plane Couette flow [38].

The plane Couette system has been verified numerically to be linearly stable for all Re [39], yet experimentally turbulence is observed at $Re_c \sim 360$ [40]. This implies the existence of coherent structures above Re_c and as such various methods have been used in attempts to locate them. Initially, a continuation approach that located Taylor-Couette solutions and then increased the radii of the cylinders whilst keeping the gap separation the same (known as the narrow-gap limit) was undertaken, though this proved to be unsuccessful. Nagata [34, 41] approached the problem by considering the Taylor-Couette system in a rotating frame of reference in the large radii limit. This combination allowed for description of the fluid via the Navier-Stokes equations with a Coriolis forcing term. The system rotates on its axis with angular frequency ω, which when increased above a critical ω_c allows for the location of the Taylor vortices via a linear instability. The 2-dimensional Taylor vortex flow is then linearly unstable to 3-dimensional wavy vortex flow and higher order turbulence. These solutions could then be traced as the radii ratio is increased 1 (corresponding to plane Couette flow) and then the rotation rate ω reduced to zero.

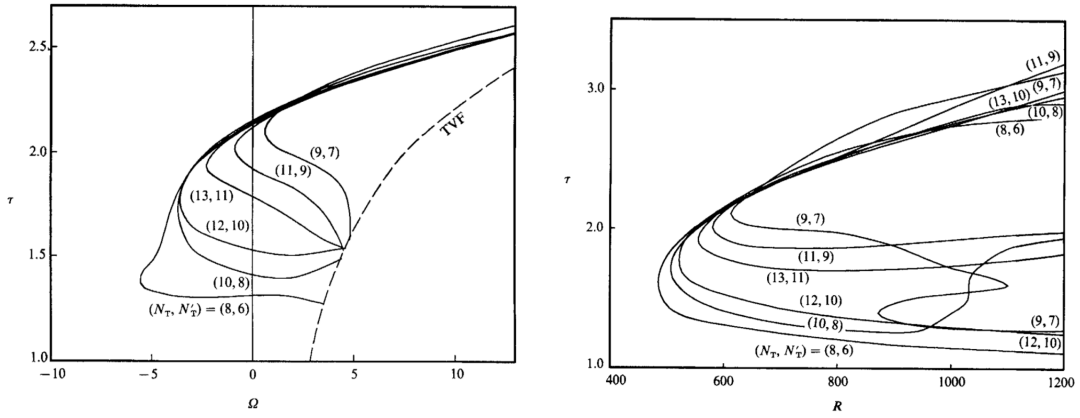

Figure 1.5 *Left - The bifurcation diagram for Nagata's system at various numerical resolutions (represented by the numbers in brackets) for* $Re = 600$*. Here, the torque* τ *represents the drag on the walls of the inner cylinder and is used as an order parameter. The laminar flow corresponds to* $\tau = 1$ *in dimensionless units. Right - An equivalent diagram instead varying Re in the PCF limit, clearly showing the bifurcation from infinity. Both reproduced with permission from [41].*

Nagata's results, shown in Fig. 1.5, show that using the continuation approach from the Taylor-Couette system can locate solutions disconnected to the laminar state in the plane Couette case. These solutions only connect with the laminar state at $Re \to \infty$. This explains the lack of linear instability to infinitesimal perturbations, but the generation of turbulent flow from finite amplitude perturbations. This scenario was first proposed by Rosenblat & Davis [42] and matches the experimental observations of Tillmark & Alfredsson [40].

A subcategory of coherent structures, known as edge states, may be observed experimentally for short times at Re very close to the transition point [43] and represent the boundary states between trajectories that will remain chaotic and those that will relaminarise [44]. These structures can serve to locally modify the shape of the $\epsilon \propto Re^{-1}$ decaying amplitude of perturbation required to ignite turbulence [45]. As Re increases more coherent structures appear [46], which can in some cases cause the location of the edge state to jump discontinuously in phase space [47]. Typically, these lower branch structures organise the dynamics in the transition region of Re, especially in the near wall region [48]. See the work of Schneider and Eckhardt for a full description of innovative numerical methods used in relation to tracking the edge state [49].

Typically, finding exact coherent structures numerically requires a very high

dimensional model and as such is computationally very expensive. As will be explained in Section 1.1.4 and Section 1.1.5, the dynamics in the transition region are remarkably well confined to a manifold constructed from just several important dynamical modes. As such, it motivates the use of low dimensional models in the study of the transition.

1.1.3 Spatio-temporal dynamics of the transition

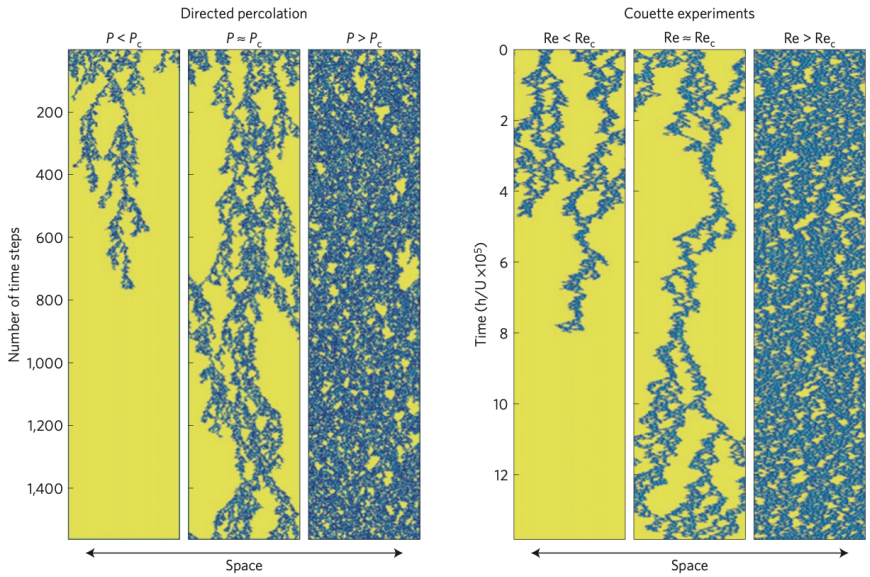

Figure 1.6 *A comparison between the spatio-temporal dynamics of 1+1D directed percolation and what is experimentally observed for plane Couette flow. Here blue represents the active sites and yellow represents the inactive laminar sites. For spreading probability P less than the critical probability P_c, the active state will always decay to the absorbing inactive state in a finite time, as with the turbulent stripes at $Re < Re_c$. Reproduced with permission from [50].*

The transition to turbulence is typically marked by localised coherent structures embedded in the laminar flow. These structures then can either relaminarise, infect neighbouring laminar flow, or continue travelling as they are [51]. The turbulent patch may infect the surrounding laminar flow by the boundary between the states fluctuating in a manner that provides a perturbation of large enough amplitude to generate turbulence. Dynamics of this nature are suitably modelled as a directed percolation process, with experiments [50] and numerical investigations [52, 53] showing promising signs that directed percolation may define the universality class of the transition, as shown in Fig. 1.6.

A similar conclusion as to the spatio-temporal dynamics of spatially localised turbulence in the transition region was reached by Barkley et. al [54], by considering the conditions for which a moving patch of turbulent flow can spread to neighbouring regions of laminar flow (in a co-moving frame) by its bounding upstream and downstream fronts travelling with velocity faster or slower respectively to the frame.

Specifically for plane Couette flow, the flow geometry primarily considered in this Thesis, the significance of spatio-temporal effects was first discussed in [55]. In this flow regime, turbulence appears as spatially localised turbulent 'stripes' at subcritical Re. The direct numerical simulations of Shi, Avila & Hof [56] have shown that the splitting rate of these stripes exceeds their decay rate at $Re = 325$, providing remarkable validation of the experimental critical $Re_c = 325 \pm 5$ as quoted in [57] two decades prior. This was then further verified by experimental and numerical work of Lemoult et. al [50] that showed that the critical exponent of the steady state turbulent fraction versus the Re of 1+1D directed percolation matched that of the plane Couette system, as shown in Fig. 1.7.

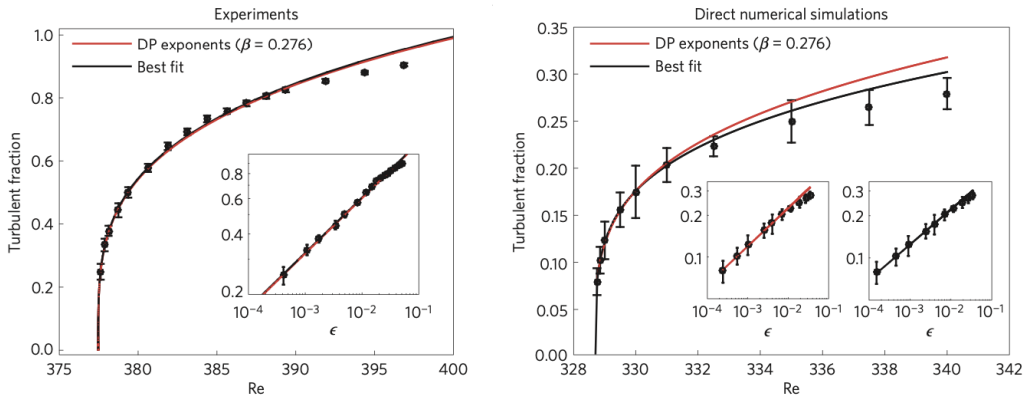

Figure 1.7 *The turbulent fraction of Couette flow in the transition region of Re extracted from both experiments and full numerical DNS of the system compared to that of 1+1D directed percolation. Reproduced with permission from [50]*

1.1.4 The self-sustaining process

After the initial experimental discovery of spatially coherent streaks in the near wall region of turbulence [58], there has been a flurry of research devoted to understanding the dynamical interactions characterised by coherent structures

that sustain turbulent motion. A common tool with which to study the features of turbulence is the so-called minimal flow unit (MFU), the periodic domain (in the streamwise and spanwise directions for plane Couette flow) that is small enough to constrain the turbulent dynamics such that they are computationally realistic to generate and easier to study, whilst also being large enough that such structures can exist. As first discussed by Jiminez and Moin [59], they identified a periodic domain in space within which flows with good agreement to turbulent statistics in the near wall regions could be directly numerically simulated and sustained. Once that domain was made small enough such that the spatially coherent streaks could not exist on comparable length scales to those identified in experiments, the turbulent dynamics could not be sustained, clearly indicating the importance of these structures in turbulence regeneration.

This understanding then motivated further study of the MFU [60], culminating in the proposal for a self-sustaining process (SSP) that is generated by the streaks. They suggest a cycle by which the streaks then become unstable via the Kelvin-Helmholtz instability [61, 62], in which a velocity difference between two layers of fluid moving in a parallel direction causes the roll-up of the interface between them. A good example of this phenomena is waves caused by wind blowing across the surface of a body of water. This instability redistributes energy back into counter-rotating streamwise vortices, via a non-linear self interaction [63]. These vortices, also known as rolls, lead to the formation of regions of fluid with velocity that deviates from the mean streamwise velocity generated by the shear [64]. This occurs as the co-moving edges of the vortices push fluid either up or down, generating a pressure gradient which enhances the flow, and regenerates the streaks. These numerical predictions were then experimentally verified in [65] and [66]. The critical Re_c for which the cycle can be observed is then the lowest Re for which the amplitude of the vortex remains unchanged after one iteration of the process.

To study the dynamics of this self-sustaining process, Waleffe published the now seminal low dimensional model for the regeneration cycle in plane Couette flow [67]. For simplicity, the process was modelled using a simpler set of conditions than is physically realised, namely free-slip boundary conditions. These dictate that the fluid velocity has no component perpendicular to the wall at the walls and that the gradient of the wall-parallel component is zero at the wall. A switch to these boundary conditions has been shown to not change the phenomenology of the flow, only altering the transitional Re_c [68]. This change allows the flow to be

decomposed into simple trigonometric functions, as Waleffe did in his analysis. Further advantages are that the energy is exactly conserved by the non-linear interactions in this scheme and the laminar state itself corresponds to one of the analytical velocity modes. The disadvantage of these conditions is that the fluid can no longer be driven by motion of the walls, so a forcing term must be introduced to replicate the effects of the counter-moving walls. It has been shown in [69] that the flow contained within a periodic box with free-slip boundary conditions well described the inner region of no-slip plane Couette flow.

Waleffe produced a low-dimensional model of the process in which the flow is spectrally decomposed into combinations of Fourier modes $\mathbf{v}_n$ such that the velocity at a point $\mathbf{x}$ is given by $\mathbf{u}(\mathbf{x}) = \sum_n a_n(t)\mathbf{v}_n$. A forcing of the form $\mathbf{F}(y) = F\sin(\beta y)\mathbf{e_x}$ is introduced, where β is a constant that matches the quarter period of the force to the wall spacing, in the streamwise x direction to produce the shear used to generate the vortices. As a result, the mean flow mode $u_L = a_L(\sin(\beta y), 0, 0)$ solves the Navier-Stokes equations for the system exactly. A truncation to 8 Fourier modes is made using symmetry arguments to give the minimal number of modes that describes the dynamics. The equations that determine the time evolution of the amplitudes of these modes are then generated by performing a Galerkin projection [70–72] of the Navier-Stokes equations onto the modes $\mathbf{v}_n$. In a later work, these solutions were then traced to the unforced plane Couette flow [73], matching those found by Nagata.

Fig. 1.8 shows a pictorial representation of the self-sustaining process and a pair of diagrams representing velocity distributions of the model system at certain points during the self-sustaining process.

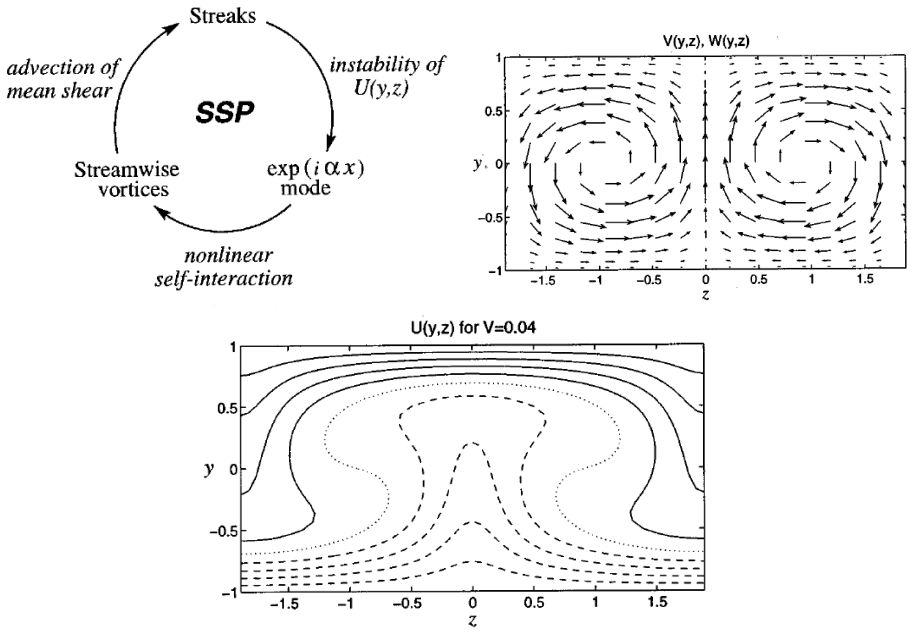

Figure 1.8 *Top left - A pictorial representation of the self-sustaining process. Top right - The velocity distribution of the streamwise rolls, where z is the infinite plane and the walls are located at $y = \pm 1$. Bottom - The streamwise velocity distribution of the streaks, where all the points along the line are of equal velocity. The dotted line represents the mean profile, dashed lines represent velocities less than the mean profile and solid lines correspond to velocities greater than the mean profile. All Reprinted from[67], with the permission of AIP Publishing.*

The 8 mode model was analysed but no fixed points beside the laminar state could be located, so a further reduction to 4 modes was made. This regime allowed dynamical systems analysis to be carried out, with a saddle node bifurcation producing two stable states, as shown in Fig. 1.9. As the upper branch solution is stable, the model captures the self-sustaining process but does not display turbulent dynamics. The system simply traces out a path from its initial condition to one of the stable branches and remains there. This is unsurprising given the low dimensionality of the model and as such the model only functions as the first step in low order modelling of the transition to turbulence.

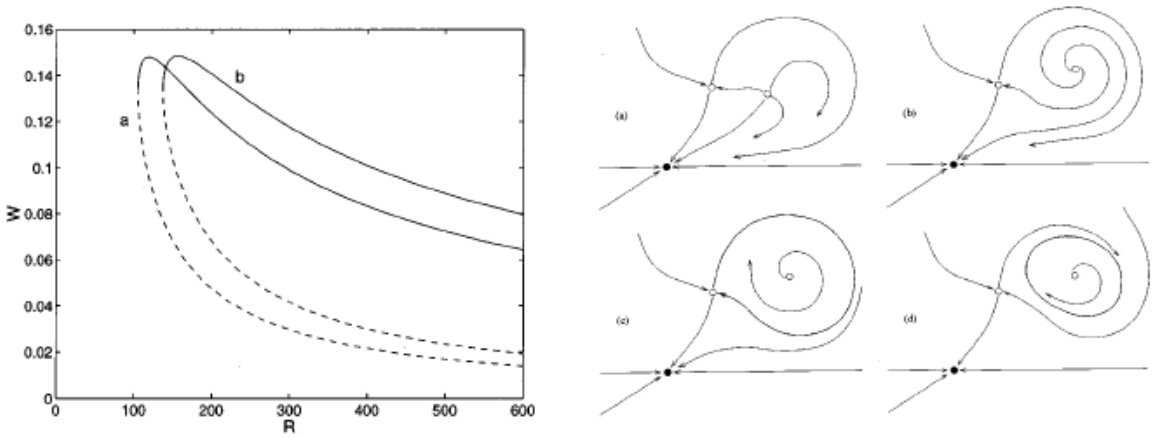

Figure 1.9 *Left - Non-trivial solutions of Waleffe's truncated 4 mode model, plotting the amplitude of the 3D instability mode W against the Reynolds number R. Right - A sketch of different dynamical scenarios for the 4 mode model. The filled black dot represents the stable laminar fixed point and the two unfilled circles represent the steady non-trivial solutions of the flow. (a) - at R slightly above R_{sn}, the value at which the saddle node bifurcation takes place, there exists a saddle and an unstable solution. (b) - at R where $R_{hc} > R > R_{sn}$, where R_{hc} represents the R at which a homoclinic bifurcation takes place. Here, exists an unstable spiral and a saddle. (c) - $R = R_{hc}$, the spiral tightens to create a homoclinic cycle. (d) - $R > R_{hc}$, a substantial portion of the phase space is contained within the periodic orbit. Reprinted from[67], with the permission of AIP Publishing.*

1.1.5 The Moehlis-Faisst-Eckhardt model

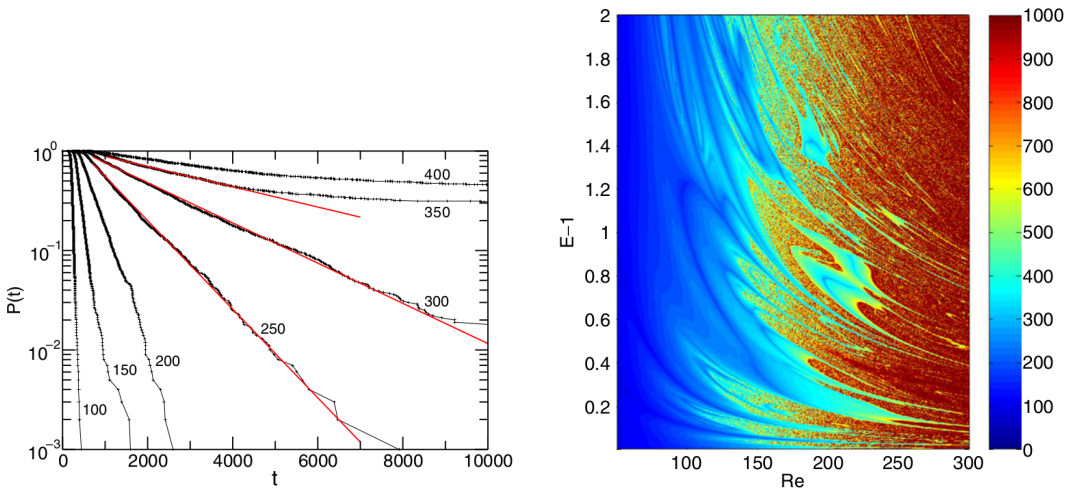

Figure 1.10 *Left - The distributions of the probability turbulence survives until time t, $P(t)$, for different values of Re in the optimal flow unit regime. The red lines correspond to the exponential fit. The discrepancy between the fit and the results for higher Re is shown to be due to a stable attractor removing some of the initial conditions in [74]. Right - Plot of turbulent lifetimes against Re and $E-1$, a measure of the energy given to an initial perturbation from the laminar flow. The colour corresponds to the lifetime of the turbulent state. This diagram shows remarkable self-similarity across different scales. Both reproduced with permission from [75].*

Building upon the work of Waleffe, the Marburg school developed an improved low order model for free-slip plane Couette flow [75]. Again the flow field was constructed from projecting the Navier-Stokes equations onto analytic Fourier modes. The modes used were a slight reformulation of the 8 mode model with an additional dimension corresponding to a modification of the laminar profile introduced. This additional mode takes the form $(\sin(3\beta y), 0, 0)$, where β again fixed the wavelength of the y-dependent velocity field to match that of the forcing. The addition of this mode is advantageous as it allows for the generation of modes with wavenumber 2β via the advective $\mathbf{u} \cdot \nabla \mathbf{u}$ term.

Analysis of the model for two different domain sizes is undertaken. The first corresponds to the minimal flow unit, the domain size corresponding to the smallest that can numerically sustain turbulence [60]. This unit corresponds to two counter-rotating vortices with a streak in between them. Simulations over periodic domains of this size do produce turbulent solutions, but they do not serve

as useful guides for the transition parameter Re_c. Localised patches of turbulent flow embedded in laminar flow will typically occur at lower Re than predicted by the minimal flow unit, as they require a larger domain size to capture. Time series of the model show turbulent trajectories through phase space, with intermittency and eventual relaminarisation as expected. A larger domain size is then tested, matching that used for the location of coherent structures in plane Couette flow in [76]. In this domain, the flow takes longer to relaminarise and has stronger intermittent bursts.

The Moehlis-Faisst-Eckhardt model produces an exponential distribution of turbulent state lifetimes, as is found in experiments [77]. The plot of the turbulent lifetimes against the strength of initial perturbation and Re shows extreme sensitivity to initial conditions, as expected for a chaotic system. A manifestation of this is that a closer inspection of Fig. 1.10 shows a fractal-like scale invariance of the plot, posing interesting questions about the topology of the turbulent portion of phase space.

1.1.6 Turbulent lifetimes

The previous two decades have seen studies of the lifetime of the turbulent state for linearly stable shear flows as a means to determine the nature of the attractor itself. Until recently, it was suggested that the lifetimes diverge to infinite length at $Re > Re_c$ [55, 77–79], though this has since been disproved in experiments [22] and numerical studies [80]. Instead, in a flow regime in which the laminar profile is linearly stable for all Re, the turbulent state is only a (potentially very long lived) transient state, when ignoring spatio-temporal effects, and as such the lifetime of a turbulent trajectory is finite.

The decay process occurs when the turbulent trajectory hits the edge state marking the boundary between the basins of attraction of the turbulent and laminar state. As the chaotic trajectory through turbulent phase is effectively memoryless, the probability that a trajectory hitting the edge state and relaminarising must also be a memoryless process and as such have a constant rate of decay λ [79]. Such a process is described by the exponential distribution, in which the probability density to decay in a time interval dt centred upon time t after an initial time delay t_0 is given by

$$p(T)dt = Pr(t \leq T < t + dt) = \lambda \exp(-\lambda(t - t_0))dt. \tag{1.6}$$

This implies that the turbulent phase space is a saddle rather than a true attractor. Special caution is given here when using the term memoryless, as the dynamics are fundamentally deterministic due to the fact that there is no stochasticity incorporated in to the Navier-Stokes equations (though of course probabilistic methods still can give an accurate description, as in Section 1.1.3). Instead, the memoryless aspect should be interpreted as the undetermined initial positions in infinite dimensional phase space within the homoclinic tangle (see [81]) of the non-trivial solutions that organise the turbulent domain combined with the fractal structure of the basin of attraction of the laminar state [82]. To obtain the probability that a turbulent trajectory remains turbulent at time t, termed the survival probability, Eq. 1.6 is integrated

$$P(t' > t) = 1 - \int_0^{t'} \lambda \exp(-\lambda(t - t_0))dt = \exp(-\lambda(t - t_0)) \tag{1.7}$$

$$P(t' > t) = \exp\left(-\frac{t - t_0}{\tau(Re)}\right), \tag{1.8}$$

where $\tau = \frac{1}{\lambda}$. The average turbulent lifetime τ has been shown experimentally [83] to increase as

$$\tau \propto \exp(\exp(Re)) \tag{1.9}$$

for high Re, and as

$$\tau \propto \exp(Re) \tag{1.10}$$

for transitional Re [22, 80]. Goldenfeld [84] has suggested that relaminarisation events occur when the largest turbulent energy fluctuation within a spatial and temporal interval is less than a threshold amplitude required to sustain turbulence, which is set by the Re of the flow. This is as if the largest fluctuation is below the threshold then necessarily all fluctuations are below the threshold and hence turbulence cannot be sustained. The turbulent energy fluctuations are proportional to $\{dv_i^2\}$, where dv is a turbulent velocity fluctuation and i labels the degree of freedom in the system. The probability that the maximum $dv_{max}^2 = x$, $P_M(x)$ is then required to calculate the relaminarisation probability. Should the set $\{dv_i^2\}$ be distributed exponentially or via a Gaussian, then the distribution of

$P_m(x)$ will follow the Gumbel distribution [85],

$$P_M(x) = \frac{1}{\beta}\exp(-(x-\mu)/\beta)\exp(\exp(-(x-\mu)/\beta)), \tag{1.11}$$

where β sets the scale and μ sets the centre point of the distribution. This is then integrated to find the cumulative distribution, ie. the probability the maximum is less than X,

$$F_M(X) = \exp(-\exp(-(X-\mu)/\beta)). \tag{1.12}$$

If we then suppose that as a turbulent trajectory is chaotic, it is possible to define a time interval τ_0 over which the flow loses any correlation to its previous state, then the typical turbulent lifetime τ will be defined as the probability that the maximum fluctuation is less than the threshold X within this correlation time,

$$\tau = \tau_0/F_M(X), \tag{1.13}$$

if $F_M(X)$ corresponds to the probability that patch of turbulence decays within the time τ_0. The functional form of the threshold X is as yet unknown, though it is supposed that it can be Taylor expanded about some Re_0 such that

$$X = X_0 + X_1(Re - Re_0) + O(Re - Re_0)^2, \tag{1.14}$$

where X_0 and X_1 are coefficients of the expansion. Re_0 corresponds to the point at which localised turbulent patches are first observed, with average lifetime of order τ_0. If these results are collated then then the functional form of the lifetime then becomes

$$\tau = \tau_0\exp(\exp(-(X_0 + X_1(Re - Re_0) + O(Re - Re_0)^2))), \tag{1.15}$$

giving a super-exponential dependence of the lifetimes upon Re. This cannot be extrapolated as a general mechanism to explain the lifetime scaling as the use of the Taylor expansion implies its validity over only a small range of Re about Re_0 [86].

In addition to this, the idea attracts some scepticism due to the semi-arbitrary choice of distribution of $\{dv_i^2\}$, required to allow for the use of Eq. 1.11 to describe the statistics of the maximal value. This, however, remains as yet best analytical explanation of the super-exponential scaling.

1.2 Non-Newtonian fluids

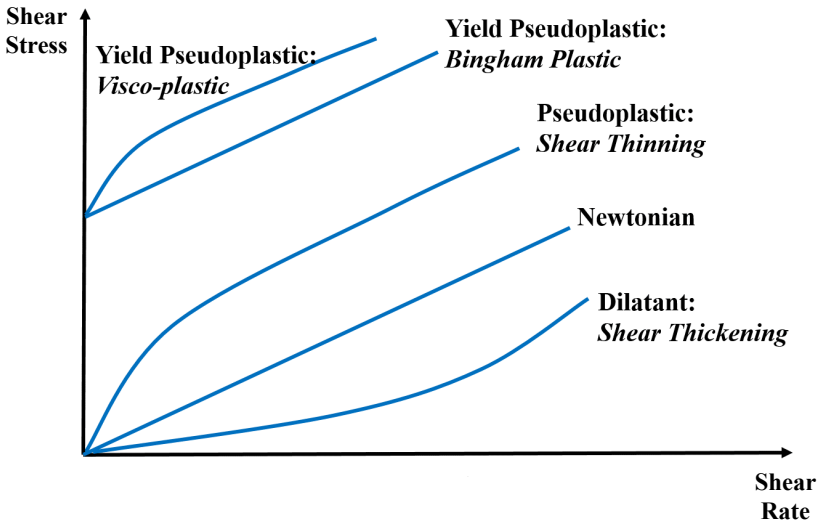

Figure 1.11 *A diagram displaying the relationship between applied shear rate and the shear stress for different types of fluid. Adapted with permission from [87]*

Thus far we have discussed results for Newtonian fluids, for which the stress tensor is defined in Eq. 1.2 for a constant temperature. These are only a generalised subset of fluids, most of which have a more complicated and often non-linear relationship between the rate of shear and the shear stress (terming them non-Newtonian fluids). This non-linearity, caused by the interaction of the molecular structure of the fluid and flow field, can then give rise to novel bulk properties and interesting phenomena. These include the so-called shear thinning, by which a fluid's viscosity decreases under an applied shear. An example of this type of fluid is paint, which is designed to flow easily when stress is applied by the brush but avoid dripping once adhered to a surface and under no further strain. The converse effect, shear thickening, describes the circumstance when a fluid's viscosity increases when a shearing force is applied, causing a resistance to flow. These types of fluids are typically colloidal suspensions and the typical fluid of study is 'oobleck' (a mixture of cornstarch and water). In addition, some materials also exhibit stress memory, in which there the fluid returns to equilibrium after an applied stress over some finite timescale. This causes hysteresis on the stress-rate of strain curve and as such corresponds to a loss of energy from the system. Finally, the introduction of some types of molecules suspended in a liquid, such as

polymer chains, introduces a degree of anisotropy to the system as the molecules exhibit different responses to normal stress depending on the direction of the application of the stress relative to the molecule alignment and state. There is also a tendency of such molecules to align their long axis parallel to the shearing force, in turn leading to the elastic stretching along the direction of the flow. Examples of the different classifications of the relationship between applied shear rate and shear stress are shown in Fig. 1.11.

1.2.1 Different models of the stress tensor

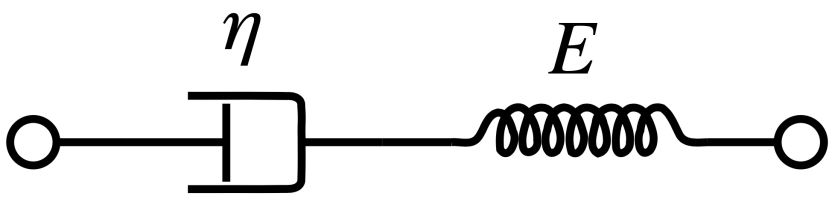

Figure 1.12 *A schematic representation of the Maxwell model for a viscoelastic fluid. Here the dashpot of viscosity η is combined in series with the spring of extension constant E.*

To describe the aforementioned effects, constitutive equations for the stress tensor must be constructed, with the aim of each model describing a certain type of fluid under certain conditions. Typically different models are selected dependent upon the scenario being modelled, together with pay-offs between numerical stability and computation time considered. Generally, constitutive relations for the stress tensor must obey three principles: the equation must be frame invariant, the stress tensor must only depend on its previous deformations, and be determined locally within a fluid parcel, though continuous across parcel boundaries [88]. See Bird and Wiest [89] for a conclusive overview of different constitutive relations.

A simple model to describe a material with both viscous and elastic properties is the so-called Maxwell model, in which the stress response of the material is regarded to behave as if described by a Hookean spring (with $\sigma_s = E\epsilon_s$, where E is the Young's modulus) and a dashpot arranged in series, see Fig. 1.12. Here the dashpot schematically represents the viscous component of the material that resists deformation to an applied shear, with stress-strain relation $\sigma_d = \mu\dot{\epsilon_d}$. As the components are arranged in series, the stress must must be experienced

equally $\sigma_{total} = \sigma_s = \sigma_d$ and their strain summed $\epsilon_{total} = \epsilon_s + \epsilon_d$. Combining all of these relations gives the Maxwell model for a viscoelastic fluid

$$\mu\dot{\epsilon} = \frac{\mu\dot{\sigma}}{E} + \sigma. \tag{1.16}$$

If the frame invariant upper convected derivative is applied to Eq. 1.16, see [88], then one arrives at the upper convected Maxwell (UCM) model

$$\boldsymbol{\tau} + \lambda\overset{\triangledown}{\boldsymbol{\tau}} = 2\mu\dot{\boldsymbol{\gamma}}, \tag{1.17}$$

where $\overset{\triangledown}{\boldsymbol{\tau}}$ represents the upper convected derivative of the stress tensor, λ denotes the stress relaxation time of the material, $\lambda = \mu/E$, and $\dot{\boldsymbol{\gamma}}$ is the aforementioned rate of strain tensor. This model, though straightforward to derive, rarely gives an adequate description of a real viscoelastic fluid.

A common situation of interest is that of a compound mixture formed by a non-Newtonian solute in a Newtonian solvent. Here, the constitutive relation is given by

$$\boldsymbol{\sigma} = -p\mathbf{I} + \mu_s\dot{\boldsymbol{\gamma}} + \boldsymbol{\tau_p}, \tag{1.18}$$

where μ_s is the solvent viscosity, and $\boldsymbol{\tau_p}$ is the polymer stress tensor. If $\boldsymbol{\tau_p}$ obeys Eq. 1.17, then Eq. 1.18 may be substituted into Eq. 1.1 to arrive at the Oldroyd-B model for viscoelastic fluids

$$\rho\left(\frac{\partial\mathbf{v}}{\partial t} + \mathbf{v}\cdot\nabla\mathbf{v}\right) = \mathbf{f} - \nabla p + \mu_s\nabla^2\mathbf{v} + \nabla\cdot\boldsymbol{\tau_p}, \tag{1.19}$$

$$\nabla\cdot\mathbf{v} = 0, \tag{1.20}$$

$$\boldsymbol{\tau_p} + \lambda\left(\frac{\partial\boldsymbol{\tau_p}}{\partial t} + \mathbf{v}\cdot\nabla\boldsymbol{\tau_p} - (\nabla\mathbf{v})^T\cdot\boldsymbol{\tau_p} - \boldsymbol{\tau_p}\cdot(\nabla\mathbf{v})\right) = \mu_p\left((\nabla\mathbf{v})^T + \nabla\mathbf{v}\right). \tag{1.21}$$

In a similar manner to the treatment of Eq. 1.4, it is possible to non-dimensionalise via scales of length L, time T and velocity $U = L/T$, such that $\mathbf{x} = \hat{\mathbf{x}}/L$, $\mathbf{v} = \hat{\mathbf{v}}/U$, $t = \hat{t}/T$, $p = \frac{\hat{p}L}{U(\mu_s+\mu_p)}$, $\mathbf{f} = \frac{\hat{\mathbf{f}}L^2}{U(\mu_s+\mu_p)}$, $\hat{\boldsymbol{\tau}}_{\boldsymbol{p}} = \frac{\boldsymbol{\tau_p}L}{U\mu_p}$ and to introduce the quantities $\beta = \frac{\mu_s}{\mu_s+\mu_p}$, the proportion of the solution viscosity provided by the solvent (which is inversely proportional to the polymer concentration in the dilute limit), and the Weissenberg number $Wi = \frac{\lambda U}{L}$, such

that Eqs. 1.19 - 1.21 become

$$Re\left(\frac{\partial \mathbf{v}}{\partial t} + \mathbf{v}\cdot\nabla\mathbf{v}\right) = \mathbf{f} - \nabla p + \beta\nabla^2\mathbf{v} + (1-\beta)\nabla\cdot\boldsymbol{\tau_p}, \tag{1.22}$$

$$\nabla\cdot\mathbf{v} = 0, \tag{1.23}$$

$$\boldsymbol{\tau_p} + Wi\left(\frac{\partial \boldsymbol{\tau_p}}{\partial t} + \mathbf{v}\cdot\nabla\boldsymbol{\tau_p} - (\nabla\mathbf{v})^T\cdot\boldsymbol{\tau_p} - \boldsymbol{\tau_p}\cdot(\nabla\mathbf{v})\right) = (\nabla\mathbf{v})^T + \nabla\mathbf{v}, \tag{1.24}$$

which are the Navier-Stokes equations for an Oldroyd-B fluid. Here, the quantity Wi can be thought of as a nondimensional number comparing the size of the elastic forces to the viscous ones, which has been shown to be the appropriate non-dimensional quantity to collapse viscoelastic flows [90]. Due to its relative simplicity, compounded by the fact that many different viscoelastic mircoconfigurations beyond the spring and dashpot model converge on Oldroyd-B model for weak flows, this is the model we shall use for the analysis in Chapter 4. Other visco-elastic models include the finitely extensible nonlinear elastic - Peterlin (FENE-P) [91], Phan–Thien-Tanner (PTT) [92] and the amusingly named Rolie-Poly [93] constitutive relations. The Oldroyd-B model must be used with a degree of caution as it does not bound the tensile stress, such that extensional flows may be thought of as being able to infinitely extend the solute polymers, which is of course unphysical. In addition to this, in reality as a polymer is forced into a configuration tending to its maximum extension, the associated spring constant will increase as the dumbbell becomes stiffer.

If the polymer solute is modelled as a Hookean dumbbell, as for the UCM and Oldroyd-B models, then using kinetic theory we may derive the relation

$$\boldsymbol{\tau_p} = nK\langle\mathbf{RR}\rangle - \frac{\mu_p\mathbf{I}}{\lambda}, \tag{1.25}$$

where n is the concentration of polymer molecules in the solution, K is the stiffness of the spring, λ is the characteristic relaxation time of the spring and $\langle\mathbf{RR}\rangle$ is the conformation tensor defined by

$$\langle\mathbf{RR}\rangle = \int \mathbf{RR}\Psi(\mathbf{R},t)d^3\mathbf{R}, \tag{1.26}$$

with $\mathbf{R}$ denoting the vector between both ends of the dumbbell, and $\Psi(\mathbf{R}, t)$ encoding the probability distribution of the $\mathbf{R}$ vector [88]. The use of $\langle\rangle$ indicates the ensemble average. This conformation tensor may be diagonalised at any instantaneous realisation of the system such that

$$\langle \mathbf{RR} \rangle = \begin{vmatrix} R_1^2 & 0 & 0 \\ 0 & R_2^2 & 0 \\ 0 & 0 & R_3^2 \end{vmatrix} \tag{1.27}$$

where R_i are the projections of the $\mathbf{R}$ vector onto its eigen frame. As the diagonalised values of the conformation tensor are the squares of R_i, they must be positive to remain physical [94]. It can be shown that if at some realisation of the system the values of R_i are positive semi-definite (i.e. not negative), then they remain so for all further times and locations within the system [95]. As the base state with zero applied stress infers $R_i = 0$, which is positive semi-definite, then all perturbations to this state must also be positive semi-definite [88]. Unfortunately, most numerical schemes to simulate Eqs. 4.1-4.3 do not enforce this condition, and, as such, care must be taken to not consider simulations and their associated results in which this condition is broken. The problem is compounded by the system typically not having an obvious indicator (eg. the amplitudes of the stress modes tending to infinity) that the positive semi-definite condition is being enforced.

In addition to this, the so-called high Wi problem must also be considered. This describes the appearances of high stress gradients that occur at moderate Wi via a loss of simulation resolution which then become numerically unstable [96].

1.2.2 Drag reduction

The phenomenon of drag reduction, as first observed by Toms [97], is the effect by which adding a small concentration of a long chain polymer one can reduce the drag force applied to a bounding stationary wall by a factor in excess of 0.7 for certain flow parameters [98]. The drag reduction effect is of great use in reducing the costs of transporting oil through pipelines as high flow rates can be obtained using less energy due to reduced losses to friction at the walls. The addition of the polymers can also cause the appearance of turbulence at a lower Re than is found in the solvent for some flow geometries, termed 'early turbulence' [99, 100]. For other flows, the converse may occur, by which the introduction of the polymers

causes the laminar profile to retain stability to a higher Re [101].

Turbulent flow exerts a much greater drag force upon the bounding walls of the flow than the laminar state, as the turbulent flow contains streamwise vortices that serve to increase the friction force applied at the wall [102]. This friction is well understood in MFU simulations to be reduced by the suppression of these vortices by the polymeric molecules, due to their application of a negative torque to the vortices [103]. This torque arises due to the resistance of a polymer being extended by two counter-rotating vortices serving to reduce the kinetic energy. Indeed the presence of polymers allows for energy transfer between the flow and polymer, altering the typical turbulent energy cascade, as described in [104], to cause drag reduction.

In the dilute limit, further addition of the high molecular weight polymer continues to reduce the drag force applied on the bounding wall, before reaching an asymptotic limit known as the maximum drag reduction (MDR) [105]. This limit serves as a lower bound for the friction factor at a certain Re. The flow structure in this regime has been shown to be remarkably invariant to changes in polymer structure, posing interesting questions about its universal nature [106], and has been shown to be similar to the edge state, as discussed in Section 1.1.2, for some flows [107].

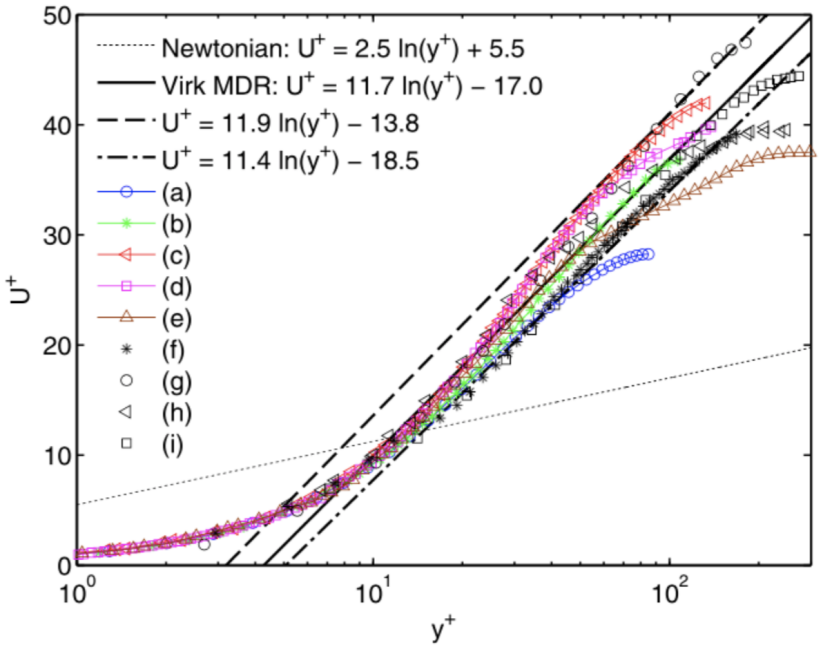

Figure 1.13 *A collation of experimental (disconnected with no colour) and numerical (connected with colour) studies in a variety of different flow geometries displaying the Virk MDR asymptote. Here y^+ encodes the distance from the bounding wall and U^+ represents the mean downstream velocity. The superscript $^+$ takes its usual definition to signal that the quantities have been non-dimensionalised via 'inner units', as detailed in [108].(a) Channel $Re = 85$ [109], (b) Channel $Re = 131$ [110] (c) Channel $Re = 100$ [111], (d) Channel $Re = 120$ [112], (e) Boundary layer $Re = 425$ [113], (f) Boundary layer $Re = 179$ [114],(g) Pipe $Re = 182$ [115], (h) Rectangular duct $Re = 253$ [116], (i) Channel $Re = 253$ [117]. Reproduced from [108], with permission from Elsevier.*

The usual characterisation of the MDR state is via its mean velocity profile, which deviates from the usual Newtonian scaling as displayed in Fig. 1.13.

1.2.3 Elasto-inertial turbulence

When a dilute solution of polymers flows at $Re > Re_c$, the fluid will exhibit qualitative and quantitative features analogous to Newtonian turbulence. The topology of the flow however, is significantly altered enough to warrant the description as a separate class of turbulence, known as elasto-inertial turbulence [118]. The addition of polymers to the flow suppresses the Newtonian coherent structures, altering the organisation of the turbulent phase space and hence

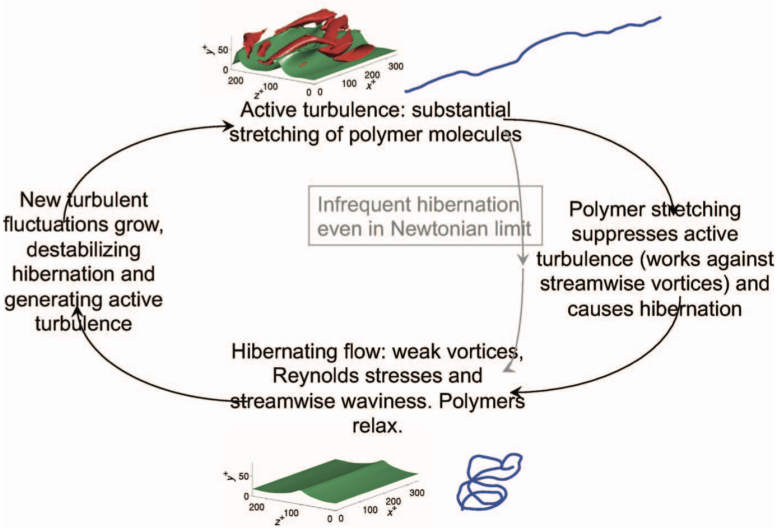

Figure 1.14 *A schematic representation of a typical cycle through phase space between the active and hibernating states. Reproduced from [108], with permission from Elsevier.*

altering the typical instantaneous flow shape of elasto-inertial turbulence [119]. Typically, the streaks are spaced further apart than Newtonian turbulence at an equivalent Re, become elongated and have smaller magnitude wavy inflections in the streamwise direction [120, 121]. It has been shown that at a high enough Wi, several ECS for plane Pouiselle flow cease to exist [122]. This elasto-inertial state is not found if the turbulence is too strong (i.e. Re too large) or the polymer solution is not elastic enough. Dubief *et al.* propose a separate self-sustaining mechanism for elasto-intertial turbulence, as described in [119].

1.2.4 Hibernating turbulence

A recent discovery in the study of elasto-inertial turbulence has been that of the so-called 'hibernating' turbulent state, discovered initially in numerical simulations of the minimum flow unit in plane Pouiselle flow [124]. In this regime, the flow is found to exhibit a reduced shear rate in the wall regions for some finite time, consequentially increasing the streamwise bulk velocity, before returning to the active turbulent state. The velocity profile in this regime is qualitatively similar to that observed at the MDR asymptote described in Section 1.2.2. Interestingly, it has been shown in numerical experiments that when the viscoelastic component is removed from the equations controlling the

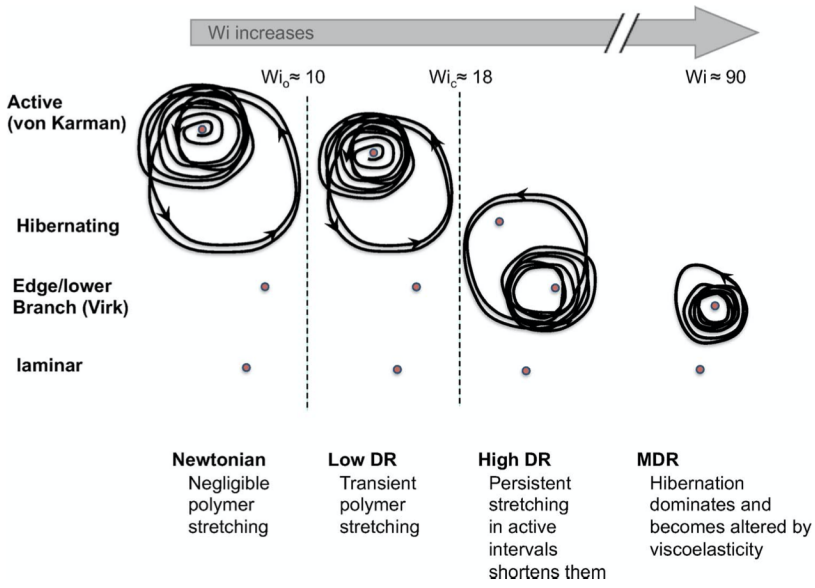

Figure 1.15 *A pictorial representation of the effects of increasing Wi on the dynamics of a turbulent trajectory. Here the description of the 'active' state as von Karman turbulence is in reference to the average downstream velocity profile taking the Prantl-von Karman form as expected in fully Newtonian turbulence [123]. Reproduced from [47], with the permission of AIP Publishing.*

time evolution of a trajectory entering the hibernating portion of phase space, the trajectory remains aligned to that of the fully viscoelastic case for a comparable time to the hibernation period [113], suggesting that the flow structures are perhaps of Newtonian nature.

In the transitional regime not dominated by either the active elasto-intertial turbulence or the MDR-like hibernating turbulence, a typical qualitative time evolution proceeds as follows: the polymer molecules are deformed at a faster rate than they can relax by the active turbulence, which reduces the available turbulent kinetic energy. This then causes the flow to enter the weaker hibernating portion of phase space, in which the polymers relax to lower energy states. This persists until a turbulent velocity fluctuation, now unopposed by the stretched polymers, grows transiently in a manner that reignites the active state. This cycle continues until the eventual relaminarisation of the flow. This cycle is shown in Fig. 1.14. As Wi is increased the amount of time spent in the active state reduces until its contribution to the velocity profile is insignificant and the flow takes on the full MDR profile [121], as shown graphically in Fig. 1.15.

Wang *et al.* have shown that the hibernating state gradually disappears in

the Newtonian regime as Re is increased [108]. This hints that this state may also play some part in the transition dynamics in the purely Newtonian case, which is supported by the detection of MDR-like structures that persist in the transitional region of Re for the Newtonian case in extended domains [125, 126]. Interestingly, experimental observations of the low drag state for transitional Newtonian turbulence appear to resemble the unit cell required for the self-sustaining process from [67], namely two counter-rotating vortices with a low speed streak in between [127].

1.3 Outline of research programme

Throughout this chapter we have seen that the use of techniques from the field of dynamical systems have proved to be a valuable endeavour in furthering the understanding of the transition to turbulence. One of the most fruitful techniques has been the use of low dimensional models to isolate qualitative features of the transition, for example in [128–134]. One feature of these models is the fact they generally are introduced using insight gained from DNS or other intuition as to the form of the model. It is therefore of interest to develop a method by which such models can be constructed without *a priori* knowledge about shape of the flow field in question. This motivates the development of an algorithm that can produce a low dimensional model 'intuition free'.

One such method is developed in Chapter 2 and then tested for plane Couette flow. In this scheme, a Nagata-like homotopy from rotating plane-Couette flow is used to determine the relevant modes to create a model that well describes the features of non-rotating plane Couette flow. When studying the series of low dimensional models created by this process, it was found that the inclusion of different combinations of velocity modes can cause dramatic differences in the length of a typical turbulent trajectory.

In Chapter 3 the mechanism that causes the difference in the length of the lifetimes is investigated. In this study, an intermittency reminiscent of that observed for hibernating turbulence in the elasto-inertial regime is observed, motivating questions as to the relationship between the observed structures and those found in the viscoelastic case. This then prompted the creation of an analogous model for elasto-inertial turbulence, for which the Oldroyd-B constitutive equations were used for simplicity. The model is then studied in Chapter 4, revealing the effects of viscoelasticity on the turbulent phase space via changes in the length of the turbulent lifetimes and modifications to the shape and stability range of periodic orbits and steady coherent structures.

Chapter 2

A recipe to generate a low order model of the transition to turbulence in plane Couette flow

The initial aim of this scheme of work was to develop a method that can be used to generate a low order model encapsulating the hallmark features of turbulent dynamics and the transition to turbulence without prior intuition as to the velocity modes required to achieve this. It is of particular interest to develop such a method as there are many systems that are typically very difficult to generate time series data for due to their numerical instability, and therefore cannot readily provide the clues as to what the turbulent flow might look like. A good example of this type of system is non-Newtonian fluid flow, as described in Section 1.2. To that end, this recipe to generate a low dimensional model was created with the intent of using it to produce a model with which we could investigate the non-Newtonian turbulence transition scenario in Chapter 4. As will be described in this chapter, and expanded upon in Chapter 3, the use of this technique for a Newtonian test case also generates results of scientific interest to the current study of the turbulence transition in this regime.

The outline of the recipe is to generate a non-degenerate set of N modes by allowing the velocity component along each axis to be drawn from a specified set of analytic spatial trigonometric functions that satisfy the boundary conditions of the flow. Once complete, the velocity modes that do not satisfy the incompressibility condition are disregarded from further analysis. The Navier-

Stokes equations are then projected onto the modes with periodic boundary conditions in the appropriate directions (depending upon chosen flow geometry), yielding a dynamical system of N simultaneous equations. Attempts could then be made to try and find the minimal set of $M < N$ modes that retain all of the qualitative features of the transition displayed in the full N mode set. This process could then lead us to infer which velocity mode interactions are critical to the existence of certain phenomena typical of the transition.

A model of this type will be unable to reproduce the spatio-temporal effects that are proposed to govern certain features of the transition, due to its low dimension. This would require the full DNS of the system, i.e. a model for which $N \to \infty$. Instead it is analogous to modelling a single turbulence 'unit', or 'site' following the naming of [84], which form the constituent building blocks of the spatio-temporal structures observed the transition or fully developed turbulence. As we shall see, regardless of the inability to model spatio-temporal effects, the models produced via this process still give interesting insight some of the features of the transition and pose questions for new avenues of research.

To test our recipe for model generation, we consider generating a model of the flow in the plane Couette geometry, due in part to its geometric simplicity, but also due to the success of Nagata [34] in using homotopy from the narrow gap approximation of rotating Taylor-Couette flow to find exact solutions in this regime, as with our outline. This flow regime has also historically been fruitful for the development of low dimensional models [67, 75], which allows us to benchmark our model against previously constructed iterations.

We use the simpler free slip boundary conditions as they allow for the flow field to be deconstructed into trigonometric Fourier modes, one of which corresponds to the laminar profile. This switch has been shown to not alter the phenomenology of the flow from wall driven plane Couette flow subject to the no slip boundary conditions, only serving to lower the critical Reynolds number at which the turbulence transition occurs [67, 68, 135]. The flow in this regime can be thought of as a representation of the inner dynamics of plane Couette flow away from the boundary layer [69]. An artificial sinusoidal forcing term is added to the Navier-Stokes equations to generate the shear, compensating for the fact that the fluid is now not required to adhere to the bounding walls.

2.1 Setup

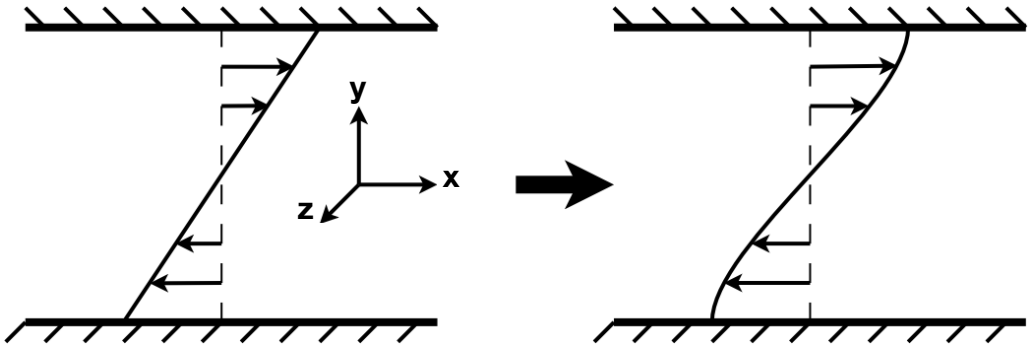

Figure 2.1 *A diagram showing the chosen coordinate system for the analysis relative to the plane Couette geometry, with the laminar profiles for the wall driven (left) and sinusoidally body forced (right) flow overlain.*

If we define the geometry of the system to have the two parallel walls located at $y = \pm 1$, with the x-coordinate pointing in the streamwise direction and the z-axis in the spanwise direction, as shown in Fig. 2.1, then the free slip conditions for the plane Couette flow system

$$\left.\frac{du}{dy}\right|_{y=\pm 1} = \left.\frac{dw}{dy}\right|_{y=\pm 1} = 0, \tag{2.1}$$

where u, v and w are the velocities in the streamwise x, wall-normal y and spanwise z directions, respectively. If we further define the walls to be impermeable we obtain the second boundary condition for the system

$$v(y = \pm 1) = 0. \tag{2.2}$$

The inclusion of the Coriolis rotation force and the shear generating sinusoidal force gives the Navier-Stokes equations for the system as

$$\rho\left(\frac{\partial \mathbf{v}}{\partial t} + \mathbf{v}\cdot\nabla\mathbf{v} + 2\omega\hat{\mathbf{k}}\times\mathbf{v}\right) = \mathbf{f}(y) - \nabla p + \mu\nabla^2\mathbf{v}, \tag{2.3}$$

$$\nabla\cdot\mathbf{v} = 0, \tag{2.4}$$

where ω is the rotation rate about the z-axis, $\hat{\mathbf{k}}$ is the unit vector in the z-direction, $\mathbf{f}(y)$ is the external body forcing, p is the pressure, ρ is the fluid density and μ is the dynamic viscosity. If we then introduce the scales of length, L, the half width of the channel and velocity U realised by the fluid at the top bounding wall, and time $T = L/U$ such that $\hat{\mathbf{x}} = \mathbf{x}/L$, $\hat{\mathbf{v}} = \mathbf{v}/U$, $\hat{t} = t/T$, $\hat{p} = \frac{Lp}{\mu U}$, $\hat{\mathbf{f}} = \frac{\mathbf{f}L^2}{\mu U}$ and $\frac{2\rho\omega L^2}{\mu} = \Omega$ we arrive at

$$Re\left(\frac{\partial \mathbf{v}}{\partial t} + \mathbf{v}\cdot\nabla\mathbf{v}\right) = \mathbf{f}(y) - \nabla p - \Omega\hat{\mathbf{k}}\times\mathbf{v} + \nabla^2\mathbf{v}, \tag{2.5}$$

$$\nabla\cdot\mathbf{v} = 0, \tag{2.6}$$

where $Re = \frac{\rho U L}{\mu}$ and the hat notation has been dropped for clarity. The forcing term $\mathbf{f}(y)$ is given by

$$\mathbf{f}(y) = \begin{pmatrix} \sqrt{2}\beta^2\sin(\beta y) \\ 0 \\ 0 \end{pmatrix}, \tag{2.7}$$

where β fixes the wavelength of the forcing to match the wall spacing as in [67, 75]. The forcing induces a pressure gradient which serves as a Lagrange multiplier to enforce the divergence free condition, though this does not affect the dynamics of the system and as such is ignored. This is as the individual modes themselves are divergence free, so any linear combination of them must also be divergence free. The resultant laminar flow $(\sqrt{2}\sin(\beta y), 0, 0)^T$ solves the Navier-Stokes equations exactly. Though this base profile has a point of inflection, it does not lead to a linear instability in the viscid regime for all Re [67, 136].

2.2 Selecting the velocity modes

We model the flow in a periodic cell in the x and z directions, with box size L_x in the x-direction and L_z in the z-direction, such that $\alpha = \frac{2\pi}{L_x}$ and $\gamma = \frac{2\pi}{L_z}$, then $\mathbf{u}(x,y,z) = \mathbf{u}(x + \frac{2\pi n}{\alpha}, y, z)$ and $\mathbf{u}(x,y,z) = \mathbf{u}(x, y, z + \frac{2\pi n}{\gamma})$ for $n \in \mathbb{Z}$. The entire domain of the box is then $0 \le x \le L_x$, $-1 \le y \le 1$ and $0 \le z \le L_z$.

We consider only Fourier modes up to the second order in the y direction, i.e. such than $m = 0, 1, 2$ for $\sin(m\beta y)$ and $\cos(m\beta y)$, and first order in x and z directions to restrict the model to a low number of dimensions. The free slip boundary conditions (2.2) and (2.1) restrict the wall normal velocity dependence

of the modes such that they are selected from the sets

$$v(y) \in [0, 1, \sin(2\beta y), \cos(\beta y)],$$

$$u(y), w(y) \in [0, 1, \cos(2\beta y), \sin(\beta y)].$$

The x-dependence and z-dependence of u, v and w is then selected from

$$u(x), v(x), w(x) \in [0, 1, \sin(\alpha x), \cos(\alpha x)],$$

$$u(z), v(z), w(z) \in [1, \sin(\gamma z), \cos(\gamma z)].$$

Velocity modes are generated by allowing each component to select one member of each of the above sets and then taking the product of these selections, i.e. generate modes in the manner of:

$$\text{Choose } u,\ v,\ w \text{ components from } \begin{bmatrix} 0 \\ 1 \\ \cos(\alpha x) \\ sin(\alpha x) \end{bmatrix} \times \begin{bmatrix} 1 \\ \cos(\beta y) \\ sin(\beta y) \\ \cos(2\beta y) \\ sin(2\beta y) \end{bmatrix} \times \begin{bmatrix} 1 \\ \cos(\gamma z) \\ sin(\gamma z) \end{bmatrix}$$

This process is repeated for each possible combination of choices from each set. The modes that do not satisfy the divergence free condition for the velocity (2.4) are then abandoned, leaving 44 unique modes. The unities are included in the velocity functional sets to allow a component of a mode to have no dependence from that specific set when multiplying through each selection. Accordingly, all modes that multiply out with a resultant velocity component of 1 in any plane are also discarded. Following [75], an additional mode corresponding to the modification of the laminar profile mode is included, resulting in 15 x-independent modes and 30 x-dependent modes (see Appendix A.1). This additional mode takes the form $(\sin(3\beta y), 0, 0)^T$ and is included as it allows for generation of modes with wavenumber 2β via the advective $\mathbf{v} \cdot \nabla \mathbf{v}$ term. The modes are normalised such that the Galerkin projection [137] over the periodic domain $x \in [0, \frac{2\pi}{\alpha}]$, $y \in [\frac{-\pi}{2\beta}, \frac{\pi}{2\beta}]$, $z \in [0, \frac{2\pi}{\gamma}]$ onto themselves gives $\frac{4\pi^3}{\alpha\beta\gamma}$, the volume of the simulated cell. The wall-normal wavenumber was fixed at $\beta = \frac{\pi}{2}$ to exactly match the forcing, again following [75], for the remainder of the work in this Thesis.

Equations for the time evolution of the amplitudes $a_n(t)$ of the modes are obtained by performing a Galerkin projection of the modes onto the Navier-Stokes equations,

$$\frac{\alpha\beta\gamma}{4\pi^3}\int_0^{\frac{2\pi}{\gamma}}\int_{-1}^{1}\int_0^{\frac{2\pi}{\alpha}} a_n(t)\mathbf{g}(x,y,z,t).\mathbf{u}_n(x,y,z)\mathrm{d}x\mathrm{d}y\mathrm{d}z, \tag{2.8}$$

where $\mathbf{g}(x,y,z,t)$ is Eq. (2.5). This produced a set of 45 equations for the time evolution of the flow (detailed in Appendix A.3), which could then be numerically integrated to define trajectories of the flow. These take the general functional form

$$\frac{\partial a_n(t)}{\partial t} = f(a_1, a_2, ..., a_N, \alpha, \beta, \gamma, Re, \Omega). \tag{2.9}$$

The numerical labelling scheme for the modes is detailed in Appendix A.1. The velocity field is comprised of the sum of the modes multiplied by their respective amplitudes, $\mathbf{v} = \sum_0^N a_n(t)\mathbf{v}_n(x,y,z)$, where $\mathbf{v} = \mathbf{v}(x,y,z,t)$ is the total velocity field, $a_n(t)$ are the mode amplitudes and $\mathbf{v}_n(x,y,z)$ are the normalised velocity modes.

2.3 2D Taylor vortices

First, we seek to construct Taylor vortices in the narrow gap limit of rotating plane Couette flow, namely when the radii of the two cylinders that form the bounding walls of the system are large and the difference said radii is small. In this approximation, the flow behaves as a plane Couette flow with an external Coriolis force, as described in the previous Section. The Taylor vortex solutions require only the 15 x-independent modes as these structures are 2-dimensional, that is to say they exist at all x, but do not vary in the x direction. As the laminar profile is well known to be linearly unstable in this regime, the Taylor vortex solutions may be obtained via linear stability analysis. The flow is linearised around the laminar state, corresponding to mode $\mathbf{u}_8$, and perturbed infinitesimally. The stability analysis is then formed as a generalised eigenvalue problem of the linearised mode amplitude evolution equations, $\mathbf{A}\mathbf{e}^{(i)} = \mathbf{e}^{(i)}\lambda_i$, where $\mathbf{e}^{(i)}$ are the eigenvectors and λ_i the eigenvalues of matrix $\mathbf{A}$. Analytic expressions for the 15 eigenvalues as a function of Re and Ω are found. Each eigenvalue, except that which corresponds to the modification of the mean profile $\mathbf{v}_{15}$, is degenerate, arising due to modes modulated by a sine or cosine in a direction perpendicular to the streamwise or

wall normal directions being topologically equivalent down to a phase shift of $\frac{\pi}{2}$. As the structures have no preferred location within the channel, this phase shift renders the different classes of modes dynamically equivalent. For example, the following two modes both encode for streamwise vortices phase shifted by $\frac{\pi}{2}$ in the z direction.

$$\begin{pmatrix} 0 \\ \gamma\cos(\beta y)\sin(\gamma z) \\ -\beta\sin(\beta y)\cos(\gamma z) \end{pmatrix} \rightarrow \begin{pmatrix} 0 \\ \gamma\cos(\beta y)\cos(\gamma z) \\ \beta\sin(\beta y)\sin(\gamma z) \end{pmatrix}$$

Of the eight distinct eigenvalue equations, only three may lead to an instability as the other five give an eigenvalue $\lambda < 0 \forall\, Re, \Omega$. The first five eigenvalue equations are;

$$\begin{aligned}
\lambda_1 =& -\frac{9\pi^2}{4}, \\
\lambda_2 =& -\pi^2, \\
\lambda_3 =& -\frac{\pi^2}{4}, \\
\lambda_{4,5} =& \frac{-24\pi\sqrt{\gamma^2+\pi^2}\sqrt{4\gamma^2+\pi^2}\gamma^2 - 15\pi^3\sqrt{\gamma^2+\pi^2}\sqrt{4\gamma^2+\pi^2}}{24\pi\sqrt{\gamma^2+\pi^2}\sqrt{4\gamma^2+\pi^2}} \\
& \pm \frac{\sqrt{(4\gamma^2+\pi^2)\left(-4096\gamma^2\Omega^2 + 81\pi^6\gamma^2 + 384\sqrt{2}\pi^2\gamma^2 \mathrm{Re}\Omega + 81\pi^8\right)}}{24\pi\sqrt{\gamma^2+\pi^2}\sqrt{4\gamma^2+\pi^2}},
\end{aligned}$$

whilst the remaining eigenvalues $\lambda_{6,7,8}$ are solutions of the polynomial

$$\begin{aligned}
&\mathrm{Real}\Big(36\sqrt{2}\pi\gamma^2\sqrt{\gamma^2+\frac{\pi^2}{4}}\Omega\left(\gamma^2+\lambda+\pi^2\right)\left(\frac{\pi^2\mathrm{Re}}{2}-2\sqrt{2}\Omega\right) - \\
&\pi\sqrt{\gamma^2+\frac{\pi^2}{4}}\left(\gamma^2+\lambda\right)\times \\
&\left(18\pi^2\left(\gamma^2+\frac{\pi^2}{4}\right)\left(\gamma^2+\lambda+\frac{\pi^2}{4}\right)\left(\gamma^2+\lambda+\pi^2\right) - 4\gamma^2\Omega\left(\frac{3\pi^2\mathrm{Re}}{\sqrt{2}}-8\Omega\right)\right)\Big)^2 = 0.
\end{aligned} \tag{2.10}$$

One of these solutions is stable $\lambda < 0$ for $Re, \Omega, \gamma > 0$, and the others form a pair of complex conjugates, which may lead to an instability. The first instability,

with the eigenvalue λ_6, corresponds to an eigenvector $\mathbf{e}_6$ comprised of the modes

$$\mathbf{u}_3 = \begin{pmatrix} 2\cos(2\beta y)\cos(\gamma z) \\ 0 \\ 0 \end{pmatrix}, \qquad \mathbf{u}_9 = \begin{pmatrix} \sqrt{2}\cos(\gamma z) \\ 0 \\ 0 \end{pmatrix},$$
$$\mathbf{u}_{13} = \frac{2}{K_{\beta\gamma}} \begin{pmatrix} 0 \\ \gamma\cos(\beta y)\cos(\gamma z) \\ \beta\sin(\beta y)\sin(\gamma z) \end{pmatrix},$$

where $K_{\beta\gamma} = \sqrt{\beta^2 + \gamma^2}$, and to the topologically equivalent eigenvector $\mathbf{e}_{6'} = [\mathbf{u}_4, \mathbf{u}_{10}, \mathbf{u}_{14}]$. These modes correspond to the ingredients from Waleffe's self sustaining process [67], where $\mathbf{u}_{3,4}$ and $\mathbf{u}_{9,10}$ encode the streaks and $\mathbf{u}_{13,14}$ the 2-dimensional vortices. The line of stability in the $Re - \Omega$ plane for these perturbations is defined by

$$Re = \frac{9(\pi^2+\gamma^2)(\pi^3+4\pi\gamma^2)^2 + 128(9\pi^2+11\gamma^2)\Omega^2}{48\sqrt{2}\pi^2(3\pi^2+4\gamma^2)\Omega}. \tag{2.11}$$

The second instability, with the eigenvalue λ_5, has the eigenvector $\mathbf{e}_5$ comprising the modes

$$\mathbf{u}_7 = \begin{pmatrix} 2\sin(\beta y)\cos(\gamma z) \\ 0 \\ 0 \end{pmatrix}, \quad \mathbf{u}_{12} = \tfrac{2}{K_{4\beta\gamma}} \begin{pmatrix} 0 \\ \gamma\cos(\gamma z)\sin(2\beta y) \\ -2\beta\cos(2\beta y)\sin(\gamma z) \end{pmatrix},$$

where $K_{4\beta\gamma} = \sqrt{4\beta^2 + \gamma^2}$, and the corresponding analogues $\mathbf{e}_{5'} = [\mathbf{u}_6, \mathbf{u}_{11}]$, both of which correspond to Taylor vortex flow with two vortices spanning the width of the channel. The associated line of stability is

$$Re = \frac{9\pi^2(\pi^2+\gamma^2)^2(\pi^2+4\gamma^2) + 256\gamma^2\Omega^2}{24\sqrt{2}\pi^2\gamma^2\Omega}, \tag{2.12}$$

At $\gamma = 1$, corresponding to the optimal domain size for locating steady solutions [76, 135], we observe that the transition Re is lower for the first instability than the second for all Ω and as such the laminar flow can always be expected to transition along the eigenvector defined by the modes of the first instability. As the two lines of stability, equations (2.11) and (2.12), are shown not to cross for any $\Omega, \gamma > 0$, this then holds for all γ. The lines of stability in the $\Omega - Re$ plane are shown in Fig. 2.2.

We turn our attention to finding the point of linear instability of the laminar

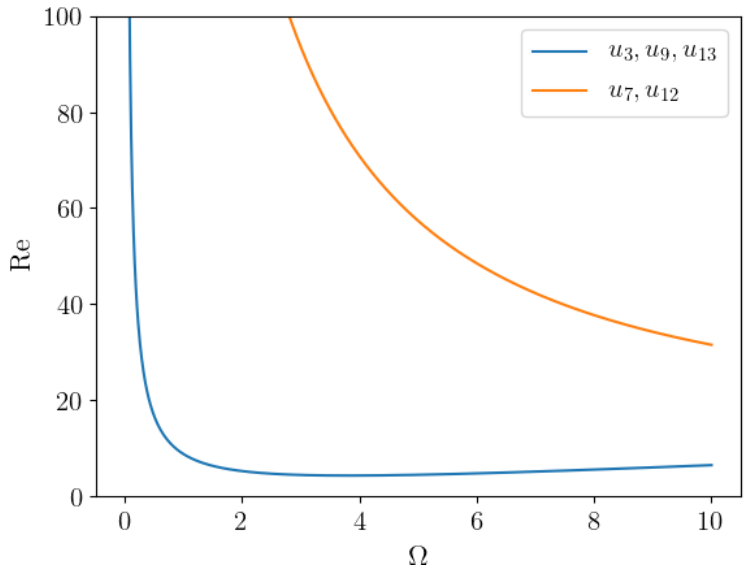

Figure 2.2 *The lines of instability for laminar profile to the two 2-dimensional perturbations in the $\Omega - Re$ plane for $\gamma = 1$. As can be seen from the plot, the flow will always transition to the structures with the line of stability that is lower in the plane. The two lines of stability have been shown not to cross for any $\Omega, \gamma > 0$.*

flow to the 2-dimensional vortices, requiring analysis of the dispersion relation Eq. (2.11) with respect to γ. Analytical minimisation of Re_c reveals a transition $\gamma = 0$, i.e. that the Taylor vortex flow begins as a bulk instability at $Re = \pi$ and $\Omega = 2.74059$. This was confirmed by numerical examination and Chebyshev collocation [138] of the flow field. We postulate that this peculiar behaviour arises from the use of free slip boundary conditions, as they do not fix the size of the structures in flow and therefore the structures first appear at the lowest allowed energy, i.e. with lowest γ. Interestingly, if a 2nd order expansion in γ is taken of the solutions to the eigenvalue equation, Eq. 2.10, and then solved for Ω, the resulting equation is not dependent upon γ. This therefore allows for the production of the stability curve, shown in Fig. 2.3, for the approximate region in which a second order expansion is valid.

The dispersion relation of the maximum eigenvalue versus γ for $Re = 5$ and $\Omega = 3$, chosen arbitrarily to be above the stability curve, is shown in Fig. 2.4.

Using these results, it is possible to construct a 5 mode model from the laminar profile $\mathbf{u}_8$, the modification to the laminar profile $\mathbf{u}_{15}$ and the modes that the laminar profile becomes first unstable to $\mathbf{u}_3, \mathbf{u}_9$ and $\mathbf{u}_{13}$, ie. the 2-dimensional

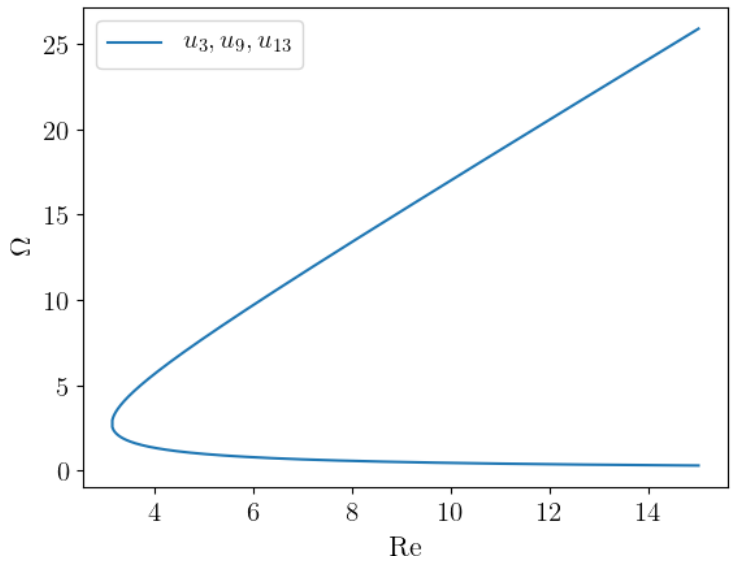

Figure 2.3 *The line of stability for the two 2-dimensional flows in the $Re - \Omega$ plane, when the equation for the eigenvalue, generated via solving Eq. 2.10, is Taylor expanded to the second order in γ. This provides a good approximation to the expected shape at the point of transition, due to the instability setting in at $\gamma = 0$. The lower branch does not connect to the $\Omega = 0$ state for all Re due to the linear stability of the base flow in the $\Omega = 0$ regime.*

streaks and vortex. Steady Taylor vortex solutions are generated by solving exactly the evolution equations for these 5 modes

$$\frac{da_3}{dt} = \frac{4\gamma\Omega a_{13}}{3\pi \mathrm{Re} K_{\beta\gamma}} - \frac{4\beta^2 a_3}{\mathrm{Re}} - \frac{\gamma^2 a_3}{\mathrm{Re}} - \frac{\beta\gamma a_8 a_{13}}{\sqrt{2}K_{\beta\gamma}} - \frac{3\beta\gamma a_{15} a_{13}}{\sqrt{2}K_{\beta\gamma}}, \tag{2.13}$$

$$\frac{da_8}{dt} = -\frac{\beta^2 a_8}{\mathrm{Re}} + \frac{\beta\gamma a_3 a_{13}}{\sqrt{2}K_{\beta\gamma}} + \frac{\beta\gamma a_{13} a_9}{K_{\beta\gamma}} + \frac{\beta^2}{\mathrm{Re}}, \tag{2.14}$$

$$\frac{da_9}{dt} = \frac{2\sqrt{2}\gamma\Omega a_{13}}{\pi \mathrm{Re} K_{\beta\gamma}} - \frac{\gamma^2 a_9}{\mathrm{Re}} - \frac{\beta\gamma a_8 a_{13}}{K_{\beta\gamma}}, \tag{2.15}$$

$$\frac{da_{13}}{dt} = -\frac{4\gamma\Omega a_3}{3\pi \mathrm{Re} K_{\beta\gamma}} - \frac{2\sqrt{2}\gamma\Omega a_9}{\pi \mathrm{Re} K_{\beta\gamma}} - \frac{(\beta^2 + \gamma^2)\, a_{13}}{\mathrm{Re}}, \tag{2.16}$$

$$\frac{da_{15}}{dt} = \frac{3\beta\gamma a_3 a_{13}}{\sqrt{2}K_{\beta\gamma}} - \frac{9\beta^2 a_{15}}{\mathrm{Re}}. \tag{2.17}$$

These solutions are located using the Newton-Raphson method [139]. As the

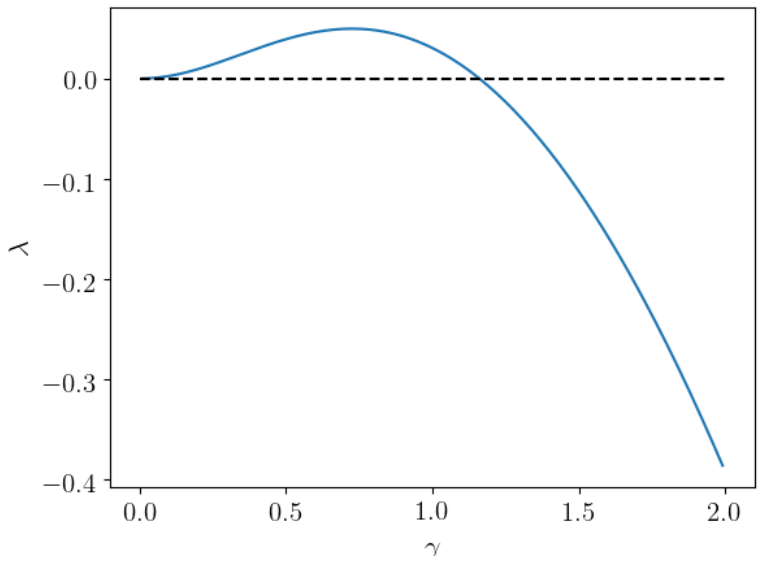

Figure 2.4 *The dispersion relation of the instability eigenvalue* λ_6 *along eigenvector* $\mathbf{e}_6 = [\boldsymbol{u}_3, \boldsymbol{u}_9, \boldsymbol{u}_{13}]$ *of the base profile* $\boldsymbol{u}_8$ *at* $Re = 5$ *and* $\Omega = 3$.

model contains explicit equations for the specific mode amplitude evolution equations, the Jacobian for the system could be analytically formed.

As before, the solutions are perturbed infinitesimally, such that the stability analysis reduces to an eigenvalue problem of the 5 linearised evolution equations. For a fixed γ and Ω the Taylor vortex solutions could be traced with increasing Re. Fig. 2.5 is the bifurcation diagram for $\gamma = 1$ and $\Omega = 3$, with the disorder parameter that measures the strength of the Taylor vortices as $D = 1 - a_8$, chosen to represent the 'distance' to the laminar solution $a_8 = 1$. Though the total energy is not conserved in this system due to the external forcing, for the stable solutions D can be thought of as quantifying the non-laminar 'energy' of the solutions.

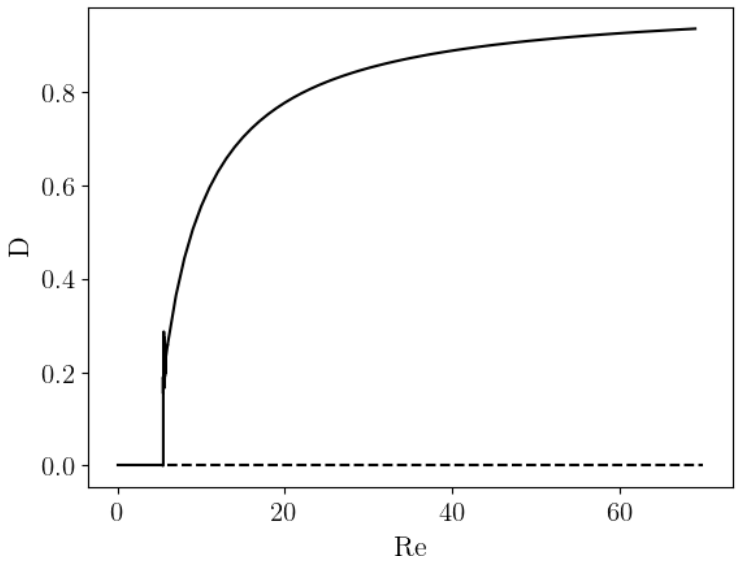

Figure 2.5 *The supercritical bifurcation diagram for the Taylor vortex solutions described by modes* $[\boldsymbol{u}_3, \boldsymbol{u}_8, \boldsymbol{u}_9, \boldsymbol{u}_{13}, \boldsymbol{u}_{15}]$ *for* $\gamma = 1$ *and* $\Omega = 3$*. The quantity* D *is defined* $D = 1 - a_8$*, chosen to represent the 'distance' to the laminar solution* $a_8 = 1$*.*

A similar picture can be produced for the second instability along $\mathbf{e}_5$ and $\mathbf{e}_{5'}$, which the laminar profile loses stability to at $Re = 31.281$ and $\Omega = 20.466$, with a resulting critical streamwise wavelength $\gamma = 1.711$. Due to the nature of the stability equation, Eq. (2.12), being solvable if Re and γ are known, this result could be calculated analytically. A tracing of the higher instability for $\gamma = 1$ and $\Omega = 20.5$ is shown in Fig. 2.6, once again using $D = 1 - a_8$ as the disorder parameter, with the lower Taylor vortex instability also shown for those parameters.

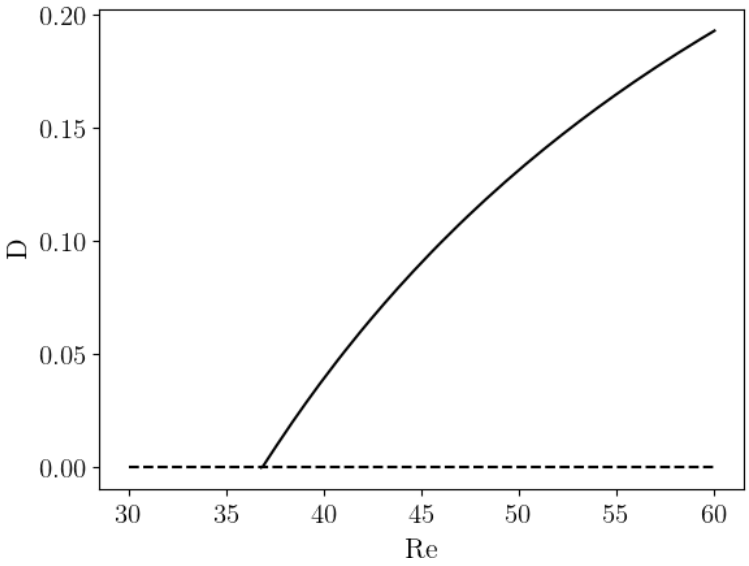

Figure 2.6 *The supercritical bifurcation diagram for the higher Taylor vortex solutions described by modes* $[\boldsymbol{u}_7, \boldsymbol{u}_8, \boldsymbol{u}_{12}, \boldsymbol{u}_{15}]$ *for* $\gamma = 1$ *and* $\Omega = 20.5$. *Here the laminar profile is unstable to the lower order vortices before the appearance of the instability to the aforementioned modes. The quantity* D *is defined* $D = 1 - a_8$, *chosen to represent the 'distance' to the laminar solution* $a_8 = 1$.

2.4 3D structures in the rotating plane Couette model

To investigate the progression to 3-dimensional structures, the flow was then linearised around the Taylor vortex solutions and their dynamic stability with respect to the 30 x-dependent modes tested. The dispersion relation of the maximum instability eigenvalue with respect to α, the streamwise wavelength, was calculated along the solution branch, allowing the point of 3-dimensional instability to be found along with its corresponding eigenvector. The analysis reveals that the Taylor vortex solutions to Eqs. 2.13-2.17 are unstable to a 3-dimensional flow. The instability was found at $Re = 5.08$ for $\Omega = 2.75$, with corresponding eigenvectors $\mathbf{e}_{10} = [\mathbf{u}_{16}, \mathbf{u}_{19}, \mathbf{u}_{25}, \mathbf{u}_{29}, \mathbf{u}_{33}, \mathbf{u}_{37}, \mathbf{u}_{39}, \mathbf{u}_{45}]$ and $\mathbf{e}_{10} = [\mathbf{u}_{17}, \mathbf{u}_{21}, \mathbf{u}_{23}, \mathbf{u}_{27}, \mathbf{u}_{32}, \mathbf{u}_{35}, \mathbf{u}_{41}, \mathbf{u}_{44}]$. Once again, the transition is found to begin as a bulk instability for $\alpha = 0$. Despite this, once past the critical point of transition the length scale of the instability is set by the maximum eigenvalue

of the dispersion curve. The dispersion relations of $\lambda_{max}(\alpha)$ for $Re = 6.0$ and $Re = 60.0$ at $\Omega = 3$ and $\gamma = 1$ are shown in Fig. 2.7.

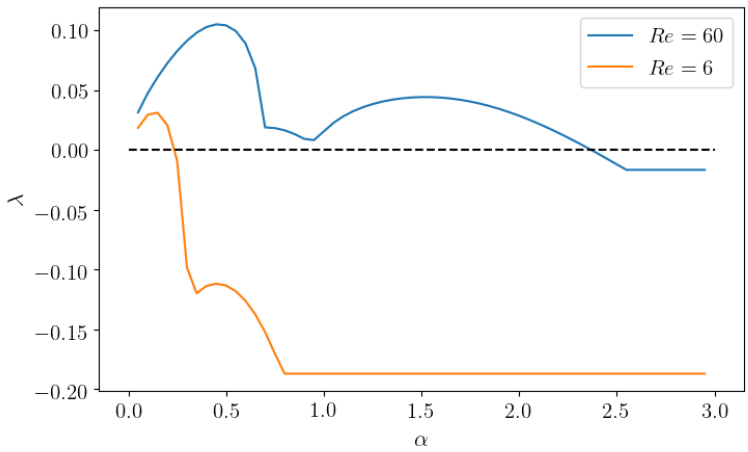

Figure 2.7 *The dispersion relation of the instability eigenvalue* λ_{10} *along eigenvector* $[\boldsymbol{u}_{16}, \boldsymbol{u}_{19}, \boldsymbol{u}_{25}, \boldsymbol{u}_{29}, \boldsymbol{u}_{33}, \boldsymbol{u}_{37}, \boldsymbol{u}_{39}, \boldsymbol{u}_{45}]$ *of the steady Taylor vortex profile defined by modes* $[\boldsymbol{u}_3, \boldsymbol{u}_8, \boldsymbol{u}_9, \boldsymbol{u}_{13}, \boldsymbol{u}_{15}]$ *for* $\gamma = 1$ *and* $\Omega = 3$. *As Re is reduced to the bifurcation point* $\lim_{Re \to Re_c} : \alpha_{critical}(\lambda_{max}) \to 0$.

If we look again at the test case $\Omega = 3$, shown in Fig. 2.8 and Fig. 2.9, the 3-dimensional stable solutions that bifurcate from the 2-dimensional Taylor vortices lose their stability to stable periodic orbits for a small range of Re, before they then become unstable and give way to the fully turbulent state. This is of particular interest as it follows the transition pathway suggested in [140] and [141], in which the non-trivial state initially appears as a chaotic orbit of infinite lifetime, which then undergoes a period doubling route to chaos.

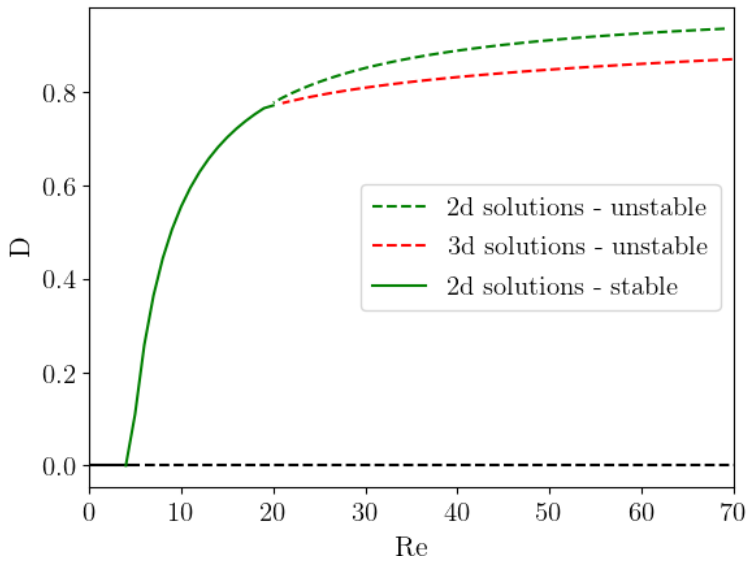

Figure 2.8 *The bifurcation diagram for $\Omega = 3$ for the 13 mode model. The laminar profile loses its stability to 2-dimensional Taylor vortices.*

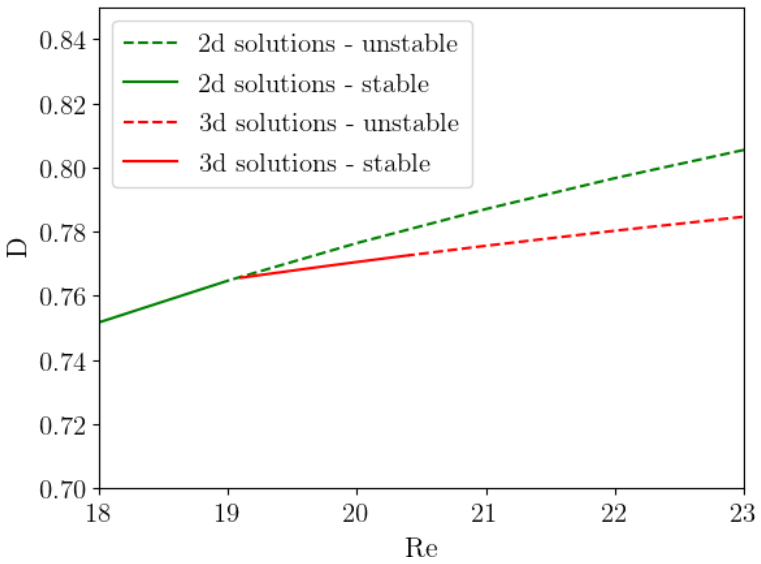

Figure 2.9 *Inset from Fig. 2.8 at the point of bifurcation between the 2-dimensional and 3-dimensional states. This shows the small region of stability of the 3-dimensional state, before the appearance of the stable periodic orbit that causes the steady solution to lose its stability.*

We see that as the stable periodic orbit appears at Re_{PO}, the mode amplitudes oscillate sinusoidally around their values at the steady state at $Re_{PO} - \delta$, just before the bifurcation. A trajectory coalescing upon the stable periodic orbit at $Re = 23$ is shown in Fig. 2.10 and Fig. 2.11.

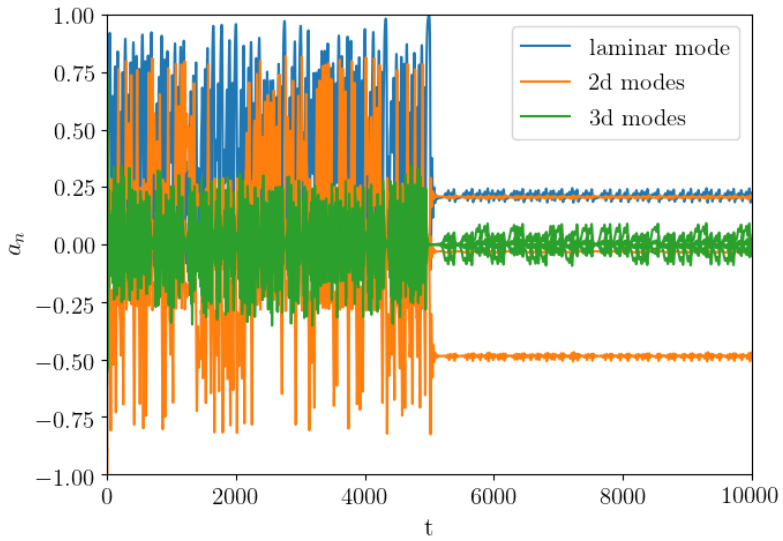

Figure 2.10 *A trajectory in the 13 mode model at $Re = 23$ and $\Omega = 3$. Here the flow can be seen to chaotically evolve in the turbulent portion of phase space before getting caught within the domain of attraction of the periodic orbit at $t \approx 5000$.*

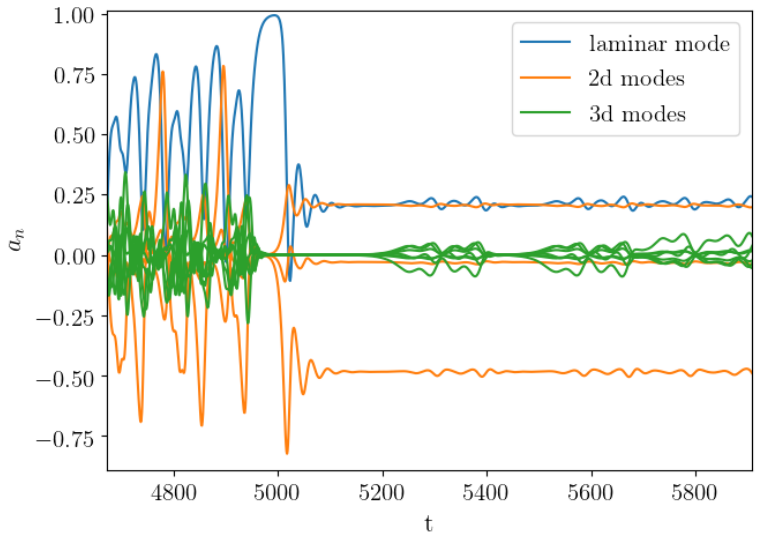

Figure 2.11 *Inset of Fig. 2.10. Interestingly the trajectory comes extremely close to relaminarising (where the laminar mode amplitude $a_8 = 1$) before entering the domain of the periodic orbit. This suggests that the orbit may act as, or interact with, the edge state for the flow. However, as the laminar profile is linearly unstable at these parameters, it is likely that the stable periodic orbit will be the globally attracting state for the system.*

Time series of the laminar mode a_8 whilst caught in the domain of the stable periodic orbit are shown in Fig 2.12 for increasing Re, with their corresponding Fourier transforms shown in Fig. 2.13. The Fourier transforms show appearance of additional frequencies before the spectrum tends towards that of the the fully turbulent system.

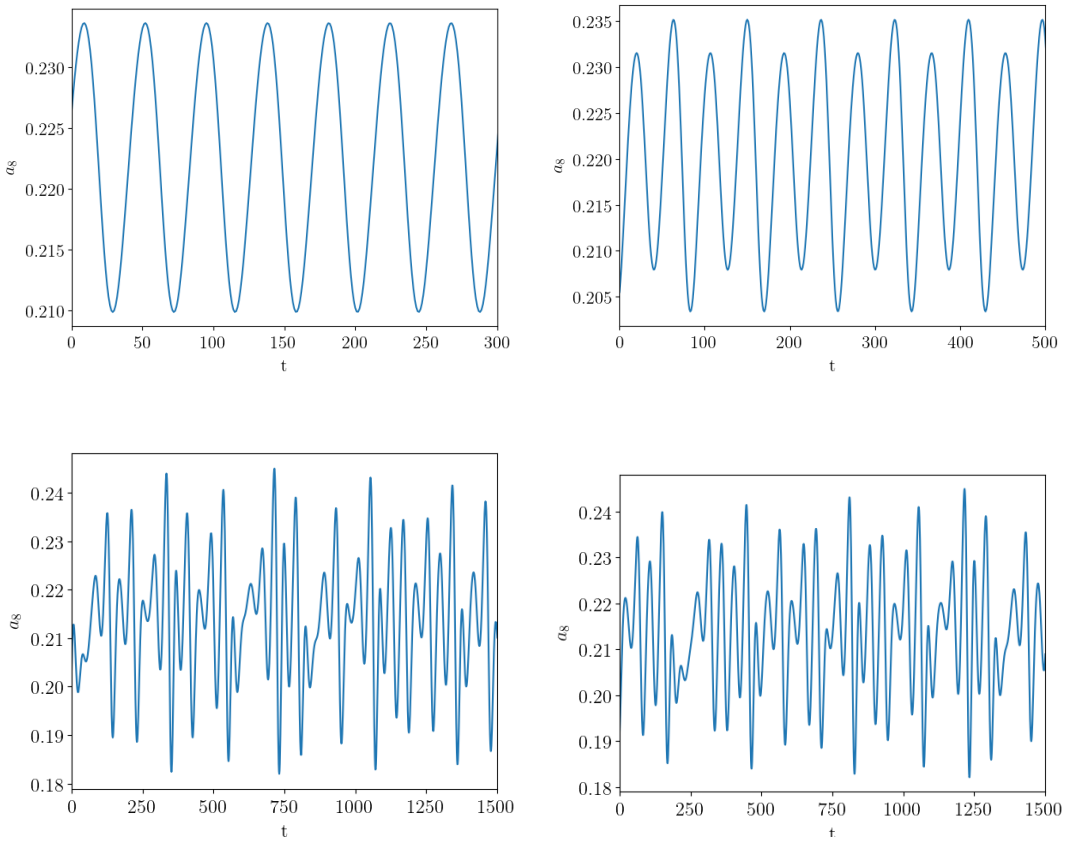

Figure 2.12 *Time series of the laminar mode a_8 for (reading from top left) $Re = 21$, $Re = 21.25$, $Re = 22$ and $Re = 23$ at $\Omega = 3$, showing the route to chaos as q is increased.*

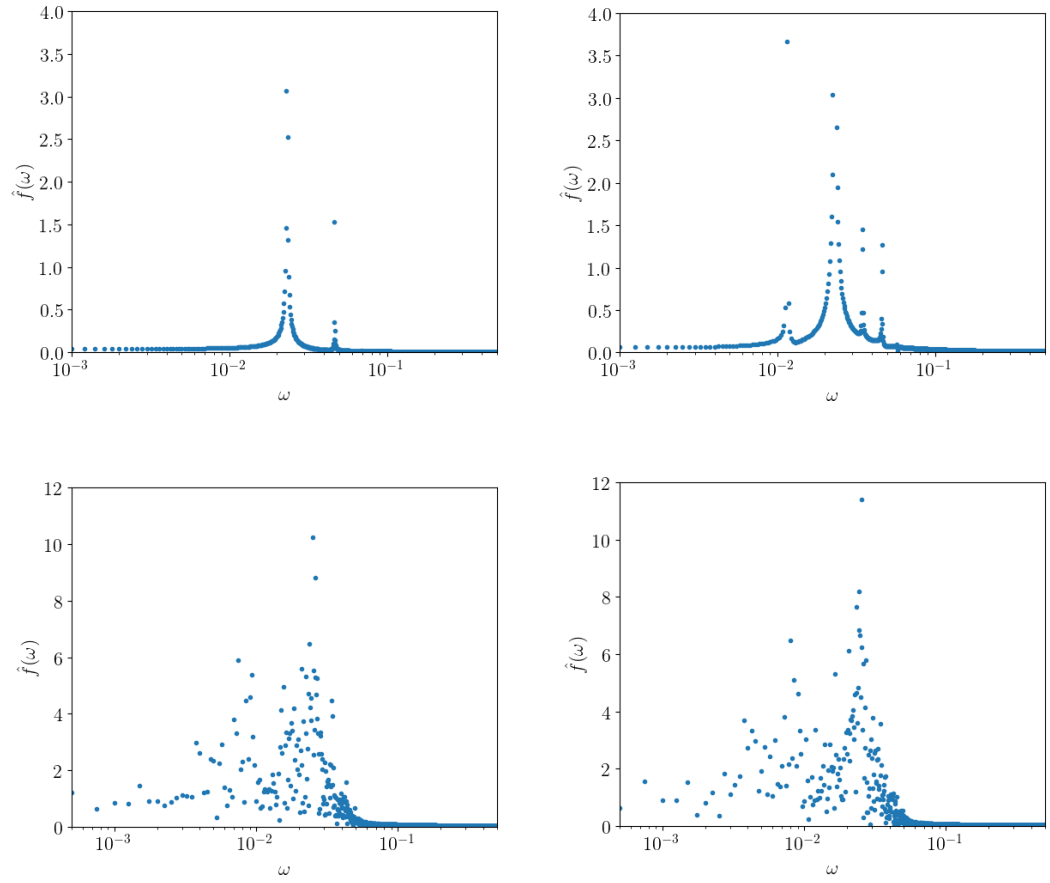

Figure 2.13 *The Fourier transforms of the laminar mode amplitude* a_8 *for (reading from top left)* $Re = 21$, $Re = 21.25$, $Re = 22$ *and* $Re = 23$ *at* $\Omega = 3$, *showing the route to chaos as Re is increased.*

2.4.1 Symmetry classes of modes

If we refer back to the findings of Sections 2.3 and 2.4, one notices that for both the laminar to 2-dimensional and 2-dimensional to 3-dimensional instabilities the two different classes of modes as defined by the instability eigenvectors contain the same dynamical information, but are merely phase shifted by $\frac{\pi}{2}$ in the spanwise z or streamwise x direction. This realisation prompted analysis of the amplitude equations, which revealed that within the thoughtlessly generated modes there exists 'symmetry classes' encoding dynamically equivalent modes. This is due to the periodicity of the sine and cosine functions, as demonstrated in Section 2.3. The non-linear interactions that generate the mode amplitudes were then also found to strictly couple classes with no exceptions. For example, if an arbitrary mode from class I, $\mathbf{u}_i$ is generated by a non-linear coupling between mode $\mathbf{u}_j$

from class J and $\mathbf{u}_k$ from class K, then for all modes in class I, A_I,

$$\frac{dA_I}{dt} = F_I(\hat{A_J} \cdot \hat{A_K}, \dots), \tag{2.18}$$

where $\hat{A_J}$ and $\hat{A_K}$ are subsets of modes from classes J and K respectively, which are specific to the mode $\mathbf{u}_i \in A_I$ in question and F_I represents a quadratic non-linear coupling specific to the chosen mode $\mathbf{u}_i$.

The mode symmetry classes are defined as follows:

Name	**Modes**	**Shift**	**Description**
L	u_8, u_{15}	-	laminar modes
A_1	u_3, u_9, u_{13}	-	streaks and vortices
A_2	u_4, u_{10}, u_{14}	$A_1 - \frac{\pi}{2}$ in z	streaks and vortices
B_1	u_7, u_{12}	-	higher order vortices and streak
B_2	u_6, u_{11}	$B_1 + \frac{\pi}{2}$ in z	higher order vortices and streak
C_1	$u_{19}, u_{25}, u_{29}, u_{37}, u_{39}$	-	Kelvin-Helmholtz instability
C_2	$u_{21}, u_{23}, u_{27}, u_{35}, u_{41}$	$C_1 + \frac{\pi}{2}$ in x	Kelvin-Helmholtz instability
D_1	$u_{18}, u_{24}, u_{28}, u_{36}, u_{38}$	$C_1 + \frac{\pi}{2}$ in z	Kelvin-Helmholtz instability
D_2	$u_{20}, u_{22}, u_{26}, u_{34}, u_{40}$	$D_1 - \frac{\pi}{2}$ in x	Kelvin-Helmholtz instability
TS_1	u_{30}, u_{43}	-	Tollmien - Schlichting like vortices
TS_2	u_{31}, u_{42}	$TS_1 - \frac{\pi}{2}$ in x	Tollmien - Schlichting like vortices
SF_1	u_{16}, u_{33}, u_{45}	-	spanwise flows
SF_2	u_{17}, u_{32}, u_{44}	$SF_1 + \frac{\pi}{2}$ in x	spanwise flows
Con	u_1, u_2, u_5	-	connector modes

Here the terming 'Tollmien - Schlichting like' refers to vortices in the $x - y$ plane, reflecting the travelling spanwise vortices observed in Tollmien - Schlichting waves. A numerical generation of such structures is shown in Fig. 2.14.

The couplings that determine the time evolution of the amplitudes of the symmetry classes are found in Appendix A.2. The non-linear couplings also completely predict the instability eigenvectors of linearised solutions when comprised of one class. The results of the linear stability analysis of the 2-dimensional symmetry classes is shown in the table below. It should be noted that for Re below the 3-dimensional instability, the B classes exhibit a linear instability to the lower order vortices described by the A modes, inferring that

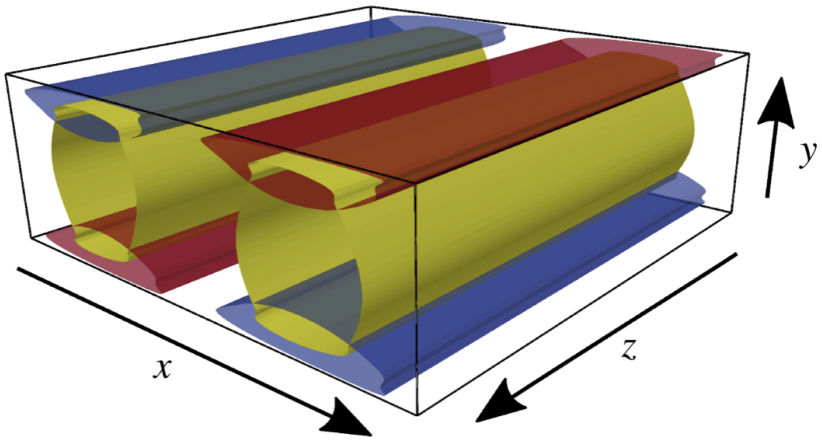

Figure 2.14 *A numerical rendering of Tollmien - Schlichting waves in plane Poiseuille flow. Though this is a pressure driven flow, the geometry is equivalent to the system currently being considered. The yellow denotes an isosurface at which the Q-vortex criterion (see [142]) is equal to* $0.3Q_{max}$*. Red and blue surfaces indicate regions at which* $u = \pm 0.5u_{max}$*. Reproduced from [143].*

they would never be observed in simulations.

2D Class	**3D instability eigenvector**	Re	Ω
A_1	C_1, SF_1 or C_1, C_2, SF_1, SF_2	5.08	2.75
A_2	$D1, SF_1$ or $D2, SF_2$	6.78	2.75
B_1	C_1, C_2, TS_1, TS_2	37.49	20.50
B_2	D_1, D_2, TS_1, TS_2	37.49	20.50

With this information, a hierarchy of models created by including different combinations of classes of modes were reviewed qualitatively to find the minimum model which encapsulated all of the hallmark features of turbulence. The initial 13 mode model was constructed using the laminar mode u_8, the laminar modification u_{15} and classes A_1 and C_1, chosen as they match the 2-dimensional and 3-dimensional linear instability eigenvectors as found previously. From this, the minimal route to 3-dimensional structures could be constructed in the rotating case. We compare this model with a 23 mode model comprised of modes u_8, u_{15} and classes TS_1, $SF1$, A_1, A_2, C_1 and D_1, found to be the minimal model, in terms on number of modes, which displays the greatest analogy to the transition to turbulence in plane Couette flow. This statement will be further discussed in Chapter 3. For further reference both models are compared with the model

created by the full set of 45 modes.

2.4.2 Structure of the models

Interestingly, this process that blindly creates low dimensional models produces a 13 mode model that contains very similar dynamical information to the 9 mode model [75] described in 1.1.5. The exact analytical form of the modes is different, but the same information is encoded albeit with slightly higher resolution in the 13 mode model. For example, the mode

$$\begin{pmatrix} \cos^2(\beta y)\cos(\gamma z) \\ 0 \\ 0 \end{pmatrix}$$

in [75] is instead encoded by

$$\begin{pmatrix} \cos(2\beta y)\cos(\gamma z) \\ 0 \\ 0 \end{pmatrix} \text{ and } \begin{pmatrix} \cos(\gamma z) \\ 0 \\ 0 \end{pmatrix}$$

with different amplitudes and normalisations in our 13 mode model.

The 13 mode model contains the modes that encode for a single self-sustaining process, i.e. streaks, vortices, 3-dimensional Kelvin-Helmholz instability, laminar mode, modification to the laminar mode and spanwise streaks. All of these components have the same phase in x and z. The structure of the model is

$$\frac{dL}{dt} = F_L(A_1^2, C_1^2), \tag{2.19}$$
$$\frac{dA_1}{dt} = F_{A_1}(A_1, LA_1, C_1SF_1), \tag{2.20}$$
$$\frac{dC_1}{dt} = F_{C_1}(C_1, LC_1, A_1SF_1), \tag{2.21}$$
$$\frac{dSF_1}{dt} = F_{SF_1}(SF_1, LSF_1, A_1C_1), \tag{2.22}$$

where $F_{X_i}(Y_j, Z_k)$ denotes a quadratic non-linear coupling between modes from classes Y_j and Z_k that generates modes in class X_i. We can compare this to the 23

mode model, which contains all of the above but also includes additional modes that describe vortices, streaks and 3-dimensional Kelvin Helmholz instability phase shifted in the spanwise z direction. In addition to this, this model also contains two Tollmien - Schlichting like vortices. By inspection of the dynamic mode coupling Eqs. A.3, it can be observed that this model encodes for two self sustaining processes, phase shifted by $\frac{\pi}{2}$ in the z direction, coupled through the laminar, Tollmien - Schlichting like and spanwise streak modes. The two SSPs cannot directly interact with each other due to their phase shift, and instead must transfer energy between the two domains via the previously listed modes. This is pictorially represented in Fig. 2.15. The symmetry class couplings for the 23 mode model are

$$\frac{dL}{dt} = F_L(A_1^2, A_2^2, C_1^2, D_1^2, TS_1^2), \tag{2.23}$$
$$\frac{dA_1}{dt} = F_{A_1}(A_1, LA_1, C_1SF_1, D_1TS_1), \tag{2.24}$$
$$\frac{dA_2}{dt} = F_{A_2}(A_1, LA_1, C_1TS_1, D_1SF_1), \tag{2.25}$$
$$\frac{dC_1}{dt} = F_{C_1}(C_1, LC_1, A_1SF_1, A_2TS_1), \tag{2.26}$$
$$\frac{dD_1}{dt} = F_{D_1}(D_1, LD_1, A_1TS_1, A_2SF_1), \tag{2.27}$$
$$\frac{dSF_1}{dt} = F_{SF_1}(SF_1, LSF_1, A_1C_1, A_2D_1), \tag{2.28}$$
$$\frac{dTS_1}{dt} = F_{TS_1}(TS_1, LTS_1, A_1D_1, A_2C_1) \tag{2.29}$$

For the full set of 45 modes, the symmetry class couplings are detailed in Appendix A.2. From this table we observe that the spanwise flows are the only modes that do not self interact to generate the laminar class modes.

2.4.3 Tracing the structures back to non-rotating plane Couette flow

The flow is now considered in the rotating case, for which the linear stability analysis of the laminar profile gives insight into which modes should be retained for the final non-rotating model. This final step is inspired by the work of Nagata [34, 41], who successfully located exact solutions for plane Couette flow using linear stability analysis of an analogous rotating system and then performing homotopy back to the plane Couette geometry, as described in Section 1.1.2.

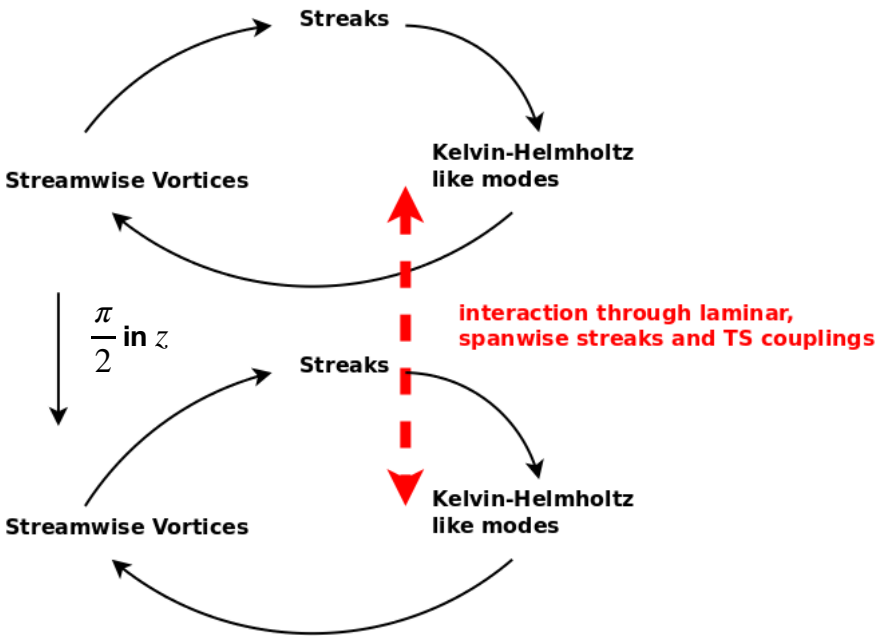

Figure 2.15 *A schematic representation of the mode interactions that sustain turbulent flow in the 23 mode model.*

Initially, the stable 2-dimensional Taylor vortex solutions to equations 2.13-2.17 are found at $\Omega = 3$ and then traced back to the $\Omega = 0$ case. This is achieved by approximating an infinitesimal reduction in Ω, via $\Omega_{current} = \Omega_{old} - \delta\Omega$, and using the state at the previous $\Omega = \Omega_{old}$ as an initial condition for a Newton-Raphson solver.

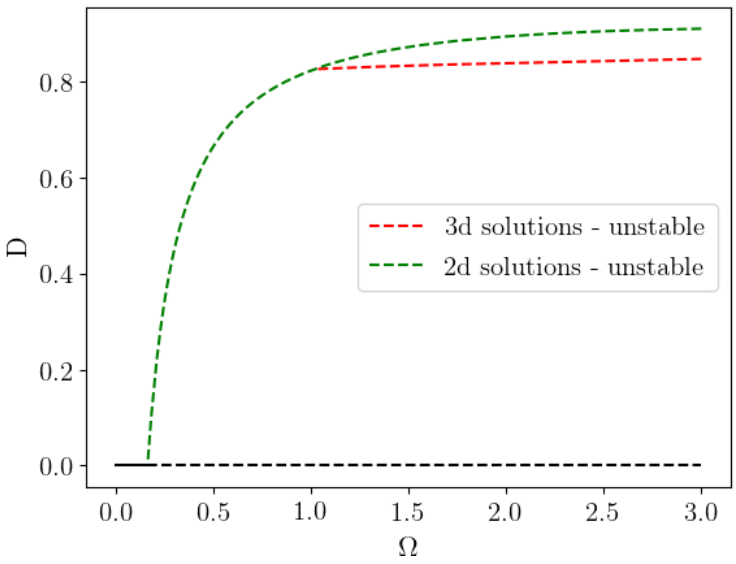

Figure 2.16 *Tracing of the steady structures from $\Omega = 3$ to $\Omega = 0$ in the 13 mode model for $Re = 50$, chosen to be above the Re at which steady solutions appear in the non-rotating case at $\Omega = 0$.*

The process was repeated for the 3-dimensional solutions found in the 13 mode model, with the results for both at $Re = 50$ shown in Fig. 2.16. The bifurcation diagram is reminiscent of Fig. 2.8, in which the increase of the control parameter causes a 3-dimensional state to bifurcate from the 2-dimensional state, following the expected phenomenology for this flow. The 2-dimensional state itself is connected to the laminar state for finite and non-zero Ω and Re, as expected for a flow with a linear instability of the laminar state.

2.5 3D structures in the plane Couette model

To consider the non-rotating case the same mode amplitude evolution equations from the rotating case could be used, simply with $\Omega = 0$. To locate coherent structures for this system, turbulent trajectories at $Re = 400$ were produced by taking random initial amplitudes for the modes and numerically timestepping the equations using the RK4 method [144]. Each instance in the time series could then be used as an initial condition for a Newton-Raphson solver to locate the coherent structures. These series were taken in the $Re >> Re_c$ regime as to ensure that turbulence had fully developed in the flow. This strategy was chosen

as it can be expected that a turbulent trajectory will for finite times be caught within the locality of a coherent structure, giving much better initial conditions for the Newton method than, for example, random initial guesses or a regular grid in phase space.

2.5.1 13 modes

For the 13 mode model we find several connected periodic orbits, whose stability is intermittent. Each has a reflective symmetry about the origin for modes $[\mathbf{v}_3, \mathbf{v}_{13}, \mathbf{v}_{15}, \mathbf{v}_{16}, \mathbf{v}_{33}, \mathbf{v}_{45}]$, meaning that the modes that correspond to the streak, vortex and spanwise streaks may oscillate between $[a, b]$ or $[-a, -b]$. The orbit first appears from $Re = 53.3$ to $Re = 85.2$, then either loses its stability or disappears before reappearing between $Re = 93.2$ and $Re = 121.4$. Turbulent dynamics do not occur at Re below $Re = 121.4$, suggesting that the loss of stability of the orbit organises the phase space such that the turbulent dynamics can occur.

The periodic orbits could be tracked through Re state space by time iterating them for a set amount of steps, ensuring that the trajectory remains within the domain of the orbit, and then infinitesimally incrementally changing Re. To keep consistency with the previous use of the parameter $D = 1 - a_8$ to demark the distance from the laminar solution, the location of the orbit on the D axis is given by $D = 1 - \langle a_8 \rangle$, averaged over several periods of oscillation.

Interestingly, the period of oscillation of the modes in the orbit remains unchanged with Re, though their position in D space alters. The presence of this stable orbit as a barrier between the trivial laminar solution and non-trivial dynamics is analogous to the short lived (in Re space) periodic orbit in the rotating case, discussed in Section 2.4, prompting the question as to whether the two orbits are dynamically connected. To test this, the usual continuation scheme infinitesimally changing Re and Ω was used. This proved challenging at the route through $Re-\Omega$ space that dynamically connects the orbits is unknown. Several different paths thorough $Re - \Omega$ space were attempted but none could connect the two features. A simple comparison of the two orbits location in D space suggests they are quite far apart, and hence unlikely to be connected. In the rotating case, the laminar mode $\mathbf{u}_8$ is far more suppressed and the flow is more dominated by the 3-dimensional modes.

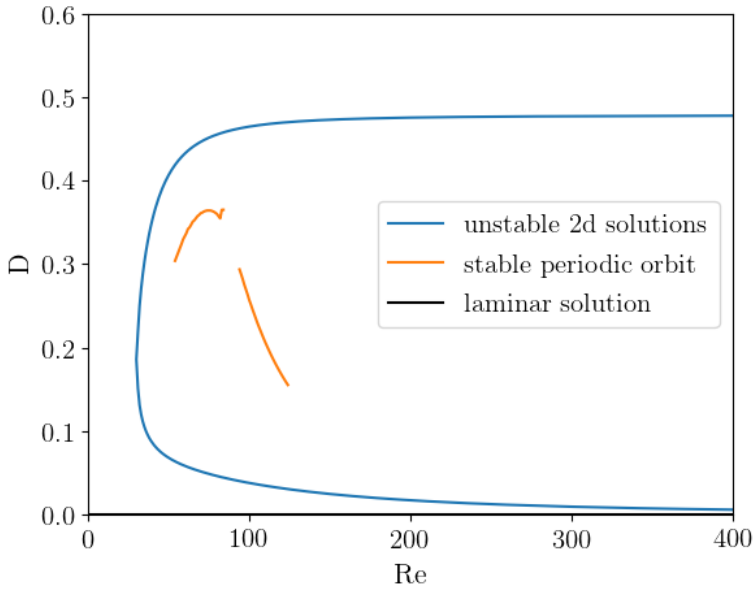

Figure 2.17 *The bifurcation diagram for the 13 mode model. Here the usual disorder parameter D is plotted against Re for the 2 unstable solutions.*

In addition, two coherent structures which bifurcate from infinity subcritically, shown in Fig. 2.17, are observed, matching the known transition scenario for plane Couette flow. These solution branches are unstable, and cannot be found below $Re = 30.6$. They are traced through Re using the same homotopy method as described in Section 2.4.3.

2.5.2 23 modes

Using the same method, the 23 mode model was found to contain four unstable steady exact coherent structures. Two of these are related to those found in the 13 mode model, such that the common modes between the models retain the same amplitudes when comparing the solutions at the same Re. In the two exact states found at lower D, all of the modes apart from those in symmetry class $TS1$ have non-zero amplitude. Conversely, the two states found at higher D have active modes in all the constituent symmetry classes with the exception of $SF1$. This perhaps suggests the significance of the TS symmetry class in accessing the higher energy turbulent state.

If a state on the 13 mode orbit is used as an initial condition for a time series of

the 23 mode model, the trajectory follows the 13 mode orbit exact and none of the modes outside of the shared set of 13 are generated. This raises the interesting observation that if the system is initialised within one set of symmetry classes, it cannot transfer energy to other classes of zero amplitude in this model. The flow instead requires a, likely infinitesimal, perturbation in the zero amplitude classes to generate an interaction with the spatially phase shifted symmetry classes. Due to this instability, the orbits are likely never observed in simulation.

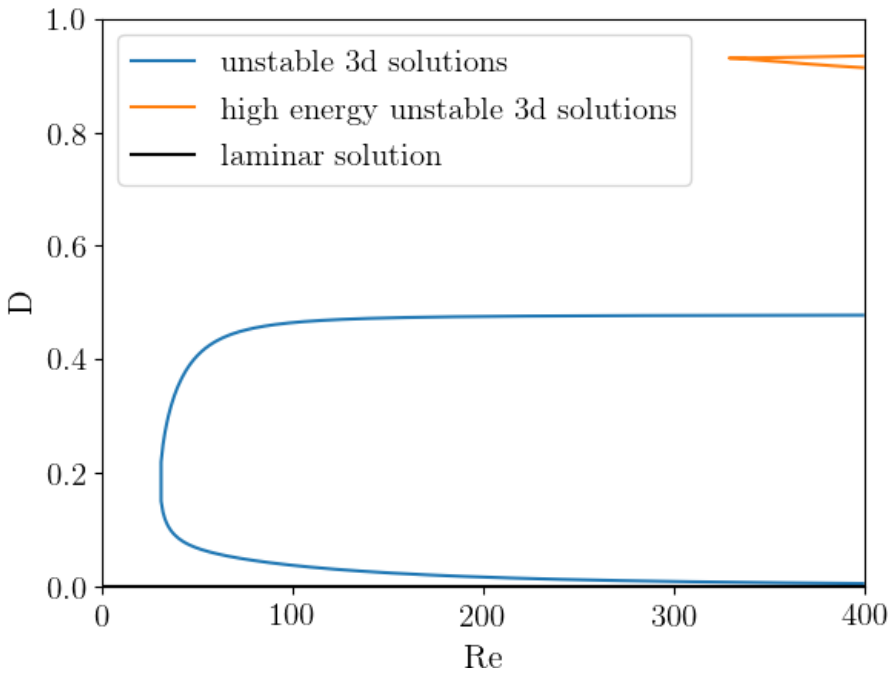

Figure 2.18 *The bifurcation diagram for the 23 mode model. Here the usual disorder parameter D is plotted against Re for the 4 unstable solutions. Interestingly, for the solution branches that overlap with those found in the 13 mode model, the common modes between the model share the same values at a specific Re. This implies that the additional modes in the 23 are themselves independently stable at their solution values.*

2.5.3 45 modes

Finally we consider the full set of 45 modes. In this regime, like the 23 mode model, the periodic orbits from the 13 mode model lose their stability. In this case, mode $\mathbf{u}_2$ is generated which allows energy transfer out of the periodic orbit localised in classes $A1, C1, L$ and $SF1$ into classes $B1$ and $B2$, which then feeds

back into the orbit, destabilising it.

A wealth of unstable coherent structures are found in this regime. We suspect that the number found is only constrained by our limited time spent searching for them. The bifurcation diagram for these structures is shown in Fig. 2.20 and Fig. 2.21.

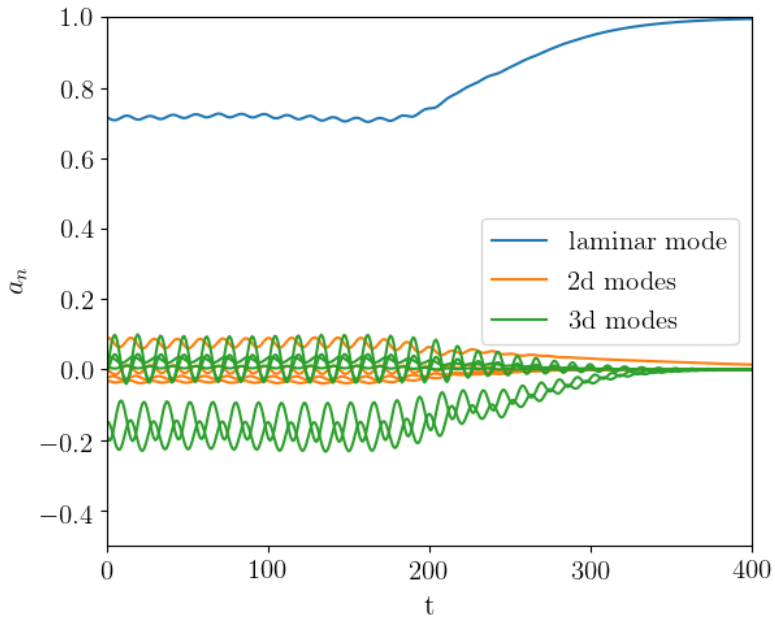

Figure 2.19 *The time evolution of a trajectory in which a point on the 13 mode periodic orbit at $Re = 95$ is used as an initial condition for the 45 mode model. This suggests that the basin of attraction of the orbit persists, but has lost its stability.*

It is an interesting observation from the 13 to 23 and then 23 to 45, each time the number of modes increases by a factor of approximately 2, and yet the number of coherent structures found dramatically increases when jumping from 23 to 45 modes. This implies that in this regime, a higher system dimensionality causes more solutions of the equations to take the form of unstable stationary states rather than unstable periodic orbits.

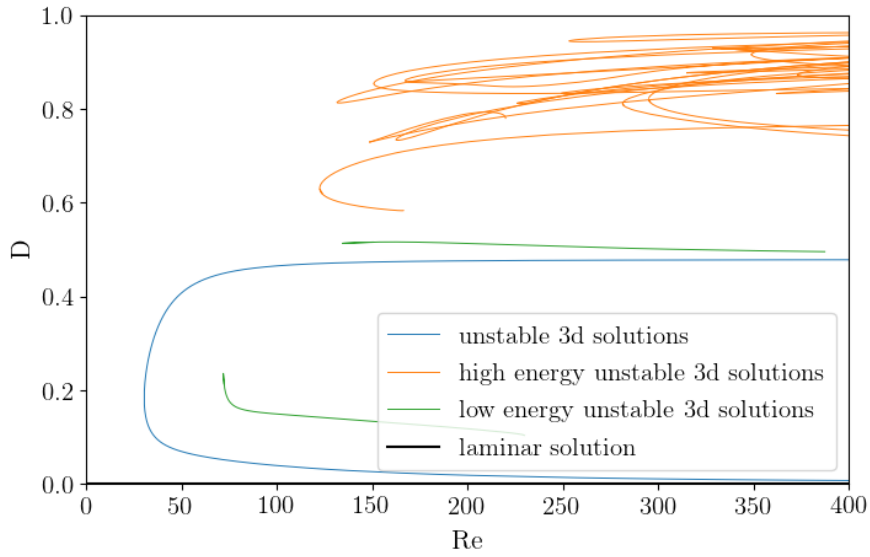

Figure 2.20 *The bifurcation diagram for the 45 mode model. Here the usual disorder parameter D is plotted against Re for the 40+ unstable solutions. The solutions common to the 13 and 23 mode models are marked in blue.*

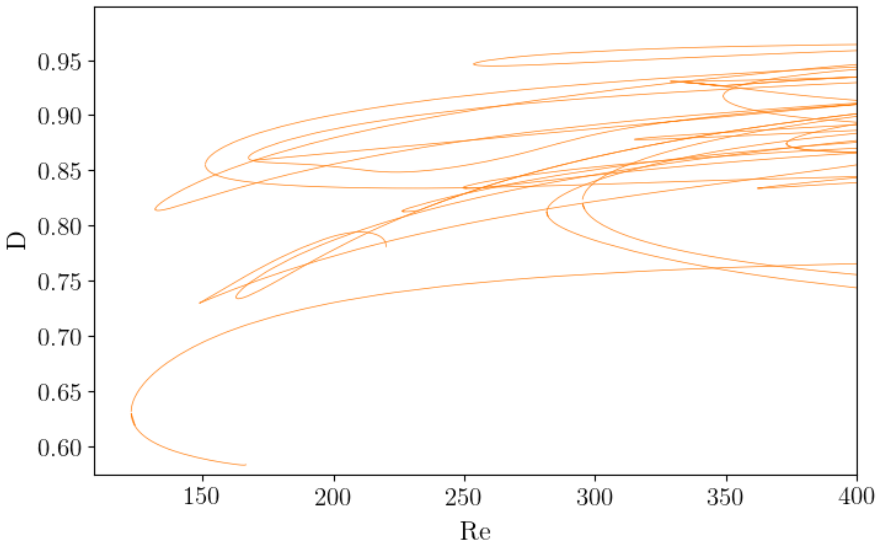

Figure 2.21 *Inset of Fig. 2.20 in the high D region of the plot, clearly showing a wealth of ECS.*

2.6 Turbulent lifetime statistics

We seek to confirm that the turbulent state is a chaotic saddle, which is characterised by a probabilistic distribution of turbulent lifetimes with an exponentially distributed survival probability (see Eq. 1.8) [75, 77, 80].To find the turbulent lifetime distributions of our models, we randomise the initial amplitudes of all the modes such that they take a value in the interval $a_{n\neq 8} \in [-p : p]$, where p controls the size of the perturbations, with the exception of the laminar mode which is drawn from the interval $a_8 \in [0 : 1]$. For these simulations $p = 1$. It has been shown that the exact form of the perturbation only effects the short time dynamics of the turbulence, and so long as the perturbation is of the required strength to access the turbulent portion of phase space then the long time averaged statistics for the system will be unchanged [145]. The time evolution equations are then numerically integrated, again using the RK4 method, producing a turbulent trajectory through phase space. The point at which a trajectory is defined to have relaminarised is when the L_2 norm η of all the non-laminar amplitudes becomes less than 10^{-5}, i.e. $\sum_{n\neq 8}^{N} a_n^2 < 10^{-5}$. This process is repeated for 10000 trials across a range of Re to construct an of ensemble from which to draw the turbulent lifetime statistical distributions. We find that the probability the system will stay turbulent for a time t, $P(t)$, is exponentially distributed as expected. We also notice that there appears to be an increasing minimum lifetime with Re, matching results from other numerical simulations [22, 75]. This time represents the time taken for the system to find the turbulent state from the initial conditions and as such was ignored when analysing the decay rates from the turbulent to laminar portions of phase space.

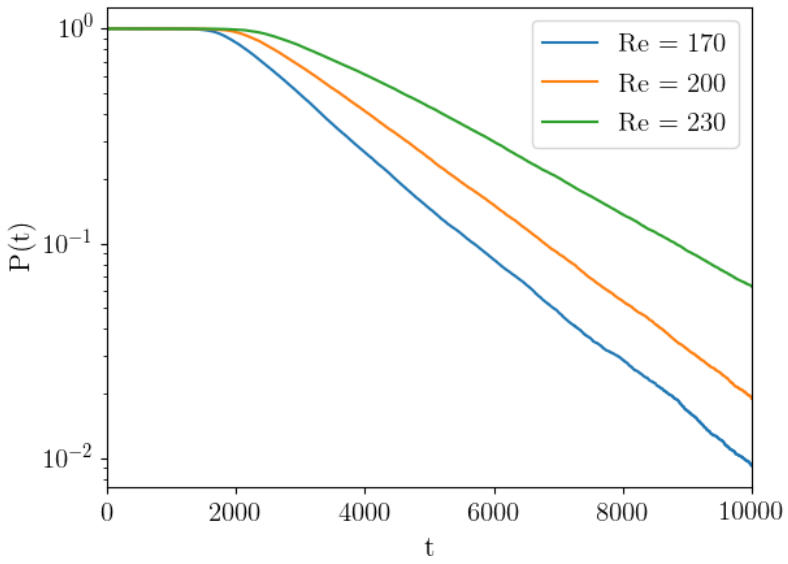

Figure 2.22 *The numerically extracted survival probability of the turbulent state $P(t)$ plotted against t for the 13 mode model.*

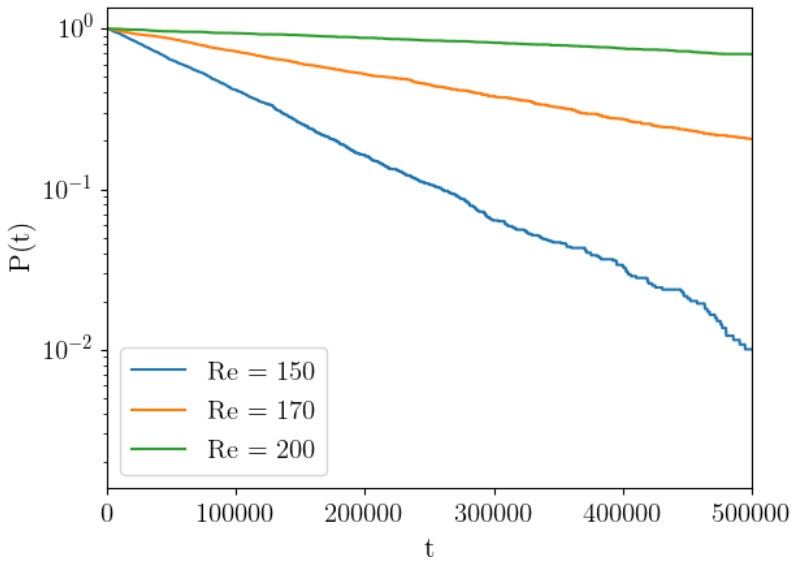

Figure 2.23 *The numerically extracted survival probability of the turbulent state $P(t)$ plotted against t for the 23 mode model. Increasing Re clearly shows a significantly more rapid increase in the average turbulent lifetime τ than for the 13 mode model.*

The mean turbulent lifetimes τ were found by using a non-linear regression in the program *xmgrace* [146], minimising the error between the numerically extracted points and the theoretical curved defined by

$$y = A_0 exp(-A_1 x), \tag{2.30}$$

where A_1 is the numerically extracted decay rate. The mean turbulent lifetime is then simply $\tau = 1/A_1$. The A_0 term represents a fitting parameter that accounts for the initial delay in reaching the turbulent manifold from the initial conditions, which varies with Re and exact form of the initial conditions. Crucially, this has no effect on the behaviour once the turbulent manifold is reached.

Due to the presence of stable periodic orbits in the 13 mode model, we exclude the runs that run to the maximum time $T_{max} = 15000$ at lower Re because they are assumed to be caught within one of the periodic orbits. A large sample of the system states that had not relaminarised at $t = T_{max}$ for these Re found them all to be caught within a periodic orbit. The proportion of trajectories that end up within the confines of a periodic orbit can be found by looking at the minimum probability for which the lifetime distribution flatlines at, giving an idea of the size of the basin of attraction for the orbits. Despite this, the presence of the stable periodic orbits modifies the phase space in such a way that chaotic saddles form around its attracting regions, which accounts for the bumps in the plot of $\tau = 1/A_1$ against Re in regions where orbits can be found. The relationship between τ and Re for each model are shown in Fig. 2.24.

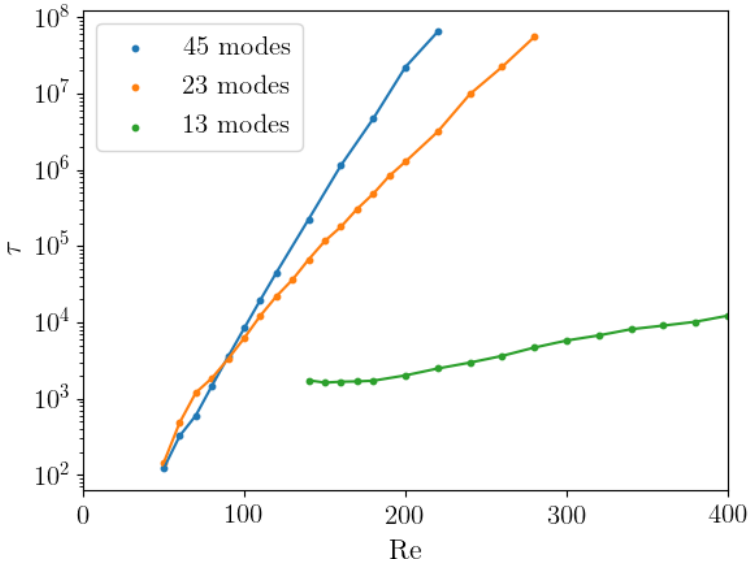

Figure 2.24 *The numerically extracted mean lifetime parameter $\tau = 1/A_1$ plotted against Re for the three different models. The lifetimes for the 13 mode model are not plotted below $Re = 140$ as the existence of stable periodic orbits in this region alters the data. Interestingly, the 23 mode model has a higher lifetime than the 45 mode model at $Re = 60$ and $Re = 70$, both of which lie within the region of stability of the 13 mode periodic orbit. This orbit has been shown to exist unstably in the 23 and 45 mode models, so due to the fact that the dynamics are confined onto a smaller dimension in the 23 mode model than the 45 mode model, it is possible that the typical trajectories interact transiently with the unstable orbit's domain in a way that increases the lifetime of the turbulent state in the 23 mode model but not in the full 45 mode model.*

Though none of the models display a super-exponential scaling of τ with the Re (which would be represented by an upward curving line in Fig. 2.24), clearly the dynamic interactions between modes in the 13 mode model and the additional 10 modes added to create the 23 mode model encapsulate some of the crucial physics that generates the long lifetimed turbulent state.

In addition to this, the lifetimes in the transitional range of Re have been shown to scale exponentially with Re [22, 80], which is reflective of the restricted degrees of freedom of the inertial manifold in this regime when compared to the fully turbulent system. As the models of this chapter are of a significantly restricted dimension, their analogy to the dynamics in the transitional may be implied by their similar lifetime scaling in this regard.

2.7 Discussion

The work detailed in this Chapter shows that the proposed algorithm for generating a low dimensional model of a turbulent system is valid. The models produced all have exact states that bifurcate from infinity, matching the known transition scenario. The increase in number of modes considered causes the model to display progressively more analogy to the full system, when selecting the modes intelligently using either the linear stability results in the rotating case or directly analysing the structure of the amplitude evolution Eqs. A.3. This gives insight into the fundamental interactions that generate different features of the transition to turbulence, allowing for greater understanding of the organisation of the infinite dimensional phase space in the full system.

The models of this Chapter have not included the stochastic effects of hydrodynamic noise into the Navier-Stokes equations as this feature is inappropriate for the objectives of this body of work. Hydrodynamic noise would make the methods used for tracking ECS used in this chapter invalid, as the system would cease behaving deterministically.

The critical Re_c demarking the point at which turbulence may be sustained for the three models are found to be lower than that expected in a full DNS of the system or indeed the experimental Re_c for plane Couette flow. This, however, is to be expected due to the use of the free-slip conditions, and may also be a manifestation of the limited order of the system.

The 13 mode model recreates the transition scenario found in [141], in which a stable periodic orbit separates the turbulent dynamics from trivial relaminarisation in the Re state space. This pathway to chaos shall be further explored in Chapter 3.

The results of this study suggest that long lifetimes arise from the ability of the structures within the flow to transfer turbulent energy into other structures at different locations within the periodic cell. The dynamical interactions of the SSP modes with the L, TS and SF mode groups cause a flow localised within one SSP to become unstable to an infinitesimal perturbation that can then ignite the other spatially phase shifted SSPs. This raises interesting questions about the nature of the decay process itself, as this energy transfer between structures at different locations within the cell is needed to access the long lifetimed state.

A decay event could require each of the phase shifted SSPs to independently 'relaminarise', such that even if the energy contained within one SSP was below the threshold required to sustain turbulence, there is some probability that the low energy SSP can receive a kick from a phase shifted SSP via the connecting modes that then reignites the turbulence in the low energy SSP. Another scenario is that perhaps these connections cause the chaotic manifolds of each SSP to collide in such a manner that creates a new chaotic saddle of considerably higher lifetime than the linear sum of the two independent manifolds. This phenomenon is termed a boundary crisis in the dynamical systems literature [147, 148] and has been shown to induce intermittency, which will be further explored in Chapter 3.

A curious observation from the investigation into the lifetime scaling versus Re is that to allow for the long lifetimed state, the required symmetry classes are phase shifted in the spanwise z direction, rather than the downstream x direction. This suggests some degree of 'width' is required in the structure to access the long lifetimed state. This corroborates recent results of a numerical investigation by Shimizu et al. [149], in which they found the lifetime of a spatially localised patch of turbulence increased exponentially with the system width at fixed Re in channel flow.

It is currently an open question as to the reason for the super-exponential lifetime scaling with Re, though if this effect does indeed arise from spatio-temporal effects then this type of modelling will not be able to capture it. A suggested further line of study would be to investigate whether by continuously increasing the maximum order of the considered modes (2 in this study), it would be possible to obtain a model that converges on the expected super-exponential scaling. However, 45 modes is already at the upper reach of what can realistically be considered a 'low dimensional' model, so this may prove impractical. Despite this, the understanding that analytic velocity modes can be divided into symmetry classes could allow for the intelligent addition of classes of higher order modes to the model, rather than thoughtlessly adding higher order modes in the hope that they provide greater analogy to physical turbulence.

In physical turbulence, the true flow field imposes no limitation on the wavelength or phase location of its constituent velocity modes. This means that the recreation of features of the transition to turbulence using a specified set of wavelengths and phase locations of the velocity modes, as in these models, can be safely generalised to explaining such features in the full flow.

Chapter 3

The origin of long lifetimes

The previous work described in Chapter 2 has shown that the inclusion of a certain combination of analytic velocity modes in a low dimensional model of plane Couette flow will cause the length in time of a turbulent trajectory to reach several orders of magnitude higher than other combinations of modes. As turbulent lifetimes are found experimentally to increase very rapidly after the point of subcritical bifurcation [56], it is possible that the long lifetime sets of modes will provide better analogy to the typical velocity profile in the transition region and that their study may help elucidate the origin of such long lifetimes. Indeed, the fact that lifetime scaling is dependent upon the inclusion of specific velocity modes and their interactions may allow the mechanism to be isolated through observing how different types of modes alter the typical trajectories through turbulent phase space such that the average lifetime increases.

The previously optimal low dimensional model for plane Couette flow [75] has lifetimes in the transition region of Re of order 10 times shorter than observed in full DNS experiments [150], shown in Fig. 3.1 and Fig. 3.2 respectively. This suggests some crucial 'physics', expressed through dynamical mode couplings, is missing from that low dimensional model. As the model from [75] is approximately analogous to our 13 mode model (which displays similarly short lifetimes), an equivalent conclusion can be made for the 13 mode model. This then motivates the question, why are the lifetimes so much longer for the 23 and 45 mode models?

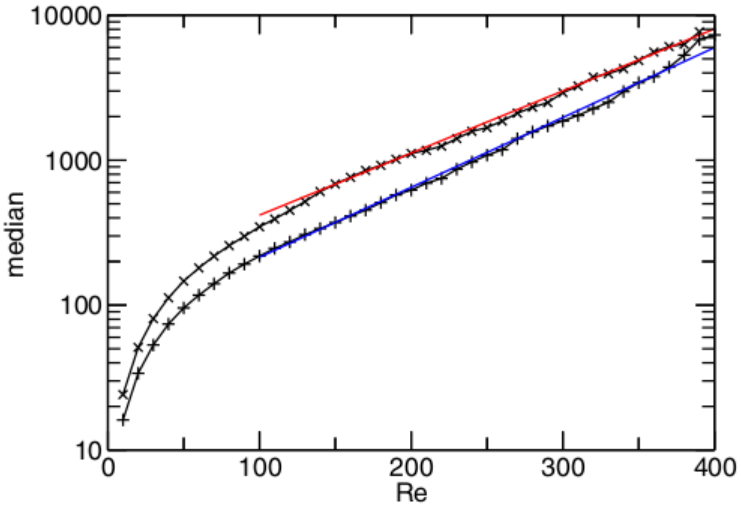

Figure 3.1 *The lifetime scaling observed in the transition region of Re for the 9 mode model in [75]. The two different data sets are plotted for different simulation box sizes, both clearly displaying an exponential dependence upon Re. Reproduced with permission from [75].*

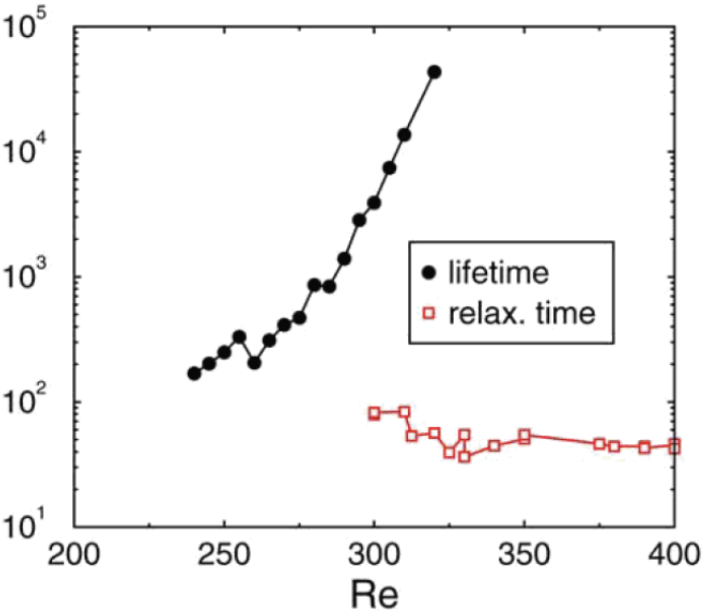

Figure 3.2 *The observed lifetime scaling in the full DNS of plane Couette flow. In the transition region of Re, which differs in exact value to the previous figure due to the low dimensional model using the free slip boundary conditions, the typical turbulent lifetime is an order of magnitude lower in the low dimensional model than the full DNS observations. This suggests that the 9 mode model is missing some crucial 'physics', expressed through dynamic mode couplings, that sustain the longer lifetime turbulence. Reproduced from [150], with permission from Springer Nature.*

3.1 Tuning the 23 mode model

The first objective was to obtain a simple parameter that could be tuned so as to produce a bifurcation between the states of different lifetime scaling. As shown in the previous chapter, the 23 mode model contains 2 SSPs coupled via non-linear interactions with the mean profile modes, spanwise streaks and the Tollmien−Schlichting like modes. The mean profile modes are necessary for a realistic model as the laminar profile $\mathbf{u}_8$ solves the Navier-Stokes equations for the system exactly, where the $a_8 = 1$, $a_{\neq 8} = 0$ state is an attractor $\forall Re$, however the spanwise streaks and Tollmien−Schlichting like modes could be removed so as to test for their significance in generating the long lifetimes observed in the 23 mode model.

If both the SF and TS modes are removed, the model cannot exhibit any turbulent dynamics and simply takes some characteristic time $T_{decay}(Re)$ to relaminarise. This is expected, as when performing the Galerkin projection to create the low dimensional models (Eq. 2.8), sets of modes form energy conserving triplets such that

$$\frac{da_i}{dt} = c_i a_j a_k + \dots \tag{3.1}$$

$$\frac{da_j}{dt} = c_j a_i a_k + \dots \tag{3.2}$$

$$\frac{da_k}{dt} = c_k a_i a_j + \dots, \tag{3.3}$$

where $c_i + c_j + c_k = 0$. If we analyse Eqs. 2.23 - 2.29, it is observed that no triplet can be created in the 23 mode model without either the SF or TS mode classes, therefore not allowing for any turbulent dynamics in the system.

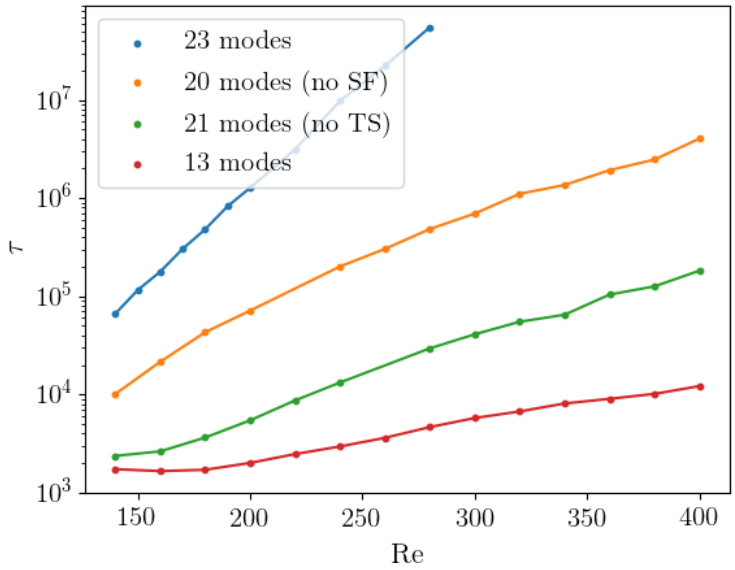

Figure 3.3 *The turbulent lifetime τ scaling versus Re for the 23 mode model and 13 mode models from the previous chapter, and models created from subsets of the 23 mode model created by removing either the TS or SF mode classes. The 23 mode model corresponds to two fully coupled SSPs, the 20 and 21 mode models correspond to two semi-coupled SSPs and the 13 mode model encodes for a single SSP.*

The results for the lifetime scaling for the different models, displayed in Fig. 3.3, show that the removal of either of the SF or TS modes causes a severe reduction in the length of the turbulent lifetimes, as a result of breaking a turbulence sustaining class interaction triplet. The lifetime scaling of the models does not become equivalent to the fully decoupled 13 mode model however, as there still exists a partial coupling between the 2 SSPs in each case. Interestingly, though the lifetimes are an order of magnitude higher for the 20 mode model (with no SF) compared to the 21 mode model (with no TS), they appear to increase with Re with a similar exponent. This suggests that the underlying arrangement of the chaotic saddle is comparable in both models, whilst distinctly different to the 13 and 23 mode models. From this it is clear that the arrangement of phase space that categorises the scaling behaviour of τ with Re is dependent upon the number of SSPs available and the degree of contact between them.

As both the removal of the TS or SF modes from the 23 mode model cause the lifetimes to scale in a similar manner, it is an arbitrary choice between them to use as the test parameter. The removal of the TS modes causes a greater reduction in the length of the turbulent lifetimes, and therefore was chosen as to

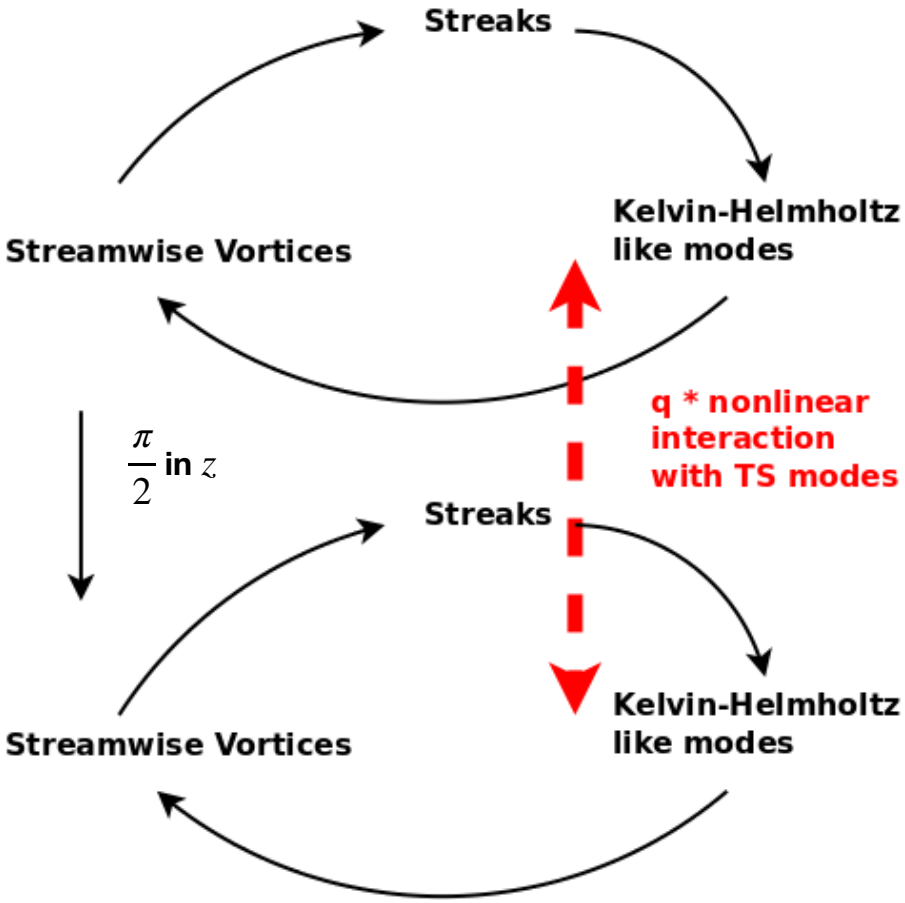

Figure 3.4 *A schematic displaying the role of the parameter q that controls the strength of the interactions between the 2 SSPs via the Tollmien−Schlichting like modes.*

make the effects more pronounced. As a result, a parameter q was chosen such that

$$\frac{da_{TS}}{dt} = -\frac{a_{TS}}{Re} + q \cdot F, \tag{3.4}$$

i.e. the parameter q controls the strength of the quadratic non-linear interactions F that generate the Tollmien−Schlichting like modes. This parameter q can be thought of in a broad sense of controlling the strength of the coupling between the two SSPs, allowing for the investigation of how the coupling alters the dynamics of the flow and gives rise to the dramatic increase in turbulent lifetimes and scaling exponent. For this parameter, the $q = 0$ case is equivalent to the 21 mode model with the TS modes removed and the $q = 1$ model is exactly equivalent to the usual 23 mode model.

3.2 Measuring velocity fluctuations

The first line of investigation undertaken was to use the model to test the hypothesis of Goldenfeld *et al.* [84], as detailed in Section 1.1.6. Namely, that the super exponential scaling of the turbulent lifetime τ with Re is an artefact of a Gaussian or exponential distribution of the turbulent energy fluctuations. This then implies that the size of the maximum fluctuation will be distributed via the Gumbel distribution, which subsequently generates a super-exponential distribution of τ with Re.

This was undertaken by calculating the distribution of velocity fluctuations for both the $q = 0$, and fully coupled $q = 1$, models and then comparing the differences. As a decay from turbulence is expected to first be characterised by a decay of the 3-dimensional modes, a norm to describe the turbulent energy fluctuations was devised as $\eta_{fluct} = (\sum_{3d} a_n^2) + (1 - a_8)^2$, which also included the squared 'distance' to the laminar solution.

To create a distribution of η_{fluct}, an ensemble of trajectories was run, using the same initial conditions as in Section 2.6, and η_{fluct} recorded at each integer value for t. The time iteration of the trajectory was terminated when the usual condition from Section 2.6 was met, signifying relaminarisation of the system. The first 500 time units of the trajectory were ignored to ensure that the trajectory had entered the turbulent portion of phase space after initialisation. Care had to be taken to ensure that the slow viscous relaxation to the laminar state was not included in the distribution, as this would suggest that lower values of η_{fluct} are much more likely than they actually are. To enforce this, the recorded η_{fluct} values were taken from the a fixed proportion of the total trajectory length after the initial 500 time units. This proportion varies with Re, as the ratio of the typical turbulent lifetime versus the typical viscous relaminarisation is itself a function of Re. An appropriate proportion of the trajectories to cut was selected by reducing the cut proportion until the distribution remained unchanged. The velocity fluctuation distributions for the 21 mode model, with the TS_1 modes removed, and the full 23 mode model are shown in Fig. 3.5 - 3.7.

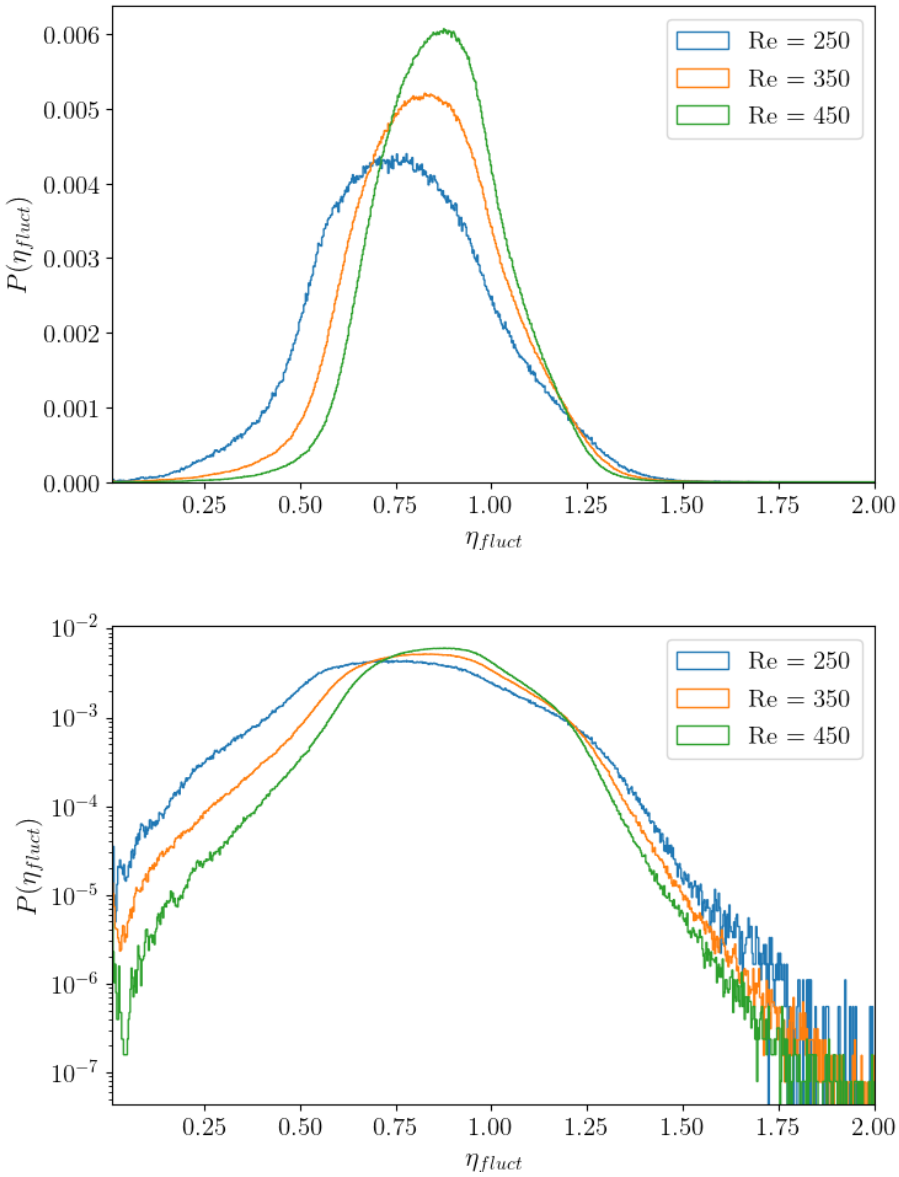

Figure 3.5 *Probability distributions of* $\eta_{fluct} = (\sum_{3d} a_n^2) + (1 - a_8)^2$ *for the 21 mode model at different Re. The approximately Gaussian functional form appears to remain the same, with the location of the peak increasing in* η_{fluct} *with Re for and its width decreasing.*

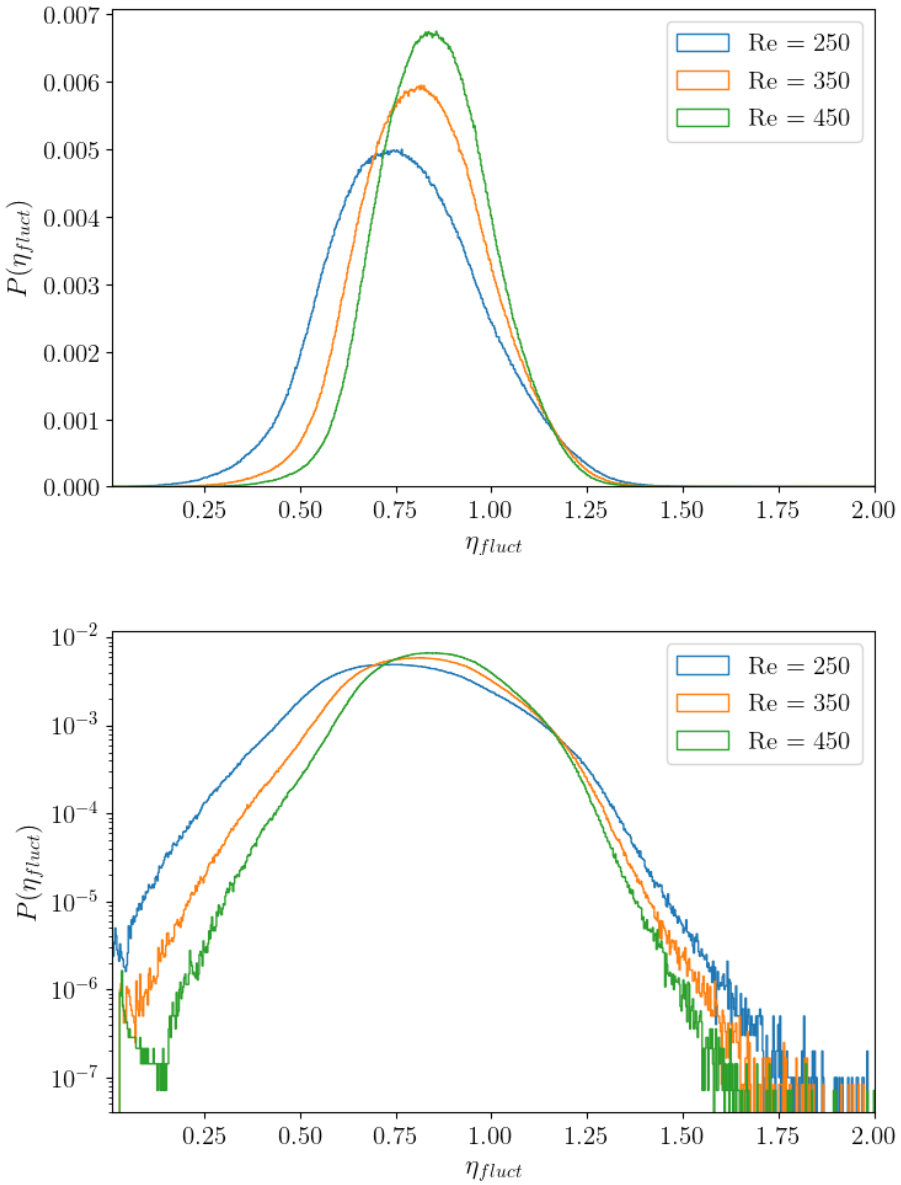

Figure 3.6 *Probability distributions of* $\eta_{fluct} = (\sum_{3d} a_n^2) + (1 - a_8)^2$ *for the 23 mode model at different Re. The distributions follow the same trends as for the 21 mode model, where an increase in Re corresponds to an increase in the modal value of* η_{fluct} *and a reduction in the width of the peak.*

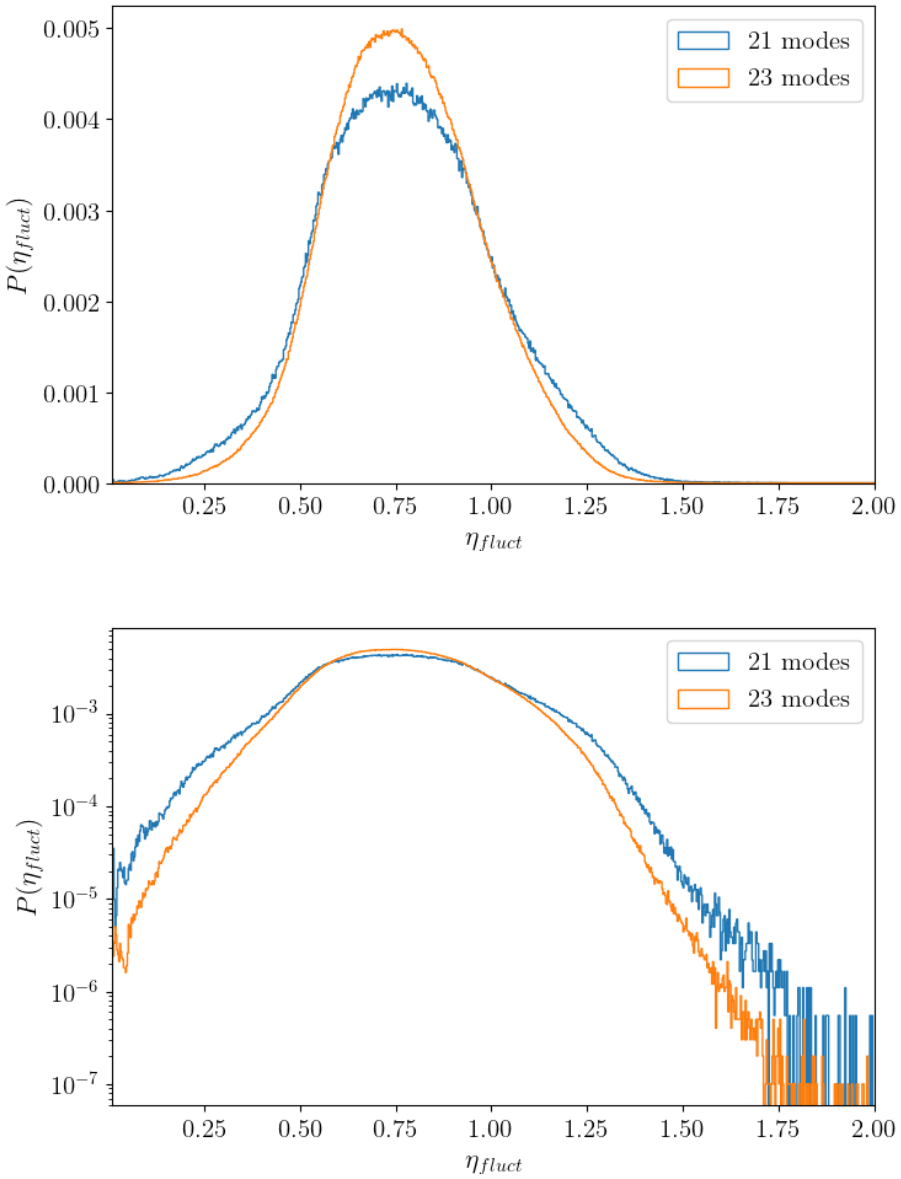

Figure 3.7 *Comparing the η_{fluct} distributions are $Re = 250$ for both models. They appear to peak at the same value of η_{fluct}, but the 21 mode model has a greater width, making extremal values more likely.*

For both models, the distribution takes an approximately Gaussian functional form, matching that observed in full DNS of plane Couette flow [151, 152]. An increase in Re corresponds to an increase in $\mu = \langle \eta_{fluct} \rangle$ and a reduction in the width of the η_{fluct} distribution. This corresponds to the turbulent attractor moving further away in the η_{fluct} space from the laminar solution (where $\eta_{fluct} = 0$) and requiring smaller deviations from $\langle \eta_{fluct} \rangle$ to sustain itself. This can be equated in dynamical system terms as an increase in Re increasing the density of local solutions in the turbulent portion of phase space, consequentially increasing the complexity of the phase space and putting more barriers between the turbulent phase space and the laminar solution. This has the effect of confining the turbulent trajectory to a smaller region of η_{fluct}.

Another metric by which we can measure the differences between the models are the distributions of the laminar mode energy $E_L = a_8^2$, where $E_L = 1$ corresponds to the laminar state. This value is suppressed whilst the trajectory is on the turbulent attractor, but increases when the trajectory makes an excursion towards the laminar state. These excursions may result in a relaminarisation event, or a dynamical interaction between with structures located between the turbulent attractor and the laminar state, for example the edge state discussed in Section 1.1.2. The distributions of E_L for the two models are displayed in Figs. 3.8 - 3.11.

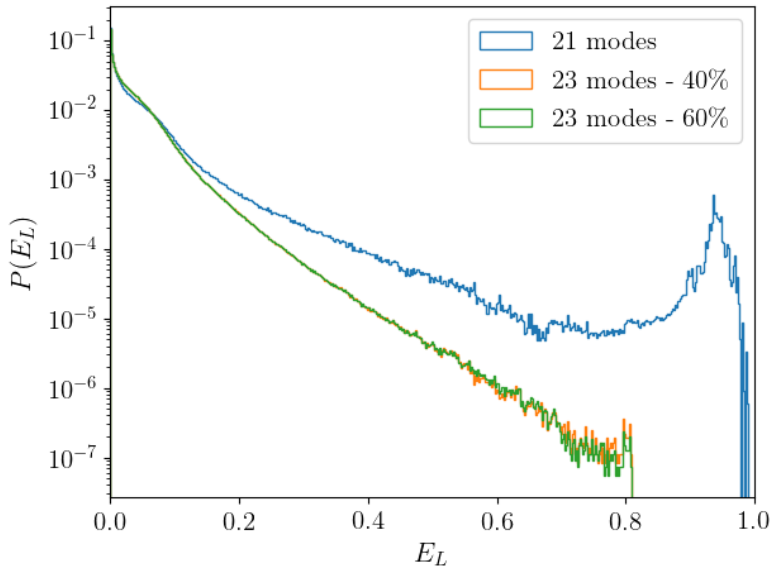

Figure 3.8 *The probability distribution of E_L for the 21 and 23 mode models at $Re = 250$. For the ensemble of 21 mode trajectories, the first 5% of the trajectory is ignored, and the following 10% considered. For the 23 mode trajectories, the first 10% of the trajectory is ignored with the following amount considered labelled on the graph. The fact that the two cuts rest upon each other suggests that the distribution is insensitive to the cutting procedure.*

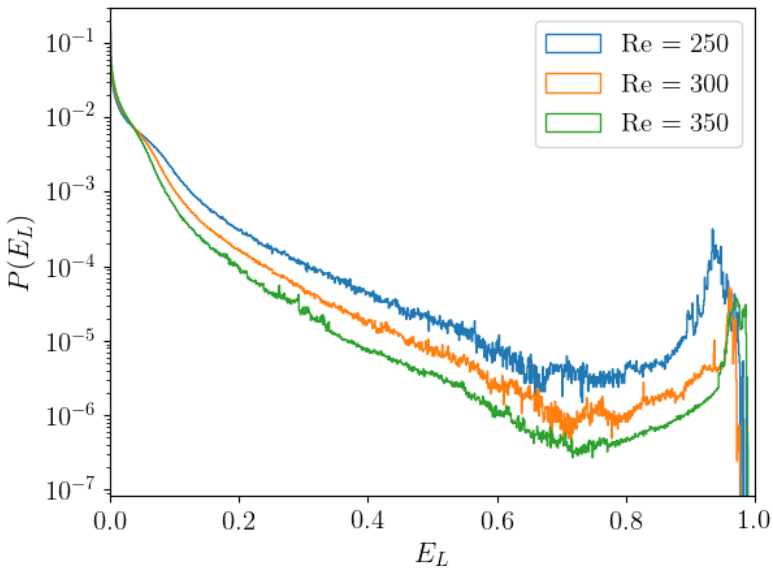

Figure 3.9 *The distribution of E_L for the 21 mode model at different values of Re.*

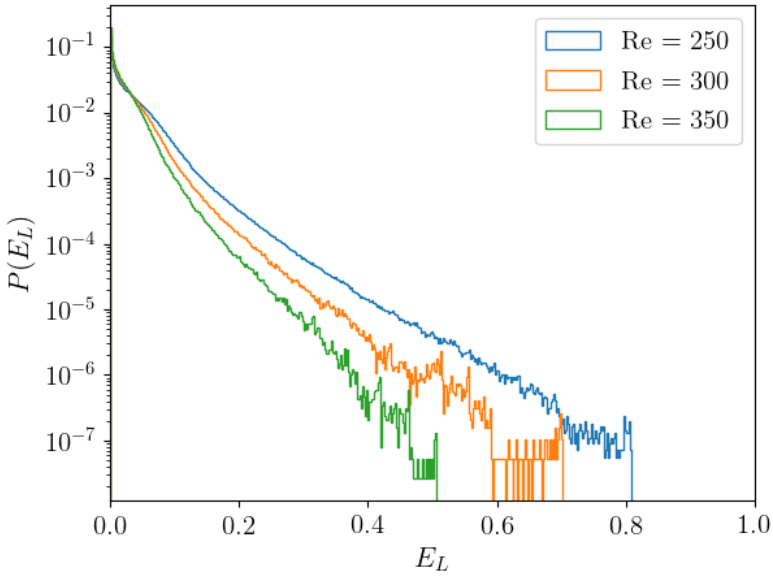

Figure 3.10 *The probability distribution of E_L for the 23 mode model for different Re. Here it can be observed that the maximum E_L fluctuation, i.e. the point beyond which no statistics are recorded in E_L, reduces with Re.*

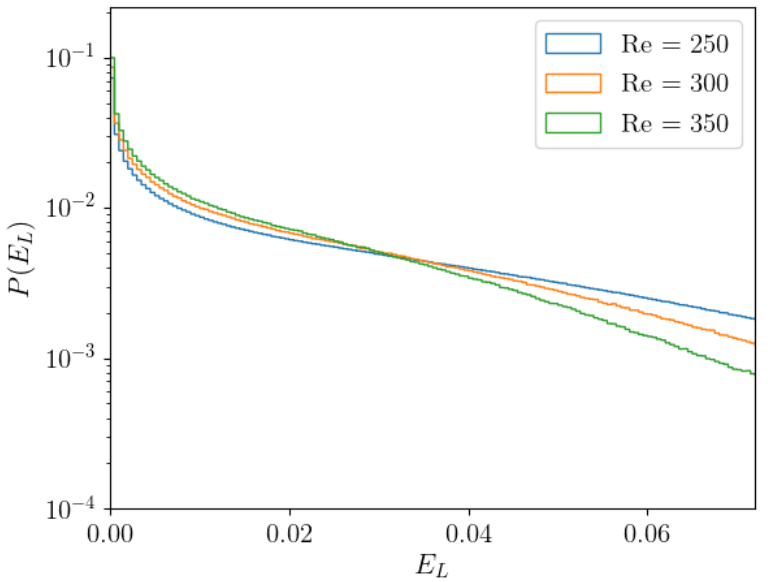

Figure 3.11 *Inset of Fig. 3.10, showing that for higher Re, there is a higher probability of E_L for low values of E_L, which is then reversed for high values of E_L past the crossover point of the distributions.*

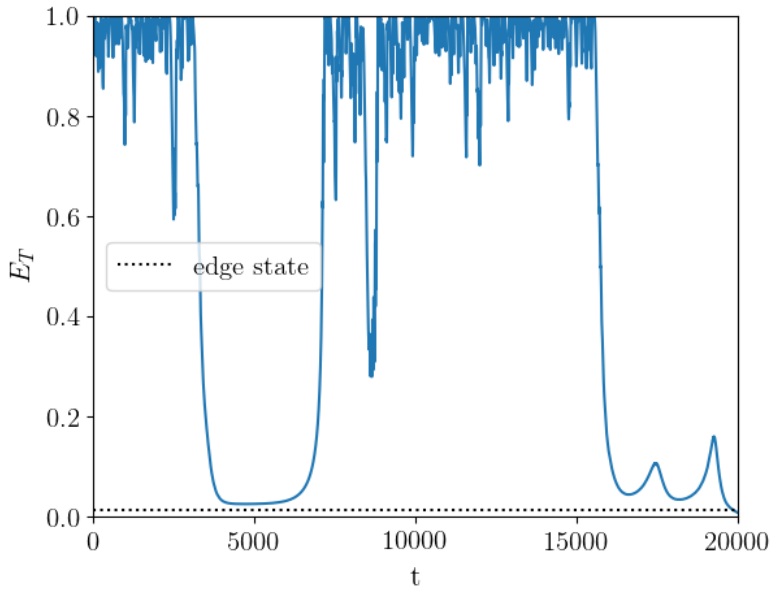

Figure 3.12 *A turbulent trajectory at $Re = 250$ for the 21 mode (no TS) model showing both a reflection back to the turbulent phase from the edge state and a long time interaction with the edge state before relaminarisation.*

As can be seen from Fig. 3.8, there is a probability peak at higher E_L close to 1 for the 21 mode model. This peak is close to the location of the lower branch solution, suggesting that some portion of the trajectories are getting caught within the attracting domain of the edge state. These trajectories can then either bounce back the turbulent part of phase space or relaminarise, as shown in Fig. 3.12. As the trajectories are cut such that the end of the trajectory (the part that corresponds to slow viscous relaminarisation) is not included in the ensemble of E_L, it is likely that this peak corresponds to either a reflection back towards the turbulent attractor by the edge state or at least a long time (when compared with the length of the trajectory considered) interaction before relaminarisation. The peak reduces in probability with an increase in Re, suggesting that the likelihood of such an interaction decreases with Re. The thinning of the peak also implies that the domain of the edge state reduces with Re. This would be expressed by the long time transient oscillations before relaminarisation reducing in amplitude of oscillation.

This phenomenon however, is not replicated in the full 23 mode model. This suggests it either becomes a rare enough event that not enough trajectories have been run with which to catch it, or that the presence of TS modes makes such

an interaction impossible via a rearrangement of the phase space.

Interestingly, for the 23 mode model there appears to be a maximum E_L that a turbulent fluctuation will reach without relaminarising, which is dependent upon Re. As Re increases the maximum E_L decreases, corroborating the earlier result that smaller fluctuations from the mean E_L are required to sustain turbulence at higher Re. These observations, compounded by those of the previous paragraph, suggest that the change of the phase space via the increase in q, such that the upper area of E_L space becomes less accessible (and likely inaccessible) to the turbulent trajectory, is intrinsically linked to the increased lifetime of the turbulent state in this regime.

3.3 Periodic orbits and the transition

Previously we have found that by increasing a control parameter q, which controls the strength of the non-linear interactions that generate the Tollmien−Schlichting like modes, we can increase the typical lifetime of a turbulent trajectory by in excess of two orders of magnitude, as shown in Fig. 3.13 and Fig. 3.14.

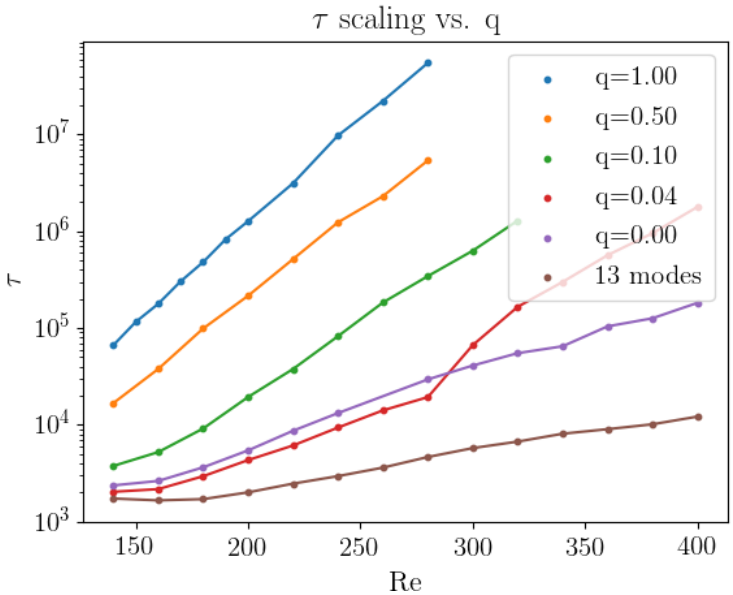

Figure 3.13 *The scaling relation of the mean turbulent lifetime τ versus Re for a range $0 \leq q \leq 1$ showing the change in the scaling relation as q is increased. A stable periodic orbit is found between $280 < Re < 300$ for $q = 0.04$, which accounts for the change in scaling behaviour between these points.*

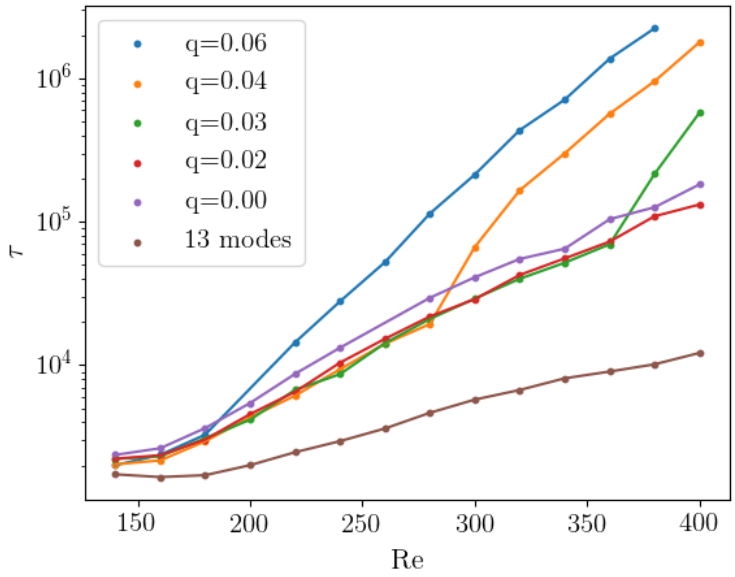

Figure 3.14 *The scaling relation of the mean turbulent lifetime τ versus Re for a range $0 \leq q \leq 0.1$ showing the change in the scaling relation as q is increased. Here it is clear to observe that for low values of q, the scaling exponent is the same as for the $q = 0$ case up to a critical Re (which is a function of q), beyond which the scaling exponent is the same as for the $q = 1$ case.*

From these figures, it can be observed that the scaling of τ versus Re can be categorised into three distinct categories: the smallest exponent characterises the lifetime scaling of the 13 mode model that encodes for a single SSP, an intermediate exponent that characterises the scaling up to a critical point in Re for low values of q, and the highest exponent for higher values of q that is common to the fully coupled $q = 1$ case. From this observation, one can conclude that the increase of q causes a discontinuous jump between lifetimes that scale as two partially coupled SSPs (common to the $q = 0$ case) and lifetimes that scale as two fully coupled SSPs, expressed through a change in the underlying phase space between the two regimes.

It can be observed that for some values of q, for example $q = 0.04$ as shown in Fig. 3.13, that at low Re the lifetimes will scale as two partially coupled SSPs and that at higher Re past a discreet point, they will scale as two fully coupled SSPs. This suggests the existence of a barrier in Re-q space between the two different lifetime scaling states. Indeed, for a narrow region of Re and q, an infinite-lifetimed state is observed, pointing to the existence of a stable periodic

orbit. To investigate this, individual trajectories were recorded in the region of Re and q of the discontinuous jump, confirming the existence of a stable periodic orbit that acts as a barrier in Re-q space between the two states. The partition of the phase space dependent upon q for $Re = 240$ is shown in Fig. 3.15.

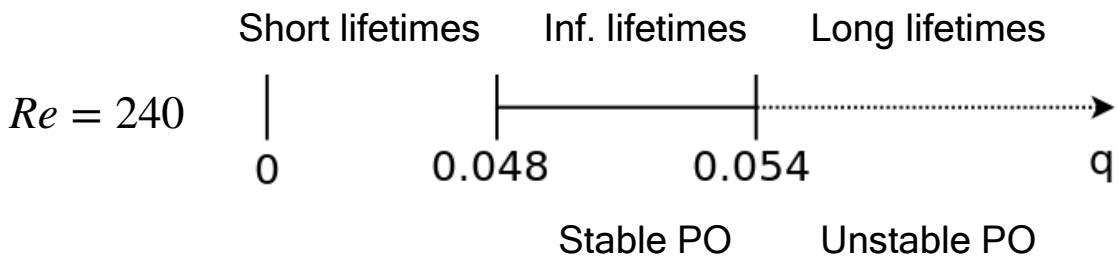

Figure 3.15 *A pictorial representation of the different classifications of the phase space for Re = 240 and their relation to the periodic orbits. Here, a bold line denotes a stable solution, a dotted line an unstable solution and an absence of a line the range before the saddle point at which the periodic orbit appears.*

When caught in the domain of the periodic orbit, the amplitudes of the modes from the A, C and D classes oscillate around zero, whilst the L, TS and SF modes oscillate around non-zero values. Interestingly, if we compare equivalent modes from each class, for example two vortices with a phase shift of $\frac{\pi}{2}$ in the z direction (i.e. modes u_{13} and u_{14} from the A_1 and A_2 classes), we see that they oscillate with quarter period phase shift in time between them, suggesting a subharmonic resonance. The amplitudes for different modes against time, when caught on the orbit at $Re = 240$ and $q = 0.05$, are shown in Figs. 3.16 - 3.18.

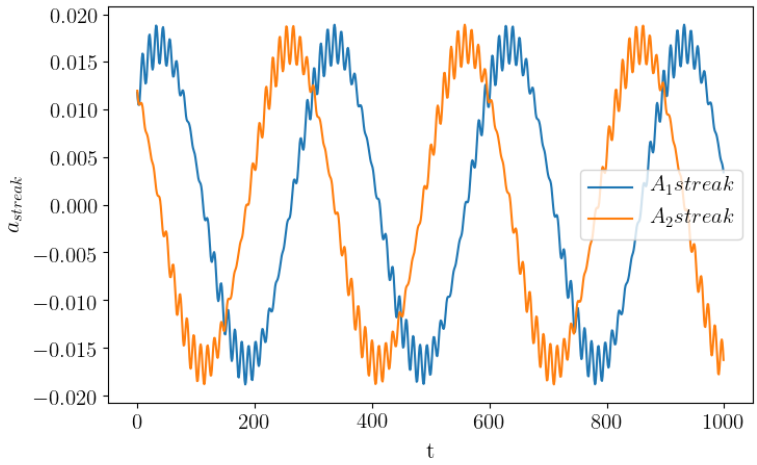

Figure 3.16 *The amplitudes of the streak modes for a trajectory caught on the stable periodic orbit at* $Re = 240$ *and* $q = 0.05$.

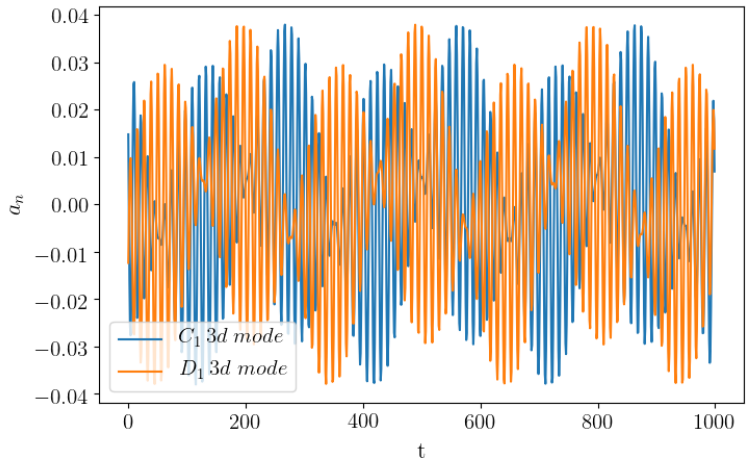

Figure 3.17 *The amplitudes of equivalent 3-dimensional modes from classes* C_1 *and* D_1 *for a trajectory caught on the stable periodic orbit at* $Re = 240$ *and* $q = 0.05$.

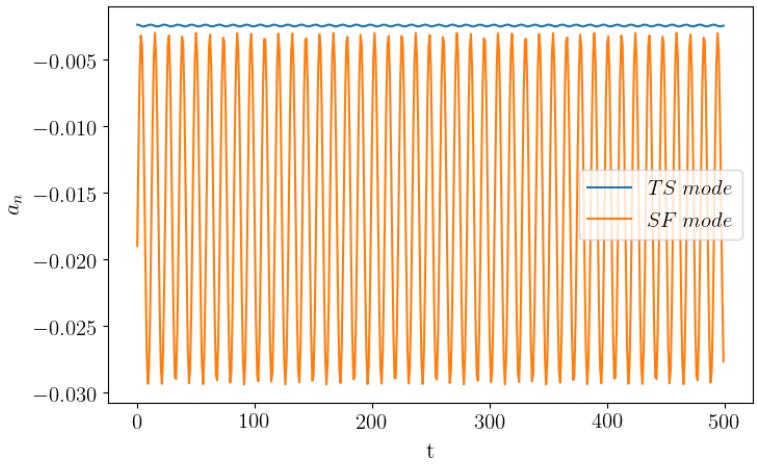

Figure 3.18 *The amplitudes of modes from the TS and SF classes for a trajectory caught on the stable periodic orbit at* $Re = 240$ *and* $q = 0.05$.

As q is increased for a fixed Re, it is observed that the orbits undertake a period doubling route to chaos, until a point at which their stability is lost. The route to chaos can be observed by tracking the E_L of an orbit as q is increased to the point of instability. The Fourier transform of this measure shows regular oscillatory flow characterised by two frequencies at $q = 0.048$, the q at which the orbit is first observed for $Re = 240$. At $q = 0.054$, just before the q at which the periodic orbit loses stability for $Re = 240$, the frequency spectrum of E_L tends towards to the typical spectrum of fully turbulent flow. Time series of E_L at $Re = 240$ for increasing q are shown in Fig. 3.19, with their respective Fourier transforms, and that of the fully coupled model, shown in Fig. 3.20.

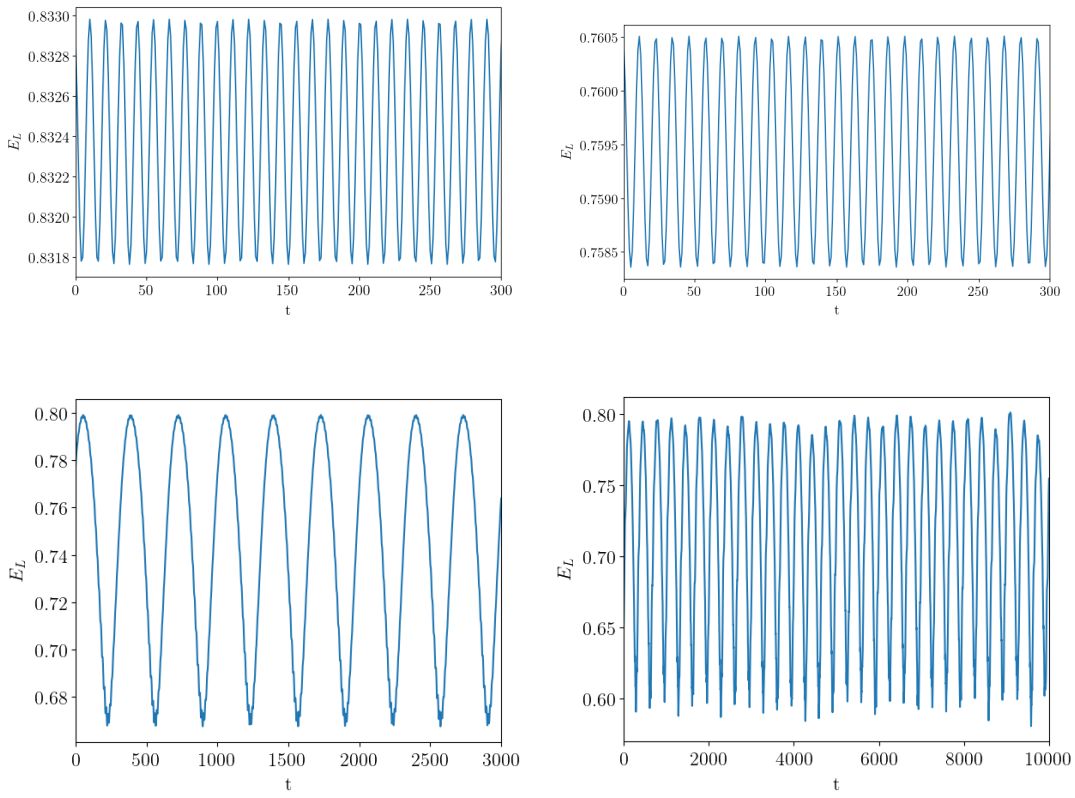

Figure 3.19 *Time series of the laminar mode energy $E_L = a_8^2$ for (reading from top left) $q = 0.048$, $q = 0.050$, $q = 0.051$, $q = 0.054$ at $Re = 240$, showing the route to chaos as q is increased. As q increases the periodic orbit becomes closer to the turbulent state, evidenced by the reduction of the average E_L of the orbit.*

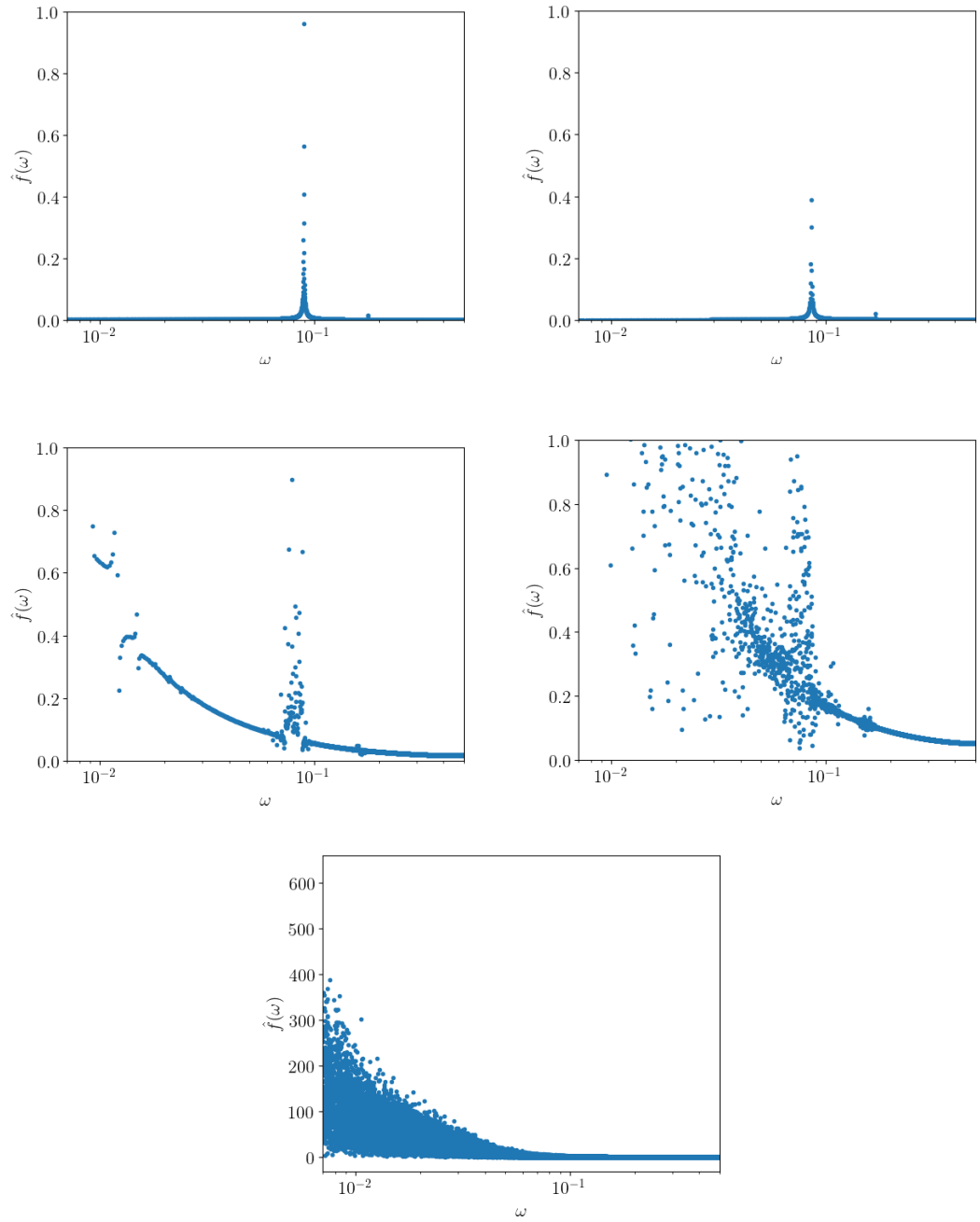

Figure 3.20 *The Fourier transforms of the laminar mode energy* $E_L = a_8^2$ *for (reading from top left)* $q = 0.048$, $q = 0.050$, $q = 0.051$ *and* $q = 0.054$ *and* $q = 1$ *at* $Re = 240$, *showing the route to chaos as* q *is increased.*

The stability range of the periodic orbit in Re-q space is found by finding the orbit for a set Re and q, then time iterating the trajectory whilst incrementally changing either q or Re. This is performed after a set number of timesteps, to ensure the trajectory has settled within the confines of the periodic orbit before

a change in Re or q. The trajectory is plotted for each value of Re and q, from which it can be ascertained the value for which the orbit loses its stability. As q is increased, the region of stability of the periodic orbit decreases in Re, until the orbit overlaps with the stability range in Re of the stable periodic orbit observed in the previous chapter for the 13 mode model, at q_{po}, where $0.12 < q_{po} < 0.13$. At this point both orbits lose their stability through a boundary crisis, as displayed below in Fig. 3.21, and are therefore no longer infinite time attractors for the turbulent trajectory. As observed in Chapter 2, the 13 mode periodic orbit is not seen in the fully coupled 23 mode model, but here it has been shown to persist between $q = 0$ and q_{po}.

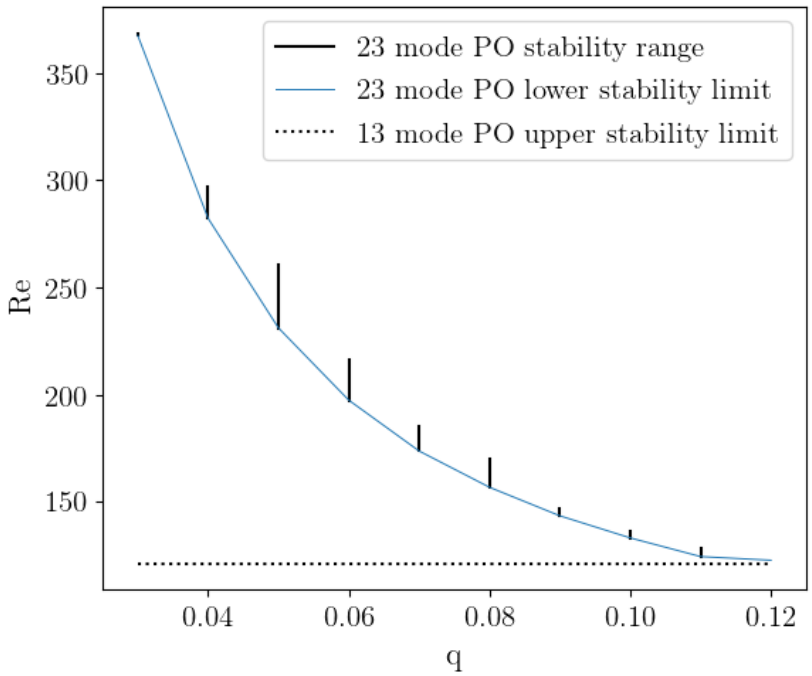

Figure 3.21 *A diagram displaying the numerically extracted ranges of stability for the periodic orbit found in Chapter 2, here labelled as the 13 mode periodic orbit, and the periodic orbit found in this chapter. The labelling of the 13 mode periodic orbit as such denotes that 13 modes are active within the orbit, but it is still observed in the 23 mode model until $q = 0.121$ at which point the domains of the two orbits collide, undergoing a boundary crisis.*

This boundary crisis can be shown by plotting the amplitude of the laminar mode, a_8, in time for $Re = 122$ and $q = 0.13$, the point just beyond the boundary crisis of the two attractors. If the two orbits are plotted at the closest point to these values that they can be traced to, $Re = 121$ for the 13 mode orbit and $Re = 123$

and $q = 0.13$ for the 23 mode orbit, the trajectory can be observed to leave the turbulent portion of the phase space to make excursions to the now unstable domains of the periodic orbits, displayed in Fig. 3.22.

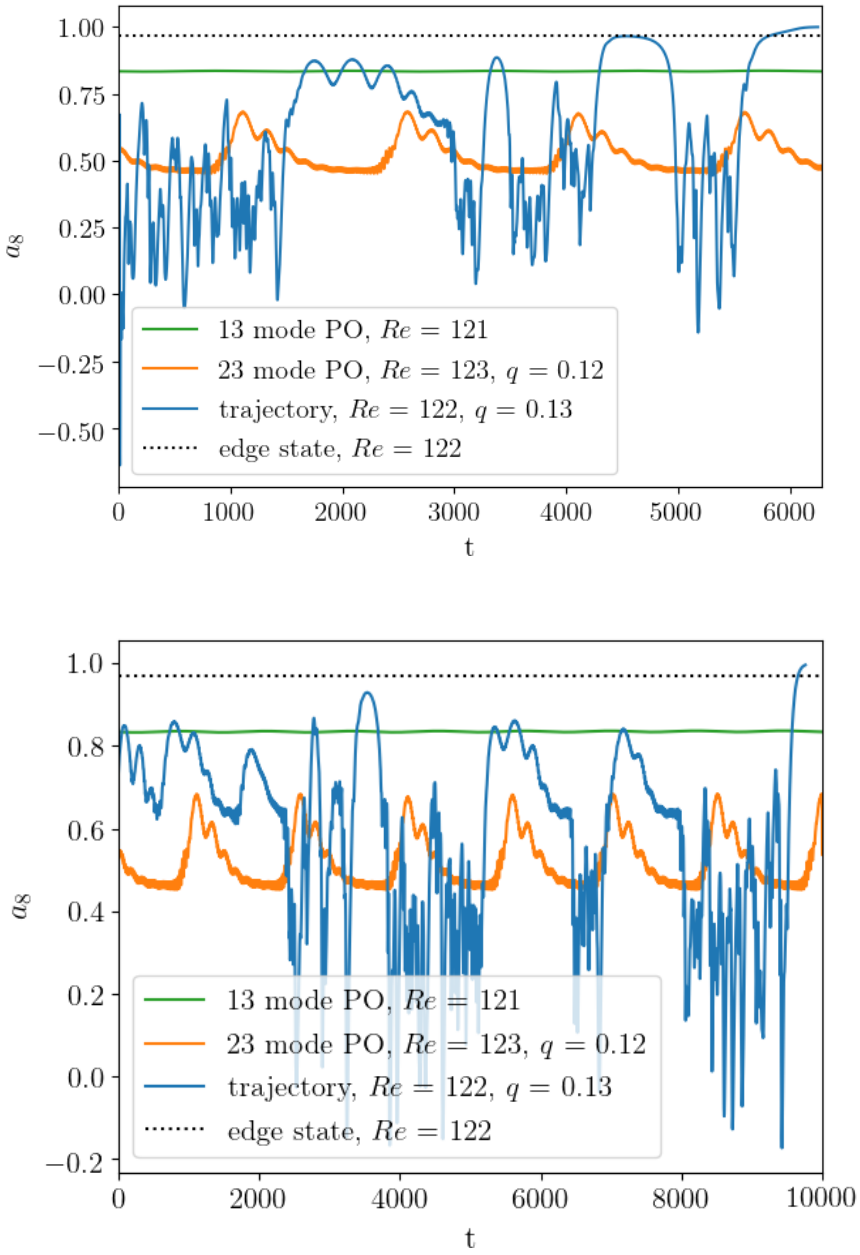

Figure 3.22 *Two typical turbulent trajectories at $Re = 122$ and $q = 0.13$, chosen to be just past the point at which both the 13 and 23 mode periodic orbits lose their stability via a boundary crisis. The flow can be seen to interact with the domains of the edge state, 13 mode periodic orbit and 23 mode periodic orbit.*

Another way to visualise this is to plot the amplitudes of two modes, chosen to be the laminar mode a_8 and a streamwise vortex mode a_{13}, for a turbulent trajectory, with the values of those modes for the POs overlain, as in Figs. 3.23 and 3.24.

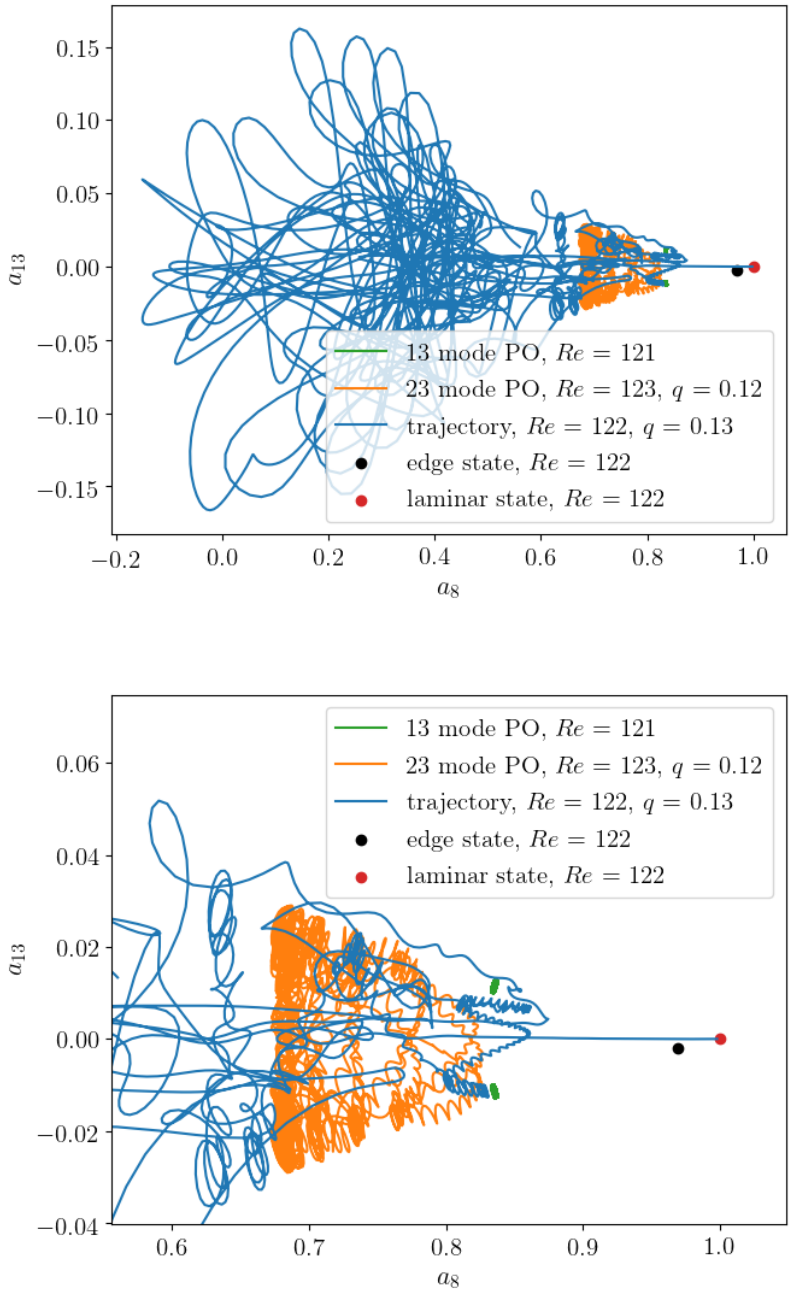

Figure 3.23 *A typical turbulent trajectory at $Re = 122$ and $q = 0.13$ shown in $a_8 - a_{13}$ space. The two periodic orbits can be seen to lie between the turbulent and laminar states, very close to each other. The trajectory interacts with the orbits when it makes excursions towards the laminar state.*

The two orbits (plotted in green and orange for the 13 mode and 23 mode POs respectively) can be observed to form a locally attracting domain between the turbulent portion of phase space and the laminar solution.

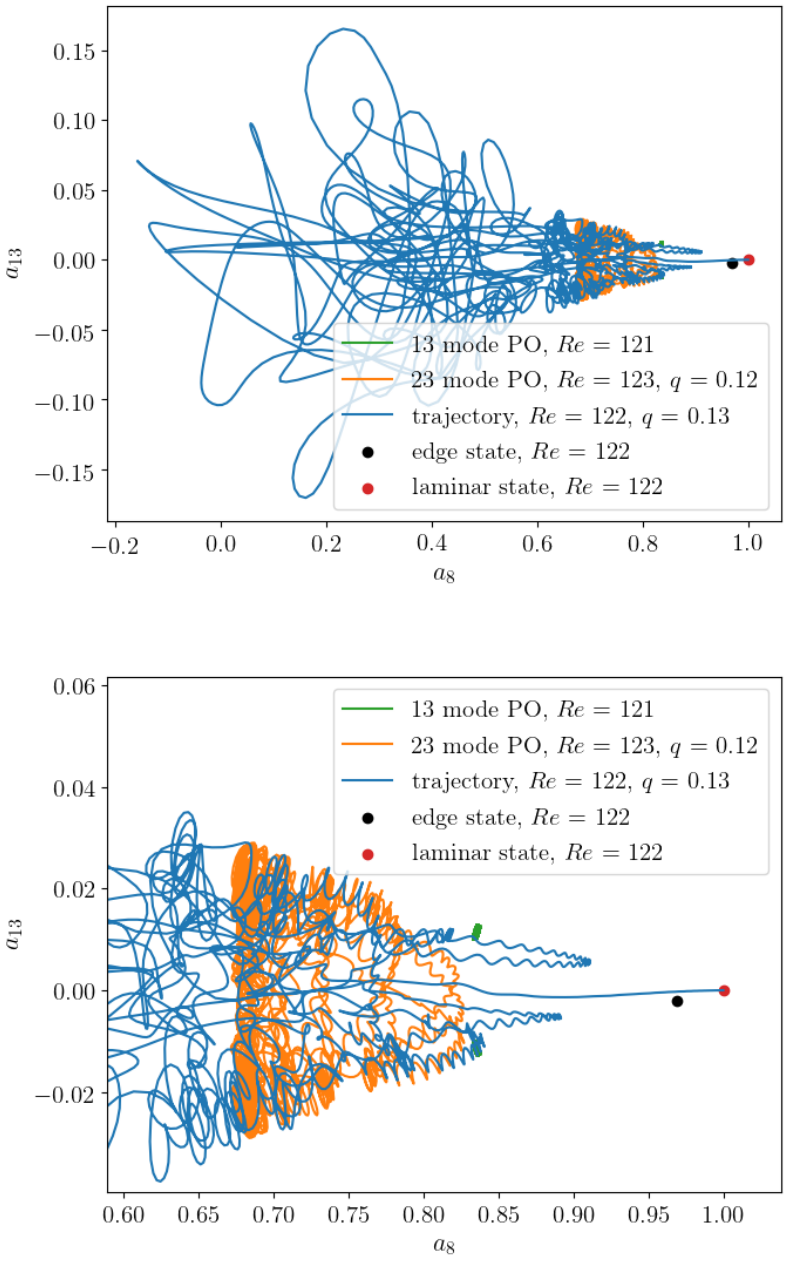

Figure 3.24 *A typical turbulent trajectory at* $Re = 122$ *and* $q = 0.13$ *shown in* $a_8 - a_{13}$ *space.*

For q just above the limit of stability of the 23 mode periodic orbit, turbulent trajectories make intermittent excursions to the domain of the now unstable

periodic orbit. In a similar manner as the excursions towards the edge state, discussed in the previous section, there is some probability that the trajectory will be reflected back towards the turbulent attractor, though now with a much higher probability than the edge state interaction.

Once q and Re are high enough that the orbit has lost its stability, the lifetimes scale with the same exponent as the fully coupled 23 mode model, suggesting the arrangement of phase space has discontinuously changed, via the creation of the orbit and its subsequent loss of stability, to match that of the 23 mode model. This then motivates the question, by what mechanism does the unstable periodic orbit cause an increase in the lifetime scaling exponent and does this reflection back from the domain of the unstable periodic orbit play a role in the generation of the long lifetimed state?

3.4 A 3-state model for the long lived state

To model the 'bouncing' mechanism we suspect could give rise to the large increase in lifetimes once the control parameter q is high enough that the transient periodic orbits lose their stability, we propose a simple 3-state model. In the region of q just beyond the upper point at which the orbit loses stability, the unstable periodic orbit places a repelling but porous barrier between the turbulent and laminar states, meaning that trajectories leaving the turbulent phase space have some probability to enter the domain of the orbit, from which they may then bounce back to the turbulent state after some time. This can be written algebraically as follows

$$\frac{dP_T}{dt} = -\alpha P_T + \beta P_H \tag{3.5}$$

$$\frac{dP_H}{dt} = \alpha P_T - (\beta + \gamma) P_H \tag{3.6}$$

$$\frac{dP_L}{dt} = \gamma P_H \tag{3.7}$$

where P_T is the probability that the trajectory is turbulent at time t, P_H is the probability that the trajectory is hibernating (a nomenclature reflective of the location of the domain of the unstable periodic orbit between the turbulent and laminar states) at time t, P_L represents the probability to be in the absorbing laminar state at time t, α and β signify the rates of decay from the turbulent to

hibernating states and vice versa respectively, with γ signifying the rate of decay from the hibernating state to laminar state. This is shown diagrammatically in Fig. 3.25.

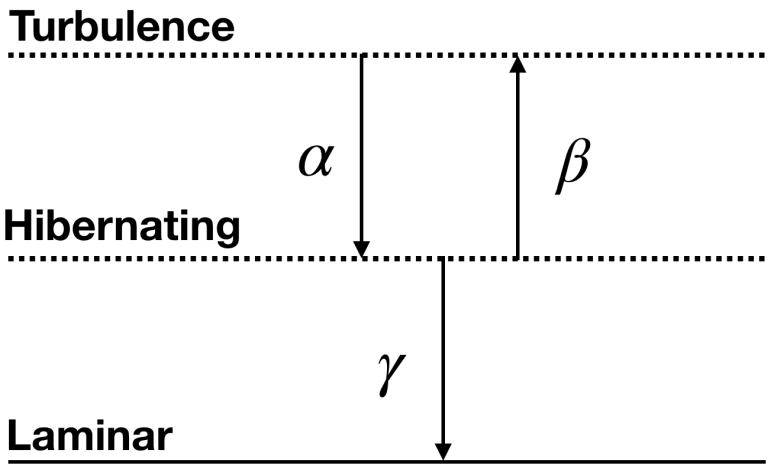

Figure 3.25 *A pictoral representation of the 3-state model for the system, with associated rate constants α, β and γ.*

To investigate the validity of this model, an ensemble of trajectories for a fixed Re and q just above the upper stability limit of the periodic orbit were generated. The square of the amplitude of the mean profile mode, E_L, was tracked against time to denote which portion of phase space the trajectory resided in. The division between the turbulent and hibernating states was taken to be the square of the minimum laminar amplitude of the quasi-sinusoidal periodic orbit, as shown in Fig. 3.26. This approach to demarking the boundary relies on the assumption that an infinitesimal change in q changes the location of the unstable periodic orbit infinitesimally in E_L space. As can be seen from Fig. 3.26, this assumption is valid.

It should be noted that by dividing the phase space in this manner, the proportion of phase space marked as hibernating includes both interactions with the domain of the periodic orbit and the edge state. At low q, before the periodic orbits appear, the interaction with the edge state's only major contribution to extending the time before full relaminarisation is by a transient oscillation observed between leaving fully developed turbulence and relaminarising.

From the ensemble of trajectories, further ensembles of lifetimes spent in each state could be extracted by calculating the amount of time units spent above

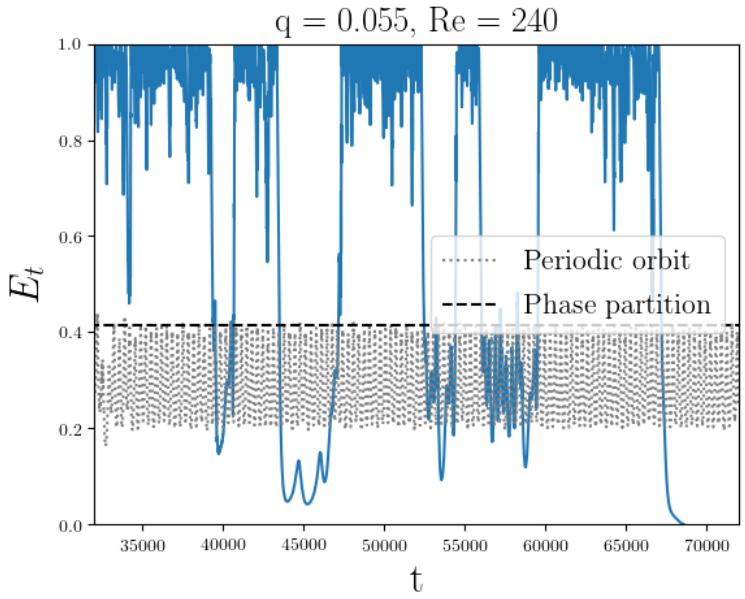

Figure 3.26 *A typical time series of the turbulent energy, defined* $E_T = 1 - E_L$*, showing the typical bouncing behaviour between the upper* T *state and the lower* H *state at* $Re = 240$ *and* $q = 0.055$*. The periodic orbit at* $q = 0.054$*, the highest* q *at which it is found to be stable, is overlain to show the location of its attractor in* E_T *space and to display the motivation for the chosen partition between the* T *and* H *states. This relies on the assumption that the location of the domain of the periodic orbit in* E_T *space only varies slightly with the increase of* q*, which is validated by the observation that the hibernation events at* $q = 0.055$ *enter the same region of phase space.*

and below the threshold value. These could then be used to find the survival probabilities and average trajectory length of each state. Times spent in each state below a threshold value are ignored, as there are often short time oscillations across the boundary between the phases when entering or leaving the hibernating state. This phenomena is typical behaviour of a chaotic trajectory crossing the boundary between two locally attracting domains.

Using standard methods for solving linear differential equations [153] and setting the initial condition $P_T(t=0)=1$ and $P_L(t=0)=P_H(t=0)=0$, the solution to Eqs. 3.5 - 3.7 takes the form

$$P_T(t) = \frac{e^{-\frac{1}{2}t\Gamma}\left(\alpha^2\left(e^{t\Delta}+1\right)+\alpha\left(-\Delta\left(e^{t\Delta}-1\right)+2\beta\left(e^{t\Delta}+1\right)-2\gamma\left(e^{t\Delta}+1\right)\right)\right)}{2\eta} + \frac{e^{-\frac{1}{2}t\Gamma}\left((\beta+\gamma)\left(\Delta\left(e^{t\Delta}-1\right)+\beta\left(e^{t\Delta}+1\right)+\gamma\left(e^{t\Delta}+1\right)\right)\right)}{2\eta} \tag{3.8}$$

$$P_H(t) = \frac{\alpha e^{-\frac{1}{2}t\Gamma}\left(e^{t\Gamma}-1\right)}{\Gamma} \tag{3.9}$$

$$\begin{aligned} P_L(t) = &-\frac{\alpha^2 e^{-\frac{1}{2}t\Gamma}\left(-2e^{\left(\frac{1}{2}t(\Delta+\alpha+\beta+\gamma)\right)}+e^{t\Delta}+1\right)}{2\eta} - \frac{\alpha\Delta e^{-\frac{1}{2}t\Gamma}\left(e^{t\Delta}-1\right)}{2\eta} \\ &-\frac{2\alpha\beta e^{-\frac{1}{2}t\Gamma}\left(-2e^{\left(\frac{1}{2}t(\Delta+\alpha+\beta+\gamma)\right)}+e^{t\Delta}+1\right)}{2\eta} \\ &+\frac{2\alpha\gamma e^{-\frac{1}{2}t\Gamma}\left(-2e^{\left(\frac{1}{2}t(\Delta+\alpha+\beta+\gamma)\right)}+e^{t\Delta}+1\right)}{2\eta} \\ &+\frac{(\beta+\gamma)e^{-\frac{1}{2}t\Gamma}\beta\left(-2e^{\left(\frac{1}{2}t(\Delta+\alpha+\beta+\gamma)\right)}+e^{t\Delta}+1\right)}{2\eta} \\ &-\frac{(\beta+\gamma)e^{-\frac{1}{2}t\Gamma}\gamma\left(-2e^{\left(\frac{1}{2}t(\Delta+\alpha+\beta+\gamma)\right)}+e^{t\Delta}+1\right)}{2\eta} \\ &-\frac{(\beta+\gamma)e^{-\frac{1}{2}t\Gamma}\left(\Delta\left(e^{t\Delta}-1\right)\right)}{2\eta} \end{aligned} \tag{3.10}$$

where $\Gamma=\sqrt{(\alpha+\beta+\gamma)^2-4\alpha\gamma}+\alpha+\beta+\gamma$, $\Delta=\sqrt{\alpha^2+2\alpha(\beta-\gamma)+(\beta+\gamma)^2}$ and $\eta=(\alpha+\beta+\gamma)^2-4\alpha\gamma$.

If we assume the the lifetime in each state to be distributed as a Poisson process,

as described in Eq. 1.8, then the rate constants α, β and γ will be

$$\alpha = \lambda_T \tag{3.11}$$

$$\beta + \gamma = \lambda_H \tag{3.12}$$

$$\frac{\beta}{\gamma} = \frac{\text{no. of } H \to T \text{ transitions}}{\text{no. of } H \to L \text{ transitions}}, \tag{3.13}$$

where λ_T and λ_H are the exponents obtained by numerically fitting the survival probability of each state. The constants can then be used to solve Eqs. 3.8 - 3.10 for t to generate an equation for the total survival probability, which can be compared to the measured survival probability to validate the model. This is shown in Fig. 3.27 for $q = 0.055$, with the survival probabilities of the T and H states at $q = 0.55$ overlain. To contrast the T survival probability at $q = 0.55$, the total survival probability at $q = 0.04$, chosen to be just before the orbit appears, is included. Interestingly, λ_T is unchanged by the presence of the orbits compared with the total survival exponent at $q = 0.04$, suggesting that the increase in the lifetimes arises solely from the reflecting interaction with the periodic orbit.

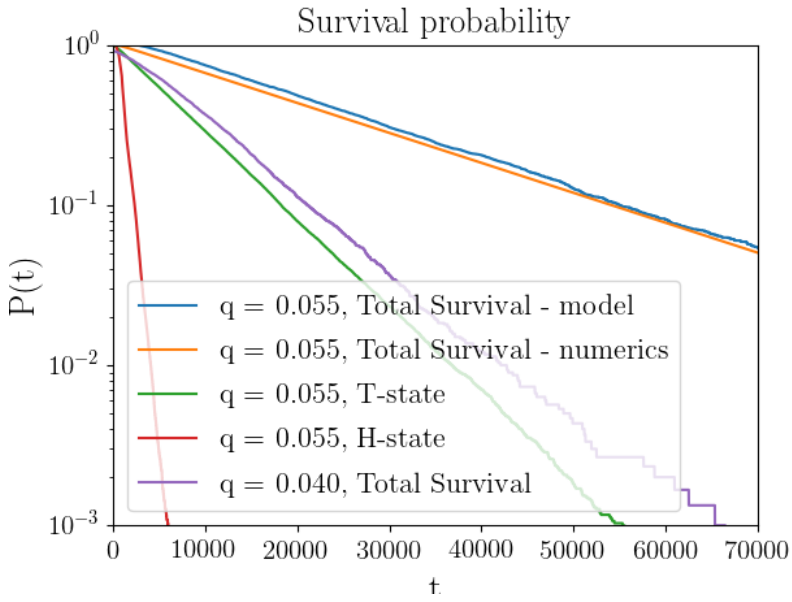

Figure 3.27 *The survival probabilities of the different turbulent T states, hibernating H states and total survival probability before relaminarising at $Re = 240$. The decay exponent of the total survival probability at $q = 0.040$, i.e. before the appearance of the periodic orbits where only the T state is possible, is very similar to the decay exponent of the T state at $q = 0.055$, at which the flow may enter the H state. This suggests that the presence of the H state does not alter the phase space topology of the T state.*

A closer inspection of the survival probability of the H state, displayed in Fig. 3.28, shows that a purely exponential distribution, as expected from a chaotic saddle, does not fully capture the entire shape of the distribution. There are two bumps in the distribution suggesting there are two processes with characteristic lifetimes that are occurring within the envelope of what is termed a H state decay.

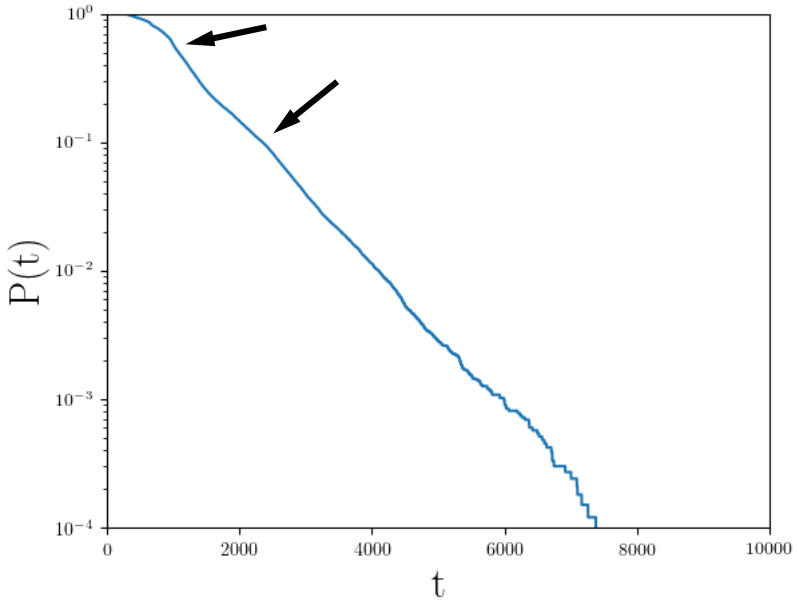

Figure 3.28 *The survival probability of the H state at $q = 0.055$ and $Re = 240$. The overall distribution shows the expected exponential relation of a chaotic saddle, though there are two bumps in the distribution. These suggest that there are events with characteristic lifetimes embedded within the overall H state lifetime.*

A decay from the T state that does not interact with the H state en route to the L state should relaminarise on a timescale that is characteristic of Re of the flow. This is as this process is governed by the viscous forces in the fluid which are of a constant comparative magnitude to the inertial forces that drive the turbulent state at constant Re.

Upon inspection of a sample of trajectories, the times taken for the trajectory to pass through the H-state without interacting and relaminarising do indeed cluster around the value of the first bump.

A selection of possible routes through the T and H domains are shown in Fig. 3.29.

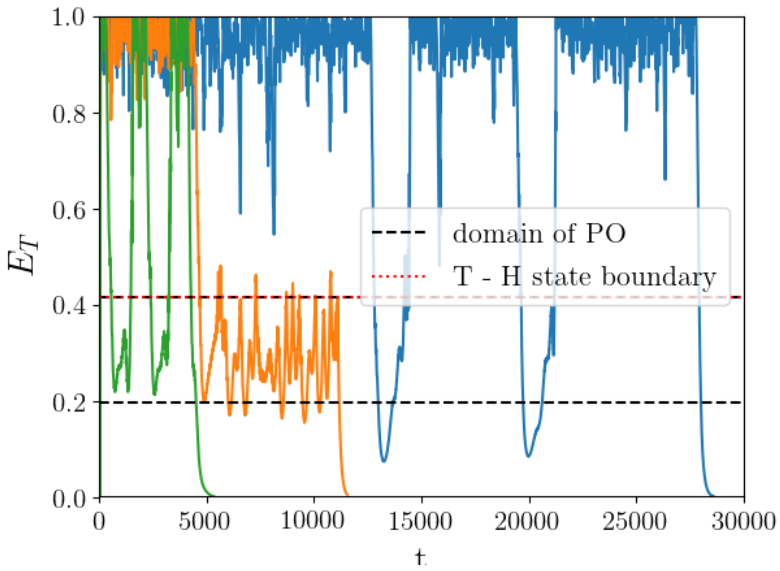

Figure 3.29 *Three typical turbulent trajectories at $q = 0.055$ and $Re = 240$. The green trajectory shows a $T \to H \to T \to H \to L$ sequence, the orange trajectory undergoes a $T \to H \to L$ and the blue trajectory undertakes a $T \to H \to T \to H \to T \to H \to L$ sequence. The domain of the periodic orbit is a chaotic saddle, with an associated memoryless decay process, but the splitting of the T and H states via the upper boundary of the domain of the PO means that two other interactions are captured within the H state lifetimes. These events are both shown in by the blue trajectory, the first is an excursion towards the laminar state that passes through the domain of the periodic orbit, but then gets reflected back in the portion of phase space between the periodic orbit and the edge state. The second is a relaminarisation event where the trajectory does not interact with the H state when passing from the T to L states.*

3.5 Discussion

The results from the investigation into the distributions of the velocity fluctuations show no discernible difference in the functional form of the tails of the $\langle dv_i^2 \rangle = \eta_{fluct}$ distributions between the 21 and 23 mode models. This, however, is perhaps not unsurprising as each model has an exponential scaling of τ versus Re. As such, these findings neither contradict nor verify the hypothesis of Goldenfeld *et al.* detailed in Section 1.1.6. The distribution of η_{fluct} for each model is indeed approximately Gaussian, which would support the use of the Gumbel distribution for describing the statistics of its extremal values. However, no conclusion can be

drawn as to its significance in relation to the lifetime scaling as both models still scale exponentially.

Instead, the findings of this chapter reveal that the lifetime scaling depends upon the degree of coupling between different SSP sites within the flow. The fact that the removal of either the SF or TS classes results in the same lifetime scaling exponent is a novel discovery, suggesting that the specific form of coupling between the SSPs (expressed through the modes couple them) is irrelevant to the specific organisation of the turbulent phase space that gives rise to the turbulent lifetime scaling behaviour. This poses the question, what is the minimal model required for a super-exponential scaling of τ with Re? Or is it even possible to replicate this phenomenon without the inclusion of spatio-temporal effects? It is perhaps likely that 'low' dimensional dynamics will not be able to reproduce this phenomenon, in a similar manner to how the model in [67] could not produce chaotic trajectories due to its limited dimension. Though this clearly affirms the obvious statement that an increase in dimensionality (of suitably chosen modes) corresponds to a increasingly realistic model. This then perhaps motivates the use of the numerical recipe from the previous chapter to intelligently select more modes to investigate the relationship between the further addition of SSP sites and coupling between such sites and the lifetime scaling with Re. This, however, likely takes any such model outside of what can be really called a low dimensional model, especially as the size of any analytical Jacobian required for a Newton-Raphson solver will scale with the square of dimensionality of the system.

The discovery of the periodic orbit embedded within the 23-dimensional phase space in this manner represents a novel framework with which to build upon the ideas of Chapter 2 to investigate features of the turbulence transition by isolating specific interactions between flow structures. Using the parameter q to investigate the change of the phase space has shown an analogous scenario to that found in [140], by which a stable periodic orbit undergoing a chaotic cascade followed by a boundary crisis increased the complexity of the chaotic saddle and hence increases the lengths of the trajectories caught within the domain of the manifold. The work presented in this chapter allows this phenomenon to be explicitly connected to a physical coupling between SSPs, enhancing our understanding of the shape of the turbulent phase space.

For plane Couette flow, a MFU short lived 'gentle' periodic orbit (with 1 unstable direction) that undergoes a boundary crisis with increased Re has been observed in numerical simulations [38]. This periodic orbit acts as the edge state for the

system and undergoes a period doubling route to chaos [154]. Transient chaos is then observed in the system when the chaotic attractor touches the domain of the orbit, creating a homoclinic tangency. This scenario resembles the observations of this chapter, with the parameter q pulling the two separate strange attractors together via increasing the coupling of the SSPs, leading to a much more repellent barrier between the laminar and turbulent portions of the phase space.

The fact that the division of the T-H boundary is somewhat coarse appears to have little effect on the validity of the three state model in describing the trajectories, as evidenced by how well the model-predicted survival probability matches the numerically extracted survival probability. As can be seen in Fig. 3.28, the bumps in the survival probability plot for the H state are small so are likely inconsequential in determining the total decay exponent.

As the orbit loses stability as q is increased, it has not been tracked to the $q = 1$ case. This makes it hard to explicitly state the effect the unstable periodic orbit has on the topology of the phase space in this regime. A better clue as to its significance is that for a q such that there is a range of stability in Re for the periodic orbit, then for Re higher than the point at which the orbit loses stability, the lifetime τ scales with the same exponent as the $q = 1$ case. This suggests that the for all q and Re beyond the point of stability for the periodic orbit the topology of the phase space can be thought of as containing the same dynamics. The difference in τ at constant Re for different values of q such that $q > q_c(Re)$ can be attributed to a smooth increase in coupling past the critical point of boundary crises between the two attractors.

The findings of this chapter build upon those from Chapter 2 in showing that the use of low dimensional models can isolate specific dynamical interactions in such a way that allows us to connect them to observed physical features and hence enhance our understanding of the transition.

Chapter 4

A low dimensional model of non-Newtonian turbulence

In recent years, there has been a wealth of experimental and numerical investigation into elasto-inertial turbulence. Various ideas have been proposed as to the nature of the phenomenon, and its relation to both Newtonian and purely elastic turbulence. To the author's knowledge, there have been no attempts to try and create a low dimensional model for non-Newtonian shear generated turbulence, therefore providing ample imperative to apply the techniques of the previous chapters to this problem. The Newtonian models of Chapter 2 behave as Oldroyd-B models, described by

$$Re\left(\frac{\partial \mathbf{v}}{\partial t}+\mathbf{v}\cdot\nabla\mathbf{v}\right)=\mathbf{f}-\nabla p+\beta\nabla^2\mathbf{v}+(1-\beta)\nabla\cdot\boldsymbol{\tau_p}, \tag{4.1}$$

$$\nabla\cdot\mathbf{v}=0, \tag{4.2}$$

$$\boldsymbol{\tau_p}+Wi\left(\frac{\partial \boldsymbol{\tau_p}}{\partial t}+\mathbf{v}\cdot\nabla\boldsymbol{\tau_p}-(\nabla\mathbf{v})^T\cdot\boldsymbol{\tau_p}-\boldsymbol{\tau_p}\cdot(\nabla\mathbf{v})\right)=(\nabla\mathbf{v})^T+\nabla\mathbf{v}, \tag{4.3}$$

as derived in Section 1.2.1, with $\beta = 1$. Here, β is used following convention to denote the property

$$\beta=\frac{\mu_s}{\mu_s+\mu_p}, \tag{4.4}$$

as opposed to the the similarly labelled β denoting the wall normal wavenumber. In these equations, Re is calculated using the total fluid viscosity, rather than solely the solvent.

As these equations collapse onto the incompressible Newtonian Navier-Stokes equations for $\beta = 1$, it is not unreasonable to use a model that well describes the Newtonian regime as a starting point for an investigation into the $\beta \approx 1$ region of phase space. This approach has been validated by the successful introduction of viscoelasticity upon Newtonian exact coherent structures to reproduce results from fully viscoelastic experiments in [122, 155].

The 23 mode model is especially relevant, as the 3-state intermittency displayed mirrors the observed flow behaviour in the elasto-inertial regime. This is compounded by the recent assertion that the MDR state is fundamentally of Newtonian nature [126, 127], motivating the search for a link between this state and any analogous one found in the non-Newtonian regime.

4.1 Adapting the Newtonian model

To investigate the ability of the 13 and 23 mode models to describe an elasto-inertial flow, the models had to be updated such that they obey the Oldroyd-B Navier-Stokes equations, as described in Section 1.2.1. The equations 4.1-4.3 were projected onto the modes, in the manner of equation 2.8, to generate a new set of equations that govern the time evolution of the velocity modes. To this end, stress modes must be introduced to be projected onto equation 4.3. These take the form

$$\mathbf{b}_i = \nabla \mathbf{a}_i + (\nabla \mathbf{a}_i)^T, \tag{4.5}$$

where $\mathbf{b}_i$ is the i^th stress mode and $\mathbf{a}_i$ is the corresponding velocity mode detailed in Appendix B.1, with the results of their projection found in Appendix B.2 for the 23 mode model. The modifications to the general form of the equations are that the velocity modes now receive an additional term such that

$$\frac{da_i}{dt} = -\frac{C\nu a_i}{Re} + \frac{C(\nu - 1)b_i}{Re} + F_i \tag{4.6}$$

where C is the constant of normalisation from equation 2.8, F_i denotes a quadratic non-linear coupling of velocity mode amplitudes and ν is a relabelling of β from equations 4.1-4.3 to avoid confusion with the wall normal wavelength. The

equations for the evolution of the stress modes take the form

$$\frac{db_i}{dt} = \frac{a_i}{Wi} - \frac{b_i}{Wi} + G_i, \tag{4.7}$$

where G_i denotes a quadratic non-linear coupling of stress and velocity modes. These modifications turn the 23 mode model into a 46 dimensional system which, combined with the smaller timestep size required for numerical stability of the stress mode equations, causes a vast increase in computational cost of this model.

4.2 The effect of Wi on lifetimes

The initial objective of this scheme of work was to investigate the effect of viscoelasticity on the lifetimes of the turbulent state using the models derived for plane Couette flow in Chapter 2. It is expected in this flow geometry that a fluid described by the Oldroyd-B model would display a delayed onset of the turbulent state in terms of the critical Re required to sustain it and shorter lifetimes of the turbulent state. Both of these features should arise from the suppression of the coherent structures that sustain turbulence by the MFU mechanism detailed in Section 1.2.3.

Initially, the 13 mode model was investigated, with the lifetime scaling results displayed in Fig. 4.1. These show the expected trend that the increase in Wi corresponds to a decrease in mean turbulent lifetime when comparing at the same Re. Additionally, the effect of the inclusion of viscoelasticity into the governing equations of the model is to elongate the region of stability of the periodic orbit that separates the turbulent and non-turbulent state space in the Re plane. This orbit is found to persist up to $Re = 121.4$ in the Newtonian case, whereas it remains stable up to $Re \approx 160$ for $Wi = 5$ and $\beta = 0.9$. This has the effect of delaying the onset of the turbulent state, following the expected phenomenology. Interestingly, this orbit was not detected at all for $Wi = 12$ and $\beta = 0.9$.

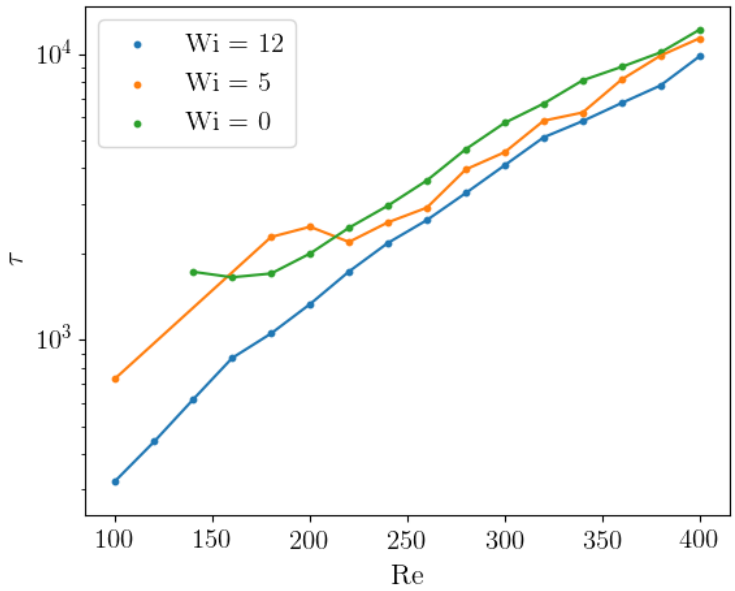

Figure 4.1 *The scaling relation of the mean turbulent lifetime τ versus Re for a range of Wi for the 13 mode model with $\beta = 0.90$. A stable periodic orbit is found between $120 < Re < 160$ for $Wi = 5$, which accounts for the bumps in lifetimes at $Re = 180, 200$, as though the orbit loses its stability, its strongly attracting domain persists in phase space. The points in the range of stability of the orbit have not been plotted. Once at Re high enough that the orbits do not affect the dynamics, the increase in Wi reduces the lifetime of the turbulent state when comparing for the same Re.*

The second investigation, concerning the 23 mode model, first sought to identify the effect that altering β makes upon the lifetime scaling behaviour with Re. The results from this investigation are shown in Fig. 4.2 and Fig. 4.3, for which the intermediate value $Wi = 4$ was used. These show that the scaling exponent is unchanged by β, at least in the range tested (which is typical of elasto-inertial turbulence), at a constant Wi. Once complete, a value of $\beta = 0.9$ was selected for the remainder of the investigation, allowing the results to be compared with the findings from the 13 mode model.

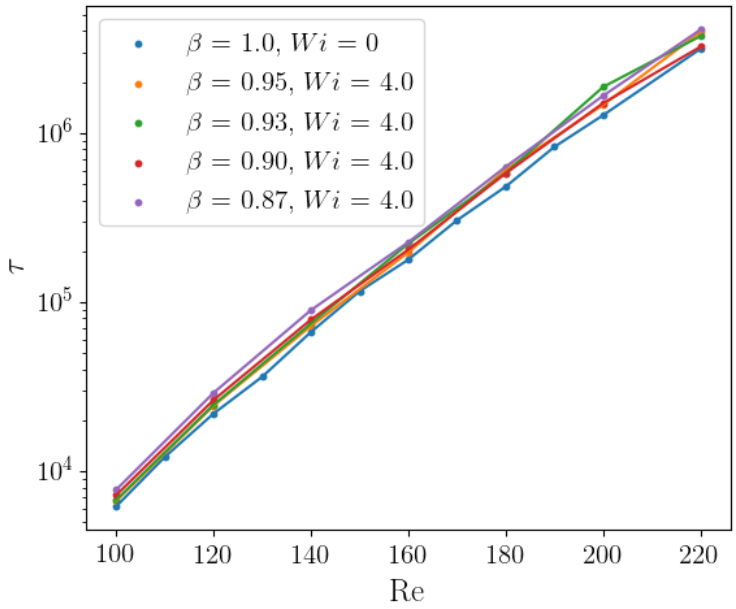

Figure 4.2 *The lifetime scaling for the 23 mode viscoelastic model for a range of β at $Wi = 4$. The scaling is shown to be completely unchanged by the choice of β, though all viscoelastic models have longer lifetimes than the $\beta = 1$, $Wi = 0$ case. This is the converse of what is found for the 13 mode model.*

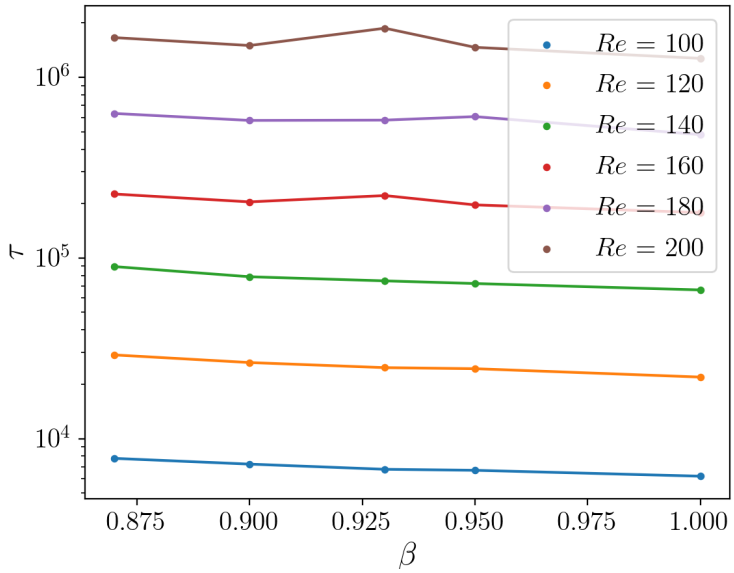

Figure 4.3 *The lifetime scaling for the 23 mode viscoelastic model for a range of β with $Wi = 4.0$.*

Replotting these results in Fig. 4.4 shows that for the 23 mode model, a decrease of β, corresponding to an increase in polymer concentration, causes an increase in the turbulent lifetime for $Wi = 4$ compared to the purely Newtonian state.

Following the line of investigation of the 13 mode model, the next relationship to investigate was the correlation between the turbulent lifetime τ and Wi for constant β, the results of which are shown in Fig. 4.4 and Fig. 4.5.

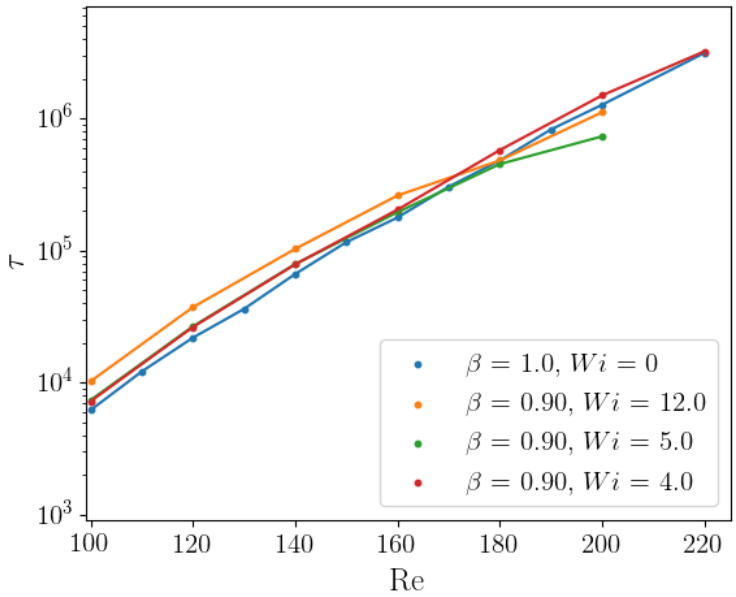

Figure 4.4 *The lifetime scaling for the 23 mode viscoelastic model for a range of Wi with $\beta = 0.9$. The scaling exponent is shown to be completely unchanged by the Wi.*

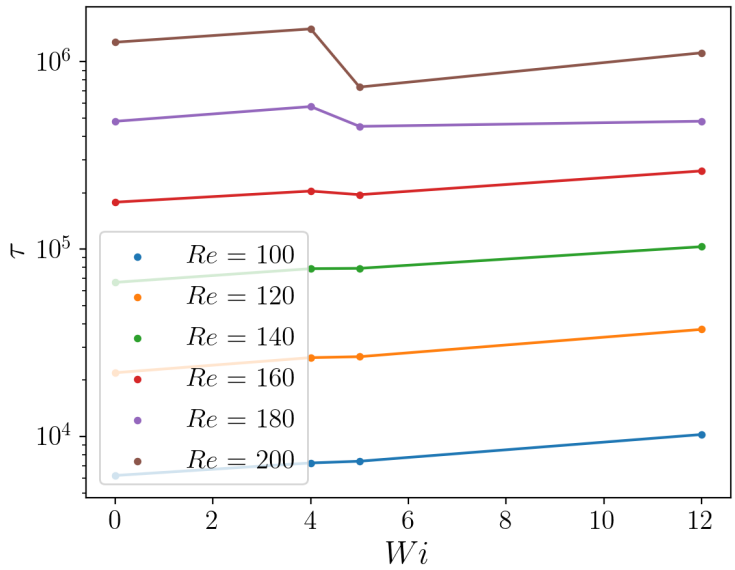

Figure 4.5 *The lifetime scaling for the 23 mode viscoelastic model for a range of Wi with $\beta = 0.9$.*

Interestingly, it appears that between $Re = 180$ and $Re = 200$, and $Wi = 4$ and $Wi = 5$, there is a change in the lifetime scaling behaviour with Wi.

For $Re < 180$, an increase in Wi causes an increase in the turbulent lifetime. However, the trend appears to change at $Re = 180$, with τ being lower for $Wi = 5$ than $Wi = 4$ for both $Re = 180$ and $Re = 200$. It is possible that this is merely a statistical effect, reflective of the progressively smaller datasets found as Re increases. However, a possible physical mechanism for this change could be the disappearance of a locally attracting structure in the elasto-inertial portion of phase between these points. To test this, sample trajectories were run at each of these points in phase space and the laminar mode amplitude a_8 tracked, though no qualitative difference could be observed. This implies the peaks are a manifestation of limited statistics when calculating τ, though this could be an interesting area for further study.

The results shown in Fig. 4.1 - Fig. 4.5 show that, as with the Newtonian case, the lifetimes are of several orders of magnitude longer in the 23 mode model than the 13 mode model. Both models also are characterised by a distinctive scaling exponent of the lifetime versus the Re, though curiously this appears to be unaffected by a change in Wi or β.

For the 23 mode model, the associated computational time to generate data due to the inherent numerical instability of the system requiring a suitably small numerical timestep, combined with the long lifetime of the turbulent state, has meant that only a low range of Re has been tested. This makes it hard to strongly infer anything from the dataset available. There may be some divergence of behaviour at higher Wi, Re or lower β, though this is an area of phase space difficult to efficiently probe with the current computational resources available.

4.3 Non-Newtonian coherent structures

A further line of study was to investigate the effect of viscoelasticity on the Newtonian coherent structures. It remains a question as to whether the dynamics in the elasto-inertial state is governed by structures that are dynamically connected to Newtonian coherent structures, or rather that new unconnected states appear, possibly with a connection to the purely elastic case instead.

The method used to locate the coherent structures was to generate a turbulent trajectory and then use its points in phase space as initial conditions for a Newton-Raphson solver, as in Section 2.5. Using this method, four coherent structures

were found at $Re = 400$, $Wi = 5$ and $\beta = 0.9$ for the 23 mode model. These states were found to be analogous to the four states found for the Newtonian case, but with small modifications to the exact mode values due to the presence of the viscoelasticity. This implies that the additional solutions resultant of the increase in system dimensionality via the stress modes are likely to be unstable periodic orbits and hence unable to be located via this regime.

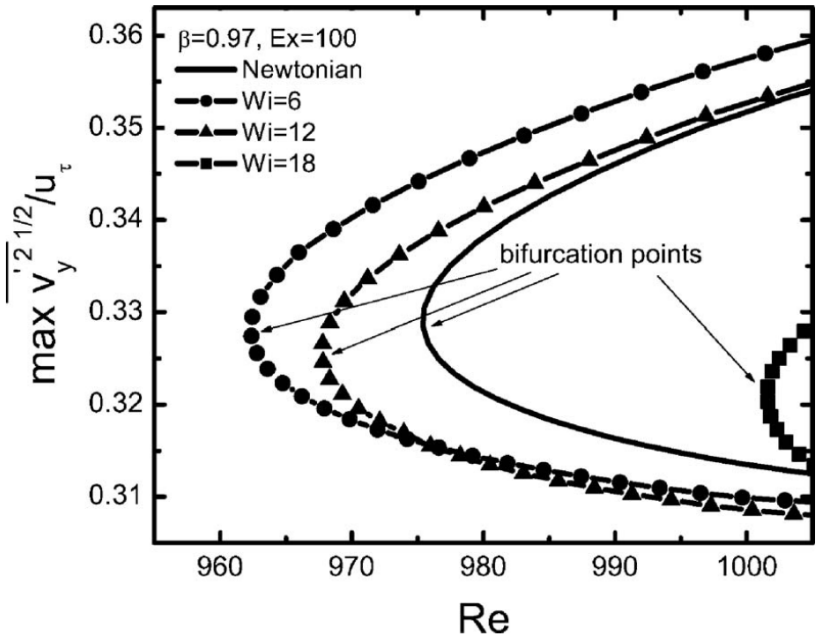

Figure 4.6 *The saddle point for a travelling wave ECS in the plane Poiseuille geometry. Here the y-axis denotes the maximum in the root mean square wall-normal velocity fluctuations for the solution. Reproduced with permission from [122].*

The saddle point at which the first coherent structures appear at could be traced in the Wi-Re plane to test how the model performs against the DNS results from [122] and [156], shown in Fig. 4.6 and Fig. 4.7 respectively. Here, a clear enhancement in the onset of the appearance of coherent structures is seen for Wi less than a threshold value, before a delay in the point of bifurcation at higher Re.

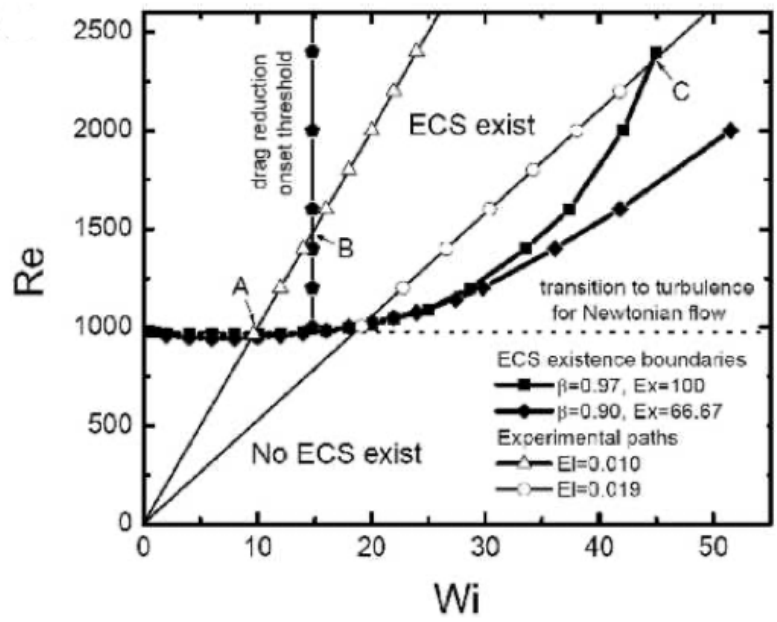

Figure 4.7 *The boundary between the portions of Wi-Re phase space in which ECS do and do not exist in the full DNS. Reproduced with permission from [156].*

Using a similar scheme to that described in Section 2.4.3, the coherent structures found previously could then be traced in the *Wi-Re* plane to find the location of the saddle point in this space. The results from this investigation for the first set of solutions to appear (the lower branch solutions) are shown in Fig. 4.8.

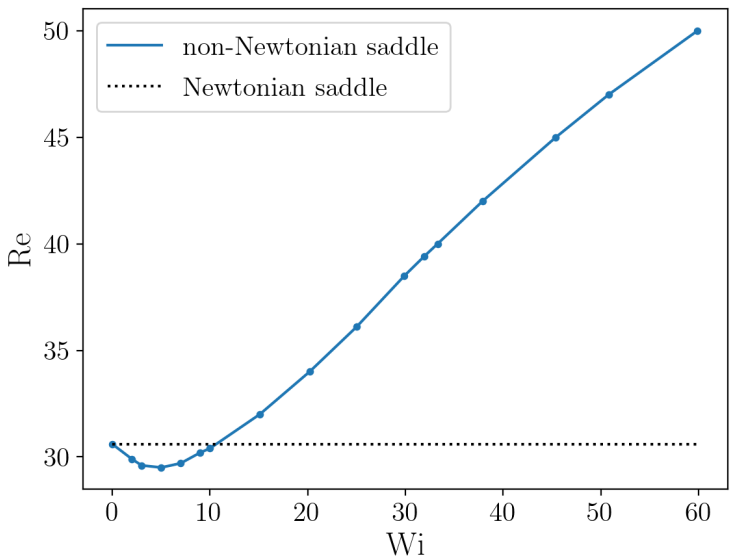

Figure 4.8 *The boundary between the portions of Wi-Re phase space in which ECS do and do not exist in the 23 mode model.*

Here the parabolic relationship between the Wi and Re from [156] is replicated up to $Wi = 30$, though for Wi greater than this value the relation appears to flatten off to a more logarithmic shape. In addition, the phenomena of low Wi values slightly enhancing the appearance of the saddle point is again replicated in the 23 mode model.

4.4 Discussion

Elucidating the origin of the phenomenon of drag reduction has been a topic of great theoretical and experimental interest over several preceding decades [115, 157–160]. As the transition to Newtonian turbulence is understood in terms of coherent structures within a dynamical systems context, a natural evolution of this idea is to study the effect of polymers on them with hope that this may aid in the understanding of the MDR state. Recent studies of this manner [24, 112, 161] have shown that polymer stretching by the coherent structures, especially the streamwise vortices, weakens said structures and consequentially suppresses the turbulent intensity.

These observations motivated the investigation detailed in this Chapter, specifically as to whether the low dimensional models derived in Chapter 2 display an interaction between the polymers and the coherent structures that suppresses the turbulent intensity and deforms the turbulent phase space. The results of this Chapter show that the results of tracking the saddle point of the coherent structures in Wi-Re space does indeed match the DNS results, by which an intermediate Wi enhances the appearance of the saddle point in Re, whilst at higher Wi the saddle point appears at higher Re. Despite this, surprisingly, we find little effect of the polymers on the turbulent lifetimes. As these are directly connected to the structure of the phase space, this implies the phase space undergoes some deformation, but not a discrete topological change as displayed for example in Chapter 3. This is most likely due to the fact that the stress modes included in the model are derived from Newtonian velocity modes and therefore cannot support the necessary structures to well describe this state.

An interesting further test would be to investigate the effect of increasing the Wi for fixed Re upon the 'hibernation frequency', the rate of excursions from the turbulent state towards the laminar domain. As shown in Fig. 4.5, an increase in Wi corresponds to an increase in τ, so it is therefore not unreasonable to assume

that the hibernation frequency will reduce. This test would serve to further probe how the effects of visco-elasticity deform the turbulent phase space.

Recent experiments [118, 162] demonstrate that the MDR state may be related to elasto-inertial turbulence, which is disconnected to the states accessible from a Newtonian derived model. The author suggests a possible line of further study is adapting the 23 mode model to describe this state or deriving a new low dimensional model with appropriate stress modes as an angle for future work in relation to this problem.

A similarly motivated additional investigation into the feasibility of adapting the 23 mode model into a purely elastic model was undertaken. The stress modes retained their form from equation 4.5, but as the Re term is taken to be small, it allows for some terms to be ignored from the velocity amplitude equations detailed in appendix A.3. The resulting form of the equations is

$$a_i = \frac{1-\beta}{\beta} b_i. \tag{4.8}$$

Eq. 4.8 allows for only the time evolution of the stress modes to be considered in a numerical time iteration algorithm, increasing its efficiency.

Several probes into the $\beta \approx 0.1$ and $Re \approx 0$ region of phase space were undertaken, but this regime was found to be extremely numerically unstable. A general trend of a perturbation igniting an oscillatory growth of the stress modes with an exponential envelope was recorded, though this could only be sustained for a short time before a numerical explosion. A further recommendation of continuing this investigation in a different region of purely elastic phase space or improving the numerical stability of the time iteration algorithm is made as a possible fruitful line of future investigations.

Chapter 5

Conclusions

The undertaking of this project was motivated by the recent progression of understanding that for both Newtonian and non-Newtonian turbulence, the phase space of the flow field is organised by states known as exact coherent structures. This discovery infers that, at least in the transition region, the dynamics of the turbulent state lie upon a somewhat low dimensional inertial manifold, and as such can be well modelled by the development of low dimensional models. This technique had been used in previous studies to produce a series of low dimensional models, with each iteration displaying greater analogy to the fully resolved system. These models however, have been created on an ad-hoc basis, often with intuition gained from full DNS of the system or high quality experimental data. This then posed the question; how can one develop a low dimensional model of a system without a priori knowledge about the turbulent state of said system?

The initial research aim of this project was to develop a recipe by which one can create a low dimensional model of a given flow without using intuition as to the useful analytical velocity modes for inclusion. In developing and testing this process, the recipe has been validated as a novel way with which to create a low dimensional model, and in addition the test model itself has furthered understanding of some features of the transition to turbulence. This model has been further extended to non-Newtonian turbulence domain, showing the use of the model generation technique beyond the standard incompressible Navier-Stokes equations.

The findings of Chapter 2 have shown how the exact spatial configuration of analytic velocity modes corresponds to the manner in which they couple with

other velocity modes after the Navier-Stokes equations have been projected on to them. The different combinations of these couplings alter the nature of the turbulent phase space, via the coupling of different SSP sites. The work of this Chapter has also revealed a wealth of coherent structures. Some of these are likely to be products of the reduced nature of the system, though they would however at least provide good initial conditions for the search for coherent structures in the fully resolved system.

Chapter 3 builds upon the findings of Chapter 2 by investigating how the coupling between SSP sites alters the turbulent portion of phase space. The SSPs are revealed to be coupled through classes of modes that non-linearly interact with SSPs of a different phase shift in space. A parameter q is introduced to control the coupling between two SSPs, encoded in a 23 mode model, of phase shift $\frac{\pi}{2}$ in the z direction. For a fixed Re, the behaviour of the model is categorised into 3 distinct domains; for $q < q_{lb}$, where q_{lb} is the q at which the orbit appears for a specific Re, the model behaves as partially coupled SSPs, for $q_{lb} < q < q_{ub}$, where q_{ub} is the upper limit of stability of the periodic orbit for a specific Re, there exists a stable attracting periodic orbit that captures some proportion of the initial conditions within its domain where they remain for infinite times, and for $q_{ub} < q < 1$ the turbulent phase space is analogous to that of two fully coupled SSPs. It is shown that the increase of q corresponds to pulling two chaotic saddles together to the point of a boundary crisis, which increases the complexity of the resulting chaotic domain, expressed through the creation of repelling structures that exist between the turbulent and laminar basins of attraction. This in turn causes an increase of the magnitude and scaling exponent of the turbulent lifetime.

In the intermediate range of q a strongly intermittent behaviour is displayed in the turbulent state, via excursions to an unstable state that lies between the turbulent attractor and the laminar state. This is shown to be remarkably well modelled via a 3-state system. This intermittency bears resemblance to the so-called hibernating turbulence phenomenon observed in elasto-inertial turbulence. This is especially interesting as recent work has suggested that the hibernating turbulence state is of a fully Newtonian nature.

These observations, combined with the success of previous studies using homotopy on Newtonian coherent structures in the viscoelastic case, motivated the investigation of the elasto-inertial turbulence regime using previously created low dimensional models. These were adapted via projecting the Navier-Stokes equations for an Oldroyd-B viscoelastic fluid onto the modes, creating new sets

of non-linear equations that govern the dynamics of the modes, which now necessarily also include stress modes, derived from the Newtonian velocity modes.

The effect of the addition of viscoelasticity was found to elongate the stability region of the stable periodic orbit that serves as the barrier between the turbulent and non-turbulent portions of phase space in the Re plane in the 13 mode model. For the range tested, modifying Wi or β did not change the scaling exponent of the turbulent lifetime τ versus Re, the measure we suppose gives a description of the topography of the turbulent phase space. These parameters do however deform the phase space to some extent, as they are seen to change the measured values of τ at specific Re. In addition, we have found that for the 23 mode model the location of the saddle point at which non-trivial unstable coherent structures appear at in Wi-Re space mirrors the expected relationship established by previous studies using full DNS. These observations serve as a promising starting point for further investigations into non-Newtonian turbulence via an updated version of the models derived in this Thesis, or a new model derived using the algorithm detailed in Chapter 2.

A final note is made towards the recent discovery of a Tollmien–Schlichting like mode possibly driving a self-sustaining process for the elasto-inertial turbulence state [163, 164]. A low dimensional model of the manner discussed in this Thesis would be an ideal tool with which to investigate the underlying dynamics of such a state, due its simplicity and the ease at which Tollmien–Schlichting like modes can be directly simulated through analytic Fourier modes. This avenue of research looks particularly fruitful due to the implied progression of understanding of elasto-inertial turbulence once a self-sustaining mechanism has been identified, analogous to the leap forward in understanding of Newtonian turbulence following the identification of its own self-sustaining process.

In conclusion, in relation to the initial scheme of work, as detailed in Section 1.3, all major objectives have been completed. This work may form the basis for further studies into both the Newtonian and non-Newtonian turbulence transition regimes, and has both answered and posed further questions about the nature of this state.

Appendix A

Chapter 2: Supplementary information

A.1 List of modes

Num.	Nrm.	u	v	w
u_1	$\sqrt{2}$	0	0	$\cos(2\beta y)$
u_2	$\sqrt{2}$	0	0	$\sin(\beta y)$
u_3	2	$\cos(2\beta y)\cos(\gamma z)$	0	0
u_4	2	$\cos(2\beta y)\sin(\gamma z)$	0	0
u_5	$\sqrt{2}$	$\cos(2\beta y)$	0	0
u_6	2	$\sin(\beta y)\cos(\gamma z)$	0	0
u_7	2	$\sin(\beta y)\sin(\gamma z)$	0	0
u_8	$\sqrt{2}$	$\sin(\beta y)$	0	0
u_9	$\sqrt{2}$	$\cos(\gamma z)$	0	0
u_{10}	$\sqrt{2}$	$\sin(\gamma z)$	0	0
u_{11}	$\frac{2}{K_{4\beta\gamma}}$	0	$\gamma\sin(2\beta y)\cos(\gamma z)$	$-2\beta\cos(2\beta y)\sin(\gamma z)$
u_{12}	$\frac{2}{K_{4\beta\gamma}}$	0	$\gamma\sin(2\beta y)\sin(\gamma z)$	$2\beta\cos(2\beta y)\cos(\gamma z)$
u_{13}	$\frac{2}{K_{\beta\gamma}}$	0	$\gamma\cos(\beta y)\cos(\gamma z)$	$\beta\sin(\beta y)\sin(\gamma z)$
u_{14}	$\frac{2}{K_{\beta\gamma}}$	0	$\gamma\cos(\beta y)\sin(\gamma z)$	$-\beta\sin(\beta y)\cos(\gamma z)$
u_{15}	$\sqrt{2}$	$\sin(3\beta y)$	0	0
u_{16}	2	0	0	$\cos(\alpha x)\sin(\beta y)$
u_{17}	2	0	0	$\sin(\alpha x)\sin(\beta y)$
u_{18}	$\frac{2\sqrt{2}}{K_{\alpha\gamma}}$	$\gamma\cos(\alpha x)\sin(\beta y)\cos(\gamma z)$	0	$\alpha\sin(\alpha x)\sin(\beta y)\sin(\gamma z)$
u_{19}	$\frac{2\sqrt{2}}{K_{\alpha\gamma}}$	$\gamma\cos(\alpha x)\sin(\beta y)\sin(\gamma z)$	0	$-\alpha\sin(\alpha x)\sin(\beta y)\cos(\gamma z)$
u_{20}	$\frac{2\sqrt{2}}{K_{\alpha\gamma}}$	$\gamma\sin(\alpha x)\sin(\beta y)\cos(\gamma z)$	0	$-\alpha\cos(\alpha x)\sin(\beta y)\sin(\gamma z)$
u_{21}	$\frac{2\sqrt{2}}{K_{\alpha\gamma}}$	$\gamma\sin(\alpha x)\sin(\beta y)\sin(\gamma z)$	0	$\alpha\cos(\alpha x)\sin(\beta y)\cos(\gamma z)$
u_{22}	$\frac{2}{K_{\alpha\gamma}}$	$\gamma\cos(\alpha x)\cos(\gamma z)$	0	$\alpha\sin(\alpha x)\sin(\gamma z)$

Num.	Nrm.	u	v	w
u_{23}	$\frac{2}{K_{\alpha\gamma}}$	$\gamma\cos(\alpha x)\sin(\gamma z)$	0	$-\alpha\sin(\alpha x)\cos(\gamma z)$
u_{24}	$\frac{2}{K_{\alpha\gamma}}$	$\gamma\sin(\alpha x)\cos(\gamma z)$	0	$-\alpha\cos(\alpha x)\sin(\gamma z)$
u_{25}	$\frac{2}{K_{\alpha\gamma}}$	$\gamma\sin(\alpha x)\sin(\gamma z)$	0	$\alpha\cos(\alpha x)\cos(\gamma z)$
u_{26}	$\frac{2\sqrt{2}}{K_{\beta\gamma}}$	0	$\gamma\cos(\alpha x)\cos(\beta y)\cos(\gamma z)$	$\beta\cos(\alpha x)\sin(\beta y)\sin(\gamma z)$
u_{27}	$\frac{2\sqrt{2}}{K_{\beta\gamma}}$	0	$\gamma\cos(\alpha x)\cos(\beta y)\sin(\gamma z)$	$-\beta\cos(\alpha x)\sin(\beta y)\cos(\gamma z)$
u_{28}	$\frac{2\sqrt{2}}{K_{\beta\gamma}}$	0	$\gamma\sin(\alpha x)\cos(\beta y)\cos(\gamma z)$	$\beta\sin(\alpha x)\sin(\beta y)\sin(\gamma z)$
u_{29}	$\frac{2\sqrt{2}}{K_{\beta\gamma}}$	0	$\gamma\sin(\alpha x)\cos(\beta y)\sin(\gamma z)$	$-\beta\sin(\alpha x)\sin(\beta y)\cos(\gamma z)$
u_{30}	$\frac{2}{K_{\alpha\beta}}$	$\beta\sin(\alpha x)\sin(\beta y)$	$\alpha\cos(\alpha x)\cos(\beta y)$	0
u_{31}	$\frac{2}{K_{\alpha\beta}}$	$-\beta\cos(\alpha x)\sin(\beta y)$	$\alpha\sin(\alpha x)\cos(\beta y)$	0
u_{32}	2	0	0	$\cos(\alpha x)\cos(2\beta y)$
u_{33}	2	0	0	$\cos(2\beta y)\sin(\alpha x)$
u_{34}	$\frac{2\sqrt{2}}{K_{\alpha\gamma}}$	$\gamma\cos(\alpha x)\cos(2\beta y)\cos(\gamma z)$	0	$\alpha\sin(\alpha x)\cos(2\beta y)\sin(\gamma z)$
u_{35}	$\frac{2\sqrt{2}}{K_{\alpha\gamma}}$	$\gamma\cos(\alpha x)\cos(2\beta y)\sin(\gamma z)$	0	$-\alpha\sin(\alpha x)\cos(2\beta y)\cos(\gamma z)$
u_{36}	$\frac{2\sqrt{2}}{K_{\alpha\gamma}}$	$\gamma\sin(\alpha x)\cos(2\beta y)\cos(\gamma z)$	0	$-\alpha\cos(\alpha x)\cos(2\beta y)\sin(\gamma z)$
u_{37}	$\frac{2\sqrt{2}}{K_{\alpha\gamma}}$	$\gamma\sin(\alpha x)\cos(2\beta y)\sin(\gamma z)$	0	$\alpha\cos(\alpha x)\cos(2\beta y)\cos(\gamma z)$
u_{38}	$\frac{2\sqrt{2}}{K_{4\beta\gamma}}$	0	$\gamma\cos(\alpha x)\sin(2\beta y)\cos(\gamma z)$	$2\beta\cos(\alpha x)\cos(2\beta y)\sin(\gamma z)$
u_{39}	$\frac{2\sqrt{2}}{K_{4\beta\gamma}}$	0	$\gamma\cos(\alpha x)\sin(2\beta y)\sin(\gamma z)$	$2\beta\cos(\alpha x)\cos(2\beta y)\cos(\gamma z)$
u_{40}	$\frac{2\sqrt{2}}{K_{4\beta\gamma}}$	0	$\gamma\sin(\alpha x)\sin(2\beta y)\cos(\gamma z)$	$-2\beta\sin(\alpha x)\cos(2\beta y)\sin(\gamma z)$
u_{41}	$\frac{2\sqrt{2}}{K_{4\beta\gamma}}$	0	$\gamma\sin(\alpha x)\sin(2\beta y)\sin(\gamma z)$	$2\beta\sin(\alpha x)\cos(2\beta y)\cos(\gamma z)$
u_{42}	$\frac{2}{K_{\alpha 4\beta}}$	$-2\beta\sin(\alpha x)\cos(2\beta y)$	$\alpha\cos(\alpha x)\sin(2\beta y)$	0
u_{43}	$\frac{2}{K_{\alpha 4\beta}}$	$2\beta\cos(\alpha x)\cos(2\beta y)$	$\alpha\sin(\alpha x)\sin(2\beta y)$	0
u_{44}	$\sqrt{2}$	0	0	$\cos(\alpha x)$
u_{45}	$\sqrt{2}$	0	0	$\sin(\alpha x)$

The solid line demarks the boundary between x-independent and x-dependent modes.

Where $K_{\alpha\beta} = \sqrt{\alpha^2+\beta^2}, K_{\alpha\gamma} = \sqrt{\alpha^2+\gamma^2}, K_{\beta\gamma} = \sqrt{\beta^2+\gamma^2}, K_{4\beta\gamma} = \sqrt{4\beta^2+\gamma^2}$ and $K_{\alpha 4\beta} = \sqrt{\alpha^2+4\beta^2}$.

A.2 Mode class interactions

The mode symmetry classes are defined as;

Name	Modes	Shift	Description
A_1	u_3, u_9, u_{13}	-	streaks and vortices
A_2	u_4, u_{10}, u_{14}	$A_1 - \frac{\pi}{2}$ in z	streaks and vortices
B_1	u_7, u_{12}	-	higher order vortex and streak
B_2	u_6, u_{11}	$B_1 + \frac{\pi}{2}$ in z	higher order vortex and streak
C_1	$u_{19}, u_{25}, u_{29}, u_{37}, u_{39}$	-	Kelvin-Helmholtz instability
C_2	$u_{21}, u_{23}, u_{27}, u_{35}, u_{41}$	$C_1 - \frac{\pi}{2}$ in x	Kelvin-Helmholtz instability
D_1	$u_{18}, u_{24}, u_{28}, u_{36}, u_{38}$		Kelvin-Helmholtz instability
D_2	$u_{20}, u_{22}, u_{26}, u_{34}, u_{40}$	$D_1 - \frac{\pi}{2}$ in x	Kelvin-Helmholtz instability
TS_1	u_{30}, u_{43}	-	Tollmien - Schlichting like vortices
TS_2	u_{31}, u_{42}	-	Tollmien - Schlichting like vortices
SF_1	u_{16}, u_{33}, u_{45}	-	spanwise flows
SF_2	u_{17}, u_{32}, u_{44}	$SF_1 - \frac{\pi}{2}$ in x	spanwise flows

Leaving modes u_1, u_2 and u_5 uncategorised. They are y-dependant modes with components in either the downstream x direction or spanwise z direction. As can be seen from the symbolic interactions below, these modes from 'connectors' that allow energy transfer between different classes of modes.

The time evolution of the symmetry classes for the full set of 45 modes is defined by the following interactions;

$$\frac{dA_1}{dt} = F(A_1, LA_1, u_1A_2, u_2B_1, u_5B_2, C_1SF_1, C_2SF_2, D_1TS_1, D_2TS_2)$$
$$\frac{dA_2}{dt} = F(A_2, LA_2, u_1A_1, u_2B_2, u_5B_1, C_1TS_1, C_2TS_2, D_1SF_1, D_2SF_2)$$
$$\frac{dB_1}{dt} = F(B_1, LB_1, u_1B_2, u_2A_1, u_5A_2, C_1TS_2, C_2TS_1, D_1SF_2, D_2SF_1)$$
$$\frac{dB_2}{dt} = F(B_2, LB_2, u_1B_1, u_2A_2, u_5A_1, C_1SF_2, C_2SF_1, D_1TS_2, D_2TS_1)$$
$$\frac{dC_1}{dt} = F(C_1, LC_1, u_1D_1, u_2D_2, u_5C_2, A_1SF_1, A_2TS_1, B_1TS_2, B_2SF_2)$$
$$\frac{dC_2}{dt} = F(C_2, LC_2, u_1D_2, u_2D_1, u_5C_1, A_1SF_2, A_2TS_2, B_1TS_1, B_2SF_1)$$
$$\frac{dD_1}{dt} = F(D_1, LD_1, u_1C_1, u_2C_2, u_5D_2, A_1TS_1, A_2SF_1, B_1SF_2, B_2TS_2)$$
$$\frac{dD_2}{dt} = F(D_2, LD_2, u_1C_2, u_2C_1, u_5D_1, A_1TS_2, A_2SF_2, B_1SF_1, B_2TS_1)$$
$$\frac{dTS_1}{dt} = F(TS_1, LTS_1, u_5TS_2, A_1D_1, A_2C_1, B_1C_2, B_2D_2)$$
$$\frac{dTS_2}{dt} = F(TS_2, LTS_2, u_5TS_1, A_1D_2, A_2C_2, B_1C_1, B_2D_1)$$
$$\frac{dSF_1}{dt} = F(SF_1, LSF_1, u_1TS_1, u_2TS_2, u_5SF_2, A_1C_1, A_2D_1, B_1D_2, B_2C_2)$$
$$\frac{dSF_2}{dt} = F(SF_2, LSF_2, u_1TS_2, u_2TS_1, u_5SF_1, A_1C_2, A_2D_2, B_1D_1, B_2C_1)$$
$$\frac{du_1}{dt} = F(u_1, C_1D_1, C_2D_2, TS_1SF_1, TS_2SF_2)$$
$$\frac{du_2}{dt} = F(u_2, A_1B_1, A_2B_2, C_1D_2, C_2D_1, SF_1TS_2, SF_2TS_1)$$
$$\frac{du_5}{dt} = F(u_5, A_1B_2, A_2B_1, C_1C_2, D_1D_2,)$$

A.3 List of velocity mode equations

$$\begin{aligned}\frac{da_1}{dt} =& -\frac{4\beta^2 a_1}{\mathrm{Re}} - \frac{\sqrt{2}\alpha\beta\gamma a_{21}a_{26}}{K_{\alpha\gamma}K_{\beta\gamma}} + \frac{\sqrt{2}\alpha\beta\gamma a_{20}a_{27}}{K_{\alpha\gamma}K_{\beta\gamma}} + \frac{\sqrt{2}\alpha\beta\gamma a_{19}a_{28}}{K_{\alpha\gamma}K_{\beta\gamma}} - \frac{\sqrt{2}\alpha\beta\gamma a_{18}a_{29}}{K_{\alpha\gamma}K_{\beta\gamma}} - \frac{2\alpha\beta\gamma a_{25}a_{38}}{K_{\alpha\gamma}K_{4\beta\gamma}} \\ &+ \frac{2\alpha\beta\gamma a_{24}a_{39}}{K_{\alpha\gamma}K_{4\beta\gamma}} + \frac{2\alpha\beta\gamma a_{23}a_{40}}{K_{\alpha\gamma}K_{4\beta\gamma}} - \frac{2\alpha\beta\gamma a_{22}a_{41}}{K_{\alpha\gamma}K_{4\beta\gamma}} - \frac{\sqrt{2}\alpha\beta a_{16}a_{30}}{K_{\alpha\beta}} - \frac{\sqrt{2}\alpha\beta a_{17}a_{31}}{K_{\alpha\beta}} - \frac{2\sqrt{2}\alpha\beta a_{42}a_{44}}{K_{\alpha4\beta}} \\ &- \frac{2\alpha\beta a_{43}a_{45}}{K_{\alpha4\beta}}\end{aligned}$$

$$\begin{aligned}\frac{da_2}{dt} =& -\frac{a_2\beta^2}{\mathrm{Re}} + \frac{3\gamma a_{12}a_{13}\beta^2}{\sqrt{2}K_{\beta\gamma}K_{4\beta\gamma}} - \frac{3\gamma a_{11}a_{14}\beta^2}{\sqrt{2}K_{\beta\gamma}K_{4\beta\gamma}} - \frac{3\gamma a_{27}a_{38}\beta^2}{\sqrt{2}K_{\beta\gamma}K_{4\beta\gamma}} + \frac{3\gamma a_{26}a_{39}\beta^2}{\sqrt{2}K_{\beta\gamma}K_{4\beta\gamma}} - \frac{3\gamma a_{29}a_{40}\beta^2}{\sqrt{2}K_{\beta\gamma}K_{4\beta\gamma}} \\ &+ \frac{3\gamma a_{28}a_{41}\beta^2}{\sqrt{2}K_{\beta\gamma}K_{4\beta\gamma}} + \frac{\alpha\gamma a_{25}a_{26}\beta}{K_{\alpha\gamma}K_{\beta\gamma}} - \frac{\alpha\gamma a_{24}a_{27}\beta}{K_{\alpha\gamma}K_{\beta\gamma}} - \frac{\alpha\gamma a_{23}a_{28}\beta}{K_{\alpha\gamma}K_{\beta\gamma}} + \frac{\alpha\gamma a_{22}a_{29}\beta}{K_{\alpha\gamma}K_{\beta\gamma}} + \frac{\alpha a_{30}a_{32}\beta}{\sqrt{2}K_{\alpha\beta}} \\ &+ \frac{\alpha a_{31}a_{33}\beta}{\sqrt{2}K_{\alpha\beta}} + \frac{\alpha\gamma a_{29}a_{34}\beta}{\sqrt{2}K_{\alpha\gamma}K_{\beta\gamma}} - \frac{\alpha\gamma a_{28}a_{35}\beta}{\sqrt{2}K_{\alpha\gamma}K_{\beta\gamma}} - \frac{\alpha\gamma a_{27}a_{36}\beta}{\sqrt{2}K_{\alpha\gamma}K_{\beta\gamma}} + \frac{\alpha\gamma a_{26}a_{37}\beta}{\sqrt{2}K_{\alpha\gamma}K_{\beta\gamma}} + \frac{\alpha\gamma a_{21}a_{38}\beta}{\sqrt{2}K_{\alpha\gamma}K_{4\beta\gamma}} \\ &- \frac{\alpha\gamma a_{20}a_{39}\beta}{\sqrt{2}K_{\alpha\gamma}K_{4\beta\gamma}} - \frac{\alpha\gamma a_{19}a_{40}\beta}{\sqrt{2}K_{\alpha\gamma}K_{4\beta\gamma}} + \frac{\alpha\gamma a_{18}a_{41}\beta}{\sqrt{2}K_{\alpha\gamma}K_{4\beta\gamma}} + \frac{\alpha a_{16}a_{42}\beta}{K_{\alpha4\beta}} + \frac{\alpha a_{17}a_{43}\beta}{\sqrt{2}K_{\alpha4\beta}} \\ &+ \frac{\alpha a_{30}a_{44}\beta}{K_{\alpha\beta}} + \frac{\alpha a_{31}a_{45}\beta}{K_{\alpha\beta}}\end{aligned}$$

$$\begin{aligned}\frac{da_3}{dt} =& \frac{4\gamma\Omega a_{13}}{3\pi\mathrm{Re}K_{\beta\gamma}} - \frac{4\beta^2 a_3}{\mathrm{Re}} - \frac{\gamma^2 a_3}{\mathrm{Re}} - \frac{\beta^2\gamma a_{28}a_{30}}{\sqrt{2}K_{\alpha\beta}K_{\beta\gamma}} + \frac{\beta^2\gamma a_{26}a_{31}}{\sqrt{2}K_{\alpha\beta}K_{\beta\gamma}} - \frac{\alpha\beta\gamma a_{18}a_{30}}{\sqrt{2}K_{\alpha\beta}K_{\alpha\gamma}} \\ &- \frac{\alpha\beta\gamma a_{20}a_{31}}{\sqrt{2}K_{\alpha\beta}K_{\alpha\gamma}} + \frac{\gamma^2 a_{16}a_{19}}{\sqrt{2}K_{\alpha\gamma}} + \frac{\gamma^2 a_{17}a_{21}}{\sqrt{2}K_{\alpha\gamma}} - \frac{\gamma^2 a_{23}a_{32}}{K_{\alpha\gamma}} - \frac{\gamma^2 a_{25}a_{33}}{K_{\alpha\gamma}} - \frac{\gamma^2 a_{35}a_{44}}{K_{\alpha\gamma}} - \frac{\gamma^2 a_{37}a_{45}}{K_{\alpha\gamma}} \\ &- \frac{\beta\gamma a_8 a_{13}}{\sqrt{2}K_{\beta\gamma}} - \frac{3\beta\gamma a_{13}a_{15}}{\sqrt{2}K_{\beta\gamma}} + \frac{\gamma a_2 a_7}{\sqrt{2}} - \gamma a_1 a_{10}\end{aligned}$$

$$\begin{aligned}\frac{da_4}{dt} =& \frac{4\gamma\Omega a_{14}}{3\pi\mathrm{Re}K_{\beta\gamma}} - \frac{4\beta^2 a_4}{\mathrm{Re}} - \frac{\gamma^2 a_4}{\mathrm{Re}} - \frac{\beta^2\gamma a_{29}a_{30}}{\sqrt{2}K_{\alpha\beta}K_{\beta\gamma}} + \frac{\beta^2\gamma a_{27}a_{31}}{\sqrt{2}K_{\alpha\beta}K_{\beta\gamma}} - \frac{\alpha\beta\gamma a_{19}a_{30}}{\sqrt{2}K_{\alpha\beta}K_{\alpha\gamma}} \\ &- \frac{\alpha\beta\gamma a_{21}a_{31}}{\sqrt{2}K_{\alpha\beta}K_{\alpha\gamma}} - \frac{\gamma^2 a_{16}a_{18}}{\sqrt{2}K_{\alpha\gamma}} - \frac{\gamma^2 a_{17}a_{20}}{\sqrt{2}K_{\alpha\gamma}} + \frac{\gamma^2 a_{22}a_{32}}{K_{\alpha\gamma}} + \frac{\gamma^2 a_{24}a_{33}}{K_{\alpha\gamma}} + \frac{\gamma^2 a_{34}a_{44}}{K_{\alpha\gamma}} + \frac{\gamma^2 a_{36}a_{45}}{K_{\alpha\gamma}} \\ &- \frac{\beta\gamma a_8 a_{14}}{\sqrt{2}K_{\beta\gamma}} - \frac{3\beta\gamma a_{14}a_{15}}{\sqrt{2}K_{\beta\gamma}} - \frac{\gamma a_2 a_6}{\sqrt{2}} + \gamma a_1 a_9\end{aligned}$$

$$\frac{da_5}{dt} = -\frac{4\beta^2 a_5}{\mathrm{Re}} - \frac{\sqrt{2}\beta\gamma^2 a_{18}a_{26}}{K_{\alpha\gamma}K_{\beta\gamma}} - \frac{\sqrt{2}\beta\gamma^2 a_{19}a_{27}}{K_{\alpha\gamma}K_{\beta\gamma}} - \frac{\sqrt{2}\beta\gamma^2 a_{20}a_{28}}{K_{\alpha\gamma}K_{\beta\gamma}} - \frac{\sqrt{2}\beta\gamma^2 a_{21}a_{29}}{K_{\alpha\gamma}K_{\beta\gamma}} - \frac{2\beta\gamma^2 a_{22}a_{38}}{K_{\alpha\gamma}K_{4\beta\gamma}}$$
$$- \frac{2\beta\gamma^2 a_{23}a_{39}}{K_{\alpha\gamma}K_{4\beta\gamma}} - \frac{2\beta\gamma^2 a_{24}a_{40}}{K_{\alpha\gamma}K_{4\beta\gamma}} - \frac{2\beta\gamma^2 a_{25}a_{41}}{K_{\alpha\gamma}K_{4\beta\gamma}} - \frac{2\beta\gamma a_9 a_{11}}{K_{4\beta\gamma}} - \frac{2\beta\gamma a_{10}a_{12}}{K_{4\beta\gamma}} - \frac{\sqrt{2}\beta\gamma a_6 a_{13}}{K_{\beta\gamma}}$$
$$- \frac{\sqrt{2}\beta\gamma a_7 a_{14}}{K_{\beta\gamma}}$$

$$\frac{da_6}{dt} = \frac{8\gamma\Omega a_{11}}{3\pi\mathrm{Re}K_{4\beta\gamma}} - \frac{\beta^2 a_6}{\mathrm{Re}} - \frac{\gamma^2 a_6}{\mathrm{Re}} + \frac{\beta^2\gamma a_{31}a_{38}}{\sqrt{2}K_{\alpha\beta}K_{4\beta\gamma}} - \frac{\beta^2\gamma a_{30}a_{40}}{\sqrt{2}K_{\alpha\beta}K_{4\beta\gamma}} - \frac{4\beta^2\gamma a_{28}a_{42}}{K_{\alpha4\beta}K_{\beta\gamma}} + \frac{2\sqrt{2}\beta^2\gamma a_{26}a_{43}}{K_{\alpha4\beta}K_{\beta\gamma}}$$
$$+ \frac{\sqrt{2}\alpha\beta\gamma a_{30}a_{34}}{K_{\alpha\beta}K_{\alpha\gamma}} + \frac{\sqrt{2}\alpha\beta\gamma a_{31}a_{36}}{K_{\alpha\beta}K_{\alpha\gamma}} - \frac{\alpha\beta\gamma a_{18}a_{42}}{K_{\alpha4\beta}K_{\alpha\gamma}} - \frac{\alpha\beta\gamma a_{20}a_{43}}{\sqrt{2}K_{\alpha4\beta}K_{\alpha\gamma}} - \frac{\gamma^2 a_{16}a_{23}}{K_{\alpha\gamma}} - \frac{\gamma^2 a_{17}a_{25}}{K_{\alpha\gamma}}$$
$$+ \frac{\gamma^2 a_{19}a_{32}}{\sqrt{2}K_{\alpha\gamma}} + \frac{\gamma^2 a_{21}a_{33}}{\sqrt{2}K_{\alpha\gamma}} + \frac{\gamma^2 a_{16}a_{35}}{\sqrt{2}K_{\alpha\gamma}} + \frac{\gamma^2 a_{17}a_{37}}{\sqrt{2}K_{\alpha\gamma}} - \frac{\gamma^2 a_{19}a_{44}}{K_{\alpha\gamma}} - \frac{\gamma^2 a_{21}a_{45}}{K_{\alpha\gamma}} - \frac{\beta\gamma a_8 a_{11}}{\sqrt{2}K_{4\beta\gamma}} + \frac{\sqrt{2}\beta\gamma a_5 a_{13}}{K_{\beta\gamma}}$$
$$+ \frac{3\beta\gamma a_{11}a_{15}}{\sqrt{2}K_{4\beta\gamma}} + \frac{\gamma a_2 a_4}{\sqrt{2}} + \frac{\gamma a_1 a_7}{\sqrt{2}} - \gamma a_2 a_{10}$$

$$\frac{da_7}{dt} = \frac{8\gamma\Omega a_{12}}{3\pi\mathrm{Re}K_{4\beta\gamma}} - \frac{\beta^2 a_7}{\mathrm{Re}} - \frac{\gamma^2 a_7}{\mathrm{Re}} + \frac{\beta^2\gamma a_{31}a_{39}}{\sqrt{2}K_{\alpha\beta}K_{4\beta\gamma}} - \frac{\beta^2\gamma a_{30}a_{41}}{\sqrt{2}K_{\alpha\beta}K_{4\beta\gamma}} - \frac{4\beta^2\gamma a_{29}a_{42}}{K_{\alpha4\beta}K_{\beta\gamma}} + \frac{2\sqrt{2}\beta^2\gamma a_{27}a_{43}}{K_{\alpha4\beta}K_{\beta\gamma}}$$
$$+ \frac{\sqrt{2}\alpha\beta\gamma a_{30}a_{35}}{K_{\alpha\beta}K_{\alpha\gamma}} + \frac{\sqrt{2}\alpha\beta\gamma a_{31}a_{37}}{K_{\alpha\beta}K_{\alpha\gamma}} - \frac{\alpha\beta\gamma a_{19}a_{42}}{K_{\alpha4\beta}K_{\alpha\gamma}} - \frac{\alpha\beta\gamma a_{21}a_{43}}{\sqrt{2}K_{\alpha4\beta}K_{\alpha\gamma}} + \frac{\gamma^2 a_{16}a_{22}}{K_{\alpha\gamma}} + \frac{\gamma^2 a_{17}a_{24}}{K_{\alpha\gamma}}$$
$$- \frac{\gamma^2 a_{18}a_{32}}{\sqrt{2}K_{\alpha\gamma}} - \frac{\gamma^2 a_{20}a_{33}}{\sqrt{2}K_{\alpha\gamma}} - \frac{\gamma^2 a_{16}a_{34}}{\sqrt{2}K_{\alpha\gamma}} - \frac{\gamma^2 a_{17}a_{36}}{\sqrt{2}K_{\alpha\gamma}} + \frac{\gamma^2 a_{18}a_{44}}{K_{\alpha\gamma}} + \frac{\gamma^2 a_{20}a_{45}}{K_{\alpha\gamma}} - \frac{\beta\gamma a_8 a_{12}}{\sqrt{2}K_{4\beta\gamma}} + \frac{\sqrt{2}\beta\gamma a_5 a_{14}}{K_{\beta\gamma}}$$
$$+ \frac{3\beta\gamma a_{12}a_{15}}{\sqrt{2}K_{4\beta\gamma}} - \frac{\gamma a_2 a_3}{\sqrt{2}} - \frac{\gamma a_1 a_6}{\sqrt{2}} + \gamma a_2 a_9$$

$$\frac{da_8}{dt} = -\frac{\beta^2 a_8}{\mathrm{Re}} + \frac{\beta\gamma^2 a_{22}a_{26}}{K_{\alpha\gamma}K_{\beta\gamma}} + \frac{\beta\gamma^2 a_{23}a_{27}}{K_{\alpha\gamma}K_{\beta\gamma}} + \frac{\beta\gamma^2 a_{24}a_{28}}{K_{\alpha\gamma}K_{\beta\gamma}} + \frac{\beta\gamma^2 a_{25}a_{29}}{K_{\alpha\gamma}K_{\beta\gamma}} + \frac{\beta\gamma^2 a_{26}a_{34}}{\sqrt{2}K_{\alpha\gamma}K_{\beta\gamma}} + \frac{\beta\gamma^2 a_{27}a_{35}}{\sqrt{2}K_{\alpha\gamma}K_{\beta\gamma}}$$
$$+ \frac{\beta\gamma^2 a_{28}a_{36}}{\sqrt{2}K_{\alpha\gamma}K_{\beta\gamma}} + \frac{\beta\gamma^2 a_{29}a_{37}}{\sqrt{2}K_{\alpha\gamma}K_{\beta\gamma}} + \frac{\beta\gamma^2 a_{18}a_{38}}{\sqrt{2}K_{\alpha\gamma}K_{4\beta\gamma}} + \frac{\beta\gamma^2 a_{19}a_{39}}{\sqrt{2}K_{\alpha\gamma}K_{4\beta\gamma}} + \frac{\beta\gamma^2 a_{20}a_{40}}{\sqrt{2}K_{\alpha\gamma}K_{4\beta\gamma}} + \frac{\beta\gamma^2 a_{21}a_{41}}{\sqrt{2}K_{\alpha\gamma}K_{4\beta\gamma}}$$
$$- \frac{3\alpha\beta^2 a_{31}a_{42}}{K_{\alpha\beta}K_{\alpha4\beta}} + \frac{3\alpha\beta^2 a_{30}a_{43}}{\sqrt{2}K_{\alpha\beta}K_{\alpha4\beta}} + \frac{\beta\gamma a_6 a_{11}}{\sqrt{2}K_{4\beta\gamma}} + \frac{\beta\gamma a_7 a_{12}}{\sqrt{2}K_{4\beta\gamma}} + \frac{\beta\gamma a_3 a_{13}}{\sqrt{2}K_{\beta\gamma}} + \frac{\beta\gamma a_9 a_{13}}{K_{\beta\gamma}} + \frac{\beta\gamma a_4 a_{14}}{\sqrt{2}K_{\beta\gamma}}$$
$$+ \frac{\beta\gamma a_{10}a_{14}}{K_{\beta\gamma}} + \frac{\beta^2}{\mathrm{Re}}$$

$$\frac{da_9}{dt} = \frac{2\sqrt{2}\gamma\Omega a_{13}}{\pi\mathrm{Re}K_{\beta\gamma}} - \frac{\gamma^2 a_9}{\mathrm{Re}} - \frac{\beta^2\gamma a_{28}a_{30}}{K_{\alpha\beta}K_{\beta\gamma}} + \frac{\beta^2\gamma a_{26}a_{31}}{K_{\alpha\beta}K_{\beta\gamma}} - \frac{4\sqrt{2}\beta^2\gamma a_{40}a_{42}}{K_{\alpha4\beta}K_{4\beta\gamma}} + \frac{4\beta^2\gamma a_{38}a_{43}}{K_{\alpha4\beta}K_{4\beta\gamma}} - \frac{\alpha\beta\gamma a_{18}a_{30}}{K_{\alpha\beta}K_{\alpha\gamma}}$$
$$- \frac{\alpha\beta\gamma a_{20}a_{31}}{K_{\alpha\beta}K_{\alpha\gamma}} + \frac{2\sqrt{2}\alpha\beta\gamma a_{34}a_{42}}{K_{\alpha4\beta}K_{\alpha\gamma}} + \frac{2\alpha\beta\gamma a_{36}a_{43}}{K_{\alpha4\beta}K_{\alpha\gamma}} - \frac{\gamma^2 a_{16}a_{19}}{K_{\alpha\gamma}} - \frac{\gamma^2 a_{17}a_{21}}{K_{\alpha\gamma}} - \frac{\gamma^2 a_{32}a_{35}}{K_{\alpha\gamma}} - \frac{\gamma^2 a_{33}a_{37}}{K_{\alpha\gamma}}$$
$$- \frac{\gamma^2 a_{23}a_{44}}{K_{\alpha\gamma}} - \frac{\gamma^2 a_{25}a_{45}}{K_{\alpha\gamma}} + \frac{2\beta\gamma a_5 a_{11}}{K_{4\beta\gamma}} - \frac{\beta\gamma a_8 a_{13}}{K_{\beta\gamma}} - \gamma a_1 a_4 - \gamma a_2 a_7$$

$$\frac{da_{10}}{dt} = \frac{2\sqrt{2}\gamma\Omega a_{14}}{\pi \mathrm{Re} K_{\beta\gamma}} - \frac{\gamma^2 a_{10}}{\mathrm{Re}} - \frac{\beta^2\gamma a_{29}a_{30}}{K_{\alpha\beta}K_{\beta\gamma}} + \frac{\beta^2\gamma a_{27}a_{31}}{K_{\alpha\beta}K_{\beta\gamma}} - \frac{4\sqrt{2}\beta^2\gamma a_{41}a_{42}}{K_{\alpha4\beta}K_{4\beta\gamma}} + \frac{4\beta^2\gamma a_{39}a_{43}}{K_{\alpha4\beta}K_{4\beta\gamma}}$$
$$- \frac{\alpha\beta\gamma a_{19}a_{30}}{K_{\alpha\beta}K_{\alpha\gamma}} - \frac{\alpha\beta\gamma a_{21}a_{31}}{K_{\alpha\beta}K_{\alpha\gamma}} + \frac{2\sqrt{2}\alpha\beta\gamma a_{35}a_{42}}{K_{\alpha4\beta}K_{\alpha\gamma}} + \frac{2\alpha\beta\gamma a_{37}a_{43}}{K_{\alpha4\beta}K_{\alpha\gamma}} + \frac{\gamma^2 a_{16}a_{18}}{K_{\alpha\gamma}} + \frac{\gamma^2 a_{17}a_{20}}{K_{\alpha\gamma}}$$
$$+ \frac{\gamma^2 a_{32}a_{34}}{K_{\alpha\gamma}} + \frac{\gamma^2 a_{33}a_{36}}{K_{\alpha\gamma}} + \frac{\gamma^2 a_{22}a_{44}}{K_{\alpha\gamma}} + \frac{\gamma^2 a_{24}a_{45}}{K_{\alpha\gamma}} + \frac{2\beta\gamma a_5 a_{12}}{K_{4\beta\gamma}} - \frac{\beta\gamma a_8 a_{14}}{K_{\beta\gamma}} + \gamma a_1 a_3 + \gamma a_2 a_6$$

$$\frac{da_{11}}{dt} = - \frac{8\gamma\Omega a_6}{3\pi \mathrm{Re} K_{4\beta\gamma}} - \frac{\left(4\beta^2+\gamma^2\right)a_{11}}{\mathrm{Re}} - \frac{2\sqrt{2}\alpha\beta\gamma a_{17}a_{19}}{K_{\alpha\gamma}K_{4\beta\gamma}} + \frac{2\sqrt{2}\alpha\beta\gamma a_{16}a_{21}}{K_{\alpha\gamma}K_{4\beta\gamma}} - \frac{4\alpha\beta\gamma a_{25}a_{32}}{K_{\alpha\gamma}K_{4\beta\gamma}}$$
$$+ \frac{4\alpha\beta\gamma a_{23}a_{33}}{K_{\alpha\gamma}K_{4\beta\gamma}} - \frac{4\alpha\beta\gamma a_{37}a_{44}}{K_{\alpha\gamma}K_{4\beta\gamma}} + \frac{4\alpha\beta\gamma a_{35}a_{45}}{K_{\alpha\gamma}K_{4\beta\gamma}} - \frac{\alpha^2\left(4\beta^2-\gamma^2\right)a_{20}a_{30}}{\sqrt{2}K_{\alpha\beta}K_{\alpha\gamma}K_{4\beta\gamma}} + \frac{\alpha^2\left(4\beta^2-\gamma^2\right)a_{18}a_{31}}{\sqrt{2}K_{\alpha\beta}K_{\alpha\gamma}K_{4\beta\gamma}}$$
$$+ \frac{\sqrt{2}\alpha^2\left(\gamma^2-4\beta^2\right)a_{24}a_{42}}{K_{\alpha4\beta}K_{\alpha\gamma}K_{4\beta\gamma}} + \frac{\alpha^2\left(4\beta^2-\gamma^2\right)a_{22}a_{43}}{K_{\alpha4\beta}K_{\alpha\gamma}K_{4\beta\gamma}} + \frac{\alpha\left(4\beta^3+3\beta\gamma^2\right)a_{26}a_{30}}{\sqrt{2}K_{\alpha\beta}K_{\beta\gamma}K_{4\beta\gamma}}$$
$$+ \frac{\alpha\left(4\beta^3+3\beta\gamma^2\right)a_{28}a_{31}}{\sqrt{2}K_{\alpha\beta}K_{\beta\gamma}K_{4\beta\gamma}} - \frac{\gamma^3 a_2 a_{14}}{\sqrt{2}K_{\beta\gamma}K_{4\beta\gamma}} - \frac{\gamma^3 a_{16}a_{27}}{\sqrt{2}K_{\beta\gamma}\sqrt{4\beta^2+\gamma^2}} - \frac{\gamma^3 a_{17}a_{29}}{\sqrt{2}K_{\beta\gamma}K_{4\beta\gamma}}$$
$$- \gamma a_{39}a_{44} - \gamma a_{41}a_{45}$$

$$\frac{da_{12}}{dt} = - \frac{8\gamma\Omega a_7}{3\pi \mathrm{Re} K_{4\beta\gamma}} - \frac{\left(4\beta^2+\gamma^2\right)a_{12}}{\mathrm{Re}} + \frac{2\sqrt{2}\alpha\beta\gamma a_{17}a_{18}}{K_{\alpha\gamma}K_{4\beta\gamma}} - \frac{2\sqrt{2}\alpha\beta\gamma a_{16}a_{20}}{K_{\alpha\gamma}K_{4\beta\gamma}} + \frac{4\alpha\beta\gamma a_{24}a_{32}}{K_{\alpha\gamma}K_{4\beta\gamma}}$$
$$- \frac{4\alpha\beta\gamma a_{22}a_{33}}{K_{\alpha\gamma}K_{4\beta\gamma}} + \frac{4\alpha\beta\gamma a_{36}a_{44}}{K_{\alpha\gamma}K_{4\beta\gamma}} - \frac{4\alpha\beta\gamma a_{34}a_{45}}{K_{\alpha\gamma}K_{4\beta\gamma}} - \frac{\alpha^2\left(4\beta^2-\gamma^2\right)a_{21}a_{30}}{\sqrt{2}K_{\alpha\beta}K_{\alpha\gamma}K_{4\beta\gamma}} + \frac{\alpha^2\left(4\beta^2-\gamma^2\right)a_{19}a_{31}}{\sqrt{2}K_{\alpha\beta}K_{\alpha\gamma}K_{4\beta\gamma}}$$
$$+ \frac{\sqrt{2}\alpha^2\left(\gamma^2-4\beta^2\right)a_{25}a_{42}}{K_{\alpha4\beta}K_{\alpha\gamma}K_{4\beta\gamma}} + \frac{\alpha^2\left(4\beta^2-\gamma^2\right)a_{23}a_{43}}{K_{\alpha4\beta}K_{\alpha\gamma}K_{4\beta\gamma}} + \frac{\alpha\left(4\beta^3+3\beta\gamma^2\right)a_{27}a_{30}}{\sqrt{2}K_{\alpha\beta}K_{\beta\gamma}K_{4\beta\gamma}}$$
$$+ \frac{\alpha\left(4\beta^3+3\beta\gamma^2\right)a_{29}a_{31}}{\sqrt{2}K_{\alpha\beta}K_{\beta\gamma}K_{4\beta\gamma}} + \frac{\gamma^3 a_2 a_{13}}{\sqrt{2}K_{\beta\gamma}K_{4\beta\gamma}} + \frac{\gamma^3 a_{16}a_{26}}{\sqrt{2}K_{\beta\gamma}K_{4\beta\gamma}} + \frac{\gamma^3 a_{17}a_{28}}{\sqrt{2}K_{\beta\gamma}K_{4\beta\gamma}}$$
$$+ \gamma a_{38}a_{44} + \gamma a_{40}a_{45}$$

$$\frac{da_{13}}{dt} = -\frac{\sqrt{2}\alpha a_{30}a_{38}\beta^3}{K_{\alpha\beta}K_{\beta\gamma}K_{4\beta\gamma}} - \frac{\sqrt{2}\alpha a_{31}a_{40}\beta^3}{K_{\alpha\beta}K_{\beta\gamma}K_{4\beta\gamma}} - \frac{2\alpha\gamma a_{17}a_{23}\beta}{K_{\alpha\gamma}K_{\beta\gamma}} + \frac{2\alpha\gamma a_{16}a_{25}\beta}{K_{\alpha\gamma}K_{\beta\gamma}} - \frac{\sqrt{2}\alpha\gamma a_{21}a_{32}\beta}{K_{\alpha\gamma}K_{\beta\gamma}}$$
$$+ \frac{\sqrt{2}\alpha\gamma a_{19}a_{33}\beta}{K_{\alpha\gamma}K_{\beta\gamma}} + \frac{\sqrt{2}\alpha\gamma a_{17}a_{35}\beta}{K_{\alpha\gamma}K_{\beta\gamma}} - \frac{\sqrt{2}\alpha\gamma a_{16}a_{37}\beta}{K_{\alpha\gamma}K_{\beta\gamma}} + \frac{\alpha\left(\beta^2-3\gamma^2\right)a_{26}a_{42}\beta}{K_{\alpha4\beta}\left(\beta^2+\gamma^2\right)}$$
$$+ \frac{\alpha\left(\beta^2-3\gamma^2\right)a_{28}a_{43}\beta}{\sqrt{2}K_{\alpha4\beta}\left(\beta^2+\gamma^2\right)} + \frac{2\alpha\gamma a_{21}a_{44}\beta}{K_{\alpha\gamma}K_{\beta\gamma}} - \frac{2\alpha\gamma a_{19}a_{45}\beta}{K_{\alpha\gamma}K_{\beta\gamma}} - \frac{4\gamma\Omega a_3}{3\pi\mathrm{Re}K_{\beta\gamma}} - \frac{2\sqrt{2}\gamma\Omega a_9}{\pi\mathrm{Re}K_{\beta\gamma}}$$
$$- \frac{\gamma\left(3\beta^2+\gamma^2\right)a_2a_{12}}{\sqrt{2}K_{\beta\gamma}K_{4\beta\gamma}} - \frac{\left(\beta^2+\gamma^2\right)a_{13}}{\mathrm{Re}} - \frac{\gamma\left(\gamma^2-3\beta^2\right)a_1a_{14}}{\sqrt{2}\left(\beta^2+\gamma^2\right)} + \frac{\alpha^2\left(\gamma^2-\beta^2\right)a_{24}a_{30}}{K_{\alpha\beta}K_{\alpha\gamma}K_{\beta\gamma}}$$
$$+ \frac{\alpha^2\left(\beta^2-\gamma^2\right)a_{22}a_{31}}{K_{\alpha\beta}K_{\alpha\gamma}K_{\beta\gamma}} - \frac{\gamma\left(\gamma^2-3\beta^2\right)a_{27}a_{32}}{\sqrt{2}\left(\beta^2+\gamma^2\right)} - \frac{\gamma\left(\gamma^2-3\beta^2\right)a_{29}a_{33}}{\sqrt{2}\left(\beta^2+\gamma^2\right)} + \frac{\alpha^2\left(\beta^2-\gamma^2\right)a_{31}a_{34}}{\sqrt{2}K_{\alpha\beta}K_{\alpha\gamma}K_{\beta\gamma}}$$
$$+ \frac{\alpha^2\left(\gamma^2-\beta^2\right)a_{30}a_{36}}{\sqrt{2}K_{\alpha\beta}K_{\alpha\gamma}K_{\beta\gamma}} - \frac{\gamma\left(3\beta^2+\gamma^2\right)a_{16}a_{39}}{\sqrt{2}K_{\beta\gamma}K_{4\beta\gamma}} - \frac{\gamma\left(3\beta^2+\gamma^2\right)a_{17}a_{41}}{\sqrt{2}K_{\beta\gamma}K_{4\beta\gamma}} + \frac{\alpha^2\left(\gamma^2-\beta^2\right)a_{20}a_{42}}{K_{\alpha4\beta}K_{\alpha\gamma}K_{\beta\gamma}}$$
$$+ \frac{\alpha^2\left(\beta^2-\gamma^2\right)a_{18}a_{43}}{\sqrt{2}K_{\alpha4\beta}K_{\alpha\gamma}K_{\beta\gamma}} - \gamma a_{27}a_{44} - \gamma a_{29}a_{45}$$

$$\frac{da_{14}}{dt} = -\frac{\sqrt{2}\alpha a_{30}a_{39}\beta^3}{K_{\alpha\beta}K_{\beta\gamma}K_{4\beta\gamma}} - \frac{\sqrt{2}\alpha a_{31}a_{41}\beta^3}{K_{\alpha\beta}K_{\beta\gamma}K_{4\beta\gamma}} + \frac{2\alpha\gamma a_{17}a_{22}\beta}{K_{\alpha\gamma}K_{\beta\gamma}} - \frac{2\alpha\gamma a_{16}a_{24}\beta}{K_{\alpha\gamma}K_{\beta\gamma}} + \frac{\sqrt{2}\alpha\gamma a_{20}a_{32}\beta}{K_{\alpha\gamma}K_{\beta\gamma}}$$
$$- \frac{\sqrt{2}\alpha\gamma a_{18}a_{33}\beta}{K_{\alpha\gamma}K_{\beta\gamma}} - \frac{\sqrt{2}\alpha\gamma a_{17}a_{34}\beta}{K_{\alpha\gamma}K_{\beta\gamma}} + \frac{\sqrt{2}\alpha\gamma a_{16}a_{36}\beta}{K_{\alpha\gamma}K_{\beta\gamma}} + \frac{\alpha\left(\beta^2-3\gamma^2\right)a_{27}a_{42}\beta}{K_{\alpha4\beta}\left(\beta^2+\gamma^2\right)}$$
$$+ \frac{\alpha\left(\beta^2-3\gamma^2\right)a_{29}a_{43}\beta}{\sqrt{2}K_{\alpha4\beta}\left(\beta^2+\gamma^2\right)} - \frac{2\alpha\gamma a_{20}a_{44}\beta}{K_{\alpha\gamma}K_{\beta\gamma}} + \frac{2\alpha\gamma a_{18}a_{45}\beta}{K_{\alpha\gamma}K_{\beta\gamma}} - \frac{4\gamma\Omega a_4}{3\pi\mathrm{Re}K_{\beta\gamma}} - \frac{2\sqrt{2}\gamma\Omega a_{10}}{\pi\mathrm{Re}K_{\beta\gamma}}$$
$$+ \frac{\gamma\left(3\beta^2+\gamma^2\right)a_2a_{11}}{\sqrt{2}K_{\beta\gamma}K_{4\beta\gamma}} + \frac{\gamma\left(\gamma^2-3\beta^2\right)a_1a_{13}}{\sqrt{2}\left(\beta^2+\gamma^2\right)} - \frac{\left(\beta^2+\gamma^2\right)a_{14}}{\mathrm{Re}} + \frac{\alpha^2\left(\gamma^2-\beta^2\right)a_{25}a_{30}}{K_{\alpha\beta}K_{\alpha\gamma}K_{\beta\gamma}}$$
$$+ \frac{\alpha^2\left(\beta^2-\gamma^2\right)a_{23}a_{31}}{K_{\alpha\beta}K_{\alpha\gamma}K_{\beta\gamma}} + \frac{\gamma\left(\gamma^2-3\beta^2\right)a_{26}a_{32}}{\sqrt{2}\left(\beta^2+\gamma^2\right)} + \frac{\gamma\left(\gamma^2-3\beta^2\right)a_{28}a_{33}}{\sqrt{2}\left(\beta^2+\gamma^2\right)} + \frac{\alpha^2\left(\beta^2-\gamma^2\right)a_{31}a_{35}}{\sqrt{2}K_{\alpha\beta}K_{\alpha\gamma}K_{\beta\gamma}}$$
$$+ \frac{\alpha^2\left(\gamma^2-\beta^2\right)a_{30}a_{37}}{\sqrt{2}K_{\alpha\beta}K_{\alpha\gamma}K_{\beta\gamma}} + \frac{\gamma\left(3\beta^2+\gamma^2\right)a_{16}a_{38}}{\sqrt{2}K_{\beta\gamma}K_{4\beta\gamma}} + \frac{\gamma\left(3\beta^2+\gamma^2\right)a_{17}a_{40}}{\sqrt{2}K_{\beta\gamma}K_{4\beta\gamma}} + \frac{\alpha^2\left(\gamma^2-\beta^2\right)a_{21}a_{42}}{K_{\alpha4\beta}K_{\alpha\gamma}K_{\beta\gamma}}$$
$$+ \frac{\alpha^2\left(\beta^2-\gamma^2\right)a_{19}a_{43}}{\sqrt{2}K_{\alpha4\beta}K_{\alpha\gamma}K_{\beta\gamma}} + \gamma a_{26}a_{44} + \gamma a_{28}a_{45}$$

$$\frac{da_{15}}{dt} = -\frac{9\beta^2a_{15}}{\mathrm{Re}} + \frac{3\beta\gamma^2a_{26}a_{34}}{\sqrt{2}K_{\alpha\gamma}K_{\beta\gamma}} + \frac{3\beta\gamma^2a_{27}a_{35}}{\sqrt{2}K_{\alpha\gamma}K_{\beta\gamma}} + \frac{3\beta\gamma^2a_{28}a_{36}}{\sqrt{2}K_{\alpha\gamma}K_{\beta\gamma}} + \frac{3\beta\gamma^2a_{29}a_{37}}{\sqrt{2}K_{\alpha\gamma}K_{\beta\gamma}} - \frac{3\beta\gamma^2a_{18}a_{38}}{\sqrt{2}K_{\alpha\gamma}K_{4\beta\gamma}}$$
$$- \frac{3\beta\gamma^2a_{19}a_{39}}{\sqrt{2}K_{\alpha\gamma}K_{4\beta\gamma}} - \frac{3\beta\gamma^2a_{20}a_{40}}{\sqrt{2}K_{\alpha\gamma}K_{4\beta\gamma}} - \frac{3\beta\gamma^2a_{21}a_{41}}{\sqrt{2}K_{\alpha\gamma}K_{4\beta\gamma}} - \frac{3\alpha\beta^2a_{31}a_{42}}{K_{\alpha\beta}K_{\alpha4\beta}} + \frac{3\alpha\beta^2a_{30}a_{43}}{\sqrt{2}K_{\alpha\beta}K_{\alpha4\beta}} - \frac{3\beta\gamma a_6a_{11}}{\sqrt{2}K_{4\beta\gamma}}$$
$$- \frac{3\beta\gamma a_7a_{12}}{\sqrt{2}K_{4\beta\gamma}} + \frac{3\beta\gamma a_3a_{13}}{\sqrt{2}K_{\beta\gamma}} + \frac{3\beta\gamma a_4a_{14}}{\sqrt{2}K_{\beta\gamma}}$$

$$\begin{aligned}\frac{da_{16}}{dt} =& -\frac{\alpha^2 a_{16}}{\mathrm{Re}} - \frac{\beta^2 a_{16}}{\mathrm{Re}} + \frac{\alpha\beta\gamma a_{12}a_{20}}{\sqrt{2}K_{\alpha\gamma}K_{4\beta\gamma}} - \frac{\alpha\beta\gamma a_{11}a_{21}}{\sqrt{2}K_{\alpha\gamma}K_{4\beta\gamma}} - \frac{\sqrt{2}\alpha\beta\gamma a_{14}a_{36}}{K_{\alpha\gamma}K_{\beta\gamma}} + \frac{\sqrt{2}\alpha\beta\gamma a_{13}a_{37}}{K_{\alpha\gamma}K_{\beta\gamma}} \\ &+ \frac{\sqrt{2}\alpha\beta a_1 a_{30}}{K_{\alpha\beta}} - \frac{\alpha\beta a_2 a_{42}}{K_{\alpha 4\beta}} + \frac{\alpha^2 a_4 a_{18}}{\sqrt{2}K_{\alpha\gamma}} - \frac{\alpha^2 a_{10}a_{18}}{K_{\alpha\gamma}} - \frac{\alpha^2 a_3 a_{19}}{\sqrt{2}K_{\alpha\gamma}} + \frac{\alpha^2 a_9 a_{19}}{K_{\alpha\gamma}} - \frac{\alpha^2 a_7 a_{22}}{K_{\alpha\gamma}} \\ &+ \frac{\alpha^2 a_6 a_{23}}{K_{\alpha\gamma}} + \frac{\alpha^2 a_7 a_{34}}{\sqrt{2}K_{\alpha\gamma}} - \frac{\alpha^2 a_6 a_{35}}{\sqrt{2}K_{\alpha\gamma}} + \frac{\alpha\beta a_4 a_{28}}{\sqrt{2}K_{\beta\gamma}} - \frac{\alpha\beta a_{10}a_{28}}{K_{\beta\gamma}} - \frac{\alpha\beta a_3 a_{29}}{\sqrt{2}K_{\beta\gamma}} + \frac{\alpha\beta a_9 a_{29}}{K_{\beta\gamma}} - \frac{\sqrt{2}\alpha\beta a_7 a_{40}}{K_{4\beta\gamma}} \\ &+ \frac{\sqrt{2}\alpha\beta a_6 a_{41}}{K_{4\beta\gamma}} + \frac{\alpha a_5 a_{17}}{\sqrt{2}} + \frac{\alpha a_8 a_{33}}{\sqrt{2}} - \frac{\alpha a_{15}a_{33}}{\sqrt{2}} - \alpha a_8 a_{45} + \frac{3\beta^2\gamma a_{12}a_{26}}{\sqrt{2}K_{\beta\gamma}K_{4\beta\gamma}} - \frac{3\beta^2\gamma a_{11}a_{27}}{\sqrt{2}K_{\beta\gamma}K_{4\beta\gamma}} \\ &- \frac{3\beta^2\gamma a_{14}a_{38}}{\sqrt{2}K_{\beta\gamma}K_{4\beta\gamma}} + \frac{3\beta^2\gamma a_{13}a_{39}}{\sqrt{2}K_{\beta\gamma}K_{4\beta\gamma}}\end{aligned}$$

$$\begin{aligned}\frac{da_{17}}{dt} =& -\frac{\alpha^2 a_{17}}{\mathrm{Re}} - \frac{\beta^2 a_{17}}{\mathrm{Re}} - \frac{\alpha\beta\gamma a_{12}a_{18}}{\sqrt{2}K_{\alpha\gamma}K_{4\beta\gamma}} + \frac{\alpha\beta\gamma a_{11}a_{19}}{\sqrt{2}K_{\alpha\gamma}K_{4\beta\gamma}} + \frac{\sqrt{2}\alpha\beta\gamma a_{14}a_{34}}{K_{\alpha\gamma}K_{\beta\gamma}} - \frac{\sqrt{2}\alpha\beta\gamma a_{13}a_{35}}{K_{\alpha\gamma}K_{\beta\gamma}} \\ &+ \frac{\sqrt{2}\alpha\beta a_1 a_{31}}{K_{\alpha\beta}} - \frac{\alpha\beta a_2 a_{43}}{\sqrt{2}K_{\alpha 4\beta}} + \frac{\alpha^2 a_4 a_{20}}{\sqrt{2}K_{\alpha\gamma}} - \frac{\alpha^2 a_{10}a_{20}}{K_{\alpha\gamma}} - \frac{\alpha^2 a_3 a_{21}}{\sqrt{2}K_{\alpha\gamma}} + \frac{\alpha^2 a_9 a_{21}}{K_{\alpha\gamma}} - \frac{\alpha^2 a_7 a_{24}}{K_{\alpha\gamma}} + \frac{\alpha^2 a_6 a_{25}}{K_{\alpha\gamma}} \\ &+ \frac{\alpha^2 a_7 a_{36}}{\sqrt{2}K_{\alpha\gamma}} - \frac{\alpha^2 a_6 a_{37}}{\sqrt{2}K_{\alpha\gamma}} - \frac{\alpha\beta a_4 a_{26}}{\sqrt{2}K_{\beta\gamma}} + \frac{\alpha\beta a_{10}a_{26}}{K_{\beta\gamma}} + \frac{\alpha\beta a_3 a_{27}}{\sqrt{2}K_{\beta\gamma}} - \frac{\alpha\beta a_9 a_{27}}{K_{\beta\gamma}} + \frac{\sqrt{2}\alpha\beta a_7 a_{38}}{K_{4\beta\gamma}} \\ &- \frac{\sqrt{2}\alpha\beta a_6 a_{39}}{K_{4\beta\gamma}} - \frac{\alpha a_5 a_{16}}{\sqrt{2}} - \frac{\alpha a_8 a_{32}}{\sqrt{2}} + \frac{\alpha a_{15}a_{32}}{\sqrt{2}} + \alpha a_8 a_{44} + \frac{3\beta^2\gamma a_{12}a_{28}}{\sqrt{2}K_{\beta\gamma}K_{4\beta\gamma}} - \frac{3\beta^2\gamma a_{11}a_{29}}{\sqrt{2}K_{\beta\gamma}K_{4\beta\gamma}} \\ &- \frac{3\beta^2\gamma a_{14}a_{40}}{\sqrt{2}K_{\beta\gamma}K_{4\beta\gamma}} + \frac{3\beta^2\gamma a_{13}a_{41}}{\sqrt{2}K_{\beta\gamma}K_{4\beta\gamma}}\end{aligned}$$

$$\begin{aligned}\frac{da_{18}}{dt} =& \frac{K_{\alpha\gamma}\left(-3\alpha^2+\beta^2+\gamma^2\right)a_{11}a_{31}\beta^2}{\sqrt{2}K_{\alpha\beta}\left(\alpha^2+\beta^2+\gamma^2\right)K_{4\beta\gamma}} + \frac{2\sqrt{2}K_{\alpha\gamma}K_{\beta\gamma}a_{13}a_{43}\beta^2}{K_{\alpha 4\beta}\left(\alpha^2+\beta^2+\gamma^2\right)} - \frac{\sqrt{2}\alpha\gamma K_{\alpha\gamma}a_{12}a_{17}\beta}{\left(\alpha^2+\beta^2+\gamma^2\right)K_{4\beta\gamma}} \\ &+ \frac{2\sqrt{2}\alpha\Omega a_{24}\beta}{\pi\mathrm{Re}\left(\alpha^2+\beta^2+\gamma^2\right)} + \frac{\sqrt{2}K_{\alpha\gamma}\left(-\alpha^2+\beta^2+\gamma^2\right)a_5 a_{26}\beta}{K_{\beta\gamma}\left(\alpha^2+\beta^2+\gamma^2\right)} + \frac{2\sqrt{2}\alpha\gamma K_{\alpha\gamma}a_1 a_{29}\beta}{K_{\beta\gamma}\left(\alpha^2+\beta^2+\gamma^2\right)} \\ &- \frac{\alpha K_{\alpha\gamma}\left(\alpha^2-3\left(\beta^2+\gamma^2\right)\right)a_3 a_{30}\beta}{\sqrt{2}K_{\alpha\beta}\gamma\left(\alpha^2+\beta^2+\gamma^2\right)} - \frac{\alpha K_{\alpha\gamma}a_9 a_{30}\beta}{K_{\alpha\beta}\gamma} + \frac{2\sqrt{2}\alpha\gamma K_{\alpha\gamma}a_{14}a_{33}\beta}{K_{\beta\gamma}\left(\alpha^2+\beta^2+\gamma^2\right)} \\ &+ \frac{4\alpha\Omega a_{36}\beta}{3\pi\mathrm{Re}\left(\alpha^2+\beta^2+\gamma^2\right)} - \frac{K_{\alpha\gamma}\left(-\alpha^2+\beta^2+\gamma^2\right)a_8 a_{38}\beta}{\sqrt{2}\left(\alpha^2+\beta^2+\gamma^2\right)K_{4\beta\gamma}} + \frac{3K_{\alpha\gamma}\left(-\alpha^2+\beta^2+\gamma^2\right)a_{15}a_{38}\beta}{\sqrt{2}\left(\alpha^2+\beta^2+\gamma^2\right)K_{4\beta\gamma}} \\ &- \frac{\sqrt{2}\alpha\gamma K_{\alpha\gamma}a_2 a_{41}\beta}{\left(\alpha^2+\beta^2+\gamma^2\right)K_{4\beta\gamma}} - \frac{\alpha K_{\alpha\gamma}\left(\alpha^2+3\left(\beta^2+\gamma^2\right)\right)a_6 a_{42}\beta}{K_{\alpha 4\beta}\gamma\left(\alpha^2+\beta^2+\gamma^2\right)} - \frac{\left(\alpha^2-\beta^2-\gamma^2\right)K_{\alpha\gamma}a_4 a_{16}}{\sqrt{2}\left(\alpha^2+\beta^2+\gamma^2\right)} \\ &+ \frac{\left(\alpha^2-\beta^2-\gamma^2\right)K_{\alpha\gamma}a_{10}a_{16}}{\alpha^2+\beta^2+\gamma^2} - \frac{\left(\alpha^2+\beta^2+\gamma^2\right)a_{18}}{\mathrm{Re}} + \frac{\gamma a_1 a_{19}}{\sqrt{2}} + \frac{\alpha a_5 a_{20}}{\sqrt{2}} - \gamma a_2 a_{23} - \alpha a_8 a_{24} \\ &- \frac{\left(\alpha^2-\beta^2-\gamma^2\right)K_{\alpha\gamma}a_7 a_{32}}{\sqrt{2}\left(\alpha^2+\beta^2+\gamma^2\right)} + \frac{\gamma a_2 a_{35}}{\sqrt{2}} + \frac{\alpha a_8 a_{36}}{\sqrt{2}} - \frac{\alpha a_{15}a_{36}}{\sqrt{2}} + \frac{8K_{\alpha\gamma}\left(\beta^2+\gamma^2\right)\Omega a_{38}}{3\pi\mathrm{Re}\left(\alpha^2+\beta^2+\gamma^2\right)K_{4\beta\gamma}} \\ &+ \frac{\left(\alpha^2-\beta^2-\gamma^2\right)K_{\alpha\gamma}a_7 a_{44}}{\alpha^2+\beta^2+\gamma^2}\end{aligned}$$

$$\frac{da_{19}}{dt} =\frac{K_{\alpha\gamma}\left(-3\alpha^2+\beta^2+\gamma^2\right)a_{12}a_{31}\beta^2}{\sqrt{2}K_{\alpha\beta}\left(\alpha^2+\beta^2+\gamma^2\right)K_{4\beta\gamma}}+\frac{2\sqrt{2}K_{\alpha\gamma}K_{\beta\gamma}a_{14}a_{43}\beta^2}{K_{\alpha4\beta}\left(\alpha^2+\beta^2+\gamma^2\right)}+\frac{\sqrt{2}\alpha\gamma K_{\alpha\gamma}a_{11}a_{17}\beta}{\left(\alpha^2+\beta^2+\gamma^2\right)K_{4\beta\gamma}}$$
$$+\frac{2\sqrt{2}\alpha\Omega a_{25}\beta}{\pi\mathrm{Re}\left(\alpha^2+\beta^2+\gamma^2\right)}+\frac{\sqrt{2}K_{\alpha\gamma}\left(-\alpha^2+\beta^2+\gamma^2\right)a_5a_{27}\beta}{K_{\beta\gamma}\left(\alpha^2+\beta^2+\gamma^2\right)}-\frac{2\sqrt{2}\alpha\gamma\sqrt{\alpha^2+\gamma^2}a_1a_{28}\beta}{K_{\beta\gamma}\left(\alpha^2+\beta^2+\gamma^2\right)}$$
$$-\frac{\alpha K_{\alpha\gamma}\left(\alpha^2-3\left(\beta^2+\gamma^2\right)\right)a_4a_{30}\beta}{\sqrt{2}K_{\alpha\beta}\gamma\left(\alpha^2+\beta^2+\gamma^2\right)}-\frac{\alpha K_{\alpha\gamma}a_{10}a_{30}\beta}{K_{\alpha\beta}\gamma}-\frac{2\sqrt{2}\alpha\gamma K_{\alpha\gamma}a_{13}a_{33}\beta}{K_{\beta\gamma}\left(\alpha^2+\beta^2+\gamma^2\right)}$$
$$+\frac{4\alpha\Omega a_{37}\beta}{3\pi\mathrm{Re}\left(\alpha^2+\beta^2+\gamma^2\right)}-\frac{K_{\alpha\gamma}\left(-\alpha^2+\beta^2+\gamma^2\right)a_8a_{39}\beta}{\sqrt{2}\left(\alpha^2+\beta^2+\gamma^2\right)K_{4\beta\gamma}}+\frac{3K_{\alpha\gamma}\left(-\alpha^2+\beta^2+\gamma^2\right)a_{15}a_{39}\beta}{\sqrt{2}\left(\alpha^2+\beta^2+\gamma^2\right)K_{4\beta\gamma}}$$
$$+\frac{\sqrt{2}\alpha\gamma K_{\alpha\gamma}a_2a_{40}\beta}{\left(\alpha^2+\beta^2+\gamma^2\right)K_{4\beta\gamma}}-\frac{\alpha K_{\alpha\gamma}\left(\alpha^2+3\left(\beta^2+\gamma^2\right)\right)a_7a_{42}\beta}{K_{\alpha4\beta}\gamma\left(\alpha^2+\beta^2+\gamma^2\right)}+\frac{\left(\alpha^2-\beta^2-\gamma^2\right)K_{\alpha\gamma}a_3a_{16}}{\sqrt{2}\left(\alpha^2+\beta^2+\gamma^2\right)}$$
$$-\frac{\left(\alpha^2-\beta^2-\gamma^2\right)K_{\alpha\gamma}a_9a_{16}}{\alpha^2+\beta^2+\gamma^2}-\frac{\gamma a_1a_{18}}{\sqrt{2}}-\frac{\left(\alpha^2+\beta^2+\gamma^2\right)a_{19}}{\mathrm{Re}}+\frac{\alpha a_5a_{21}}{\sqrt{2}}+\gamma a_2a_{22}-\alpha a_8a_{25}$$
$$+\frac{\left(\alpha^2-\beta^2-\gamma^2\right)K_{\alpha\gamma}a_6a_{32}}{\sqrt{2}\left(\alpha^2+\beta^2+\gamma^2\right)}-\frac{\gamma a_2a_{34}}{\sqrt{2}}+\frac{\alpha a_8a_{37}}{\sqrt{2}}-\frac{\alpha a_{15}a_{37}}{\sqrt{2}}+\frac{8K_{\alpha\gamma}\left(\beta^2+\gamma^2\right)\Omega a_{39}}{3\pi\mathrm{Re}\left(\alpha^2+\beta^2+\gamma^2\right)K_{4\beta\gamma}}$$
$$-\frac{\left(\alpha^2-\beta^2-\gamma^2\right)K_{\alpha\gamma}a_6a_{44}}{\alpha^2+\beta^2+\gamma^2}$$

$$\frac{da_{20}}{dt} =-\frac{K_{\alpha\gamma}\left(-3\alpha^2+\beta^2+\gamma^2\right)a_{11}a_{30}\beta^2}{\sqrt{2}K_{\alpha\beta}\left(\alpha^2+\beta^2+\gamma^2\right)K_{4\beta\gamma}}-\frac{4K_{\alpha\gamma}K_{\beta\gamma}a_{13}a_{42}\beta^2}{K_{\alpha4\beta}\left(\alpha^2+\beta^2+\gamma^2\right)}+\frac{\sqrt{2}\alpha\gamma K_{\alpha\gamma}a_{12}a_{16}\beta}{\left(\alpha^2+\beta^2+\gamma^2\right)K_{4\beta\gamma}}$$
$$-\frac{2\sqrt{2}\alpha\Omega a_{22}\beta}{\pi\mathrm{Re}\left(\alpha^2+\beta^2+\gamma^2\right)}-\frac{2\sqrt{2}\alpha\gamma K_{\alpha\gamma}a_1a_{27}\beta}{K_{\beta\gamma}\left(\alpha^2+\beta^2+\gamma^2\right)}+\frac{\sqrt{2}K_{\alpha\gamma}\left(-\alpha^2+\beta^2+\gamma^2\right)a_5a_{28}\beta}{K_{\beta\gamma}\left(\alpha^2+\beta^2+\gamma^2\right)}$$
$$-\frac{\alpha K_{\alpha\gamma}\left(\alpha^2-3\left(\beta^2+\gamma^2\right)\right)a_3a_{31}\beta}{\sqrt{2}K_{\alpha\beta}\gamma\left(\alpha^2+\beta^2+\gamma^2\right)}-\frac{\alpha K_{\alpha\gamma}a_9a_{31}\beta}{K_{\alpha\beta}\gamma}-\frac{2\sqrt{2}\alpha\gamma K_{\alpha\gamma}a_{14}a_{32}\beta}{K_{\beta\gamma}\left(\alpha^2+\beta^2+\gamma^2\right)}$$
$$-\frac{4\alpha\Omega a_{34}\beta}{3\pi\mathrm{Re}\left(\alpha^2+\beta^2+\gamma^2\right)}+\frac{\sqrt{2}\alpha\gamma K_{\alpha\gamma}a_2a_{39}\beta}{\left(\alpha^2+\beta^2+\gamma^2\right)K_{4\beta\gamma}}-\frac{K_{\alpha\gamma}\left(-\alpha^2+\beta^2+\gamma^2\right)a_8a_{40}\beta}{\sqrt{2}\left(\alpha^2+\beta^2+\gamma^2\right)K_{4\beta\gamma}}$$
$$+\frac{3K_{\alpha\gamma}\left(-\alpha^2+\beta^2+\gamma^2\right)a_{15}a_{40}\beta}{\sqrt{2}\left(\alpha^2+\beta^2+\gamma^2\right)K_{4\beta\gamma}}-\frac{\alpha K_{\alpha\gamma}\left(\alpha^2+3\left(\beta^2+\gamma^2\right)\right)a_6a_{43}\beta}{\sqrt{2}K_{\alpha4\beta}\gamma\left(\alpha^2+\beta^2+\gamma^2\right)}$$
$$-\frac{\left(\alpha^2-\beta^2-\gamma^2\right)K_{\alpha\gamma}a_4a_{17}}{\sqrt{2}\left(\alpha^2+\beta^2+\gamma^2\right)}+\frac{\left(\alpha^2-\beta^2-\gamma^2\right)K_{\alpha\gamma}a_{10}a_{17}}{\alpha^2+\beta^2+\gamma^2}-\frac{\alpha a_5a_{18}}{\sqrt{2}}-\frac{\left(\alpha^2+\beta^2+\gamma^2\right)a_{20}}{\mathrm{Re}}$$
$$+\frac{\gamma a_1a_{21}}{\sqrt{2}}+\alpha a_8a_{22}-\gamma a_2a_{25}-\frac{\left(\alpha^2-\beta^2-\gamma^2\right)K_{\alpha\gamma}a_7a_{33}}{\sqrt{2}\left(\alpha^2+\beta^2+\gamma^2\right)}-\frac{\alpha a_8a_{34}}{\sqrt{2}}+\frac{\alpha a_{15}a_{34}}{\sqrt{2}}+\frac{\gamma a_2a_{37}}{\sqrt{2}}$$
$$+\frac{8K_{\alpha\gamma}\left(\beta^2+\gamma^2\right)\Omega a_{40}}{3\pi\mathrm{Re}\left(\alpha^2+\beta^2+\gamma^2\right)K_{4\beta\gamma}}+\frac{\left(\alpha^2-\beta^2-\gamma^2\right)K_{\alpha\gamma}a_7a_{45}}{\alpha^2+\beta^2+\gamma^2}$$

$$\frac{da_{21}}{dt} = -\frac{K_{\alpha\gamma}\left(-3\alpha^2+\beta^2+\gamma^2\right)a_{12}a_{30}\beta^2}{\sqrt{2}K_{\alpha\beta}\left(\alpha^2+\beta^2+\gamma^2\right)K_{4\beta\gamma}} - \frac{4K_{\alpha\gamma}K_{\beta\gamma}a_{14}a_{42}\beta^2}{K_{\alpha4\beta}\left(\alpha^2+\beta^2+\gamma^2\right)} - \frac{\sqrt{2}\alpha\gamma K_{\alpha\gamma}a_{11}a_{16}\beta}{\left(\alpha^2+\beta^2+\gamma^2\right)K_{4\beta\gamma}}$$
$$- \frac{2\sqrt{2}\alpha\Omega a_{23}\beta}{\pi\mathrm{Re}\left(\alpha^2+\beta^2+\gamma^2\right)} + \frac{2\sqrt{2}\alpha\gamma K_{\alpha\gamma}a_1a_{26}\beta}{K_{\beta\gamma}\left(\alpha^2+\beta^2+\gamma^2\right)} + \frac{\sqrt{2}K_{\alpha\gamma}\left(-\alpha^2+\beta^2+\gamma^2\right)a_5a_{29}\beta}{K_{\beta\gamma}\left(\alpha^2+\beta^2+\gamma^2\right)}$$
$$- \frac{\alpha K_{\alpha\gamma}\left(\alpha^2-3\left(\beta^2+\gamma^2\right)\right)a_4a_{31}\beta}{\sqrt{2}K_{\alpha\beta}\gamma\left(\alpha^2+\beta^2+\gamma^2\right)} - \frac{\alpha K_{\alpha\gamma}a_{10}a_{31}\beta}{K_{\alpha\beta}\gamma} + \frac{2\sqrt{2}\alpha\gamma K_{\alpha\gamma}a_{13}a_{32}\beta}{K_{\beta\gamma}\left(\alpha^2+\beta^2+\gamma^2\right)}$$
$$- \frac{4\alpha\Omega a_{35}\beta}{3\pi\mathrm{Re}\left(\alpha^2+\beta^2+\gamma^2\right)} - \frac{\sqrt{2}\alpha\gamma K_{\alpha\gamma}a_2a_{38}\beta}{\left(\alpha^2+\beta^2+\gamma^2\right)K_{4\beta\gamma}} - \frac{K_{\alpha\gamma}\left(-\alpha^2+\beta^2+\gamma^2\right)a_8a_{41}\beta}{\sqrt{2}\left(\alpha^2+\beta^2+\gamma^2\right)K_{4\beta\gamma}}$$
$$+ \frac{3K_{\alpha\gamma}\left(-\alpha^2+\beta^2+\gamma^2\right)a_{15}a_{41}\beta}{\sqrt{2}\left(\alpha^2+\beta^2+\gamma^2\right)K_{4\beta\gamma}} - \frac{\alpha K_{\alpha\gamma}\left(\alpha^2+3\left(\beta^2+\gamma^2\right)\right)a_7a_{43}\beta}{\sqrt{2}K_{\alpha4\beta}\gamma\left(\alpha^2+\beta^2+\gamma^2\right)}$$
$$+ \frac{\left(\alpha^2-\beta^2-\gamma^2\right)K_{\alpha\gamma}a_3a_{17}}{\sqrt{2}\left(\alpha^2+\beta^2+\gamma^2\right)} - \frac{\left(\alpha^2-\beta^2-\gamma^2\right)K_{\alpha\gamma}a_9a_{17}}{\alpha^2+\beta^2+\gamma^2} - \frac{\alpha a_5a_{19}}{\sqrt{2}} - \frac{\gamma a_1a_{20}}{\sqrt{2}}$$
$$- \frac{\left(\alpha^2+\beta^2+\gamma^2\right)a_{21}}{\mathrm{Re}} + \alpha a_8a_{23} + \gamma a_2a_{24} + \frac{\left(\alpha^2-\beta^2-\gamma^2\right)K_{\alpha\gamma}a_6a_{33}}{\sqrt{2}\left(\alpha^2+\beta^2+\gamma^2\right)} - \frac{\alpha a_8a_{35}}{\sqrt{2}} + \frac{\alpha a_{15}a_{35}}{\sqrt{2}}$$
$$- \frac{\gamma a_2a_{36}}{\sqrt{2}} + \frac{8K_{\alpha\gamma}\left(\beta^2+\gamma^2\right)\Omega a_{41}}{3\pi\mathrm{Re}\left(\alpha^2+\beta^2+\gamma^2\right)K_{4\beta\gamma}} - \frac{\left(\alpha^2-\beta^2-\gamma^2\right)K_{\alpha\gamma}a_6a_{45}}{\alpha^2+\beta^2+\gamma^2}$$

$$\frac{da_{22}}{dt} = \frac{2\sqrt{2}\gamma^2\Omega a_{26}}{\pi\mathrm{Re}K_{\alpha\gamma}K_{\beta\gamma}} - \frac{\left(\alpha^2+\gamma^2\right)a_{22}}{\mathrm{Re}} + \frac{\beta^2\left(\gamma^2-\alpha^2\right)a_{13}a_{31}}{K_{\alpha\beta}K_{\alpha\gamma}K_{\beta\gamma}} + \frac{4\beta^2\left(\gamma^2-\alpha^2\right)a_{11}a_{43}}{K_{\alpha4\beta}K_{\alpha\gamma}K_{4\beta\gamma}} - \frac{2\alpha\beta\gamma a_{14}a_{17}}{K_{\alpha\gamma}K_{\beta\gamma}}$$
$$+ \frac{\beta\left(\alpha^2-\gamma^2\right)a_8a_{26}}{K_{\alpha\gamma}K_{\beta\gamma}} - \frac{2\alpha\beta\gamma a_2a_{29}}{K_{\alpha\gamma}K_{\beta\gamma}} - \frac{2\alpha\beta\gamma a_6a_{30}}{K_{\alpha\beta}K_{\alpha\gamma}} + \frac{4\alpha\beta\gamma a_{12}a_{33}}{K_{\alpha\gamma}K_{4\beta\gamma}} + \frac{2\beta\left(\gamma^2-\alpha^2\right)a_5a_{38}}{K_{\alpha\gamma}K_{4\beta\gamma}}$$
$$+ \frac{4\alpha\beta\gamma a_1a_{41}}{K_{\alpha\gamma}K_{4\beta\gamma}} + \frac{4\sqrt{2}\alpha\beta\gamma a_3a_{42}}{K_{\alpha4\beta}K_{\alpha\gamma}} + \frac{\left(\alpha^2-\gamma^2\right)a_7a_{16}}{K_{\alpha\gamma}} + \frac{\left(\alpha^2-\gamma^2\right)a_4a_{32}}{K_{\alpha\gamma}} + \frac{\left(\alpha^2-\gamma^2\right)a_{10}a_{44}}{K_{\alpha\gamma}}$$
$$- \alpha a_8a_{20} - \alpha a_5a_{36} - \gamma a_2a_{19} - \gamma a_1a_{35}$$

$$\frac{da_{23}}{dt} = \frac{2\sqrt{2}\gamma^2\Omega a_{27}}{\pi\mathrm{Re}K_{\alpha\gamma}K_{\beta\gamma}} - \frac{\left(\alpha^2+\gamma^2\right)a_{23}}{\mathrm{Re}} + \frac{\beta^2\left(\gamma^2-\alpha^2\right)a_{14}a_{31}}{K_{\alpha\beta}K_{\alpha\gamma}K_{\beta\gamma}} + \frac{4\beta^2\left(\gamma^2-\alpha^2\right)a_{12}a_{43}}{K_{\alpha4\beta}K_{\alpha\gamma}K_{4\beta\gamma}} + \frac{2\alpha\beta\gamma a_{13}a_{17}}{K_{\alpha\gamma}K_{\beta\gamma}}$$
$$+ \frac{\beta\left(\alpha^2-\gamma^2\right)a_8a_{27}}{K_{\alpha\gamma}K_{\beta\gamma}} + \frac{2\alpha\beta\gamma a_2a_{28}}{K_{\alpha\gamma}K_{\beta\gamma}} - \frac{2\alpha\beta\gamma a_7a_{30}}{K_{\alpha\beta}K_{\alpha\gamma}} - \frac{4\alpha\beta\gamma a_{11}a_{33}}{K_{\alpha\gamma}K_{4\beta\gamma}} + \frac{2\beta\left(\gamma^2-\alpha^2\right)a_5a_{39}}{K_{\alpha\gamma}K_{4\beta\gamma}}$$
$$- \frac{4\alpha\beta\gamma a_1a_{40}}{K_{\alpha\gamma}K_{4\beta\gamma}} + \frac{4\sqrt{2}\alpha\beta\gamma a_4a_{42}}{K_{\alpha4\beta}K_{\alpha\gamma}} + \frac{\left(\gamma^2-\alpha^2\right)a_6a_{16}}{K_{\alpha\gamma}} + \frac{\left(\gamma^2-\alpha^2\right)a_3a_{32}}{K_{\alpha\gamma}} + \frac{\left(\gamma^2-\alpha^2\right)a_9a_{44}}{K_{\alpha\gamma}}$$
$$- \alpha a_8a_{21} - \alpha a_5a_{37} + \gamma a_2a_{18} + \gamma a_1a_{34}$$

$$\frac{da_{24}}{dt} = \frac{2\sqrt{2}\gamma^2\Omega a_{28}}{\pi\mathrm{Re}K_{\alpha\gamma}K_{\beta\gamma}} - \frac{\left(\alpha^2+\gamma^2\right)a_{24}}{\mathrm{Re}} + \frac{\beta^2\left(\alpha^2-\gamma^2\right)a_{13}a_{30}}{K_{\alpha\beta}K_{\alpha\gamma}K_{\beta\gamma}} + \frac{4\sqrt{2}\beta^2\left(\alpha^2-\gamma^2\right)a_{11}a_{42}}{K_{\alpha4\beta}K_{\alpha\gamma}K_{4\beta\gamma}} + \frac{2\alpha\beta\gamma a_{14}a_{16}}{K_{\alpha\gamma}K_{\beta\gamma}}$$
$$+ \frac{2\alpha\beta\gamma a_2a_{27}}{K_{\alpha\gamma}K_{\beta\gamma}} + \frac{\beta\left(\alpha^2-\gamma^2\right)a_8a_{28}}{K_{\alpha\gamma}K_{\beta\gamma}} - \frac{2\alpha\beta\gamma a_6a_{31}}{K_{\alpha\beta}K_{\alpha\gamma}} - \frac{4\alpha\beta\gamma a_{12}a_{32}}{K_{\alpha\gamma}K_{4\beta\gamma}} - \frac{4\alpha\beta\gamma a_1a_{39}}{K_{\alpha\gamma}K_{4\beta\gamma}}$$
$$+ \frac{2\beta\left(\gamma^2-\alpha^2\right)a_5a_{40}}{K_{\alpha\gamma}K_{4\beta\gamma}} + \frac{4\alpha\beta\gamma a_3a_{43}}{K_{\alpha4\beta}K_{\alpha\gamma}} + \frac{\left(\alpha^2-\gamma^2\right)a_7a_{17}}{K_{\alpha\gamma}} + \frac{\left(\alpha^2-\gamma^2\right)a_4a_{33}}{K_{\alpha\gamma}} + \frac{\left(\alpha^2-\gamma^2\right)a_{10}a_{45}}{K_{\alpha\gamma}}$$
$$+ \alpha a_8a_{18} + \alpha a_5a_{34} - \gamma a_2a_{21} - \gamma a_1a_{37}$$

$$\begin{aligned}\frac{da_{25}}{dt} =&\frac{2\sqrt{2}\gamma^2\Omega a_{29}}{\pi\mathrm{Re}K_{\alpha\gamma}K_{\beta\gamma}} - \frac{\left(\alpha^2+\gamma^2\right)a_{25}}{\mathrm{Re}} + \frac{\beta^2\left(\alpha^2-\gamma^2\right)a_{14}a_{30}}{K_{\alpha\beta}K_{\alpha\gamma}K_{\beta\gamma}} + \frac{4\sqrt{2}\beta^2\left(\alpha^2-\gamma^2\right)a_{12}a_{42}}{K_{\alpha4\beta}K_{\alpha\gamma}K_{4\beta\gamma}} - \frac{2\alpha\beta\gamma a_{13}a_{16}}{K_{\alpha\gamma}K_{\beta\gamma}}\\ &- \frac{2\alpha\beta\gamma a_2a_{26}}{K_{\alpha\gamma}K_{\beta\gamma}} + \frac{\beta\left(\alpha^2-\gamma^2\right)a_8a_{29}}{K_{\alpha\gamma}K_{\beta\gamma}} - \frac{2\alpha\beta\gamma a_7a_{31}}{K_{\alpha\beta}K_{\alpha\gamma}} + \frac{4\alpha\beta\gamma a_{11}a_{32}}{K_{\alpha\gamma}K_{4\beta\gamma}} + \frac{4\alpha\beta\gamma a_1a_{38}}{K_{\alpha\gamma}K_{4\beta\gamma}}\\ &+ \frac{2\beta\left(\gamma^2-\alpha^2\right)a_5a_{41}}{K_{\alpha\gamma}K_{4\beta\gamma}} + \frac{4\alpha\beta\gamma a_4a_{43}}{K_{\alpha4\beta}K_{\alpha\gamma}} + \frac{\left(\gamma^2-\alpha^2\right)a_6a_{17}}{K_{\alpha\gamma}} + \frac{\left(\gamma^2-\alpha^2\right)a_3a_{33}}{K_{\alpha\gamma}} + \frac{\left(\gamma^2-\alpha^2\right)a_9a_{45}}{K_{\alpha\gamma}}\\ &+ \alpha a_8a_{19} + \alpha a_5a_{35} + \gamma a_2a_{20} + \gamma a_1a_{36}\end{aligned}$$

$$\begin{aligned}\frac{da_{26}}{dt} =&- \frac{\left(\alpha^2-3\beta^2+\gamma^2\right)K_{\beta\gamma}a_3a_{31}\alpha^2}{\sqrt{2}K_{\alpha\beta}\gamma\left(\alpha^2+\beta^2+\gamma^2\right)} - \frac{K_{\beta\gamma}a_9a_{31}\alpha^2}{K_{\alpha\beta}\gamma} - \frac{K_{\beta\gamma}\left(\alpha^2+3\beta^2+\gamma^2\right)a_6a_{43}\alpha^2}{\sqrt{2}K_{\alpha4\beta}\gamma\left(\alpha^2+\beta^2+\gamma^2\right)}\\ &+ \frac{\sqrt{2}\beta K_{\beta\gamma}a_4a_{17}\alpha}{\alpha^2+\beta^2+\gamma^2} - \frac{2\beta K_{\beta\gamma}a_{10}a_{17}\alpha}{\alpha^2+\beta^2+\gamma^2} - \frac{\left(\alpha^2-3\beta^2+\gamma^2\right)a_5a_{28}\alpha}{\sqrt{2}\left(\alpha^2+\beta^2+\gamma^2\right)}\\ &- \frac{\beta K_{\beta\gamma}\left(\alpha^2+5\beta^2+\gamma^2\right)a_{11}a_{30}\alpha}{\sqrt{2}K_{\alpha\beta}\left(\alpha^2+\beta^2+\gamma^2\right)K_{4\beta\gamma}} + \frac{\sqrt{2}\beta K_{\beta\gamma}a_7a_{33}\alpha}{\alpha^2+\beta^2+\gamma^2} + \frac{8\beta K_{\beta\gamma}\Omega a_{40}\alpha}{3\pi\mathrm{Re}\left(\alpha^2+\beta^2+\gamma^2\right)K_{4\beta\gamma}}\\ &- \frac{K_{\beta\gamma}\left(\alpha^2+3\beta^2+\gamma^2\right)a_8a_{40}\alpha}{\sqrt{2}\left(\alpha^2+\beta^2+\gamma^2\right)K_{4\beta\gamma}} - \frac{\left(\alpha^2-5\beta^2+\gamma^2\right)K_{\beta\gamma}a_{15}a_{40}\alpha}{\sqrt{2}\left(\alpha^2+\beta^2+\gamma^2\right)K_{4\beta\gamma}} - \frac{\beta\left(\alpha^2+5\beta^2+\gamma^2\right)a_{13}a_{42}\alpha}{K_{\alpha4\beta}\left(\alpha^2+\beta^2+\gamma^2\right)}\\ &- \frac{2\beta K_{\beta\gamma}a_7a_{45}\alpha}{\alpha^2+\beta^2+\gamma^2} - \frac{\gamma K_{\beta\gamma}\left(\alpha^2+3\beta^2+\gamma^2\right)a_{12}a_{16}}{\sqrt{2}\left(\alpha^2+\beta^2+\gamma^2\right)K_{4\beta\gamma}} - \frac{2\sqrt{2}K_{\alpha\gamma}K_{\beta\gamma}\Omega a_{22}}{\pi\mathrm{Re}\left(\alpha^2+\beta^2+\gamma^2\right)} - \frac{\left(\alpha^2+\beta^2+\gamma^2\right)a_{26}}{\mathrm{Re}}\\ &- \frac{\gamma\left(\alpha^2-3\beta^2+\gamma^2\right)a_1a_{27}}{\sqrt{2}\left(\alpha^2+\beta^2+\gamma^2\right)} - \frac{\gamma\left(\alpha^2-3\beta^2+\gamma^2\right)a_{14}a_{32}}{\sqrt{2}\left(\alpha^2+\beta^2+\gamma^2\right)} - \frac{4K_{\alpha\gamma}K_{\beta\gamma}\Omega a_{34}}{3\pi\mathrm{Re}\left(\alpha^2+\beta^2+\gamma^2\right)}\\ &- \frac{\gamma K_{\beta\gamma}\left(\alpha^2+3\beta^2+\gamma^2\right)a_2a_{39}}{\sqrt{2}\left(\alpha^2+\beta^2+\gamma^2\right)K_{4\beta\gamma}} - \gamma a_{14}a_{44}\end{aligned}$$

$$\begin{aligned}\frac{da_{27}}{dt} =&- \frac{\left(\alpha^2-3\beta^2+\gamma^2\right)K_{\beta\gamma}a_4a_{31}\alpha^2}{\sqrt{2}K_{\alpha\beta}\gamma\left(\alpha^2+\beta^2+\gamma^2\right)} - \frac{K_{\beta\gamma}a_{10}a_{31}\alpha^2}{K_{\alpha\beta}\gamma} - \frac{K_{\beta\gamma}\left(\alpha^2+3\beta^2+\gamma^2\right)a_7a_{43}\alpha^2}{\sqrt{2}K_{\alpha4\beta}\gamma\left(\alpha^2+\beta^2+\gamma^2\right)}\\ &- \frac{\sqrt{2}\beta K_{\beta\gamma}a_3a_{17}\alpha}{\alpha^2+\beta^2+\gamma^2} + \frac{2\beta K_{\beta\gamma}a_9a_{17}\alpha}{\alpha^2+\beta^2+\gamma^2} - \frac{\left(\alpha^2-3\beta^2+\gamma^2\right)a_5a_{29}\alpha}{\sqrt{2}\left(\alpha^2+\beta^2+\gamma^2\right)} - \frac{\beta K_{\beta\gamma}\left(\alpha^2+5\beta^2+\gamma^2\right)a_{12}a_{30}\alpha}{\sqrt{2}K_{\alpha\beta}\left(\alpha^2+\beta^2+\gamma^2\right)K_{4\beta\gamma}}\\ &- \frac{\sqrt{2}\beta K_{\beta\gamma}a_6a_{33}\alpha}{\alpha^2+\beta^2+\gamma^2} + \frac{8\beta K_{\beta\gamma}\Omega a_{41}\alpha}{3\pi\mathrm{Re}\left(\alpha^2+\beta^2+\gamma^2\right)K_{4\beta\gamma}} - \frac{K_{\beta\gamma}\left(\alpha^2+3\beta^2+\gamma^2\right)a_8a_{41}\alpha}{\sqrt{2}\left(\alpha^2+\beta^2+\gamma^2\right)K_{4\beta\gamma}}\\ &- \frac{\left(\alpha^2-5\beta^2+\gamma^2\right)K_{\beta\gamma}a_{15}a_{41}\alpha}{\sqrt{2}\left(\alpha^2+\beta^2+\gamma^2\right)K_{4\beta\gamma}} - \frac{\beta\left(\alpha^2+5\beta^2+\gamma^2\right)a_{14}a_{42}\alpha}{K_{\alpha4\beta}\left(\alpha^2+\beta^2+\gamma^2\right)} + \frac{2\beta K_{\beta\gamma}a_6a_{45}\alpha}{\alpha^2+\beta^2+\gamma^2}\\ &+ \frac{\gamma K_{\beta\gamma}\left(\alpha^2+3\beta^2+\gamma^2\right)a_{11}a_{16}}{\sqrt{2}\left(\alpha^2+\beta^2+\gamma^2\right)K_{4\beta\gamma}} - \frac{2\sqrt{2}K_{\alpha\gamma}K_{\beta\gamma}\Omega a_{23}}{\pi\mathrm{Re}\left(\alpha^2+\beta^2+\gamma^2\right)} + \frac{\gamma\left(\alpha^2-3\beta^2+\gamma^2\right)a_1a_{26}}{\sqrt{2}\left(\alpha^2+\beta^2+\gamma^2\right)}\\ &- \frac{\left(\alpha^2+\beta^2+\gamma^2\right)a_{27}}{\mathrm{Re}} + \frac{\gamma\left(\alpha^2-3\beta^2+\gamma^2\right)a_{13}a_{32}}{\sqrt{2}\left(\alpha^2+\beta^2+\gamma^2\right)} - \frac{4K_{\alpha\gamma}K_{\beta\gamma}\Omega a_{35}}{3\pi\mathrm{Re}\left(\alpha^2+\beta^2+\gamma^2\right)}\\ &+ \frac{\gamma K_{\beta\gamma}\left(\alpha^2+3\beta^2+\gamma^2\right)a_2a_{38}}{\sqrt{2}\left(\alpha^2+\beta^2+\gamma^2\right)K_{4\beta\gamma}} + \gamma a_{13}a_{44}\end{aligned}$$

$$\begin{aligned}\frac{da_{28}}{dt} =&\frac{\left(\alpha^2-3\beta^2+\gamma^2\right)K_{\beta\gamma}a_3a_{30}\alpha^2}{\sqrt{2}K_{\alpha\beta}\gamma\left(\alpha^2+\beta^2+\gamma^2\right)}+\frac{K_{\beta\gamma}a_9a_{30}\alpha^2}{K_{\alpha\beta}\gamma}+\frac{K_{\beta\gamma}\left(\alpha^2+3\beta^2+\gamma^2\right)a_6a_{42}\alpha^2}{K_{\alpha4\beta}\gamma\left(\alpha^2+\beta^2+\gamma^2\right)}\\&-\frac{\sqrt{2}\beta K_{\beta\gamma}a_4a_{16}\alpha}{\alpha^2+\beta^2+\gamma^2}+\frac{2\beta K_{\beta\gamma}a_{10}a_{16}\alpha}{\alpha^2+\beta^2+\gamma^2}+\frac{\left(\alpha^2-3\beta^2+\gamma^2\right)a_5a_{26}\alpha}{\sqrt{2}\left(\alpha^2+\beta^2+\gamma^2\right)}\\&-\frac{\beta K_{\beta\gamma}\left(\alpha^2+5\beta^2+\gamma^2\right)a_{11}a_{31}\alpha}{\sqrt{2}K_{\alpha\beta}\left(\alpha^2+\beta^2+\gamma^2\right)K_{4\beta\gamma}}-\frac{\sqrt{2}\beta K_{\beta\gamma}a_7a_{32}\alpha}{\alpha^2+\beta^2+\gamma^2}-\frac{8\beta K_{\beta\gamma}\Omega a_{38}\alpha}{3\pi\mathrm{Re}\left(\alpha^2+\beta^2+\gamma^2\right)K_{4\beta\gamma}}\\&+\frac{K_{\beta\gamma}\left(\alpha^2+3\beta^2+\gamma^2\right)a_8a_{38}\alpha}{\sqrt{2}\left(\alpha^2+\beta^2+\gamma^2\right)K_{4\beta\gamma}}+\frac{\left(\alpha^2-5\beta^2+\gamma^2\right)K_{\beta\gamma}a_{15}a_{38}\alpha}{\sqrt{2}\left(\alpha^2+\beta^2+\gamma^2\right)K_{4\beta\gamma}}-\frac{\beta\left(\alpha^2+5\beta^2+\gamma^2\right)a_{13}a_{43}\alpha}{\sqrt{2}K_{\alpha4\beta}\left(\alpha^2+\beta^2+\gamma^2\right)}\\&+\frac{2\beta K_{\beta\gamma}a_7a_{44}\alpha}{\alpha^2+\beta^2+\gamma^2}-\frac{\gamma K_{\beta\gamma}\left(\alpha^2+3\beta^2+\gamma^2\right)a_{12}a_{17}}{\sqrt{2}\left(\alpha^2+\beta^2+\gamma^2\right)K_{4\beta\gamma}}-\frac{2\sqrt{2}K_{\alpha\gamma}K_{\beta\gamma}\Omega a_{24}}{\pi\mathrm{Re}\left(\alpha^2+\beta^2+\gamma^2\right)}-\frac{\left(\alpha^2+\beta^2+\gamma^2\right)a_{28}}{\mathrm{Re}}\\&-\frac{\gamma\left(\alpha^2-3\beta^2+\gamma^2\right)a_1a_{29}}{\sqrt{2}\left(\alpha^2+\beta^2+\gamma^2\right)}-\frac{\gamma\left(\alpha^2-3\beta^2+\gamma^2\right)a_{14}a_{33}}{\sqrt{2}\left(\alpha^2+\beta^2+\gamma^2\right)}-\frac{4K_{\alpha\gamma}K_{\beta\gamma}\Omega a_{36}}{3\pi\mathrm{Re}\left(\alpha^2+\beta^2+\gamma^2\right)}\\&-\frac{\gamma K_{\beta\gamma}\left(\alpha^2+3\beta^2+\gamma^2\right)a_2a_{41}}{\sqrt{2}\left(\alpha^2+\beta^2+\gamma^2\right)K_{4\beta\gamma}}-\gamma a_{14}a_{45}\end{aligned}$$

$$\begin{aligned}\frac{da_{29}}{dt} =&\frac{\left(\alpha^2-3\beta^2+\gamma^2\right)K_{\beta\gamma}a_4a_{30}\alpha^2}{\sqrt{2}K_{\alpha\beta}\gamma\left(\alpha^2+\beta^2+\gamma^2\right)}+\frac{K_{\beta\gamma}a_{10}a_{30}\alpha^2}{K_{\alpha\beta}\gamma}+\frac{K_{\beta\gamma}\left(\alpha^2+3\beta^2+\gamma^2\right)a_7a_{42}\alpha^2}{K_{\alpha4\beta}\gamma\left(\alpha^2+\beta^2+\gamma^2\right)}\\&+\frac{\sqrt{2}\beta K_{\beta\gamma}a_3a_{16}\alpha}{\alpha^2+\beta^2+\gamma^2}-\frac{2\beta K_{\beta\gamma}a_9a_{16}\alpha}{\alpha^2+\beta^2+\gamma^2}+\frac{\left(\alpha^2-3\beta^2+\gamma^2\right)a_5a_{27}\alpha}{\sqrt{2}\left(\alpha^2+\beta^2+\gamma^2\right)}\\&-\frac{\beta K_{\beta\gamma}\left(\alpha^2+5\beta^2+\gamma^2\right)a_{12}a_{31}\alpha}{\sqrt{2}K_{\alpha\beta}\left(\alpha^2+\beta^2+\gamma^2\right)K_{4\beta\gamma}}+\frac{\sqrt{2}\beta K_{\beta\gamma}a_6a_{32}\alpha}{\alpha^2+\beta^2+\gamma^2}-\frac{8\beta K_{\beta\gamma}\Omega a_{39}\alpha}{3\pi\mathrm{Re}\left(\alpha^2+\beta^2+\gamma^2\right)K_{4\beta\gamma}}\\&+\frac{K_{\beta\gamma}\left(\alpha^2+3\beta^2+\gamma^2\right)a_8a_{39}\alpha}{\sqrt{2}\left(\alpha^2+\beta^2+\gamma^2\right)K_{4\beta\gamma}}+\frac{\left(\alpha^2-5\beta^2+\gamma^2\right)K_{\beta\gamma}a_{15}a_{39}\alpha}{\sqrt{2}\left(\alpha^2+\beta^2+\gamma^2\right)K_{4\beta\gamma}}-\frac{\beta\left(\alpha^2+5\beta^2+\gamma^2\right)a_{14}a_{43}\alpha}{\sqrt{2}K_{\alpha4\beta}\left(\alpha^2+\beta^2+\gamma^2\right)}\\&-\frac{2\beta K_{\beta\gamma}a_6a_{44}\alpha}{\alpha^2+\beta^2+\gamma^2}+\frac{\gamma K_{\beta\gamma}\left(\alpha^2+3\beta^2+\gamma^2\right)a_{11}a_{17}}{\sqrt{2}\left(\alpha^2+\beta^2+\gamma^2\right)K_{4\beta\gamma}}-\frac{2\sqrt{2}K_{\alpha\gamma}K_{\beta\gamma}\Omega a_{25}}{\pi\mathrm{Re}\left(\alpha^2+\beta^2+\gamma^2\right)}\\&+\frac{\gamma\left(\alpha^2-3\beta^2+\gamma^2\right)a_1a_{28}}{\sqrt{2}\left(\alpha^2+\beta^2+\gamma^2\right)}-\frac{\left(\alpha^2+\beta^2+\gamma^2\right)a_{29}}{\mathrm{Re}}+\frac{\gamma\left(\alpha^2-3\beta^2+\gamma^2\right)a_{13}a_{33}}{\sqrt{2}\left(\alpha^2+\beta^2+\gamma^2\right)}\\&-\frac{4K_{\alpha\gamma}K_{\beta\gamma}\Omega a_{37}}{3\pi\mathrm{Re}\left(\alpha^2+\beta^2+\gamma^2\right)}+\frac{\gamma K_{\beta\gamma}\left(\alpha^2+3\beta^2+\gamma^2\right)a_2a_{40}}{\sqrt{2}\left(\alpha^2+\beta^2+\gamma^2\right)K_{4\beta\gamma}}+\gamma a_{13}a_{45}\end{aligned}$$

$$\begin{aligned}\frac{da_{30}}{dt} =&\frac{(\beta^2-\alpha^2)\,a_{11}a_{20}\gamma^2}{\sqrt{2}K_{\alpha\beta}K_{\alpha\gamma}K_{4\beta\gamma}}+\frac{(\beta^2-\alpha^2)\,a_{12}a_{21}\gamma^2}{\sqrt{2}K_{\alpha\beta}K_{\alpha\gamma}K_{4\beta\gamma}}+\frac{(\beta^2-\alpha^2)\,a_{13}a_{24}\gamma^2}{K_{\alpha\beta}K_{\alpha\gamma}K_{\beta\gamma}}+\frac{(\beta^2-\alpha^2)\,a_{14}a_{25}\gamma^2}{K_{\alpha\beta}K_{\alpha\gamma}K_{\beta\gamma}}\\&-\frac{\sqrt{2}\alpha\beta a_{11}a_{26}\gamma^2}{K_{\alpha\beta}K_{\beta\gamma}K_{4\beta\gamma}}-\frac{\sqrt{2}\alpha\beta a_{12}a_{27}\gamma^2}{K_{\alpha\beta}K_{\beta\gamma}K_{4\beta\gamma}}+\frac{(\beta^2-\alpha^2)\,a_{13}a_{36}\gamma^2}{\sqrt{2}K_{\alpha\beta}K_{\alpha\gamma}K_{\beta\gamma}}+\frac{(\beta^2-\alpha^2)\,a_{14}a_{37}\gamma^2}{\sqrt{2}K_{\alpha\beta}K_{\alpha\gamma}K_{\beta\gamma}}\\&-\frac{\sqrt{2}\alpha\beta a_{13}a_{38}\gamma^2}{K_{\alpha\beta}K_{\beta\gamma}K_{4\beta\gamma}}-\frac{\sqrt{2}\alpha\beta a_{14}a_{39}\gamma^2}{K_{\alpha\beta}K_{\beta\gamma}K_{4\beta\gamma}}-\frac{\sqrt{2}\alpha\beta a_{3}a_{18}\gamma}{K_{\alpha\beta}K_{\alpha\gamma}}+\frac{2\alpha\beta a_{9}a_{18}\gamma}{K_{\alpha\beta}K_{\alpha\gamma}}-\frac{\sqrt{2}\alpha\beta a_{4}a_{19}\gamma}{K_{\alpha\beta}K_{\alpha\gamma}}\\&+\frac{2\alpha\beta a_{10}a_{19}\gamma}{K_{\alpha\beta}K_{\alpha\gamma}}+\frac{2\alpha\beta a_{6}a_{22}\gamma}{K_{\alpha\beta}K_{\alpha\gamma}}+\frac{2\alpha\beta a_{7}a_{23}\gamma}{K_{\alpha\beta}K_{\alpha\gamma}}+\frac{(\beta^2-\alpha^2)\,a_{3}a_{28}\gamma}{\sqrt{2}K_{\alpha\beta}K_{\beta\gamma}}+\frac{(\beta^2-\alpha^2)\,a_{9}a_{28}\gamma}{K_{\alpha\beta}K_{\beta\gamma}}\\&+\frac{(\beta^2-\alpha^2)\,a_{4}a_{29}\gamma}{\sqrt{2}K_{\alpha\beta}K_{\beta\gamma}}+\frac{(\beta^2-\alpha^2)\,a_{10}a_{29}\gamma}{K_{\alpha\beta}K_{\beta\gamma}}-\frac{\sqrt{2}\alpha\beta a_{6}a_{34}\gamma}{K_{\alpha\beta}K_{\alpha\gamma}}-\frac{\sqrt{2}\alpha\beta a_{7}a_{35}\gamma}{K_{\alpha\beta}K_{\alpha\gamma}}+\frac{(\beta^2-\alpha^2)\,a_{6}a_{40}\gamma}{\sqrt{2}K_{\alpha\beta}K_{4\beta\gamma}}\\&+\frac{(\beta^2-\alpha^2)\,a_{7}a_{41}\gamma}{\sqrt{2}K_{\alpha\beta}K_{4\beta\gamma}}-\frac{(\alpha^2+\beta^2)\,a_{30}}{\mathrm{Re}}-\frac{\alpha\,(\alpha^2-3\beta^2)\,a_{5}a_{31}}{\sqrt{2}\,(\alpha^2+\beta^2)}-\frac{\alpha\,(\alpha^2+3\beta^2)\,a_{8}a_{43}}{\sqrt{2}K_{\alpha\beta}K_{\alpha4\beta}}\\&-\frac{\alpha\,(\alpha^2-5\beta^2)\,a_{15}a_{43}}{\sqrt{2}K_{\alpha\beta}K_{\alpha4\beta}}\end{aligned}$$

$$\begin{aligned}\frac{da_{31}}{dt} =&\frac{(\alpha^2-\beta^2)\,a_{11}a_{18}\gamma^2}{\sqrt{2}K_{\alpha\beta}K_{\alpha\gamma}K_{4\beta\gamma}}+\frac{(\alpha^2-\beta^2)\,a_{12}a_{19}\gamma^2}{\sqrt{2}K_{\alpha\beta}K_{\alpha\gamma}K_{4\beta\gamma}}+\frac{(\alpha^2-\beta^2)\,a_{13}a_{22}\gamma^2}{K_{\alpha\beta}K_{\alpha\gamma}K_{\beta\gamma}}+\frac{(\alpha^2-\beta^2)\,a_{14}a_{23}\gamma^2}{K_{\alpha\beta}K_{\alpha\gamma}K_{\beta\gamma}}\\&-\frac{\sqrt{2}\alpha\beta a_{11}a_{28}\gamma^2}{K_{\alpha\beta}K_{\beta\gamma}K_{4\beta\gamma}}-\frac{\sqrt{2}\alpha\beta a_{12}a_{29}\gamma^2}{K_{\alpha\beta}K_{\beta\gamma}K_{4\beta\gamma}}+\frac{(\alpha^2-\beta^2)\,a_{13}a_{34}\gamma^2}{\sqrt{2}K_{\alpha\beta}K_{\alpha\gamma}K_{\beta\gamma}}+\frac{(\alpha^2-\beta^2)\,a_{14}a_{35}\gamma^2}{\sqrt{2}K_{\alpha\beta}K_{\alpha\gamma}K_{\beta\gamma}}\\&-\frac{\sqrt{2}\alpha\beta a_{13}a_{40}\gamma^2}{K_{\alpha\beta}K_{\beta\gamma}K_{4\beta\gamma}}-\frac{\sqrt{2}\alpha\beta a_{14}a_{41}\gamma^2}{K_{\alpha\beta}K_{\beta\gamma}K_{4\beta\gamma}}-\frac{\sqrt{2}\alpha\beta a_{3}a_{20}\gamma}{K_{\alpha\beta}K_{\alpha\gamma}}+\frac{2\alpha\beta a_{9}a_{20}\gamma}{K_{\alpha\beta}K_{\alpha\gamma}}-\frac{\sqrt{2}\alpha\beta a_{4}a_{21}\gamma}{K_{\alpha\beta}K_{\alpha\gamma}}\\&+\frac{2\alpha\beta a_{10}a_{21}\gamma}{K_{\alpha\beta}K_{\alpha\gamma}}+\frac{2\alpha\beta a_{6}a_{24}\gamma}{K_{\alpha\beta}K_{\alpha\gamma}}+\frac{2\alpha\beta a_{7}a_{25}\gamma}{K_{\alpha\beta}K_{\alpha\gamma}}+\frac{(\alpha^2-\beta^2)\,a_{3}a_{26}\gamma}{\sqrt{2}K_{\alpha\beta}K_{\beta\gamma}}+\frac{(\alpha^2-\beta^2)\,a_{9}a_{26}\gamma}{K_{\alpha\beta}K_{\beta\gamma}}\\&+\frac{(\alpha^2-\beta^2)\,a_{4}a_{27}\gamma}{\sqrt{2}K_{\alpha\beta}K_{\beta\gamma}}+\frac{(\alpha^2-\beta^2)\,a_{10}a_{27}\gamma}{K_{\alpha\beta}K_{\beta\gamma}}-\frac{\sqrt{2}\alpha\beta a_{6}a_{36}\gamma}{K_{\alpha\beta}K_{\alpha\gamma}}-\frac{\sqrt{2}\alpha\beta a_{7}a_{37}\gamma}{K_{\alpha\beta}K_{\alpha\gamma}}+\frac{(\alpha^2-\beta^2)\,a_{6}a_{38}\gamma}{\sqrt{2}K_{\alpha\beta}K_{4\beta\gamma}}\\&+\frac{(\alpha^2-\beta^2)\,a_{7}a_{39}\gamma}{\sqrt{2}K_{\alpha\beta}K_{4\beta\gamma}}+\frac{\alpha\,(\alpha^2-3\beta^2)\,a_{5}a_{30}}{\sqrt{2}\,(\alpha^2+\beta^2)}-\frac{(\alpha^2+\beta^2)\,a_{31}}{\mathrm{Re}}+\frac{\alpha\,(\alpha^2+3\beta^2)\,a_{8}a_{42}}{K_{\alpha\beta}K_{\alpha4\beta}}\\&+\frac{\alpha\,(\alpha^2-5\beta^2)\,a_{15}a_{42}}{K_{\alpha\beta}K_{\alpha4\beta}}\end{aligned}$$

$$\begin{aligned}\frac{da_{32}}{dt} =&-\frac{\alpha^2a_{32}}{\mathrm{Re}}-\frac{4\beta^2a_{32}}{\mathrm{Re}}+\frac{\alpha\beta\gamma a_{14}a_{20}}{\sqrt{2}K_{\alpha\gamma}K_{\beta\gamma}}-\frac{\alpha\beta\gamma a_{13}a_{21}}{\sqrt{2}K_{\alpha\gamma}K_{\beta\gamma}}-\frac{\alpha\beta a_{2}a_{30}}{\sqrt{2}K_{\alpha\beta}}+\frac{\alpha^2a_{7}a_{18}}{\sqrt{2}K_{\alpha\gamma}}-\frac{\alpha^2a_{6}a_{19}}{\sqrt{2}K_{\alpha\gamma}}\\&-\frac{\alpha^2a_{4}a_{22}}{K_{\alpha\gamma}}+\frac{\alpha^2a_{3}a_{23}}{K_{\alpha\gamma}}-\frac{\alpha^2a_{10}a_{34}}{K_{\alpha\gamma}}+\frac{\alpha^2a_{9}a_{35}}{K_{\alpha\gamma}}+\frac{\alpha\beta a_{7}a_{28}}{\sqrt{2}K_{\beta\gamma}}-\frac{\alpha\beta a_{6}a_{29}}{\sqrt{2}K_{\beta\gamma}}+\frac{2\alpha\beta a_{10}a_{40}}{K_{4\beta\gamma}}\\&-\frac{2\alpha\beta a_{9}a_{41}}{K_{4\beta\gamma}}+\frac{\alpha a_{8}a_{17}}{\sqrt{2}}-\frac{\alpha a_{15}a_{17}}{\sqrt{2}}-\alpha a_{5}a_{45}\end{aligned}$$

$$\frac{da_{33}}{dt} = -\frac{\alpha^2 a_{33}}{\mathrm{Re}} - \frac{4\beta^2 a_{33}}{\mathrm{Re}} - \frac{\alpha\beta\gamma a_{14}a_{18}}{\sqrt{2}K_{\alpha\gamma}K_{\beta\gamma}} + \frac{\alpha\beta\gamma a_{13}a_{19}}{\sqrt{2}K_{\alpha\gamma}K_{\beta\gamma}} - \frac{\alpha\beta a_2 a_{31}}{\sqrt{2}K_{\alpha\beta}} + \frac{\alpha^2 a_7 a_{20}}{\sqrt{2}K_{\alpha\gamma}} - \frac{\alpha^2 a_6 a_{21}}{\sqrt{2}K_{\alpha\gamma}}$$
$$- \frac{\alpha^2 a_4 a_{24}}{K_{\alpha\gamma}} + \frac{\alpha^2 a_3 a_{25}}{K_{\alpha\gamma}} - \frac{\alpha^2 a_{10}a_{36}}{K_{\alpha\gamma}} + \frac{\alpha^2 a_9 a_{37}}{K_{\alpha\gamma}} - \frac{\alpha\beta a_7 a_{26}}{\sqrt{2}K_{\beta\gamma}} + \frac{\alpha\beta a_6 a_{27}}{\sqrt{2}K_{\beta\gamma}} - \frac{2\alpha\beta a_{10}a_{38}}{K_{4\beta\gamma}}$$
$$+ \frac{2\alpha\beta a_9 a_{39}}{K_{4\beta\gamma}} - \frac{\alpha a_8 a_{16}}{\sqrt{2}} + \frac{\alpha a_{15}a_{16}}{\sqrt{2}} + \alpha a_5 a_{44}$$

$$\frac{da_{34}}{dt} = -\frac{16\alpha\beta\Omega a_{20}}{3\pi\mathrm{Re}\left(\alpha^2+4\beta^2+\gamma^2\right)} + \frac{4\Omega K_{\alpha\gamma}\left(4\beta^2+\gamma^2\right)a_{26}}{3\pi\mathrm{Re}K_{\beta\gamma}\left(\alpha^2+4\beta^2+\gamma^2\right)} - \frac{a_{34}\left(\alpha^2+4\beta^2+\gamma^2\right)}{\mathrm{Re}}$$
$$- \frac{\sqrt{2}\alpha\beta\gamma K_{\alpha\gamma}a_{14}a_{17}}{K_{\beta\gamma}\left(\alpha^2+4\beta^2+\gamma^2\right)} - \frac{\sqrt{2}\alpha\beta\gamma K_{\alpha\gamma}a_2 a_{29}}{K_{\beta\gamma}\left(\alpha^2+4\beta^2+\gamma^2\right)} + \frac{2\sqrt{2}\alpha\beta K_{\alpha\gamma}a_9 a_{42}}{\gamma K_{\alpha4\beta}}$$
$$- \frac{K_{\alpha\gamma}a_7 a_{16}\left(\alpha^2-4\beta^2-\gamma^2\right)}{\sqrt{2}\left(\alpha^2+4\beta^2+\gamma^2\right)} + \frac{\beta K_{\alpha\gamma}a_8 a_{26}\left(\alpha^2-4\beta^2-\gamma^2\right)}{\sqrt{2}K_{\beta\gamma}\left(\alpha^2+4\beta^2+\gamma^2\right)} + \frac{3\beta K_{\alpha\gamma}a_{15}a_{26}\left(\alpha^2-4\beta^2-\gamma^2\right)}{\sqrt{2}K_{\beta\gamma}\left(\alpha^2+4\beta^2+\gamma^2\right)}$$
$$+ \frac{\beta^2 K_{\alpha\gamma}a_{13}a_{31}\left(3\alpha^2+4\beta^2+\gamma^2\right)}{\sqrt{2}K_{\alpha\beta}K_{\beta\gamma}\left(\alpha^2+4\beta^2+\gamma^2\right)} + \frac{K_{\alpha\gamma}a_{10}a_{32}\left(\alpha^2-4\beta^2-\gamma^2\right)}{\alpha^2+4\beta^2+\gamma^2} + \frac{K_{\alpha\gamma}a_4 a_{44}\left(\alpha^2-4\beta^2-\gamma^2\right)}{\alpha^2+4\beta^2+\gamma^2}$$
$$+ \frac{\sqrt{2}\alpha^3\beta K_{\alpha\gamma}a_6 a_{30}}{K_{\alpha\beta}\left(\alpha^2\gamma+4\beta^2\gamma+\gamma^3\right)} + \frac{\alpha a_8 a_{20}}{\sqrt{2}} - \frac{\alpha a_{15}a_{20}}{\sqrt{2}} - \alpha a_5 a_{24} + \frac{\gamma a_2 a_{19}}{\sqrt{2}} - \gamma a_1 a_{23}$$

$$\frac{da_{35}}{dt} = -\frac{16\alpha\beta\Omega a_{21}}{3\pi\mathrm{Re}\left(\alpha^2+4\beta^2+\gamma^2\right)} + \frac{4\Omega K_{\alpha\gamma}\left(4\beta^2+\gamma^2\right)a_{27}}{3\pi\mathrm{Re}K_{\beta\gamma}\left(\alpha^2+4\beta^2+\gamma^2\right)} - \frac{a_{35}\left(\alpha^2+4\beta^2+\gamma^2\right)}{\mathrm{Re}}$$
$$+ \frac{\sqrt{2}\alpha\beta\gamma K_{\alpha\gamma}a_{13}a_{17}}{K_{\beta\gamma}\left(\alpha^2+4\beta^2+\gamma^2\right)} + \frac{\sqrt{2}\alpha\beta\gamma K_{\alpha\gamma}a_2 a_{28}}{K_{\beta\gamma}\left(\alpha^2+4\beta^2+\gamma^2\right)} + \frac{2\sqrt{2}\alpha\beta K_{\alpha\gamma}a_{10}a_{42}}{\gamma K_{\alpha4\beta}}$$
$$+ \frac{K_{\alpha\gamma}a_6 a_{16}\left(\alpha^2-4\beta^2-\gamma^2\right)}{\sqrt{2}\left(\alpha^2+4\beta^2+\gamma^2\right)} + \frac{\beta K_{\alpha\gamma}a_8 a_{27}\left(\alpha^2-4\beta^2-\gamma^2\right)}{\sqrt{2}K_{\beta\gamma}\left(\alpha^2+4\beta^2+\gamma^2\right)} + \frac{3\beta K_{\alpha\gamma}a_{15}a_{27}\left(\alpha^2-4\beta^2-\gamma^2\right)}{\sqrt{2}K_{\beta\gamma}\left(\alpha^2+4\beta^2+\gamma^2\right)}$$
$$+ \frac{\beta^2 K_{\alpha\gamma}a_{14}a_{31}\left(3\alpha^2+4\beta^2+\gamma^2\right)}{\sqrt{2}K_{\alpha\beta}K_{\beta\gamma}\left(\alpha^2+4\beta^2+\gamma^2\right)} - \frac{K_{\alpha\gamma}a_9 a_{32}\left(\alpha^2-4\beta^2-\gamma^2\right)}{\alpha^2+4\beta^2+\gamma^2} - \frac{K_{\alpha\gamma}a_3 a_{44}\left(\alpha^2-4\beta^2-\gamma^2\right)}{\alpha^2+4\beta^2+\gamma^2}$$
$$+ \frac{\sqrt{2}\alpha^3\beta K_{\alpha\gamma}a_7 a_{30}}{K_{\alpha\beta}\left(\alpha^2\gamma+4\beta^2\gamma+\gamma^3\right)} + \frac{\alpha a_8 a_{21}}{\sqrt{2}} - \frac{\alpha a_{15}a_{21}}{\sqrt{2}} - \alpha a_5 a_{25} - \frac{\gamma a_2 a_{18}}{\sqrt{2}} + \gamma a_1 a_{22}$$

$$\frac{da_{36}}{dt} = \frac{16\alpha\beta\Omega a_{18}}{3\pi\mathrm{Re}\left(\alpha^2+4\beta^2+\gamma^2\right)} + \frac{4\Omega K_{\alpha\gamma}\left(4\beta^2+\gamma^2\right)a_{28}}{3\pi\mathrm{Re}K_{\beta\gamma}\left(\alpha^2+4\beta^2+\gamma^2\right)} - \frac{a_{36}\left(\alpha^2+4\beta^2+\gamma^2\right)}{\mathrm{Re}}$$
$$+ \frac{\sqrt{2}\alpha\beta\gamma K_{\alpha\gamma}a_{14}a_{16}}{K_{\beta\gamma}\left(\alpha^2+4\beta^2+\gamma^2\right)} + \frac{\sqrt{2}\alpha\beta\gamma K_{\alpha\gamma}a_2 a_{27}}{K_{\beta\gamma}\left(\alpha^2+4\beta^2+\gamma^2\right)} + \frac{2\alpha\beta K_{\alpha\gamma}a_9 a_{43}}{\gamma K_{\alpha4\beta}} - \frac{K_{\alpha\gamma}a_7 a_{17}\left(\alpha^2-4\beta^2-\gamma^2\right)}{\sqrt{2}\left(\alpha^2+4\beta^2+\gamma^2\right)}$$
$$+ \frac{\beta K_{\alpha\gamma}a_8 a_{28}\left(\alpha^2-4\beta^2-\gamma^2\right)}{\sqrt{2}K_{\beta\gamma}\left(\alpha^2+4\beta^2+\gamma^2\right)} + \frac{3\beta K_{\alpha\gamma}a_{15}a_{28}\left(\alpha^2-4\beta^2-\gamma^2\right)}{\sqrt{2}K_{\beta\gamma}\left(\alpha^2+4\beta^2+\gamma^2\right)}$$
$$- \frac{\beta^2 K_{\alpha\gamma}a_{13}a_{30}\left(3\alpha^2+4\beta^2+\gamma^2\right)}{\sqrt{2}K_{\alpha\beta}K_{\beta\gamma}\left(\alpha^2+4\beta^2+\gamma^2\right)} + \frac{K_{\alpha\gamma}a_{10}a_{33}\left(\alpha^2-4\beta^2-\gamma^2\right)}{\alpha^2+4\beta^2+\gamma^2} + \frac{K_{\alpha\gamma}a_4 a_{45}\left(\alpha^2-4\beta^2-\gamma^2\right)}{\alpha^2+4\beta^2+\gamma^2}$$
$$+ \frac{\sqrt{2}\alpha^3\beta K_{\alpha\gamma}a_6 a_{31}}{K_{\alpha\beta}\left(\alpha^2\gamma+4\beta^2\gamma+\gamma^3\right)} - \frac{\alpha a_8 a_{18}}{\sqrt{2}} + \frac{\alpha a_{15}a_{18}}{\sqrt{2}} + \alpha a_5 a_{22} + \frac{\gamma a_2 a_{21}}{\sqrt{2}} - \gamma a_1 a_{25}$$

$$\frac{da_{37}}{dt} =\frac{16\alpha\beta\Omega a_{19}}{3\pi\mathrm{Re}\left(\alpha^2+4\beta^2+\gamma^2\right)}+\frac{4\Omega K_{\alpha\gamma}\left(4\beta^2+\gamma^2\right)a_{29}}{3\pi\mathrm{Re}K_{\beta\gamma}\left(\alpha^2+4\beta^2+\gamma^2\right)}-\frac{a_{37}\left(\alpha^2+4\beta^2+\gamma^2\right)}{\mathrm{Re}}$$
$$-\frac{\sqrt{2}\alpha\beta\gamma K_{\alpha\gamma}a_{13}a_{16}}{K_{\beta\gamma}\left(\alpha^2+4\beta^2+\gamma^2\right)}-\frac{\sqrt{2}\alpha\beta\gamma K_{\alpha\gamma}a_{2}a_{26}}{K_{\beta\gamma}\left(\alpha^2+4\beta^2+\gamma^2\right)}+\frac{2\alpha\beta K_{\alpha\gamma}a_{10}a_{43}}{\gamma K_{\alpha4\beta}}+\frac{K_{\alpha\gamma}a_{6}a_{17}\left(\alpha^2-4\beta^2-\gamma^2\right)}{\sqrt{2}\left(\alpha^2+4\beta^2+\gamma^2\right)}$$
$$+\frac{\beta K_{\alpha\gamma}a_{8}a_{29}\left(\alpha^2-4\beta^2-\gamma^2\right)}{\sqrt{2}K_{\beta\gamma}\left(\alpha^2+4\beta^2+\gamma^2\right)}+\frac{3\beta K_{\alpha\gamma}a_{15}a_{29}\left(\alpha^2-4\beta^2-\gamma^2\right)}{\sqrt{2}K_{\beta\gamma}\left(\alpha^2+4\beta^2+\gamma^2\right)}$$
$$-\frac{\beta^2 K_{\alpha\gamma}a_{14}a_{30}\left(3\alpha^2+4\beta^2+\gamma^2\right)}{\sqrt{2}K_{\alpha\beta}K_{\beta\gamma}\left(\alpha^2+4\beta^2+\gamma^2\right)}-\frac{K_{\alpha\gamma}a_{9}a_{33}\left(\alpha^2-4\beta^2-\gamma^2\right)}{\alpha^2+4\beta^2+\gamma^2}$$
$$-\frac{K_{\alpha\gamma}a_{3}a_{45}\left(\alpha^2-4\beta^2-\gamma^2\right)}{\alpha^2+4\beta^2+\gamma^2}+\frac{\sqrt{2}\alpha^3\beta K_{\alpha\gamma}a_{7}a_{31}}{K_{\alpha\beta}\left(\alpha^2\gamma+4\beta^2\gamma+\gamma^3\right)}-\frac{\alpha a_{8}a_{19}}{\sqrt{2}}+\frac{\alpha a_{15}a_{19}}{\sqrt{2}}+\alpha a_{5}a_{23}$$
$$-\frac{\gamma a_{2}a_{20}}{\sqrt{2}}+\gamma a_{1}a_{24}$$

$$\frac{da_{38}}{dt} =-\frac{8\alpha\beta\Omega K_{4\beta\gamma}a_{28}}{3\pi\mathrm{Re}K_{\beta\gamma}\left(\alpha^2+4\beta^2+\gamma^2\right)}-\frac{8\Omega K_{\alpha\gamma}K_{4\beta\gamma}a_{18}}{3\pi\mathrm{Re}\left(\alpha^2+4\beta^2+\gamma^2\right)}-\frac{a_{38}\left(\alpha^2+4\beta^2+\gamma^2\right)}{\mathrm{Re}}$$
$$-\frac{\alpha^2\left(\alpha^2+\gamma^2\right)K_{4\beta\gamma}a_{6}a_{31}}{\sqrt{2}\gamma K_{\alpha\beta}\left(\alpha^2+4\beta^2+\gamma^2\right)}-\frac{\alpha^2 K_{4\beta\gamma}a_{9}a_{43}}{\gamma\sqrt{\alpha^2+4\beta^2}}-\frac{2\sqrt{2}\alpha\beta K_{4\beta\gamma}a_{7}a_{17}}{\alpha^2+4\beta^2+\gamma^2}-\frac{\alpha\left(\alpha^2+\gamma^2\right)K_{4\beta\gamma}a_{8}a_{28}}{\sqrt{2}K_{\beta\gamma}\left(\alpha^2+4\beta^2+\gamma^2\right)}$$
$$-\frac{\alpha K_{4\beta\gamma}a_{15}a_{28}\left(\alpha^2-8\beta^2+\gamma^2\right)}{\sqrt{2}K_{\beta\gamma}\left(\alpha^2+4\beta^2+\gamma^2\right)}+\frac{\sqrt{2}\alpha\beta K_{4\beta\gamma}a_{13}a_{30}\left(\alpha^2+2\beta^2+\gamma^2\right)}{K_{\alpha\beta}K_{\beta\gamma}\left(\alpha^2+4\beta^2+\gamma^2\right)}+\frac{4\alpha\beta K_{4\beta\gamma}a_{10}a_{33}}{\alpha^2+4\beta^2+\gamma^2}$$
$$+\frac{4\alpha\beta K_{4\beta\gamma}a_{4}a_{45}}{\alpha^2+4\beta^2+\gamma^2}-\frac{\gamma\left(\alpha^2+\gamma^2\right)K_{4\beta\gamma}a_{14}a_{16}}{\sqrt{2}K_{\beta\gamma}\left(\alpha^2+4\beta^2+\gamma^2\right)}-\frac{\gamma\left(\alpha^2+\gamma^2\right)K_{4\beta\gamma}a_{2}a_{27}}{\sqrt{2}K_{\beta\gamma}\left(\alpha^2+4\beta^2+\gamma^2\right)}-\gamma a_{12}a_{44}$$

$$\frac{da_{39}}{dt} =-\frac{8\alpha\beta\Omega K_{4\beta\gamma}a_{29}}{3\pi\mathrm{Re}K_{\beta\gamma}\left(\alpha^2+4\beta^2+\gamma^2\right)}-\frac{8\Omega K_{\alpha\gamma}K_{4\beta\gamma}a_{19}}{3\pi\mathrm{Re}\left(\alpha^2+4\beta^2+\gamma^2\right)}-\frac{a_{39}\left(\alpha^2+4\beta^2+\gamma^2\right)}{\mathrm{Re}}$$
$$-\frac{\alpha^2\left(\alpha^2+\gamma^2\right)K_{4\beta\gamma}a_{7}a_{31}}{\sqrt{2}\gamma K_{\alpha\beta}\left(\alpha^2+4\beta^2+\gamma^2\right)}-\frac{\alpha^2 K_{4\beta\gamma}a_{10}a_{43}}{\gamma\sqrt{\alpha^2+4\beta^2}}+\frac{2\sqrt{2}\alpha\beta K_{4\beta\gamma}a_{6}a_{17}}{\alpha^2+4\beta^2+\gamma^2}-\frac{\alpha\left(\alpha^2+\gamma^2\right)K_{4\beta\gamma}a_{8}a_{29}}{\sqrt{2}K_{\beta\gamma}\left(\alpha^2+4\beta^2+\gamma^2\right)}$$
$$-\frac{\alpha K_{4\beta\gamma}a_{15}a_{29}\left(\alpha^2-8\beta^2+\gamma^2\right)}{\sqrt{2}K_{\beta\gamma}\left(\alpha^2+4\beta^2+\gamma^2\right)}+\frac{\sqrt{2}\alpha\beta K_{4\beta\gamma}a_{14}a_{30}\left(\alpha^2+2\beta^2+\gamma^2\right)}{K_{\alpha\beta}K_{\beta\gamma}\left(\alpha^2+4\beta^2+\gamma^2\right)}-\frac{4\alpha\beta K_{4\beta\gamma}a_{9}a_{33}}{\alpha^2+4\beta^2+\gamma^2}$$
$$-\frac{4\alpha\beta K_{4\beta\gamma}a_{3}a_{45}}{\alpha^2+4\beta^2+\gamma^2}+\frac{\gamma\left(\alpha^2+\gamma^2\right)K_{4\beta\gamma}a_{13}a_{16}}{\sqrt{2}K_{\beta\gamma}\left(\alpha^2+4\beta^2+\gamma^2\right)}+\frac{\gamma\left(\alpha^2+\gamma^2\right)K_{4\beta\gamma}a_{2}a_{26}}{\sqrt{2}K_{\beta\gamma}\left(\alpha^2+4\beta^2+\gamma^2\right)}+\gamma a_{11}a_{44}$$

$$\frac{da_{40}}{dt} =\frac{8\alpha\beta\Omega K_{4\beta\gamma}a_{26}}{3\pi\mathrm{Re}K_{\beta\gamma}\left(\alpha^2+4\beta^2+\gamma^2\right)}-\frac{8\Omega K_{\alpha\gamma}K_{4\beta\gamma}a_{20}}{3\pi\mathrm{Re}\left(\alpha^2+4\beta^2+\gamma^2\right)}-\frac{a_{40}\left(\alpha^2+4\beta^2+\gamma^2\right)}{\mathrm{Re}}$$
$$+\frac{\alpha^2\left(\alpha^2+\gamma^2\right)K_{4\beta\gamma}a_{6}a_{30}}{\sqrt{2}\gamma K_{\alpha\beta}\left(\alpha^2+4\beta^2+\gamma^2\right)}+\frac{\sqrt{2}\alpha^2 K_{4\beta\gamma}a_{9}a_{42}}{\gamma K_{\alpha4\beta}}+\frac{2\sqrt{2}\alpha\beta K_{4\beta\gamma}a_{7}a_{16}}{\alpha^2+4\beta^2+\gamma^2}+\frac{\alpha\left(\alpha^2+\gamma^2\right)K_{4\beta\gamma}a_{8}a_{26}}{\sqrt{2}K_{\beta\gamma}\left(\alpha^2+4\beta^2+\gamma^2\right)}$$
$$+\frac{\alpha K_{4\beta\gamma}a_{15}a_{26}\left(\alpha^2-8\beta^2+\gamma^2\right)}{\sqrt{2}K_{\beta\gamma}\left(\alpha^2+4\beta^2+\gamma^2\right)}+\frac{\sqrt{2}\alpha\beta K_{4\beta\gamma}a_{13}a_{31}\left(\alpha^2+2\beta^2+\gamma^2\right)}{K_{\alpha\beta}K_{\beta\gamma}\left(\alpha^2+4\beta^2+\gamma^2\right)}-\frac{4\alpha\beta K_{4\beta\gamma}a_{10}a_{32}}{\alpha^2+4\beta^2+\gamma^2}$$
$$-\frac{4\alpha\beta K_{4\beta\gamma}a_{4}a_{44}}{\alpha^2+4\beta^2+\gamma^2}-\frac{\gamma\left(\alpha^2+\gamma^2\right)K_{4\beta\gamma}a_{14}a_{17}}{\sqrt{2}K_{\beta\gamma}\left(\alpha^2+4\beta^2+\gamma^2\right)}-\frac{\gamma\left(\alpha^2+\gamma^2\right)K_{4\beta\gamma}a_{2}a_{29}}{\sqrt{2}K_{\beta\gamma}\left(\alpha^2+4\beta^2+\gamma^2\right)}-\gamma a_{12}a_{45}$$

$$\frac{da_{41}}{dt} =\frac{8\alpha\beta\Omega K_{4\beta\gamma}a_{27}}{3\pi\mathrm{Re}K_{\beta\gamma}\left(\alpha^2+4\beta^2+\gamma^2\right)}-\frac{8\Omega K_{\alpha\gamma}K_{4\beta\gamma}a_{21}}{3\pi\mathrm{Re}\left(\alpha^2+4\beta^2+\gamma^2\right)}-\frac{a_{41}\left(\alpha^2+4\beta^2+\gamma^2\right)}{\mathrm{Re}}$$
$$+\frac{\alpha^2\left(\alpha^2+\gamma^2\right)K_{4\beta\gamma}a_7a_{30}}{\sqrt{2}\gamma K_{\alpha\beta}\left(\alpha^2+4\beta^2+\gamma^2\right)}+\frac{\sqrt{2}\alpha^2K_{4\beta\gamma}a_{10}a_{42}}{\gamma K_{\alpha4\beta}}-\frac{2\sqrt{2}\alpha\beta K_{4\beta\gamma}a_6a_{16}}{\alpha^2+4\beta^2+\gamma^2}$$
$$+\frac{\alpha\left(\alpha^2+\gamma^2\right)K_{4\beta\gamma}a_8a_{27}}{\sqrt{2}K_{\beta\gamma}\left(\alpha^2+4\beta^2+\gamma^2\right)}+\frac{\alpha K_{4\beta\gamma}a_{15}a_{27}\left(\alpha^2-8\beta^2+\gamma^2\right)}{\sqrt{2}K_{\beta\gamma}\left(\alpha^2+4\beta^2+\gamma^2\right)}$$
$$+\frac{\sqrt{2}\alpha\beta K_{4\beta\gamma}a_{14}a_{31}\left(\alpha^2+2\beta^2+\gamma^2\right)}{K_{\alpha\beta}K_{\beta\gamma}\left(\alpha^2+4\beta^2+\gamma^2\right)}+\frac{4\alpha\beta K_{4\beta\gamma}a_9a_{32}}{\alpha^2+4\beta^2+\gamma^2}+\frac{4\alpha\beta K_{4\beta\gamma}a_3a_{44}}{\alpha^2+4\beta^2+\gamma^2}$$
$$+\frac{\gamma\left(\alpha^2+\gamma^2\right)K_{4\beta\gamma}a_{13}a_{17}}{\sqrt{2}K_{\beta\gamma}\left(\alpha^2+4\beta^2+\gamma^2\right)}+\frac{\gamma\left(\alpha^2+\gamma^2\right)K_{4\beta\gamma}a_2a_{28}}{\sqrt{2}K_{\beta\gamma}\left(\alpha^2+4\beta^2+\gamma^2\right)}+\gamma a_{11}a_{45}$$

$$\frac{da_{42}}{dt} =-\frac{a_8a_{31}\alpha^3}{2K_{\alpha\beta}K_{\alpha4\beta}}+\frac{2\beta\gamma a_6a_{18}\alpha}{K_{\alpha4\beta}K_{\alpha\gamma}}+\frac{2\beta\gamma a_7a_{19}\alpha}{K_{\alpha4\beta}K_{\alpha\gamma}}-\frac{2\sqrt{2}\beta\gamma a_3a_{22}\alpha}{K_{\alpha4\beta}K_{\alpha\gamma}}-\frac{2\sqrt{2}\beta\gamma a_4a_{23}\alpha}{K_{\alpha4\beta}K_{\alpha\gamma}}+\frac{2\beta\gamma^2a_{13}a_{26}\alpha}{K_{\alpha4\beta}\left(\beta^2+\gamma^2\right)}$$
$$+\frac{2\beta\gamma^2a_{14}a_{27}\alpha}{K_{\alpha4\beta}\left(\beta^2+\gamma^2\right)}-\frac{\left(\alpha^2-8\beta^2\right)a_{15}a_{31}\alpha}{2K_{\alpha\beta}K_{\alpha4\beta}}-\frac{2\sqrt{2}\beta\gamma a_9a_{34}\alpha}{K_{\alpha4\beta}K_{\alpha\gamma}}-\frac{2\sqrt{2}\beta\gamma a_{10}a_{35}\alpha}{K_{\alpha4\beta}K_{\alpha\gamma}}$$
$$-\frac{\left(\alpha^2-4\beta^2\right)\gamma^2a_{13}a_{20}}{2K_{\alpha4\beta}K_{\alpha\gamma}K_{\beta\gamma}}-\frac{\left(\alpha^2-4\beta^2\right)\gamma^2a_{14}a_{21}}{2K_{\alpha4\beta}K_{\alpha\gamma}K_{\beta\gamma}}-\frac{\left(\alpha^2-4\beta^2\right)\gamma^2a_{11}a_{24}}{\sqrt{2}K_{\alpha4\beta}K_{\alpha\gamma}K_{4\beta\gamma}}-\frac{\left(\alpha^2-4\beta^2\right)\gamma^2a_{12}a_{25}}{\sqrt{2}K_{\alpha4\beta}K_{\alpha\gamma}K_{4\beta\gamma}}$$
$$-\frac{\left(\alpha^2-4\beta^2\right)\gamma a_6a_{28}}{2K_{\alpha4\beta}K_{\beta\gamma}}-\frac{\left(\alpha^2-4\beta^2\right)\gamma a_7a_{29}}{2K_{\alpha4\beta}K_{\beta\gamma}}-\frac{\left(\alpha^2-4\beta^2\right)\gamma a_9a_{40}}{\sqrt{2}K_{\alpha4\beta}K_{4\beta\gamma}}-\frac{\left(\alpha^2-4\beta^2\right)\gamma a_{10}a_{41}}{\sqrt{2}K_{\alpha4\beta}K_{4\beta\gamma}}$$
$$-\frac{\left(\alpha^2+4\beta^2\right)a_{42}}{\mathrm{Re}}$$

$$\frac{da_{43}}{dt} =\frac{a_8a_{30}\alpha^3}{\sqrt{2}K_{\alpha\beta}K_{\alpha4\beta}}+\frac{2\sqrt{2}\beta\gamma a_6a_{20}\alpha}{K_{\alpha4\beta}K_{\alpha\gamma}}+\frac{2\sqrt{2}\beta\gamma a_7a_{21}\alpha}{K_{\alpha4\beta}K_{\alpha\gamma}}-\frac{4\beta\gamma a_3a_{24}\alpha}{K_{\alpha4\beta}K_{\alpha\gamma}}-\frac{4\beta\gamma a_4a_{25}\alpha}{K_{\alpha4\beta}K_{\alpha\gamma}}+\frac{2\sqrt{2}\beta\gamma^2a_{13}a_{28}\alpha}{K_{\alpha4\beta}\left(\beta^2+\gamma^2\right)}$$
$$+\frac{2\sqrt{2}\beta\gamma^2a_{14}a_{29}\alpha}{K_{\alpha4\beta}\left(\beta^2+\gamma^2\right)}-\frac{4\beta\gamma a_9a_{36}\alpha}{K_{\alpha4\beta}K_{\alpha\gamma}}-\frac{4\beta\gamma a_{10}a_{37}\alpha}{K_{\alpha4\beta}K_{\alpha\gamma}}+\frac{\left(\alpha^2-4\beta^2\right)\gamma^2a_{13}a_{18}}{\sqrt{2}K_{\alpha4\beta}K_{\alpha\gamma}K_{\beta\gamma}}+\frac{\left(\alpha^2-4\beta^2\right)\gamma^2a_{14}a_{19}}{\sqrt{2}K_{\alpha4\beta}K_{\alpha\gamma}K_{\beta\gamma}}$$
$$+\frac{\left(\alpha^2-4\beta^2\right)\gamma^2a_{11}a_{22}}{K_{\alpha4\beta}K_{\alpha\gamma}K_{4\beta\gamma}}+\frac{\left(\alpha^2-4\beta^2\right)\gamma^2a_{12}a_{23}}{K_{\alpha4\beta}K_{\alpha\gamma}K_{4\beta\gamma}}+\frac{\left(\alpha^2-4\beta^2\right)\gamma a_6a_{26}}{\sqrt{2}K_{\alpha4\beta}K_{\beta\gamma}}+\frac{\left(\alpha^2-4\beta^2\right)\gamma a_7a_{27}}{\sqrt{2}K_{\alpha4\beta}K_{\beta\gamma}}$$
$$+\frac{\left(\alpha^3-8\alpha\beta^2\right)a_{15}a_{30}}{\sqrt{2}K_{\alpha\beta}K_{\alpha4\beta}}+\frac{\left(\alpha^2-4\beta^2\right)\gamma a_9a_{38}}{K_{\alpha4\beta}K_{4\beta\gamma}}+\frac{\left(\alpha^2-4\beta^2\right)\gamma a_{10}a_{39}}{K_{\alpha4\beta}K_{4\beta\gamma}}-\frac{\left(\alpha^2+4\beta^2\right)a_{43}}{\mathrm{Re}}$$

$$\frac{da_{44}}{dt} =-\frac{\alpha^2a_{44}}{\mathrm{Re}}+\frac{\alpha\beta\gamma a_{14}a_{20}}{K_{\alpha\gamma}K_{\beta\gamma}}-\frac{\alpha\beta\gamma a_{13}a_{21}}{K_{\alpha\gamma}K_{\beta\gamma}}-\frac{2\alpha\beta\gamma a_{12}a_{36}}{K_{\alpha\gamma}K_{4\beta\gamma}}+\frac{2\alpha\beta\gamma a_{11}a_{37}}{K_{\alpha\gamma}K_{4\beta\gamma}}-\frac{\alpha\beta a_2a_{30}}{K_{\alpha\beta}}+\frac{2\sqrt{2}\alpha\beta a_1a_{42}}{K_{\alpha4\beta}}$$
$$-\frac{\alpha^2a_7a_{18}}{K_{\alpha\gamma}}+\frac{\alpha^2a_6a_{19}}{K_{\alpha\gamma}}-\frac{\alpha^2a_{10}a_{22}}{K_{\alpha\gamma}}+\frac{\alpha^2a_9a_{23}}{K_{\alpha\gamma}}-\frac{\alpha^2a_4a_{34}}{K_{\alpha\gamma}}+\frac{\alpha^2a_3a_{35}}{K_{\alpha\gamma}}-\frac{\alpha\beta a_7a_{28}}{K_{\beta\gamma}}+\frac{\alpha\beta a_6a_{29}}{K_{\beta\gamma}}$$
$$+\frac{2\alpha\beta a_4a_{40}}{K_{4\beta\gamma}}-\frac{2\alpha\beta a_3a_{41}}{K_{4\beta\gamma}}-\alpha a_8a_{17}-\alpha a_5a_{33}$$

$$\frac{da_{45}}{dt} = -\frac{\alpha^2 a_{45}}{\mathrm{Re}} - \frac{\alpha\beta\gamma a_{14}a_{18}}{K_{\alpha\gamma}K_{\beta\gamma}} + \frac{\alpha\beta\gamma a_{13}a_{19}}{K_{\alpha\gamma}K_{\beta\gamma}} + \frac{2\alpha\beta\gamma a_{12}a_{34}}{K_{\alpha\gamma}K_{4\beta\gamma}} - \frac{2\alpha\beta\gamma a_{11}a_{35}}{K_{\alpha\gamma}K_{4\beta\gamma}} - \frac{\alpha\beta a_2 a_{31}}{K_{\alpha\beta}} + \frac{2\alpha\beta a_1 a_{43}}{K_{\alpha 4\beta}}$$
$$- \frac{\alpha^2 a_7 a_{20}}{K_{\alpha\gamma}} + \frac{\alpha^2 a_6 a_{21}}{K_{\alpha\gamma}} - \frac{\alpha^2 a_{10}a_{24}}{K_{\alpha\gamma}} + \frac{\alpha^2 a_9 a_{25}}{K_{\alpha\gamma}} - \frac{\alpha^2 a_4 a_{36}}{K_{\alpha\gamma}} + \frac{\alpha^2 a_3 a_{37}}{K_{\alpha\gamma}} + \frac{\alpha\beta a_7 a_{26}}{K_{\beta\gamma}} - \frac{\alpha\beta a_6 a_{27}}{K_{\beta\gamma}}$$
$$- \frac{2\alpha\beta a_4 a_{38}}{K_{4\beta\gamma}} + \frac{2\alpha\beta a_3 a_{39}}{K_{4\beta\gamma}} + \alpha a_8 a_{16} + \alpha a_5 a_{32}$$

A.4 Mode interaction table for 23 mode model

j/k	3	8	9	13	15	16	19	25	29	33	37	39	45
3	-			8,15		19,29	16	33	16	25	45	45	37,39
8		-		3,9		33,45	25,37	19	25,37,39	16	19	19,29	16
9			-	8		19,29	16	45	16	37,39	33	33	25
13				-	3	25,37,39	33,45			19,29	16	16	29
15					-	33	37		37,39	16	19	19,29	
16						-	3,9	13			13	13	
19							-		13			8,15	13
25								-	8	3			9
29									-	13	8,15		13
33										-	9		
37											-		3
39												-	
45													-

Table A.2 *A table to show the nonlinear couplings that generate a_i via $\dot{a}_i = N_{ijk}a_j a_k$, with the 13 modes that encode the same information as the Marburg model [75].*

j/k	4	10	14	18	24	28	30	36	38	43
4	-		8,15	16	33	16	19,29	45	45	25
10		-	8	16	45	16	19,29	33	33	37,39
14			-	33,45			25, 37, 39	16	16	19,29
18				-			3, 9		8,15	13
24					-	8	13			
28						-	3,9	8,15		13
30							-	13	13	8,15
36								-		9
38									-	9
43										-

Table A.3 *A table to show the nonlinear couplings that generate a_i via $\dot{a}_i = N_{ijk}a_j a_k$ for the new modes not included in the Marburg model [75].*

j/k	3	8	9	13	15	16	19	25	29	33	37	39	45
4						18,28	30	43	30	24			36,38
10						18,28	30		30	36,38	43	43	24
14		4,10			4	24,36,38	43	30	43	18, 28	30	30	28
18	30	24,36	30	43	36	4,10				14			14
24	43	18		30		14				4			10
28	30	24,36,38	30	43	36,38					14			14
30	18,28		18,28	24,36,38	43		4,10	14	4,10		14	14	
36		18	43	30	18	14				10			4
38		18,28	43	30	18,28	14							
43	24	30	36,38	18,28	30		14		14		10	10	

Table A.4 *A table to show the cross-term non-linear couplings that generate a_i via $\dot{a}_i = N_{ijk}a_j a_k$ between the 2 sets of modes.*

Appendix B

Chapter 4: Supplementary information

B.1 Re-labelling table

For brevity the 23 modes are relabelled in the chronological order that they appear in in the original model. The stress tensor mode b_i is generated via $\mathbf{b}_i = \nabla \mathbf{a}_i + (\nabla \mathbf{a}_i)^T$.

Num.	**Nrm.**	**u**	**v**	**w**
u_1	2	$\cos(2\beta y)\cos(\gamma z)$	0	0
u_2	2	$\cos(2\beta y)\sin(\gamma z)$	0	0
u_3	$\sqrt{2}$	$\sin(\beta y)$	0	0
u_4	$\sqrt{2}$	$\cos(\gamma z)$	0	0
u_5	$\sqrt{2}$	$\sin(\gamma z)$	0	0
u_6	$\frac{2}{K_{\beta\gamma}}$	0	$\gamma\cos(\beta y)\cos(\gamma z)$	$\beta\sin(\beta y)\sin(\gamma z)$
u_7	$\frac{2}{K_{\beta\gamma}}$	0	$\gamma\cos(\beta y)\sin(\gamma z)$	$-\beta\sin(\beta y)\cos(\gamma z)$
u_8	$\sqrt{2}$	$\sin(3\beta y)$	0	0
u_9	2	0	0	$\cos(\alpha x)\sin(\beta y)$
u_{10}	$\frac{2\sqrt{2}}{K_{\alpha\gamma}}$	$\gamma\cos(\alpha x)\sin(\beta y)\cos(\gamma z)$	0	$\alpha\sin(\alpha x)\sin(\beta y)\sin(\gamma z)$
u_{11}	$\frac{2\sqrt{2}}{K_{\alpha\gamma}}$	$\gamma\cos(\alpha x)\sin(\beta y)\sin(\gamma z)$	0	$-\alpha\sin(\alpha x)\sin(\beta y)\cos(\gamma z)$
u_{12}	$\frac{2}{K_{\alpha\gamma}}$	$\gamma\sin(\alpha x)\cos(\gamma z)$	0	$-\alpha\cos(\alpha x)\sin(\gamma z)$
u_{13}	$\frac{2}{K_{\alpha\gamma}}$	$\gamma\sin(\alpha x)\sin(\gamma z)$	0	$\alpha\cos(\alpha x)\cos(\gamma z)$
u_{14}	$\frac{2\sqrt{2}}{K_{\beta\gamma}}$	0	$\gamma\sin(\alpha x)\cos(\beta y)\cos(\gamma z)$	$\beta\sin(\alpha x)\sin(\beta y)\sin(\gamma z)$
u_{15}	$\frac{2\sqrt{2}}{K_{\beta\gamma}}$	0	$\gamma\sin(\alpha x)\cos(\beta y)\sin(\gamma z)$	$-\beta\sin(\alpha x)\sin(\beta y)\cos(\gamma z)$
u_{16}	$\frac{2}{K_{\alpha\beta}}$	$\beta\sin(\alpha x)\sin(\beta y)$	$\alpha\cos(\alpha x)\cos(\beta y)$	0
u_{17}	2	0	0	$\cos(2\beta y)\sin(\alpha x)$
u_{18}	$\frac{2\sqrt{2}}{K_{\alpha\gamma}}$	$\gamma\sin(\alpha x)\cos(2\beta y)\cos(\gamma z)$	0	$-\alpha\cos(\alpha x)\cos(2\beta y)\sin(\gamma z)$
u_{19}	$\frac{2\sqrt{2}}{K_{\alpha\gamma}}$	$\gamma\sin(\alpha x)\cos(2\beta y)\sin(\gamma z)$	0	$\alpha\cos(\alpha x)\cos(2\beta y)\cos(\gamma z)$
u_{20}	$\frac{2\sqrt{2}}{K_{4\beta\gamma}}$	0	$\gamma\cos(\alpha x)\sin(2\beta y)\cos(\gamma z)$	$2\beta\cos(\alpha x)\cos(2\beta y)\sin(\gamma z)$

u_{21}	$\frac{2\sqrt{2}}{K_{4\beta\gamma}}$	0	$\gamma\cos(\alpha x)\sin(2\beta y)\sin(\gamma z)$	$2\beta\cos(\alpha x)\cos(2\beta y)\cos(\gamma z)$
u_{22}	$\frac{2}{K_{\alpha 4\beta}}$	$2\beta\cos(\alpha x)\cos(2\beta y)$	$\alpha\sin(\alpha x)\sin(2\beta y)$	0
u_{23}	$\sqrt{2}$	0	0	$\sin(\alpha x)$

B.2 List of stress mode equations

$$\begin{aligned}\frac{db_1}{dt} =& + \frac{\gamma^2 a_9 b_{11}\left(\alpha^2+\beta^2+\gamma^2\right)}{\sqrt{2}K_{\alpha\gamma}\left(4\beta^2+\gamma^2\right)} - \frac{\alpha\beta\gamma\left(\alpha^2-7\beta^2\right)a_{10}b_{16}}{\sqrt{2}K_{\alpha\beta}K_{\alpha\gamma}\left(4\beta^2+\gamma^2\right)} + \frac{\gamma^2\left(\alpha^2-3\beta^2\right)a_{11}b_9}{\sqrt{2}K_{\alpha\gamma}\left(4\beta^2+\gamma^2\right)} + \frac{16\alpha\beta^3\gamma a_{12}b_{22}}{K_{\alpha 4\beta}K_{\alpha\gamma}\left(4\beta^2+\gamma^2\right)} \\ & - \frac{\gamma^2\left(\alpha^2-4\beta^2\right)a_{13}b_{17}}{K_{\alpha\gamma}\left(4\beta^2+\gamma^2\right)} - \frac{\beta^2\gamma K_{\alpha\beta}a_{14}b_{16}}{\sqrt{2}K_{\beta\gamma}\left(4\beta^2+\gamma^2\right)} - \frac{\alpha\beta\gamma a_{16}b_{10}\left(\alpha^2+5\beta^2+3\gamma^2\right)}{\sqrt{2}K_{\alpha\beta}K_{\alpha\gamma}\left(4\beta^2+\gamma^2\right)} \\ & + \frac{\beta^2\gamma a_{16}b_{14}\left(-\alpha^2+3\beta^2+\gamma^2\right)}{\sqrt{2}K_{\alpha\beta}K_{\beta\gamma}\left(4\beta^2+\gamma^2\right)} - \frac{\gamma^2 K_{\alpha\gamma}a_{17}b_{13}}{4\beta^2+\gamma^2} + \frac{a_1}{\mathrm{Wi}} - \frac{\alpha^2\gamma^2 a_{19}b_{23}}{K_{\alpha\gamma}\left(4\beta^2+\gamma^2\right)} \\ & - \frac{4\alpha\beta\gamma^3 a_{22}b_{12}}{K_{\alpha 4\beta}K_{\alpha\gamma}\left(4\beta^2+\gamma^2\right)} - \frac{\gamma^2 a_{23}b_{19}\left(\alpha^2+4\beta^2+\gamma^2\right)}{K_{\alpha\gamma}\left(4\beta^2+\gamma^2\right)} + \frac{\beta\gamma a_3\left(3\beta^2+\gamma^2\right)b_6}{\sqrt{2}K_{\beta\gamma}\left(4\beta^2+\gamma^2\right)} - \frac{\beta^3\gamma a_6 b_3}{\sqrt{2}K_{\beta\gamma}\left(4\beta^2+\gamma^2\right)} \\ & - \frac{27\beta^3\gamma a_6 b_8}{\sqrt{2}K_{\beta\gamma}\left(4\beta^2+\gamma^2\right)} + \frac{3\beta\gamma a_8\left(\gamma^2-5\beta^2\right)b_6}{\sqrt{2}K_{\beta\gamma}\left(4\beta^2+\gamma^2\right)} - \frac{b_1}{\mathrm{Wi}}\end{aligned} \tag{B.1}$$

$$\begin{aligned}\frac{db_2}{dt} =& - \frac{\gamma^2 a_9 b_{10}\left(\alpha^2+\beta^2+\gamma^2\right)}{\sqrt{2}K_{\alpha\gamma}\left(4\beta^2+\gamma^2\right)} - \frac{\gamma^2\left(\alpha^2-3\beta^2\right)a_{10}b_9}{\sqrt{2}K_{\alpha\gamma}\left(4\beta^2+\gamma^2\right)} - \frac{\alpha\beta\gamma\left(\alpha^2-7\beta^2\right)a_{11}b_{16}}{\sqrt{2}K_{\alpha\beta}K_{\alpha\gamma}\left(4\beta^2+\gamma^2\right)} + \frac{\gamma^2\left(\alpha^2-4\beta^2\right)a_{12}b_{17}}{K_{\alpha\gamma}\left(4\beta^2+\gamma^2\right)} \\ & + \frac{16\alpha\beta^3\gamma a_{13}b_{22}}{K_{\alpha 4\beta}K_{\alpha\gamma}\left(4\beta^2+\gamma^2\right)} - \frac{\beta^2\gamma K_{\alpha\beta}a_{15}b_{16}}{\sqrt{2}K_{\beta\gamma}\left(4\beta^2+\gamma^2\right)} - \frac{\alpha\beta\gamma a_{16}b_{11}\left(\alpha^2+5\beta^2+3\gamma^2\right)}{\sqrt{2}K_{\alpha\beta}K_{\alpha\gamma}\left(4\beta^2+\gamma^2\right)} \\ & + \frac{\beta^2\gamma a_{16}b_{15}\left(-\alpha^2+3\beta^2+\gamma^2\right)}{\sqrt{2}K_{\alpha\beta}K_{\beta\gamma}\left(4\beta^2+\gamma^2\right)} + \frac{\gamma^2 K_{\alpha\gamma}a_{17}b_{12}}{4\beta^2+\gamma^2} + \frac{\alpha^2\gamma^2 a_{18}b_{23}}{K_{\alpha\gamma}\left(4\beta^2+\gamma^2\right)} - \frac{4\alpha\beta\gamma^3 a_{22}b_{13}}{K_{\alpha 4\beta}K_{\alpha\gamma}\left(4\beta^2+\gamma^2\right)} \\ & + \frac{\gamma^2 a_{23}b_{18}\left(\alpha^2+4\beta^2+\gamma^2\right)}{K_{\alpha\gamma}\left(4\beta^2+\gamma^2\right)} + \frac{a_2}{\mathrm{Wi}} + \frac{\beta\gamma a_3\left(3\beta^2+\gamma^2\right)b_7}{\sqrt{2}K_{\beta\gamma}\left(4\beta^2+\gamma^2\right)} - \frac{\beta^3\gamma a_7 b_3}{\sqrt{2}K_{\beta\gamma}\left(4\beta^2+\gamma^2\right)} - \frac{27\beta^3\gamma a_7 b_8}{\sqrt{2}K_{\beta\gamma}\left(4\beta^2+\gamma^2\right)} \\ & + \frac{3\beta\gamma a_8\left(\gamma^2-5\beta^2\right)b_7}{\sqrt{2}K_{\beta\gamma}\left(4\beta^2+\gamma^2\right)} - \frac{b_2}{\mathrm{Wi}}\end{aligned} \tag{B.2}$$

$$\frac{db_3}{dt} = + \frac{a_6 b_4 \gamma^3}{\beta K_{\beta\gamma}} + \frac{a_7 b_5 \gamma^3}{\beta K_{\beta\gamma}} + \frac{(\alpha^2+\beta^2+\gamma^2)\, a_{20} b_{10} \gamma^2}{\sqrt{2}\beta K_{\alpha\gamma} K_{4\beta\gamma}} + \frac{(\alpha^2+\beta^2+\gamma^2)\, a_{21} b_{11} \gamma^2}{\sqrt{2}\beta K_{4\beta\gamma}} + \frac{K_{\alpha\gamma} a_{14} b_{12} \gamma^2}{\beta K_{\beta\gamma}} \tag{B.3}$$
$$+ \frac{K_{\alpha\gamma} a_{15} b_{13} \gamma^2}{\beta K_{\beta\gamma}} + \frac{(\alpha^2-\beta^2+\gamma^2)\, a_{12} b_{14} \gamma^2}{\beta K_{\alpha\gamma} K_{\beta\gamma}} + \frac{(\alpha^2+3\beta^2+\gamma^2)\, a_{18} b_{14} \gamma^2}{\sqrt{2}\beta K_{\alpha\gamma} K_{\beta\gamma}} + \frac{(\alpha^2-\beta^2+\gamma^2)\, a_{13} b_{15} \gamma^2}{\beta K_{\alpha\gamma} K_{\beta\gamma}}$$
$$+ \frac{(\alpha^2+3\beta^2+\gamma^2)\, a_{19} b_{15} \gamma^2}{\sqrt{2}\beta K_{\alpha\gamma} K_{\beta\gamma}} + \frac{(\alpha^2+4\beta^2+\gamma^2)\, a_{14} b_{18} \gamma^2}{\sqrt{2}\beta K_{\alpha\gamma} K_{\beta\gamma}} + \frac{(\alpha^2+4\beta^2+\gamma^2)\, a_{15} b_{19} \gamma^2}{\sqrt{2}\beta K_{\alpha\gamma} K_{\beta\gamma}} + \frac{K_{\alpha\gamma} a_{10} b_{20} \gamma^2}{\sqrt{2}\beta K_{4\beta\gamma}}$$
$$+ \frac{K_{\alpha\gamma} a_{11} b_{21} \gamma^2}{\sqrt{2}\beta K_{4\beta\gamma}} + \frac{(\gamma^2-\beta^2)\, a_4 b_6 \gamma}{\beta K_{\beta\gamma}} + \frac{(\gamma^2-\beta^2)\, a_5 b_7 \gamma}{\beta K_{\beta\gamma}} + \frac{a_3}{\mathrm{Wi}} + \frac{\alpha\,(3\alpha^2+7\beta^2)\, a_{22} b_{16}}{\sqrt{2} K_{\alpha\beta} K_{\alpha 4\beta}} + \frac{(\gamma^3+4\beta^2\gamma)\, a_6 b_1}{\sqrt{2}\beta K_{\beta\gamma}}$$
$$+ \frac{(3\alpha^3+8\beta^2\alpha)\, a_{16} b_{22}}{\sqrt{2} K_{\alpha\beta} K_{\alpha 4\beta}} + \frac{(\gamma^3+4\beta^2\gamma)\, a_7 b_2}{\sqrt{2}\beta K_{\beta\gamma}} - \frac{b_3}{\mathrm{Wi}} + \frac{(\gamma^3+3\beta^2\gamma)\, a_1 b_6}{\sqrt{2}\beta K_{\beta\gamma}} + \frac{(\gamma^3+3\beta^2\gamma)\, a_2 b_7}{\sqrt{2}\beta K_{\beta\gamma}}$$

$$\frac{db_4}{dt} = - \frac{a_9 b_{11}\,(\alpha^2+\beta^2+\gamma^2)}{K_{\alpha\gamma}} - \frac{\alpha\beta K_{\alpha\beta} a_{10} b_{16}}{\gamma K_{\alpha\gamma}} - \frac{(\alpha^2+\beta^2)\, a_{11} b_9}{K_{\alpha\gamma}} - \frac{\alpha^2 a_{13} b_{23}}{K_{\alpha\gamma}} - \frac{\beta^2 K_{\alpha\beta} a_{14} b_{16}}{\gamma K_{\beta\gamma}} \tag{B.4}$$
$$- \frac{\alpha\beta a_{16} b_{10}\,(\alpha^2+\beta^2-\gamma^2)}{\gamma K_{\alpha\beta} K_{\alpha\gamma}} - \frac{\beta^2 a_{16} b_{14}\,(\alpha^2+\beta^2-\gamma^2)}{\gamma K_{\alpha\beta} K_{\beta\gamma}} - \frac{a_{17} b_{19}\,(\alpha^2+4\beta^2+\gamma^2)}{K_{\alpha\gamma}} + \frac{2\alpha\beta K_{\alpha 4\beta} a_{18} b_{22}}{\gamma K_{\alpha\gamma}}$$
$$- \frac{(\alpha^2+4\beta^2)\, a_{19} b_{17}}{K_{\alpha\gamma}} + \frac{4\beta^2 K_{\alpha 4\beta} a_{20} b_{22}}{\gamma K_{4\beta\gamma}} + \frac{2\alpha\beta a_{22} b_{18}\,(\alpha^2+4\beta^2-\gamma^2)}{\gamma K_{\alpha 4\beta} K_{\alpha\gamma}} + \frac{4\beta^2 a_{22} b_{20}\,(\alpha^2+4\beta^2-\gamma^2)}{\gamma K_{\alpha 4\beta} K_{4\beta\gamma}}$$
$$- K_{\alpha\gamma} a_{23} b_{13} + \frac{a_3\,(\beta\gamma^2-\beta^3)\, b_6}{K_{\beta\gamma}} + \frac{a_4}{\mathrm{Wi}} - \frac{\beta^3 a_6 b_3}{\gamma K_{\beta\gamma}} - \frac{b_4}{\mathrm{Wi}}$$

$$\frac{db_5}{dt} = \frac{a_9 b_{10}\,(\alpha^2+\beta^2+\gamma^2)}{K_{\alpha\gamma}} + \frac{(\alpha^2+\beta^2)\, a_{10} b_9}{K_{\alpha\gamma}} - \frac{\alpha\beta K_{\alpha\beta} a_{11} b_{16}}{\gamma K_{\alpha\gamma}} + \frac{\alpha^2 a 7_{12} b_{23}}{K_{\alpha\gamma}} - \frac{\beta^2 K_{\alpha\beta} a_{15} b_{16}}{\gamma K_{\beta\gamma}} \tag{B.5}$$
$$- \frac{\alpha\beta a_{16} b_{11}\,(\alpha^2+\beta^2-\gamma^2)}{\gamma K_{\alpha\beta} K_{\alpha\gamma}} - \frac{\beta^2 a_{16} b_{15}\,(\alpha^2+\beta^2-\gamma^2)}{\gamma K_{\alpha\beta} K_{\beta\gamma}} + \frac{a_{17} b_{18}\,(\alpha^2+4\beta^2+\gamma^2)}{K_{\alpha\gamma}} + \frac{(\alpha^2+4\beta^2)\, a_{18} b_{17}}{K_{\alpha\gamma}}$$
$$+ \frac{2\alpha\beta K_{\alpha 4\beta} a_{19} b_{22}}{\gamma K_{\alpha\gamma}} + \frac{4\beta^2 K_{\alpha 4\beta} a_{21} b_{22}}{\gamma K_{4\beta\gamma}} + \frac{2\alpha\beta a_{22} b_{19}\,(\alpha^2+4\beta^2-\gamma^2)}{\gamma K_{\alpha 4\beta} K_{\alpha\gamma}} + \frac{4\beta^2 a_{22} b_{21}\,(\alpha^2+4\beta^2-\gamma^2)}{\gamma K_{\alpha 4\beta} K_{4\beta\gamma}}$$
$$+ K_{\alpha\gamma} a_{23} b_{12} + \frac{a_3\,(\beta\gamma^2-\beta^3)\, b_7}{\gamma K_{\beta\gamma}} + \frac{a_5}{\mathrm{Wi}} - \frac{\beta^3 a_7 b_3}{\gamma K_{\beta\gamma}} - \frac{b_5}{\mathrm{Wi}}$$

$$
\begin{aligned}
\frac{db_6}{dt} = &- \frac{\sqrt{2}\alpha\left(\alpha^2+3\beta^2+\gamma^2\right)a_{20}b_{16}\beta^3}{K_{\alpha\beta}\left(\beta^2+\gamma^2\right)^{3/2}K_{4\beta\gamma}} + \frac{2\alpha^3\gamma a_{13}b_9\beta}{K_{\alpha\gamma}\left(\beta^2+\gamma^2\right)^{3/2}} - \frac{\sqrt{2}\alpha\left(\alpha^2+2\beta^2\right)\gamma a_{19}b_9\beta}{K_{\alpha\gamma}\left(\beta^2+\gamma^2\right)^{3/2}} \\
&+ \frac{\sqrt{2}\alpha\left(\alpha^2+2\beta^2\right)\gamma a_{17}b_{11}\beta}{K_{\alpha\gamma}\left(\beta^2+\gamma^2\right)^{3/2}} - \frac{2\alpha^3\gamma a_{23}b_{11}\beta}{K_{\alpha\gamma}\left(\beta^2+\gamma^2\right)^{3/2}} + \frac{2\alpha^3\gamma a_9 b_{13}\beta}{K_{\alpha\gamma}\left(\beta^2+\gamma^2\right)^{3/2}} \\
&+ \frac{\alpha\left(\beta^4-6\gamma^2\beta^2+\gamma^4+\alpha^2\left(\beta^2-3\gamma^2\right)\right)a_{22}b_{14}\beta}{\sqrt{2}K_{\alpha4\beta}\left(\beta^2+\gamma^2\right)^2} + \frac{\sqrt{2}\alpha\left(\alpha^2+2\beta^2\right)\gamma a_{11}b_{17}\beta}{K_{\alpha\gamma}\left(\beta^2+\gamma^2\right)^{3/2}} - \frac{\sqrt{2}\alpha\left(\alpha^2+2\beta^2\right)\gamma a_9 b_{19}\beta}{K_{\alpha\gamma}\left(\beta^2+\gamma^2\right)^{3/2}} \\
&- \frac{\sqrt{2}\alpha\left(4\beta^4+\alpha^2\beta^2+3\gamma^2\beta^2+\gamma^4\right)a_{16}b_{20}\beta}{K_{\alpha\beta}\left(\beta^2+\gamma^2\right)^{3/2}K_{4\beta\gamma}} + \frac{\alpha\left(\alpha^2\left(\beta^2-3\gamma^2\right)-8\beta^2\gamma^2\right)a_{14}b_{22}\beta}{\sqrt{2}K_{\alpha4\beta}\left(\beta^2+\gamma^2\right)^2} - \frac{2\alpha^3\gamma a_{11}b_{23}\beta}{K_{\alpha\gamma}\left(\beta^2+\gamma^2\right)^{3/2}} \\
&+ \frac{a_6}{\mathrm{Wi}} - \frac{\gamma\left(7\beta^4+3\gamma^2\beta^2+\alpha^2\left(3\beta^2+\gamma^2\right)\right)a_{21}b_9}{\sqrt{2}\left(\beta^2+\gamma^2\right)^{3/2}K_{4\beta\gamma}} + \frac{\alpha^2\left(\beta^2-\gamma^2\right)\left(\alpha^2+\beta^2-\gamma^2\right)a_{22}b_{10}}{\sqrt{2}K_{\alpha4\beta}K_{\alpha\gamma}\left(\beta^2+\gamma^2\right)^{3/2}} \\
&- \frac{\alpha^2\left(\left(\beta^2-\gamma^2\right)\alpha^2+\gamma^2\left(\beta^2+\gamma^2\right)\right)a_{16}b_{12}}{K_{\alpha\beta}K_{\alpha\gamma}\left(\beta^2+\gamma^2\right)^{3/2}} - \frac{\gamma\left(-7\beta^4+2\gamma^2\beta^2+\gamma^4+\alpha^2\left(\gamma^2-3\beta^2\right)\right)a_{17}b_{15}}{\sqrt{2}\left(\beta^2+\gamma^2\right)^2} \\
&- \frac{\gamma\left(\alpha^2+\beta^2+\gamma^2\right)a_{23}b_{15}}{\beta^2+\gamma^2} + \frac{\alpha^2\left(\left(\gamma^2-\beta^2\right)\alpha^2+\beta^2\left(\beta^2+\gamma^2\right)\right)a_{12}b_{16}}{K_{\alpha\beta}K_{\alpha\gamma}\left(\beta^2+\gamma^2\right)^{3/2}} \\
&+ \frac{\alpha^2\left(-3\beta^4+\gamma^2\beta^2+\alpha^2\left(\gamma^2-\beta^2\right)\right)a_{18}b_{16}}{\sqrt{2}K_{\alpha\beta}K_{\alpha\gamma}\left(\beta^2+\gamma^2\right)^{3/2}} + \frac{\gamma\left(8\beta^4+\alpha^2\left(3\beta^2-\gamma^2\right)\right)a_{15}b_{17}}{\sqrt{2}\left(\beta^2+\gamma^2\right)^2} \\
&- \frac{\alpha^2\left(4\beta^4+\gamma^2\beta^2+\gamma^4+\alpha^2\left(\beta^2-\gamma^2\right)\right)a_{16}b_{18}}{\sqrt{2}K_{\alpha\beta}K_{\alpha\gamma}\left(\beta^2+\gamma^2\right)^{3/2}} - \frac{\gamma\left(8\beta^4+5\gamma^2\beta^2+\gamma^4+\alpha^2\left(3\beta^2+\gamma^2\right)\right)a_9b_{21}}{\sqrt{2}\left(\beta^2+\gamma^2\right)^{3/2}K_{4\beta\gamma}} \\
&+ \frac{\alpha^2\left(\alpha^2\left(\beta^2-\gamma^2\right)-4\beta^2\gamma^2\right)a_{10}b_{22}}{\sqrt{2}K_{\alpha4\beta}K_{\alpha\gamma}\left(\beta^2+\gamma^2\right)^{3/2}} - \frac{\alpha^2\gamma a_{15}b_{23}}{\beta^2+\gamma^2} - \frac{b_6}{\mathrm{Wi}}
\end{aligned}
\tag{B.6}
$$

$$\frac{db_7}{dt} = -\frac{\sqrt{2}\alpha\left(\alpha^2+3\beta^2+\gamma^2\right)a_{21}b_{16}\beta^3}{K_{\alpha\beta}\left(\beta^2+\gamma^2\right)^{3/2}K_{4\beta\gamma}} - \frac{2\alpha^3\gamma a_{12}b_9\beta}{K_{\alpha\gamma}\left(\beta^2+\gamma^2\right)^{3/2}} + \frac{\sqrt{2}\alpha\left(\alpha^2+2\beta^2\right)\gamma a_{18}b_9\beta}{K_{\alpha\gamma}\left(\beta^2+\gamma^2\right)^{3/2}} \tag{B.7}$$
$$- \frac{\sqrt{2}\alpha\left(\alpha^2+2\beta^2\right)\gamma a_{17}b_{10}\beta}{K_{\alpha\gamma}\left(\beta^2+\gamma^2\right)^{3/2}} + \frac{2\alpha^3\gamma a_{23}b_{10}\beta}{K_{\alpha\gamma}\left(\beta^2+\gamma^2\right)^{3/2}} - \frac{2\alpha^3\gamma a_9 b_{12}\beta}{K_{\alpha\gamma}\left(\beta^2+\gamma^2\right)^{3/2}}$$
$$+ \frac{\alpha\left(\beta^4-6\gamma^2\beta^2+\gamma^4+\alpha^2\left(\beta^2-3\gamma^2\right)\right)a_{22}b_{15}\beta}{\sqrt{2}K_{\alpha4\beta}\left(\beta^2+\gamma^2\right)^2} - \frac{\sqrt{2}\alpha\left(\alpha^2+2\beta^2\right)\gamma a_{10}b_{17}\beta}{K_{\alpha\gamma}\left(\beta^2+\gamma^2\right)^{3/2}} + \frac{\sqrt{2}\alpha\left(\alpha^2+2\beta^2\right)\gamma a_9 b_{18}\beta}{K_{\alpha\gamma}\left(\beta^2+\gamma^2\right)^{3/2}}$$
$$- \frac{\sqrt{2}\alpha\left(4\beta^4+\alpha^2\beta^2+3\gamma^2\beta^2+\gamma^4\right)a_{16}b_{21}\beta}{K_{\alpha\beta}\left(\beta^2+\gamma^2\right)^{3/2}K_{4\beta\gamma}} + \frac{\alpha\left(\alpha^2\left(\beta^2-3\gamma^2\right)-8\beta^2\gamma^2\right)a_{15}b_{22}\beta}{\sqrt{2}K_{\alpha4\beta}\left(\beta^2+\gamma^2\right)^2} + \frac{2\alpha^3\gamma a_{10}b_{23}\beta}{K_{\alpha\gamma}\left(\beta^2+\gamma^2\right)^{3/2}}$$
$$+ \frac{a_7}{\mathrm{Wi}} + \frac{\gamma\left(7\beta^4+3\gamma^2\beta^2+\alpha^2\left(3\beta^2+\gamma^2\right)\right)a_{20}b_9}{\sqrt{2}\left(\beta^2+\gamma^2\right)^{3/2}K_{4\beta\gamma}} + \frac{\alpha^2\left(\beta^2-\gamma^2\right)\left(\alpha^2+\beta^2-\gamma^2\right)a_{22}b_{11}}{\sqrt{2}K_{\alpha4\beta}K_{\alpha\gamma}\left(\beta^2+\gamma^2\right)^{3/2}}$$
$$- \frac{\alpha^2\left(\left(\beta^2-\gamma^2\right)\alpha^2+\gamma^2\left(\beta^2+\gamma^2\right)\right)a_{16}b_{13}}{K_{\alpha\beta}K_{\alpha\gamma}\left(\beta^2+\gamma^2\right)^{3/2}} + \frac{\gamma\left(-7\beta^4+2\gamma^2\beta^2+\gamma^4+\alpha^2\left(\gamma^2-3\beta^2\right)\right)a_{17}b_{14}}{\sqrt{2}\left(\beta^2+\gamma^2\right)^2}$$
$$+ \frac{\gamma\left(\alpha^2+\beta^2+\gamma^2\right)a_{23}b_{14}}{\beta^2+\gamma^2} + \frac{\alpha^2\left(\left(\gamma^2-\beta^2\right)\alpha^2+\beta^2\left(\beta^2+\gamma^2\right)\right)a_{13}b_{16}}{K_{\alpha\beta}K_{\alpha\gamma}\left(\beta^2+\gamma^2\right)^{3/2}}$$
$$+ \frac{\alpha^2\left(-3\beta^4+\gamma^2\beta^2+\alpha^2\left(\gamma^2-\beta^2\right)\right)a_{19}b_{16}}{\sqrt{2}K_{\alpha\beta}K_{\alpha\gamma}\left(\beta^2+\gamma^2\right)^{3/2}} + \frac{\gamma\left(\alpha^2\left(\gamma^2-3\beta^2\right)-8\beta^4\right)a_{14}b_{17}}{\sqrt{2}\left(\beta^2+\gamma^2\right)^2}$$
$$- \frac{\alpha^2\left(4\beta^4+\gamma^2\beta^2+\gamma^4+\alpha^2\left(\beta^2-\gamma^2\right)\right)a_{16}b_{19}}{\sqrt{2}K_{\alpha\beta}K_{\alpha\gamma}\left(\beta^2+\gamma^2\right)^{3/2}} + \frac{\gamma\left(8\beta^4+5\gamma^2\beta^2+\gamma^4+\alpha^2\left(3\beta^2+\gamma^2\right)\right)a_9b_{20}}{\sqrt{2}\left(\beta^2+\gamma^2\right)^{3/2}K_{4\beta\gamma}}$$
$$+ \frac{\alpha^2\left(\alpha^2\left(\beta^2-\gamma^2\right)-4\beta^2\gamma^2\right)a_{11}b_{22}}{\sqrt{2}K_{\alpha4\beta}K_{\alpha\gamma}\left(\beta^2+\gamma^2\right)^{3/2}} + \frac{\alpha^2\gamma a_{14}b_{23}}{\beta^2+\gamma^2} - \frac{b_7}{\mathrm{Wi}}$$

$$\frac{db_8}{dt} = -\frac{\gamma^2 a_{10}b_{20}\left(\alpha^2-8\beta^2+\gamma^2\right)}{3\sqrt{2}\beta K_{\alpha\gamma}K_{4\beta\gamma}} - \frac{\gamma^2 a_{11}b_{21}\left(\alpha^2-8\beta^2+\gamma^2\right)}{3\sqrt{2}\beta K_{\alpha\gamma}K_{4\beta\gamma}} + \frac{\gamma^2 a_{14}b_{18}\left(\alpha^2+4\beta^2+\gamma^2\right)}{3\sqrt{2}\beta K_{\alpha\gamma}K_{\beta\gamma}}$$
(B.8)
$$+ \frac{\gamma^2 a_{15}b_{19}\left(\alpha^2+4\beta^2+\gamma^2\right)}{3\sqrt{2}\beta K_{\alpha\gamma}K_{\beta\gamma}} + \frac{\left(\alpha^3+16\alpha\beta^2\right)a_{16}b_{22}}{3\sqrt{2}K_{\alpha\beta}K_{\alpha4\beta}} + \frac{\gamma^2 a_{18}b_{14}\left(\alpha^2-5\beta^2+\gamma^2\right)}{3\sqrt{2}\beta K_{\alpha\gamma}K_{\beta\gamma}} - \frac{a_1\left(5\beta^2\gamma-\gamma^3\right)b_6}{3\sqrt{2}\beta K_{\beta\gamma}}$$
$$+ \frac{\gamma^2 a_{19}b_{15}\left(\alpha^2-5\beta^2+\gamma^2\right)}{3\sqrt{2}\beta K_{\alpha\gamma}K_{\beta\gamma}} - \frac{\gamma^2 a_{20}b_{10}\left(\alpha^2+\beta^2+\gamma^2\right)}{3\sqrt{2}\beta K_{\alpha\gamma}K_{4\beta\gamma}} - \frac{\gamma^2 a_{21}b_{11}\left(\alpha^2+\beta^2+\gamma^2\right)}{3\sqrt{2}\beta K_{\alpha\gamma}K_{4\beta\gamma}}$$
$$+ \frac{\alpha\left(\alpha^2-11\beta^2\right)a_{22}b_{16}}{3\sqrt{2}K_{\alpha\beta}K_{\alpha4\beta}} - \frac{a_2\left(5\beta^2\gamma-\gamma^3\right)b_7}{3\sqrt{2}\beta K_{\beta\gamma}} + \frac{a_6\left(4\beta^2\gamma+\gamma^3\right)b_1}{3\sqrt{2}\beta K_{\beta\gamma}} + \frac{a_7\left(4\beta^2\gamma+\gamma^3\right)b_2}{3\sqrt{2}\beta K_{\beta\gamma}} + \frac{a_8}{\mathrm{Wi}} - \frac{b_8}{\mathrm{Wi}}$$

$$\frac{db_9}{dt} = -\frac{2\beta\gamma a_7 b_{12}\alpha^3}{(\alpha^2+\beta^2)K_{\alpha\gamma}K_{\beta\gamma}} + \frac{2\beta\gamma a_6 b_{13}\alpha^3}{(\alpha^2+\beta^2)K_{\alpha\gamma}K_{\beta\gamma}} - \frac{a_3 b_{23}\alpha^3}{\alpha^2+\beta^2} + \frac{(\alpha^2+\beta^2+\gamma^2)a_2 b_{10}\alpha^2}{\sqrt{2}(\alpha^2+\beta^2)K_{\alpha\gamma}} \tag{B.9}$$
$$- \frac{(\alpha^2+\beta^2+\gamma^2)a_5 b_{10}\alpha^2}{(\alpha^2+\beta^2)K_{\alpha\gamma}} - \frac{(\alpha^2+\beta^2+\gamma^2)a_1 b_{11}\alpha^2}{\sqrt{2}(\alpha^2+\beta^2)K_{\alpha\gamma}} + \frac{(\alpha^2+\beta^2+\gamma^2)a_4 b_{11}\alpha^2}{(\alpha^2+\beta^2)K_{\alpha\gamma}} - \frac{\gamma^2 a_{11}b_1\alpha^2}{\sqrt{2}(\alpha^2+\beta^2)K_{\alpha\gamma}}$$
$$+ \frac{\gamma^2 a_{10}b_2\alpha^2}{\sqrt{2}(\alpha^2+\beta^2)K_{\alpha\gamma}} + \frac{\gamma^2 a_{11}b_4\alpha^2}{(\alpha^2+\beta^2)K_{\alpha\gamma}} - \frac{\gamma^2 a_{10}b_5\alpha^2}{(\alpha^2+\beta^2)K_{\alpha\gamma}} + \frac{\beta(\alpha^2+\beta^2+\gamma^2)a_2 b_{14}\alpha}{\sqrt{2}(\alpha^2+\beta^2)K_{\beta\gamma}}$$
$$- \frac{\beta(\alpha^2+\beta^2+\gamma^2)a_5 b_{14}\alpha}{(\alpha^2+\beta^2)K_{\beta\gamma}} - \frac{\beta(\alpha^2+\beta^2+\gamma^2)a_1 b_{15}\alpha}{\sqrt{2}(\alpha^2+\beta^2)K_{\beta\gamma}} + \frac{\beta(\alpha^2+\beta^2+\gamma^2)a_4 b_{15}\alpha}{(\alpha^2+\beta^2)K_{\beta\gamma}} + \frac{(\alpha^2+4\beta^2)a_3 b_{17}\alpha}{\sqrt{2}(\alpha^2+\beta^2)}$$
$$- \frac{(\alpha^2+4\beta^2)a_8 b_{17}\alpha}{\sqrt{2}(\alpha^2+\beta^2)} - \frac{\sqrt{2}\beta\gamma(2\beta^2+\gamma^2)a_7 b_{18}\alpha}{(\alpha^2+\beta^2)K_{\alpha\gamma}K_{\beta\gamma}} - \frac{\beta\gamma^2 a_{15}b_1\alpha}{\sqrt{2}(\alpha^2+\beta^2)K_{\beta\gamma}} + \frac{\sqrt{2}\beta\gamma(2\beta^2+\gamma^2)a_6 b_{19}\alpha}{(\alpha^2+\beta^2)K_{\alpha\gamma}K_{\beta\gamma}}$$
$$+ \frac{\beta\gamma^2 a_{14}b_2\alpha}{\sqrt{2}(\alpha^2+\beta^2)K_{\beta\gamma}} + \frac{3\beta^2 a_{17}b_3\alpha}{\sqrt{2}(\alpha^2+\beta^2)} + \frac{\beta^2 a_{23}b_3\alpha}{\alpha^2+\beta^2} + \frac{\beta\gamma^2 a_{15}b_4\alpha}{(\alpha^2+\beta^2)K_{\beta\gamma}} - \frac{\beta\gamma^2 a_{14}b_5\alpha}{(\alpha^2+\beta^2)K_{\beta\gamma}}$$
$$- \frac{2\beta^3\gamma a_{13}b_6\alpha}{(\alpha^2+\beta^2)K_{\alpha\gamma}K_{\beta\gamma}} + \frac{\sqrt{2}\beta\gamma(2\beta^2+\gamma^2)a_{19}b_6\alpha}{(\alpha^2+\beta^2)K_{\alpha\gamma}K_{\beta\gamma}} + \frac{2\beta^3\gamma a_{12}b_7\alpha}{(\alpha^2+\beta^2)K_{\alpha\gamma}K_{\beta\gamma}} - \frac{\sqrt{2}\beta\gamma(2\beta^2+\gamma^2)a_{18}b_7\alpha}{(\alpha^2+\beta^2)K_{\alpha\gamma}K_{\beta\gamma}}$$
$$- \frac{3\beta^2 a_{17}b_8\alpha}{\sqrt{2}(\alpha^2+\beta^2)} + \frac{a_9}{\mathrm{Wi}} - \frac{b_9}{\mathrm{Wi}} - \frac{\beta^2\gamma(\alpha^2+8\beta^2+3\gamma^2)a_7 b_{20}}{\sqrt{2}(\alpha^2+\beta^2)K_{\beta\gamma}K_{4\beta\gamma}} + \frac{\beta^2\gamma(\alpha^2+8\beta^2+3\gamma^2)a_6 b_{21}}{\sqrt{2}(\alpha^2+\beta^2)K_{\beta\gamma}K_{4\beta\gamma}}$$
$$+ \frac{\beta^2\gamma(7\beta^2+3\gamma^2)a_{21}b_6}{\sqrt{2}(\alpha^2+\beta^2)K_{\beta\gamma}K_{4\beta\gamma}} - \frac{\beta^2\gamma(7\beta^2+3\gamma^2)a_{20}b_7}{\sqrt{2}(\alpha^2+\beta^2)K_{\beta\gamma}K_{4\beta\gamma}}$$

$$\frac{db_{10}}{dt} = + \frac{4\sqrt{2}\alpha\gamma K_{\alpha\gamma}a_7 b_{17}\beta^3}{K_{\beta\gamma}(\alpha^2+\beta^2+\gamma^2)^2} - \frac{K_{\alpha\gamma}(-3\alpha^2+\beta^2+\gamma^2)a_{20}b_3\beta^3}{\sqrt{2}(\alpha^2+\beta^2+\gamma^2)^2 K_{4\beta\gamma}} + \frac{4\sqrt{2}\alpha\gamma K_{\alpha\gamma}a_{17}b_7\beta^3}{K_{\beta\gamma}(\alpha^2+\beta^2+\gamma^2)^2} \tag{B.10}$$
$$- \frac{9K_{\alpha\gamma}(\alpha^2-3(\beta^2+\gamma^2))a_{20}b_8\beta^3}{\sqrt{2}(\alpha^2+\beta^2+\gamma^2)^2 K_{4\beta\gamma}} + \frac{2\sqrt{2}K_{\alpha\gamma}(\alpha^4+(3\beta^2+\gamma^2)\alpha^2+4\beta^2(\beta^2+\gamma^2))a_6 b_{22}\beta^2}{K_{\alpha4\beta}K_{\beta\gamma}(\alpha^2+\beta^2+\gamma^2)^2}$$
$$+ \frac{\alpha a_{12}b_3\beta^2}{\alpha^2+\beta^2+\gamma^2} + \frac{3\alpha a_{18}b_3\beta^2}{\sqrt{2}(\alpha^2+\beta^2+\gamma^2)} + \frac{2\sqrt{2}K_{\alpha\gamma}(3\beta^4+2\gamma^2\beta^2-\gamma^4+\alpha^2(\beta^2-\gamma^2))a_{22}b_6\beta^2}{K_{\alpha4\beta}K_{\beta\gamma}(\alpha^2+\beta^2+\gamma^2)^2}$$
$$- \frac{3\alpha a_{18}b_8\beta^2}{\sqrt{2}(\alpha^2+\beta^2+\gamma^2)} - \frac{\alpha K_{\alpha\gamma}(\alpha^4+(2\beta^2+\gamma^2)\alpha^2-7\beta^2(\beta^2+\gamma^2))a_1 b_{16}\beta}{\sqrt{2}K_{\alpha\beta}\gamma(\alpha^2+\beta^2+\gamma^2)^2} - \frac{\alpha K_{\alpha\beta}K_{\alpha\gamma}a_4 b_{16}\beta}{\gamma^3+\alpha^2\gamma+\beta^2\gamma}$$
$$+ \frac{\alpha(\gamma^6+9\beta^2\gamma^4+\alpha^4\gamma^2+8\beta^4\gamma^2+\alpha^2(8\beta^4+9\gamma^2\beta^2+2\gamma^4))a_{16}b_1\beta}{\sqrt{2}K_{\alpha\beta}\gamma K_{\alpha\gamma}(\alpha^2+\beta^2+\gamma^2)^2}$$
$$+ \frac{K_{\alpha\gamma}(\alpha^4+(5\beta^2+2\gamma^2)\alpha^2+\gamma^2(\beta^2+\gamma^2))a_3 b_{20}\beta}{\sqrt{2}(\alpha^2+\beta^2+\gamma^2)^2 K_{4\beta\gamma}}$$
$$- \frac{3K_{\alpha\gamma}(\alpha^4+(5\beta^2+2\gamma^2)\alpha^2-8\beta^4+\gamma^4-7\beta^2\gamma^2)a_8 b_{20}\beta}{\sqrt{2}(\alpha^2+\beta^2+\gamma^2)^2 K_{4\beta\gamma}} + \frac{\alpha\gamma K_{\alpha\gamma}a_{16}b_4\beta}{K_{\alpha\beta}(\alpha^2+\beta^2+\gamma^2)} + \frac{a_{10}}{\mathrm{Wi}}$$
$$- \frac{K_{\alpha\gamma}(\alpha^4+(2\beta^2+\gamma^2)\alpha^2-3\beta^2(\beta^2+\gamma^2))a_2 b_9}{\sqrt{2}(\alpha^2+\beta^2+\gamma^2)^2} + \frac{(\alpha^2+\beta^2)K_{\alpha\gamma}a_5 b_9}{\alpha^2+\beta^2+\gamma^2} - \frac{b_{10}}{\mathrm{Wi}} - \frac{\alpha(\alpha^2+\gamma^2)a_3 b_{12}}{\alpha^2+\beta^2+\gamma^2}$$
$$+ \frac{\alpha(\alpha^2+4\beta^2+\gamma^2)a_3 b_{18}}{\sqrt{2}(\alpha^2+\beta^2+\gamma^2)} - \frac{\alpha(\alpha^2+4\beta^2+\gamma^2)a_8 b_{18}}{\sqrt{2}(\alpha^2+\beta^2+\gamma^2)}$$
$$+ \frac{(\gamma^6+5\beta^2\gamma^4+\alpha^4\gamma^2+4\beta^4\gamma^2+\alpha^2(4\beta^4+5\gamma^2\beta^2+2\gamma^4))a_9 b_2}{\sqrt{2}K_{\alpha\gamma}(\alpha^2+\beta^2+\gamma^2)^2} - \frac{\gamma^2 K_{\alpha\gamma}a_9 b_5}{\alpha^2+\beta^2+\gamma^2}$$

$$\frac{db_{11}}{dt} = -\frac{4\sqrt{2}\alpha\gamma K_{\alpha\gamma} a_6 b_{17}\beta^3}{K_{\beta\gamma}\left(\alpha^2+\beta^2+\gamma^2\right)^2} - \frac{K_{\alpha\gamma}\left(-3\alpha^2+\beta^2+\gamma^2\right) a_{21} b_3 \beta^3}{\sqrt{2}\left(\alpha^2+\beta^2+\gamma^2\right)^2 K_{4\beta\gamma}} - \frac{4\sqrt{2}\alpha\gamma K_{\alpha\gamma} a_{17} b_6 \beta^3}{K_{\beta\gamma}\left(\alpha^2+\beta^2+\gamma^2\right)^2} \tag{B.11}$$
$$- \frac{9K_{\alpha\gamma}\left(\alpha^2-3\left(\beta^2+\gamma^2\right)\right) a_{21} b_8 \beta^3}{\sqrt{2}\left(\alpha^2+\beta^2+\gamma^2\right)^2 K_{4\beta\gamma}} + \frac{2\sqrt{2}K_{\alpha\gamma}\left(\alpha^4+\left(3\beta^2+\gamma^2\right)\alpha^2+4\beta^2\left(\beta^2+\gamma^2\right)\right) a_7 b_{22}\beta^2}{K_{\alpha4\beta}K_{\beta\gamma}\left(\alpha^2+\beta^2+\gamma^2\right)^2}$$
$$+ \frac{\alpha a_{13} b_3 \beta^2}{\alpha^2+\beta^2+\gamma^2} + \frac{3\alpha a_{19} b_3 \beta^2}{\sqrt{2}\left(\alpha^2+\beta^2+\gamma^2\right)} + \frac{2\sqrt{2}K_{\alpha\gamma}\left(3\beta^4+2\gamma^2\beta^2-\gamma^4+\alpha^2\left(\beta^2-\gamma^2\right)\right) a_{22} b_7 \beta^2}{K_{\alpha4\beta}K_{\beta\gamma}\left(\alpha^2+\beta^2+\gamma^2\right)^2}$$
$$- \frac{3\alpha a_{19} b_8 \beta^2}{\sqrt{2}\left(\alpha^2+\beta^2+\gamma^2\right)} - \frac{\alpha K_{\alpha\gamma}\left(\alpha^4+\left(2\beta^2+\gamma^2\right)\alpha^2-7\beta^2\left(\beta^2+\gamma^2\right)\right) a_2 b_{16}\beta}{\sqrt{2}K_{\alpha\beta}\gamma\left(\alpha^2+\beta^2+\gamma^2\right)^2} - \frac{\alpha K_{\alpha\beta}K_{\alpha\gamma} a_5 b_{16}\beta}{\gamma^3+\alpha^2\gamma+\beta^2\gamma}$$
$$+ \frac{K_{\alpha\gamma}\left(\alpha^4+\left(5\beta^2+2\gamma^2\right)\alpha^2+\gamma^2\left(\beta^2+\gamma^2\right)\right) a_3 b_{21}\beta}{\sqrt{2}\left(\alpha^2+\beta^2+\gamma^2\right)^2 K_{4\beta\gamma}}$$
$$- \frac{3K_{\alpha\gamma}\left(\alpha^4+\left(5\beta^2+2\gamma^2\right)\alpha^2-8\beta^4+\gamma^4-7\beta^2\gamma^2\right) a_8 b_{21}\beta}{\sqrt{2}\left(\alpha^2+\beta^2+\gamma^2\right)^2 K_{4\beta\gamma}}$$
$$+ \frac{\alpha\left(\gamma^6+9\beta^2\gamma^4+\alpha^4\gamma^2+8\beta^4\gamma^2+\alpha^2\left(8\beta^4+9\gamma^2\beta^2+2\gamma^4\right)\right) a_{16} b_2 \beta}{\sqrt{2}K_{\alpha\beta}\gamma K_{\alpha\gamma}\left(\alpha^2+\beta^2+\gamma^2\right)^2} + \frac{\alpha\gamma K_{\alpha\gamma} a_{16} b_5 \beta}{K_{\alpha\beta}\left(\alpha^2+\beta^2+\gamma^2\right)} + \frac{a_{11}}{\mathrm{Wi}}$$
$$+ \frac{K_{\alpha\gamma}\left(\alpha^4+\left(2\beta^2+\gamma^2\right)\alpha^2-3\beta^2\left(\beta^2+\gamma^2\right)\right) a_1 b_9}{\sqrt{2}\left(\alpha^2+\beta^2+\gamma^2\right)^2} - \frac{\left(\alpha^2+\beta^2\right) K_{\alpha\gamma} a_4 b_9}{\alpha^2+\beta^2+\gamma^2} - \frac{b_{11}}{\mathrm{Wi}} - \frac{\alpha\left(\alpha^2+\gamma^2\right) a_3 b_{13}}{\alpha^2+\beta^2+\gamma^2}$$
$$- \frac{\left(\gamma^6+5\beta^2\gamma^4+\alpha^4\gamma^2+4\beta^4\gamma^2+\alpha^2\left(4\beta^4+5\gamma^2\beta^2+2\gamma^4\right)\right) a_9 b_1}{\sqrt{2}K_{\alpha\gamma}\left(\alpha^2+\beta^2+\gamma^2\right)^2} + \frac{\alpha\left(\alpha^2+4\beta^2+\gamma^2\right) a_3 b_{19}}{\sqrt{2}\left(\alpha^2+\beta^2+\gamma^2\right)}$$
$$- \frac{\alpha\left(\alpha^2+4\beta^2+\gamma^2\right) a_8 b_{19}}{\sqrt{2}\left(\alpha^2+\beta^2+\gamma^2\right)} + \frac{\gamma^2 K_{\alpha\gamma} a_9 b_4}{\alpha^2+\beta^2+\gamma^2}$$

$$\frac{db_{12}}{dt} = +\frac{2\alpha\beta^3\gamma a_9 b_7}{\left(\alpha^2+\gamma^2\right)^{3/2} K_{\beta\gamma}} + \frac{\alpha\beta^2 a_{10} b_3}{\alpha^2+\gamma^2} + \frac{a_{12}}{\mathrm{Wi}} + \frac{\beta^3\left(\alpha^2-\gamma^2\right) a_{14} b_3}{\left(\alpha^2+\gamma^2\right)^{3/2} K_{\beta\gamma}} + \frac{\beta^2 a_{16} b_6\left(\alpha^2\left(\beta^2+\gamma^2\right)-\beta^2\gamma^2+\gamma^4\right)}{K_{\alpha\beta}\left(\alpha^2+\gamma^2\right)^{3/2} K_{\beta\gamma}} \tag{B.12}$$
$$- \frac{a_{17} b_2\left(\alpha^2\left(\gamma^2-4\beta^2\right)+4\beta^2\gamma^2+\gamma^4\right)}{\left(\alpha^2+\gamma^2\right)^{3/2}} + \frac{16\alpha\beta^3\gamma a_1 b_{22}}{K_{\alpha4\beta}\left(\alpha^2+\gamma^2\right)^{3/2}} + \frac{16\alpha\beta^3\gamma a_{22} b_1}{K_{\alpha4\beta}\left(\alpha^2+\gamma^2\right)^{3/2}} - \frac{\gamma^2 a_{23} b_5}{K_{\alpha\gamma}}$$
$$+ \frac{a_2 b_{17}\left(\alpha^4+\alpha^2\left(4\beta^2+\gamma^2\right)-4\beta^2\gamma^2\right)}{\left(\alpha^2+\gamma^2\right)^{3/2}} + \frac{\alpha a_3 b_{10}\left(\alpha^2+\beta^2+\gamma^2\right)}{\alpha^2+\gamma^2}$$
$$+ \frac{\beta a_3 b_{14}\left(\alpha^4+\alpha^2\left(\beta^2+2\gamma^2\right)-\beta^2\gamma^2+\gamma^4\right)}{\left(\alpha^2+\gamma^2\right)^{3/2} K_{\beta\gamma}} + \frac{\alpha^2 a_5 b_{23}}{K_{\alpha\gamma}} - \frac{\beta^2 a_6 b_{16}\left(\alpha^4+\alpha^2\left(\gamma^2-\beta^2\right)+\beta^2\gamma^2\right)}{K_{\alpha\beta}\left(\alpha^2+\gamma^2\right)^{3/2} K_{\beta\gamma}}$$
$$+ \frac{2\alpha\beta^3\gamma a_7 b_9}{\left(\alpha^2+\gamma^2\right)^{3/2} K_{\beta\gamma}} - \frac{b_{12}}{\mathrm{Wi}}$$

$$\frac{db_{13}}{dt} = -\frac{2\alpha\beta^3\gamma a_9 b_6}{\left(\alpha^2+\gamma^2\right)^{3/2} K_{\beta\gamma}} + \frac{\alpha\beta^2 a_{11} b_3}{\alpha^2+\gamma^2} + \frac{a_{13}}{\mathrm{Wi}} + \frac{\beta^3\left(\alpha^2-\gamma^2\right) a_{15} b_3}{\left(\alpha^2+\gamma^2\right)^{3/2} K_{\beta\gamma}} + \frac{\beta^2 a_{16} b_7\left(\alpha^2\left(\beta^2+\gamma^2\right)-\beta^2\gamma^2+\gamma^4\right)}{K_{\alpha\beta}\left(\alpha^2+\gamma^2\right)^{3/2} K_{\beta\gamma}} \tag{B.13}$$
$$+ \frac{a_{17} b_1\left(\alpha^2\left(\gamma^2-4\beta^2\right)+4\beta^2\gamma^2+\gamma^4\right)}{\left(\alpha^2+\gamma^2\right)^{3/2}} - \frac{a_1 b_{17}\left(\alpha^4+\alpha^2\left(4\beta^2+\gamma^2\right)-4\beta^2\gamma^2\right)}{\left(\alpha^2+\gamma^2\right)^{3/2}} + \frac{16\alpha\beta^3\gamma a_{22} b_2}{K_{\alpha4\beta}\left(\alpha^2+\gamma^2\right)^{3/2}}$$
$$+ \frac{\gamma^2 a_{23} b_4}{K_{\alpha\gamma}} + \frac{16\alpha\beta^3\gamma a_2 b_{22}}{K_{\alpha4\beta}\left(\alpha^2+\gamma^2\right)^{3/2}} + \frac{\alpha a_3 b_{11}\left(\alpha^2+\beta^2+\gamma^2\right)}{\alpha^2+\gamma^2} + \frac{\beta a_3 b_{15}\left(\alpha^4+\alpha^2\left(\beta^2+2\gamma^2\right)-\beta^2\gamma^2+\gamma^4\right)}{\left(\alpha^2+\gamma^2\right)^{3/2} K_{\beta\gamma}}$$
$$- \frac{\alpha^2 a_4 b_{23}}{K_{\alpha\gamma}} - \frac{2\alpha\beta^3\gamma a_6 b_9}{\left(\alpha^2+\gamma^2\right)^{3/2} K_{\beta\gamma}} - \frac{\beta^2 a_7 b_{16}\left(\alpha^4+\alpha^2\left(\gamma^2-\beta^2\right)+\beta^2\gamma^2\right)}{K_{\alpha\beta}\left(\alpha^2+\gamma^2\right)^{3/2} K_{\beta\gamma}} - \frac{b_{13}}{\mathrm{Wi}}$$

$$\frac{db_{14}}{dt} = -\frac{2\sqrt{2}\alpha K_{\beta\gamma} a_2 b_9 \beta^3}{\left(\alpha^2+\beta^2+\gamma^2\right)^2} - \frac{2\sqrt{2}\alpha K_{\beta\gamma} a_9 b_2 \beta^3}{\left(\alpha^2+\beta^2+\gamma^2\right)^2} + \frac{\alpha K_{\beta\gamma}\left(3\alpha^2+7\beta^2+3\gamma^2\right) a_{20} b_3 \beta^2}{\sqrt{2}\left(\alpha^2+\beta^2+\gamma^2\right)^2 K_{4\beta\gamma}} \tag{B.14}$$
$$+ \frac{3\alpha\left(\alpha^2-11\beta^2+\gamma^2\right) K_{\beta\gamma} a_{20} b_8 \beta^2}{\sqrt{2}\left(\alpha^2+\beta^2+\gamma^2\right)^2 K_{4\beta\gamma}} - \frac{\alpha\left(3\alpha^4+\left(11\beta^2+3\gamma^2\right)\alpha^2+8\beta^2\left(2\beta^2+\gamma^2\right)\right) a_6 b_{22}\beta}{\sqrt{2} K_{\alpha4\beta}\left(\alpha^2+\beta^2+\gamma^2\right)^2}$$
$$+ \frac{\alpha\left(-13\beta^4-2\gamma^2\beta^2+3\gamma^4+\alpha^2\left(3\gamma^2-5\beta^2\right)\right) a_{22} b_6 \beta}{\sqrt{2} K_{\alpha4\beta}\left(\alpha^2+\beta^2+\gamma^2\right)^2} + \frac{a_{14}}{\mathrm{Wi}} - \frac{b_{14}}{\mathrm{Wi}}$$
$$+ \frac{\alpha^2 K_{\beta\gamma}\left(\alpha^4+\left(2\beta^2+\gamma^2\right)\alpha^2-7\beta^4+\beta^2\gamma^2\right) a_1 b_{16}}{\sqrt{2} K_{\alpha\beta}\gamma\left(\alpha^2+\beta^2+\gamma^2\right)^2} + \frac{\alpha^2 K_{\alpha\beta} K_{\beta\gamma} a_4 b_{16}}{\gamma^3+\alpha^2\gamma+\beta^2\gamma}$$
$$+ \frac{\gamma\left(\alpha^4+\left(\beta^2+\gamma^2\right)\alpha^2+8\beta^4\right) a_7 b_{17}}{\sqrt{2}\left(\alpha^2+\beta^2+\gamma^2\right)^2} - \frac{\alpha^2 K_{\beta\gamma}\left(8\beta^4+\gamma^2\beta^2+\gamma^4+\alpha^2\gamma^2\right) a_{16} b_1}{\sqrt{2} K_{\alpha\beta}\gamma\left(\alpha^2+\beta^2+\gamma^2\right)^2}$$
$$+ \frac{\alpha K_{\beta\gamma}\left(\alpha^4+\left(5\beta^2+2\gamma^2\right)\alpha^2+8\beta^4+\gamma^4+5\beta^2\gamma^2\right) a_3 b_{20}}{\sqrt{2}\left(\alpha^2+\beta^2+\gamma^2\right)^2 K_{4\beta\gamma}}$$
$$+ \frac{\alpha K_{\beta\gamma}\left(\alpha^4+\left(5\beta^2+2\gamma^2\right)\alpha^2-32\beta^4+\gamma^4+5\beta^2\gamma^2\right) a_8 b_{20}}{\sqrt{2}\left(\alpha^2+\beta^2+\gamma^2\right)^2 K_{4\beta\gamma}} + \frac{\alpha^2\gamma a_7 b_{23}}{\alpha^2+\beta^2+\gamma^2} - \frac{\alpha^2\gamma K_{\beta\gamma} a_{16} b_4}{K_{\alpha\beta}\left(\alpha^2+\beta^2+\gamma^2\right)}$$
$$- \frac{\gamma\left(-7\beta^4+2\gamma^2\beta^2+\gamma^4+\alpha^2\left(\beta^2+\gamma^2\right)\right) a_{17} b_7}{\sqrt{2}\left(\alpha^2+\beta^2+\gamma^2\right)^2} - \frac{\gamma\left(\beta^2+\gamma^2\right) a_{23} b_7}{\alpha^2+\beta^2+\gamma^2}$$

$$
\begin{aligned}
\frac{db_{15}}{dt} = &+ \frac{2\sqrt{2}\alpha K_{\beta\gamma} a_1 b_9 \beta^3}{\left(\alpha^2+\beta^2+\gamma^2\right)^2} + \frac{2\sqrt{2}\alpha K_{\beta\gamma} a_9 b_1 \beta^3}{\left(\alpha^2+\beta^2+\gamma^2\right)^2} + \frac{\alpha K_{\beta\gamma}\left(3\alpha^2+7\beta^2+3\gamma^2\right) a_{21} b_3 \beta^2}{\sqrt{2}\left(\alpha^2+\beta^2+\gamma^2\right)^2 K_{4\beta\gamma}} \\
&+ \frac{3\alpha\left(\alpha^2-11\beta^2+\gamma^2\right) K_{\beta\gamma} a_{21} b_8 \beta^2}{\sqrt{2}\left(\alpha^2+\beta^2+\gamma^2\right)^2 K_{4\beta\gamma}} - \frac{\alpha\left(3\alpha^4+\left(11\beta^2+3\gamma^2\right)\alpha^2+8\beta^2\left(2\beta^2+\gamma^2\right)\right) a_7 b_{22}\beta}{\sqrt{2}K_{\alpha 4\beta}\left(\alpha^2+\beta^2+\gamma^2\right)^2} \\
&+ \frac{\alpha\left(-13\beta^4-2\gamma^2\beta^2+3\gamma^4+\alpha^2\left(3\gamma^2-5\beta^2\right)\right) a_{22} b_7 \beta}{\sqrt{2}K_{\alpha 4\beta}\left(\alpha^2+\beta^2+\gamma^2\right)^2} + \frac{a_{15}}{\mathrm{Wi}} - \frac{b_{15}}{\mathrm{Wi}} \\
&+ \frac{\alpha^2 K_{\beta\gamma}\left(\alpha^4+\left(2\beta^2+\gamma^2\right)\alpha^2-7\beta^4+\beta^2\gamma^2\right) a_2 b_{16}}{\sqrt{2}K_{\alpha\beta}\gamma\left(\alpha^2+\beta^2+\gamma^2\right)^2} + \frac{\alpha^2 K_{\alpha\beta} K_{\beta\gamma} a_5 b_{16}}{\gamma^3+\alpha^2\gamma+\beta^2\gamma} \\
&- \frac{\gamma\left(\alpha^4+\left(\beta^2+\gamma^2\right)\alpha^2+8\beta^4\right) a_6 b_{17}}{\sqrt{2}\left(\alpha^2+\beta^2+\gamma^2\right)^2} + \frac{\alpha K_{\beta\gamma}\left(\alpha^4+\left(5\beta^2+2\gamma^2\right)\alpha^2+8\beta^4+\gamma^4+5\beta^2\gamma^2\right) a_3 b_{21}}{\sqrt{2}\left(\alpha^2+\beta^2+\gamma^2\right)^2 K_{4\beta\gamma}} \\
&+ \frac{\alpha K_{\beta\gamma}\left(\alpha^4+\left(5\beta^2+2\gamma^2\right)\alpha^2-32\beta^4+\gamma^4+5\beta^2\gamma^2\right) a_8 b_{21}}{\sqrt{2}\left(\alpha^2+\beta^2+\gamma^2\right)^2 K_{4\beta\gamma}} - \frac{\alpha^2\gamma a_6 b_{23}}{\alpha^2+\beta^2+\gamma^2} \\
&- \frac{\alpha^2 K_{\beta\gamma}\left(8\beta^4+\gamma^2\beta^2+\gamma^4+\alpha^2\gamma^2\right) a_{16} b_2}{\sqrt{2}K_{\alpha\beta}\gamma\left(\alpha^2+\beta^2+\gamma^2\right)^2} - \frac{\alpha^2\gamma K_{\beta\gamma} a_{16} b_5}{K_{\alpha\beta}\left(\alpha^2+\beta^2+\gamma^2\right)} \\
&+ \frac{\gamma\left(-7\beta^4+2\gamma^2\beta^2+\gamma^4+\alpha^2\left(\beta^2+\gamma^2\right)\right) a_{17} b_6}{\sqrt{2}\left(\alpha^2+\beta^2+\gamma^2\right)^2} + \frac{\gamma\left(\beta^2+\gamma^2\right) a_{23} b_6}{\alpha^2+\beta^2+\gamma^2}
\end{aligned}
\tag{B.15}
$$

$$\frac{db_{16}}{dt} = \frac{2\alpha\beta a_4 b_{10}\gamma^3}{(\alpha^2+\beta^2)^{3/2} K_{\alpha\gamma}} + \frac{2\alpha\beta a_5 b_{11}\gamma^3}{(\alpha^2+\beta^2)^{3/2} K_{\alpha\gamma}} + \frac{2\alpha\beta a_{10} b_4\gamma^3}{(\alpha^2+\beta^2)^{3/2} K_{\alpha\gamma}} - \frac{(\alpha^2-\beta^2) a_{14} b_4\gamma^3}{(\alpha^2+\beta^2)^{3/2} K_{\beta\gamma}} + \frac{2\alpha\beta a_{11} b_5\gamma^3}{(\alpha^2+\beta^2)^{3/2} K_{\alpha\gamma}} \tag{B.16}$$
$$- \frac{(\alpha^2-\beta^2) a_{15} b_5\gamma^3}{(\alpha^2+\beta^2)^{3/2} K_{\beta\gamma}} + \frac{(\alpha^4+(\beta^2-\gamma^2)\alpha^2+\beta^2\gamma^2) a_6 b_{12}\gamma^2}{(\alpha^2+\beta^2)^{3/2} K_{\alpha\gamma}K_{\beta\gamma}} + \frac{(\alpha^4+(\beta^2-\gamma^2)\alpha^2+\beta^2\gamma^2) a_7 b_{13}\gamma^2}{(\alpha^2+\beta^2)^{3/2} K_{\alpha\gamma}K_{\beta\gamma}}$$
$$+ \frac{(\alpha^4+(\beta^2-\gamma^2)\alpha^2+\beta^2(4\beta^2+\gamma^2)) a_6 b_{18}\gamma^2}{\sqrt{2}(\alpha^2+\beta^2)^{3/2} K_{\alpha\gamma}K_{\beta\gamma}} + \frac{(\alpha^4+(\beta^2-\gamma^2)\alpha^2+\beta^2(4\beta^2+\gamma^2)) a_7 b_{19}\gamma^2}{\sqrt{2}(\alpha^2+\beta^2)^{3/2} K_{\alpha\gamma}K_{\beta\gamma}}$$
$$- \frac{\sqrt{2}\alpha\beta(2\beta^2+\gamma^2) a_6 b_{20}\gamma^2}{(\alpha^2+\beta^2)^{3/2} K_{\beta\gamma}K_{4\beta\gamma}} - \frac{\sqrt{2}\alpha\beta(2\beta^2+\gamma^2) a_7 b_{21}\gamma^2}{(\alpha^2+\beta^2)^{3/2} K_{\beta\gamma}K_{4\beta\gamma}} - \frac{(\beta^4-\gamma^2\beta^2+\alpha^2(\beta^2+\gamma^2)) a_{12} b_6\gamma^2}{(\alpha^2+\beta^2)^{3/2} K_{\alpha\gamma}K_{\beta\gamma}}$$
$$- \frac{(\alpha^2(\beta^2+\gamma^2)-\beta^2(3\beta^2+\gamma^2)) a_{18} b_6\gamma^2}{\sqrt{2}(\alpha^2+\beta^2)^{3/2} K_{\alpha\gamma}K_{\beta\gamma}} - \frac{\sqrt{2}\alpha\beta(2\beta^2+\gamma^2) a_{20} b_6\gamma^2}{(\alpha^2+\beta^2)^{3/2} K_{\beta\gamma}K_{4\beta\gamma}}$$
$$- \frac{(\beta^4-\gamma^2\beta^2+\alpha^2(\beta^2+\gamma^2)) a_{13} b_7\gamma^2}{(\alpha^2+\beta^2)^{3/2} K_{\alpha\gamma}K_{\beta\gamma}} - \frac{(\alpha^2(\beta^2+\gamma^2)-\beta^2(3\beta^2+\gamma^2)) a_{19} b_7\gamma^2}{\sqrt{2}(\alpha^2+\beta^2)^{3/2} K_{\alpha\gamma}K_{\beta\gamma}}$$
$$- \frac{\sqrt{2}\alpha\beta(2\beta^2+\gamma^2) a_{21} b_7\gamma^2}{(\alpha^2+\beta^2)^{3/2} K_{\beta\gamma}K_{4\beta\gamma}} - \frac{\sqrt{2}\alpha\beta(2\beta^2+\gamma^2) a_1 b_{10}\gamma}{(\alpha^2+\beta^2)^{3/2} K_{\alpha\gamma}} - \frac{\sqrt{2}\alpha\beta(2\beta^2+\gamma^2) a_2 b_{11}\gamma}{(\alpha^2+\beta^2)^{3/2} K_{\alpha\gamma}}$$
$$- \frac{(\alpha^2-\beta^2)(\alpha^2+3\beta^2+\gamma^2) a_1 b_{14}\gamma}{\sqrt{2}(\alpha^2+\beta^2)^{3/2} K_{\beta\gamma}} - \frac{(\alpha^4+(2\beta^2+\gamma^2)\alpha^2+\beta^4-\beta^2\gamma^2) a_4 b_{14}\gamma}{(\alpha^2+\beta^2)^{3/2} K_{\beta\gamma}}$$
$$- \frac{(\alpha^2-\beta^2)(\alpha^2+3\beta^2+\gamma^2) a_2 b_{15}\gamma}{\sqrt{2}(\alpha^2+\beta^2)^{3/2} K_{\beta\gamma}} - \frac{(\alpha^4+(2\beta^2+\gamma^2)\alpha^2+\beta^4-\beta^2\gamma^2) a_5 b_{15}\gamma}{(\alpha^2+\beta^2)^{3/2} K_{\beta\gamma}}$$
$$- \frac{\sqrt{2}\alpha\beta(2\beta^2+\gamma^2) a_{10} b_1\gamma}{(\alpha^2+\beta^2)^{3/2} K_{\alpha\gamma}} + \frac{(4\beta^4+\gamma^2\beta^2-\alpha^2\gamma^2) a_{14} b_1\gamma}{\sqrt{2}(\alpha^2+\beta^2)^{3/2} K_{\beta\gamma}} - \frac{\sqrt{2}\alpha\beta(2\beta^2+\gamma^2) a_{11} b_2\gamma}{(\alpha^2+\beta^2)^{3/2} K_{\alpha\gamma}}$$
$$+ \frac{(4\beta^4+\gamma^2\beta^2-\alpha^2\gamma^2) a_{15} b_2\gamma}{\sqrt{2}(\alpha^2+\beta^2)^{3/2} K_{\beta\gamma}} + \frac{a_{16}}{\mathrm{Wi}} - \frac{b_{16}}{\mathrm{Wi}} - \frac{\alpha(\alpha^4+5\beta^2\alpha^2+8\beta^4) a_3 b_{22}}{\sqrt{2}(\alpha^2+\beta^2)^{3/2} K_{\alpha 4\beta}}$$
$$- \frac{\alpha(\alpha^4+5\beta^2\alpha^2-32\beta^4) a_8 b_{22}}{\sqrt{2}(\alpha^2+\beta^2)^{3/2} K_{\alpha 4\beta}} - \frac{\alpha\beta^2(3\alpha^2+7\beta^2) a_{22} b_3}{\sqrt{2}(\alpha^2+\beta^2)^{3/2} K_{\alpha 4\beta}} - \frac{3\alpha\beta^2(\alpha^2-11\beta^2) a_{22} b_8}{\sqrt{2}(\alpha^2+\beta^2)^{3/2} K_{\alpha 4\beta}}$$

$$\frac{db_{17}}{dt} = - \frac{4\sqrt{2}\gamma a_{15} b_6\beta^4}{(\alpha^2+4\beta^2)(\beta^2+\gamma^2)} + \frac{4\sqrt{2}\gamma a_{14} b_7\beta^4}{(\alpha^2+4\beta^2)(\beta^2+\gamma^2)} - \frac{2\sqrt{2}(\alpha^2+2\beta^2)\gamma a_7 b_{14}\beta^2}{(\alpha^2+4\beta^2)(\beta^2+\gamma^2)} \tag{B.17}$$
$$+ \frac{2\sqrt{2}(\alpha^2+2\beta^2)\gamma a_6 b_{15}\beta^2}{(\alpha^2+4\beta^2)(\beta^2+\gamma^2)} + \frac{3\alpha a_9 b_3\beta^2}{\sqrt{2}(\alpha^2+4\beta^2)} - \frac{3\alpha a_9 b_8\beta^2}{\sqrt{2}(\alpha^2+4\beta^2)} - \frac{\alpha\gamma(3\alpha^2+5\beta^2+\gamma^2) a_7 b_{10}\beta}{\sqrt{2}(\alpha^2+4\beta^2) K_{\alpha\gamma}K_{\beta\gamma}}$$
$$+ \frac{\alpha\gamma(3\alpha^2+5\beta^2+\gamma^2) a_6 b_{11}\beta}{\sqrt{2}(\alpha^2+4\beta^2) K_{\alpha\gamma}K_{\beta\gamma}} - \frac{2\alpha(\alpha^2+4\beta^2+\gamma^2) a_5 b_{20}\beta}{(\alpha^2+4\beta^2) K_{4\beta\gamma}} + \frac{2\alpha(\alpha^2+4\beta^2+\gamma^2) a_4 b_{21}\beta}{(\alpha^2+4\beta^2) K_{4\beta\gamma}}$$
$$+ \frac{2\alpha\gamma^2 a_{21} b_4\beta}{(\alpha^2+4\beta^2) K_{4\beta\gamma}} - \frac{2\alpha\gamma^2 a_{20} b_5\beta}{(\alpha^2+4\beta^2) K_{4\beta\gamma}} + \frac{\alpha\gamma(\gamma^2-7\beta^2) a_{11} b_6\beta}{\sqrt{2}(\alpha^2+4\beta^2) K_{\alpha\gamma}K_{\beta\gamma}} - \frac{\alpha\gamma(\gamma^2-7\beta^2) a_{10} b_7\beta}{\sqrt{2}(\alpha^2+4\beta^2) K_{\alpha\gamma}K_{\beta\gamma}} + \frac{a_{17}}{\mathrm{Wi}}$$
$$- \frac{\alpha(\alpha^2+\beta^2) a_3 b_9}{\sqrt{2}(\alpha^2+4\beta^2)} + \frac{\alpha(\alpha^2+\beta^2) a_8 b_9}{\sqrt{2}(\alpha^2+4\beta^2)} - \frac{\alpha^2 K_{\alpha\gamma} a_2 b_{12}}{\alpha^2+4\beta^2} + \frac{\alpha^2 K_{\alpha\gamma} a_1 b_{13}}{\alpha^2+4\beta^2} - \frac{b_{17}}{\mathrm{Wi}} - \frac{\alpha^2(\alpha^2+4\beta^2+\gamma^2) a_5 b_{18}}{(\alpha^2+4\beta^2) K_{\alpha\gamma}}$$
$$+ \frac{\alpha^2(\gamma^2-4\beta^2) a_{13} b_1}{(\alpha^2+4\beta^2) K_{\alpha\gamma}} + \frac{\alpha^2(\alpha^2+4\beta^2+\gamma^2) a_4 b_{19}}{(\alpha^2+4\beta^2) K_{\alpha\gamma}} - \frac{\alpha^2(\gamma^2-4\beta^2) a_{12} b_2}{(\alpha^2+4\beta^2) K_{\alpha\gamma}} + \frac{\alpha^2\gamma^2 a_{19} b_4}{(\alpha^2+4\beta^2) K_{\alpha\gamma}}$$
$$- \frac{\alpha^2\gamma^2 a_{18} b_5}{(\alpha^2+4\beta^2) K_{\alpha\gamma}}$$

$$\frac{db_{18}}{dt} = -\frac{\sqrt{2}\alpha\gamma K_{\alpha\gamma} a_7 b_9 \beta^3}{K_{\beta\gamma}\left(\alpha^2+4\beta^2+\gamma^2\right)^2} - \frac{K_{\alpha\gamma}\left(3\alpha^2+4\beta^2+\gamma^2\right) a_{14} b_3 \beta^3}{\sqrt{2} K_{\beta\gamma}\left(\alpha^2+4\beta^2+\gamma^2\right)^2} - \frac{\sqrt{2}\alpha\gamma K_{\alpha\gamma} a_9 b_7 \beta^3}{K_{\beta\gamma}\left(\alpha^2+4\beta^2+\gamma^2\right)^2} \tag{B.18}$$
$$- \frac{9 K_{\alpha\gamma}\left(\alpha^2+3\left(4\beta^2+\gamma^2\right)\right) a_{14} b_8 \beta^3}{\sqrt{2} K_{\beta\gamma}\left(\alpha^2+4\beta^2+\gamma^2\right)^2} - \frac{K_{\alpha\gamma}\left(\alpha^4+\left(3\beta^2+\gamma^2\right)\alpha^2+\beta^2\left(4\beta^2+\gamma^2\right)\right) a_6 b_{16} \beta^2}{\sqrt{2} K_{\alpha\beta} K_{\beta\gamma}\left(\alpha^2+4\beta^2+\gamma^2\right)^2}$$
$$+ \frac{3\alpha a_{10} b_3 \beta^2}{\sqrt{2}\left(\alpha^2+4\beta^2+\gamma^2\right)} + \frac{K_{\alpha\gamma}\left(12\beta^4+7\gamma^2\beta^2+\gamma^4+\alpha^2\left(5\beta^2+\gamma^2\right)\right) a_{16} b_6 \beta^2}{\sqrt{2} K_{\alpha\beta} K_{\beta\gamma}\left(\alpha^2+4\beta^2+\gamma^2\right)^2} - \frac{3\alpha a_{10} b_8 \beta^2}{\sqrt{2}\left(\alpha^2+4\beta^2+\gamma^2\right)}$$
$$+ \frac{K_{\alpha\gamma}\left(\alpha^4+\left(5\beta^2+2\gamma^2\right)\alpha^2+12\beta^4+\gamma^4+7\beta^2\gamma^2\right) a_3 b_{14} \beta}{\sqrt{2} K_{\beta\gamma}\left(\alpha^2+4\beta^2+\gamma^2\right)^2}$$
$$+ \frac{3 K_{\alpha\gamma}\left(\alpha^4+\left(5\beta^2+2\gamma^2\right)\alpha^2-20\beta^4+\gamma^4-\beta^2\gamma^2\right) a_8 b_{14} \beta}{\sqrt{2} K_{\beta\gamma}\left(\alpha^2+4\beta^2+\gamma^2\right)^2} + \frac{2\alpha K_{\alpha4\beta} K_{\alpha\gamma} a_4 b_{22} \beta}{\gamma^3+\alpha^2\gamma+4\beta^2\gamma}$$
$$- \frac{2\alpha\gamma K_{\alpha\gamma} a_{22} b_4 \beta}{K_{\alpha4\beta}\left(\alpha^2+4\beta^2+\gamma^2\right)} + \frac{a_{18}}{\mathrm{Wi}} - \frac{\alpha\left(\alpha^2+\beta^2+\gamma^2\right) a_3 b_{10}}{\sqrt{2}\left(\alpha^2+4\beta^2+\gamma^2\right)} + \frac{\alpha\left(\alpha^2+\beta^2+\gamma^2\right) a_8 b_{10}}{\sqrt{2}\left(\alpha^2+4\beta^2+\gamma^2\right)}$$
$$+ \frac{\left(\alpha^2+4\beta^2\right) K_{\alpha\gamma} a_5 b_{17}}{\alpha^2+4\beta^2+\gamma^2} - \frac{b_{18}}{\mathrm{Wi}} + \frac{\alpha^2 K_{\alpha\gamma} a_2 b_{23}}{\alpha^2+4\beta^2+\gamma^2} - \frac{K_{\alpha\gamma}\left(4\beta^2+\gamma^2\right) a_{23} b_2}{\alpha^2+4\beta^2+\gamma^2} - \frac{\gamma^2 K_{\alpha\gamma} a_{17} b_5}{\alpha^2+4\beta^2+\gamma^2}$$

$$\frac{db_{19}}{dt} = \frac{\sqrt{2}\alpha\gamma K_{\alpha\gamma} a_6 b_9 \beta^3}{K_{\beta\gamma}\left(\alpha^2+4\beta^2+\gamma^2\right)^2} - \frac{K_{\alpha\gamma}\left(3\alpha^2+4\beta^2+\gamma^2\right) a_{15} b_3 \beta^3}{\sqrt{2} K_{\beta\gamma}\left(\alpha^2+4\beta^2+\gamma^2\right)^2} + \frac{\sqrt{2}\alpha\gamma K_{\alpha\gamma} a_9 b_6 \beta^3}{K_{\beta\gamma}\left(\alpha^2+4\beta^2+\gamma^2\right)^2} \tag{B.19}$$
$$- \frac{9 K_{\alpha\gamma}\left(\alpha^2+3\left(4\beta^2+\gamma^2\right)\right) a_{15} b_8 \beta^3}{\sqrt{2} K_{\beta\gamma}\left(\alpha^2+4\beta^2+\gamma^2\right)^2} - \frac{K_{\alpha\gamma}\left(\alpha^4+\left(3\beta^2+\gamma^2\right)\alpha^2+\beta^2\left(4\beta^2+\gamma^2\right)\right) a_7 b_{16} \beta^2}{\sqrt{2} K_{\alpha\beta} K_{\beta\gamma}\left(\alpha^2+4\beta^2+\gamma^2\right)^2}$$
$$+ \frac{3\alpha a_{11} b_3 \beta^2}{\sqrt{2}\left(\alpha^2+4\beta^2+\gamma^2\right)} + \frac{K_{\alpha\gamma}\left(12\beta^4+7\gamma^2\beta^2+\gamma^4+\alpha^2\left(5\beta^2+\gamma^2\right)\right) a_{16} b_7 \beta^2}{\sqrt{2} K_{\alpha\beta} K_{\beta\gamma}\left(\alpha^2+4\beta^2+\gamma^2\right)^2} - \frac{3\alpha a_{11} b_8 \beta^2}{\sqrt{2}\left(\alpha^2+4\beta^2+\gamma^2\right)}$$
$$+ \frac{K_{\alpha\gamma}\left(\alpha^4+\left(5\beta^2+2\gamma^2\right)\alpha^2+12\beta^4+\gamma^4+7\beta^2\gamma^2\right) a_3 b_{15} \beta}{\sqrt{2} K_{\beta\gamma}\left(\alpha^2+4\beta^2+\gamma^2\right)^2}$$
$$+ \frac{3 K_{\alpha\gamma}\left(\alpha^4+\left(5\beta^2+2\gamma^2\right)\alpha^2-20\beta^4+\gamma^4-\beta^2\gamma^2\right) a_8 b_{15} \beta}{\sqrt{2} K_{\beta\gamma}\left(\alpha^2+4\beta^2+\gamma^2\right)^2} + \frac{2\alpha K_{\alpha4\beta} K_{\alpha\gamma} a_5 b_{22} \beta}{\gamma^3+\alpha^2\gamma+4\beta^2\gamma}$$
$$- \frac{2\alpha\gamma K_{\alpha\gamma} a_{22} b_5 \beta}{K_{\alpha4\beta}\left(\alpha^2+4\beta^2+\gamma^2\right)} + \frac{a_{19}}{\mathrm{Wi}} - \frac{\alpha\left(\alpha^2+\beta^2+\gamma^2\right) a_3 b_{11}}{\sqrt{2}\left(\alpha^2+4\beta^2+\gamma^2\right)} + \frac{\alpha\left(\alpha^2+\beta^2+\gamma^2\right) a_8 b_{11}}{\sqrt{2}\left(\alpha^2+4\beta^2+\gamma^2\right)}$$
$$- \frac{\left(\alpha^2+4\beta^2\right) K_{\alpha\gamma} a_4 b_{17}}{\alpha^2+4\beta^2+\gamma^2} + \frac{K_{\alpha\gamma}\left(4\beta^2+\gamma^2\right) a_{23} b_1}{\alpha^2+4\beta^2+\gamma^2} - \frac{b_{19}}{\mathrm{Wi}} - \frac{\alpha^2 K_{\alpha\gamma} a_1 b_{23}}{\alpha^2+4\beta^2+\gamma^2} + \frac{\gamma^2 K_{\alpha\gamma} a_{17} b_4}{\alpha^2+4\beta^2+\gamma^2}$$

$$\frac{db_{20}}{dt} = -\frac{\gamma a_9 K_{4\beta\gamma} b_7 \left(\alpha^2\left(\beta^2+\gamma^2\right)+8\beta^4+5\beta^2\gamma^2+\gamma^4\right)}{\sqrt{2}K_{\beta\gamma}\left(\alpha^2+4\beta^2+\gamma^2\right)^2} + \frac{\alpha\beta^2 a_{14} K_{4\beta\gamma} b_3 \left(3\alpha^2+8\beta^2+3\gamma^2\right)}{\sqrt{2}K_{\beta\gamma}\left(\alpha^2+4\beta^2+\gamma^2\right)^2} \tag{B.20}$$
$$+ \frac{3\alpha\beta^2 a_{14} K_{4\beta\gamma} b_8 \left(\alpha^2+16\beta^2+\gamma^2\right)}{\sqrt{2}K_{\beta\gamma}\left(\alpha^2+4\beta^2+\gamma^2\right)^2} - \frac{\sqrt{2}\alpha\beta^3 a_{16} K_{4\beta\gamma} b_6 \left(\alpha^2+2\beta^2+\gamma^2\right)}{K_{\alpha\beta}K_{\beta\gamma}\left(\alpha^2+4\beta^2+\gamma^2\right)^2} + \frac{a_{20}}{\mathrm{Wi}}$$
$$+ \frac{\alpha^2\gamma a_{22} K_{4\beta\gamma} b_4}{K_{\alpha 4\beta}\left(\alpha^2+4\beta^2+\gamma^2\right)} - \frac{\alpha a_3 K_{4\beta\gamma} b_{14}\left(\alpha^4+\alpha^2\left(5\beta^2+2\gamma^2\right)+8\beta^4+5\beta^2\gamma^2+\gamma^4\right)}{\sqrt{2}K_{\beta\gamma}\left(\alpha^2+4\beta^2+\gamma^2\right)^2}$$
$$- \frac{\alpha^2 K_{\alpha 4\beta} a_4 K_{4\beta\gamma} b_{22}}{\alpha^2\gamma+4\beta^2\gamma+\gamma^3} - \frac{\sqrt{2}\alpha\beta^3 a_6 K_{4\beta\gamma} b_{16}\left(\alpha^2+2\beta^2+\gamma^2\right)}{K_{\alpha\beta}K_{\beta\gamma}\left(\alpha^2+4\beta^2+\gamma^2\right)^2}$$
$$+ \frac{\gamma a_7 K_{4\beta\gamma} b_9 \left(\alpha^4+\alpha^2\left(7\beta^2+\gamma^2\right)+8\beta^4+3\beta^2\gamma^2\right)}{\sqrt{2}K_{\beta\gamma}\left(\alpha^2+4\beta^2+\gamma^2\right)^2}$$
$$- \frac{\alpha a_8 K_{4\beta\gamma} b_{14}\left(\alpha^4+\alpha^2\left(5\beta^2+2\gamma^2\right)-32\beta^4+5\beta^2\gamma^2+\gamma^4\right)}{\sqrt{2}K_{\beta\gamma}\left(\alpha^2+4\beta^2+\gamma^2\right)^2} - \frac{b_{20}}{\mathrm{Wi}}$$

$$\frac{db_{21}}{dt} = \frac{\gamma a_9 K_{4\beta\gamma} b_6 \left(\alpha^2\left(\beta^2+\gamma^2\right)+8\beta^4+5\beta^2\gamma^2+\gamma^4\right)}{\sqrt{2}K_{\beta\gamma}\left(\alpha^2+4\beta^2+\gamma^2\right)^2} + \frac{\alpha\beta^2 a_{15} K_{4\beta\gamma} b_3 \left(3\alpha^2+8\beta^2+3\gamma^2\right)}{\sqrt{2}K_{\beta\gamma}\left(\alpha^2+4\beta^2+\gamma^2\right)^2} \tag{B.21}$$
$$+ \frac{3\alpha\beta^2 a_{15} K_{4\beta\gamma} b_8 \left(\alpha^2+16\beta^2+\gamma^2\right)}{\sqrt{2}K_{\beta\gamma}\left(\alpha^2+4\beta^2+\gamma^2\right)^2} - \frac{\sqrt{2}\alpha\beta^3 a_{16} K_{4\beta\gamma} b_7 \left(\alpha^2+2\beta^2+\gamma^2\right)}{K_{\alpha\beta}K_{\beta\gamma}\left(\alpha^2+4\beta^2+\gamma^2\right)^2} + \frac{a_{21}}{\mathrm{Wi}}$$
$$+ \frac{\alpha^2\gamma a_{22} K_{4\beta\gamma} b_5}{K_{\alpha 4\beta}\left(\alpha^2+4\beta^2+\gamma^2\right)} - \frac{\alpha a_3 K_{4\beta\gamma} b_{15}\left(\alpha^4+\alpha^2\left(5\beta^2+2\gamma^2\right)+8\beta^4+5\beta^2\gamma^2+\gamma^4\right)}{\sqrt{2}K_{\beta\gamma}\left(\alpha^2+4\beta^2+\gamma^2\right)^2}$$
$$- \frac{\alpha^2 K_{\alpha 4\beta} a_5 K_{4\beta\gamma} b_{22}}{\alpha^2\gamma+4\beta^2\gamma+\gamma^3} - \frac{\gamma a_6 K_{4\beta\gamma} b_9 \left(\alpha^4+\alpha^2\left(7\beta^2+\gamma^2\right)+8\beta^4+3\beta^2\gamma^2\right)}{\sqrt{2}K_{\beta\gamma}\left(\alpha^2+4\beta^2+\gamma^2\right)^2}$$
$$- \frac{\sqrt{2}\alpha\beta^3 a_7 K_{4\beta\gamma} b_{16}\left(\alpha^2+2\beta^2+\gamma^2\right)}{K_{\alpha\beta}K_{\beta\gamma}\left(\alpha^2+4\beta^2+\gamma^2\right)^2} - \frac{\alpha a_8 K_{4\beta\gamma} b_{15}\left(\alpha^4+\alpha^2\left(5\beta^2+2\gamma^2\right)-32\beta^4+5\beta^2\gamma^2+\gamma^4\right)}{\sqrt{2}K_{\beta\gamma}\left(\alpha^2+4\beta^2+\gamma^2\right)^2} - \frac{b_{21}}{\mathrm{Wi}}$$

$$\frac{db_{22}}{dt} = -\frac{4\alpha\beta a_1 b_{12}\gamma^3}{\left(\alpha^2+4\beta^2\right)^{3/2}K_{\alpha\gamma}} - \frac{4\alpha\beta a_2 b_{13}\gamma^3}{\left(\alpha^2+4\beta^2\right)^{3/2}K_{\alpha\gamma}} - \frac{4\alpha\beta a_4 b_{18}\gamma^3}{\left(\alpha^2+4\beta^2\right)^{3/2}K_{\alpha\gamma}} - \frac{4\alpha\beta a_{12} b_1\gamma^3}{\left(\alpha^2+4\beta^2\right)^{3/2}K_{\alpha\gamma}} \tag{B.22}$$
$$- \frac{4\alpha\beta a_5 b_{19}\gamma^3}{\left(\alpha^2+4\beta^2\right)^{3/2}K_{\alpha\gamma}} - \frac{4\alpha\beta a_{13} b_2\gamma^3}{\left(\alpha^2+4\beta^2\right)^{3/2}K_{\alpha\gamma}} - \frac{4\alpha\beta a_{18} b_4\gamma^3}{\left(\alpha^2+4\beta^2\right)^{3/2}K_{\alpha\gamma}} + \frac{\left(\alpha^2-4\beta^2\right)a_{20}b_4\gamma^3}{\left(\alpha^2+4\beta^2\right)^{3/2}K_{4\beta\gamma}}$$
$$- \frac{4\alpha\beta a_{19} b_5\gamma^3}{\left(\alpha^2+4\beta^2\right)^{3/2}K_{\alpha\gamma}} + \frac{\left(\alpha^2-4\beta^2\right)a_{21}b_5\gamma^3}{\left(\alpha^2+4\beta^2\right)^{3/2}K_{4\beta\gamma}} - \frac{\left(\alpha^4+\left(7\beta^2-\gamma^2\right)\alpha^2+4\beta^2\left(\beta^2+\gamma^2\right)\right)a_6 b_{10}\gamma^2}{\sqrt{2}\left(\alpha^2+4\beta^2\right)^{3/2}K_{\alpha\gamma}K_{\beta\gamma}}$$
$$- \frac{\left(\alpha^4+\left(7\beta^2-\gamma^2\right)\alpha^2+4\beta^2\left(\beta^2+\gamma^2\right)\right)a_7 b_{11}\gamma^2}{\sqrt{2}\left(\alpha^2+4\beta^2\right)^{3/2}K_{\alpha\gamma}K_{\beta\gamma}} + \frac{2\sqrt{2}\alpha\beta\left(\gamma^2-\beta^2\right)a_6 b_{14}\gamma^2}{\left(\alpha^2+4\beta^2\right)^{3/2}\left(\beta^2+\gamma^2\right)}$$
$$+ \frac{2\sqrt{2}\alpha\beta\left(\gamma^2-\beta^2\right)a_7 b_{15}\gamma^2}{\left(\alpha^2+4\beta^2\right)^{3/2}\left(\beta^2+\gamma^2\right)} + \frac{\left(12\beta^4-4\gamma^2\beta^2+\alpha^2\left(\beta^2+\gamma^2\right)\right)a_{10}b_6\gamma^2}{\sqrt{2}\left(\alpha^2+4\beta^2\right)^{3/2}K_{\alpha\gamma}K_{\beta\gamma}} + \frac{2\sqrt{2}\alpha\beta\left(\gamma^2-\beta^2\right)a_{14}b_6\gamma^2}{\left(\alpha^2+4\beta^2\right)^{3/2}\left(\beta^2+\gamma^2\right)}$$
$$+ \frac{\left(12\beta^4-4\gamma^2\beta^2+\alpha^2\left(\beta^2+\gamma^2\right)\right)a_{11}b_7\gamma^2}{\sqrt{2}\left(\alpha^2+4\beta^2\right)^{3/2}K_{\alpha\gamma}K_{\beta\gamma}} + \frac{2\sqrt{2}\alpha\beta\left(\gamma^2-\beta^2\right)a_{15}b_7\gamma^2}{\left(\alpha^2+4\beta^2\right)^{3/2}\left(\beta^2+\gamma^2\right)}$$
$$+ \frac{\left(\alpha^4+\left(8\beta^2+\gamma^2\right)\alpha^2+16\beta^4-4\beta^2\gamma^2\right)a_4 b_{20}\gamma}{\left(\alpha^2+4\beta^2\right)^{3/2}K_{4\beta\gamma}} + \frac{\left(\alpha^4+\left(8\beta^2+\gamma^2\right)\alpha^2+16\beta^4-4\beta^2\gamma^2\right)a_5 b_{21}\gamma}{\left(\alpha^2+4\beta^2\right)^{3/2}K_{4\beta\gamma}} + \frac{a_{22}}{\mathrm{Wi}}$$
$$+ \frac{\alpha\left(\alpha^4+5\beta^2\alpha^2+8\beta^4\right)a_3 b_{16}}{\sqrt{2}K_{\alpha\beta}\left(\alpha^2+4\beta^2\right)^{3/2}} + \frac{\alpha\left(\alpha^4+5\beta^2\alpha^2-32\beta^4\right)a_8 b_{16}}{\sqrt{2}K_{\alpha\beta}\left(\alpha^2+4\beta^2\right)^{3/2}} - \frac{b_{22}}{\mathrm{Wi}} - \frac{\alpha\beta^2\left(3\alpha^2+8\beta^2\right)a_{16}b_3}{\sqrt{2}K_{\alpha\beta}\left(\alpha^2+4\beta^2\right)^{3/2}}$$
$$- \frac{3\alpha\beta^2\left(\alpha^2+16\beta^2\right)a_{16}b_8}{\sqrt{2}K_{\alpha\beta}\left(\alpha^2+4\beta^2\right)^{3/2}}$$

$$\frac{db_{23}}{dt} = +\frac{\beta^2 a_9 b_3}{\alpha} - \frac{\beta\gamma a_{10}K_{\beta\gamma}b_7}{\alpha K_{\alpha\gamma}} + \frac{\beta\gamma a_{11}K_{\beta\gamma}b_6}{\alpha K_{\alpha\gamma}} - \frac{\gamma^2 a_{12}b_5}{K_{\alpha\gamma}} + \frac{\gamma^2 a_{13}b_4}{K_{\alpha\gamma}} - \frac{a_{18}\left(4\beta^2+\gamma^2\right)b_2}{K_{\alpha\gamma}} \tag{B.23}$$
$$+ \frac{a_1 b_{19}\left(\alpha^2+4\beta^2+\gamma^2\right)}{K_{\alpha\gamma}} + \frac{2\beta a_1 b_{21}\left(\alpha^2+4\beta^2+\gamma^2\right)}{\alpha K_{4\beta\gamma}} + \frac{a_{19}\left(4\beta^2+\gamma^2\right)b_1}{K_{\alpha\gamma}} - \frac{2\beta a_{20}K_{4\beta\gamma}b_2}{\alpha}$$
$$+ \frac{2\beta a_{21}K_{4\beta\gamma}b_1}{\alpha} + \frac{a_{23}}{\mathrm{Wi}} - \frac{a_2 b_{18}\left(\alpha^2+4\beta^2+\gamma^2\right)}{K_{\alpha\gamma}} - \frac{2\beta a_2 b_{20}\left(\alpha^2+4\beta^2+\gamma^2\right)}{\alpha K_{4\beta\gamma}} + \frac{\left(\alpha^2+\beta^2\right)a_3 b_9}{\alpha}$$
$$+ K_{\alpha\gamma}a_4 b_{13} - K_{\alpha\gamma}a_5 b_{12} + \frac{\beta\gamma a_6 b_{11}\left(-\alpha^2+\beta^2+\gamma^2\right)}{\alpha K_{\alpha\gamma}K_{\beta\gamma}} - \frac{\beta\gamma a_7 b_{10}\left(-\alpha^2+\beta^2+\gamma^2\right)}{\alpha K_{\alpha\gamma}K_{\beta\gamma}} - \frac{b_{23}}{\mathrm{Wi}}$$

Bibliography

[1] Boris Hasselblatt and Anatole Katok. *A first course in dynamics: with a panorama of recent developments*. Cambridge University Press, 2003.

[2] Jens HM Fransson, Alessandro Talamelli, Luca Brandt, and Carlo Cossu. Delaying transition to turbulence by a passive mechanism. *Physical review letters*, 96(6):064501, 2006.

[3] Genta Kawahara. Laminarization of minimal plane couette flow: going beyond the basin of attraction of turbulence. *Physics of Fluids*, 17(4):041702, 2005.

[4] Mohamed Gad-el Hak. *Flow control: passive, active, and reactive flow management*. Cambridge university press, 2006.

[5] Osborne Reynolds. An experimental investigation of the circumstances which determine whether the motion of water shall be direct or sinuous, and of the law of resistance in parallel channels. *Proceedings of the royal society of London*, 35(224-226):84–99, 1883.

[6] Osborne Reynolds. On the dynamical theory of incompressible viscous fluids and the determination of the criterion. *Proceedings of the Royal Society of London*, 56(336-339):40–45, 1894.

[7] Philip G Drazin and William Hill Reid. *Hydrodynamic stability*. Cambridge university press, 2004.

[8] AG Darbyshire and T Mullin. Transition to turbulence in constant-mass-flux pipe flow. *Journal of Fluid Mechanics*, 289:83–114, 1995.

[9] David J Tritton. *Physical fluid dynamics*. Springer Science & Business Media, 2012.

[10] George Keith Batchelor. *An introduction to fluid dynamics*. Cambridge university press, 2000.

[11] Charles L Fefferman. Existence and smoothness of the navier-stokes equation. *The millennium prize problems*, pages 57–67, 2006.

[12] WVR Malkus and G Veronis. Finite amplitude cellular convection. *Journal of Fluid Mechanics*, 4(3):225–260, 1958.

[13] KA Cliffe, A Spence, and SJ Tavener. The numerical analysis of bifurcation problems with application to fluid mechanics. *Acta Numerica*, 9:39–131, 2000.

[14] B Hof, A Juel, and T Mullin. Scaling of the turbulence transition threshold in a pipe. *Physical review letters*, 91(24):244502, 2003.

[15] Armin Schmiegel and Bruno Eckhardt. Fractal stability border in plane couette flow. *Physical review letters*, 79(26):5250, 1997.

[16] Kathryn M Butler and Brian F Farrell. Three-dimensional optimal perturbations in viscous shear flow. *Physics of Fluids A: Fluid Dynamics*, 4(8):1637–1650, 1992.

[17] Lloyd N Trefethen, Anne E Trefethen, Satish C Reddy, and Tobin A Driscoll. Hydrodynamic stability without eigenvalues. *Science*, 261(5121):578–584, 1993.

[18] Nazmi Burak Budanur, Kimberly Y Short, Mohammad Farazmand, Ashley P Willis, and Predrag Cvitanović. Relative periodic orbits form the backbone of turbulent pipe flow. *Journal of Fluid Mechanics*, 833:274–301, 2017.

[19] Björn Hof, Casimir WH van Doorne, Jerry Westerweel, Frans TM Nieuwstadt, Holger Faisst, Bruno Eckhardt, Hakan Wedin, Richard R Kerswell, and Fabian Waleffe. Experimental observation of nonlinear traveling waves in turbulent pipe flow. *Science*, 305(5690):1594–1598, 2004.

[20] HE Fiedler. Coherent structures in turbulent flows. *Progress in Aerospace Sciences*, 25(3):231–269, 1988.

[21] John F Gibson, Jonathan Halcrow, and Predrag Cvitanović. Visualizing the geometry of state space in plane couette flow. *Journal of Fluid Mechanics*, 611:107–130, 2008.

[22] Björn Hof, Jerry Westerweel, Tobias M Schneider, and Bruno Eckhardt. Finite lifetime of turbulence in shear flows. *Nature*, 443(7107):59, 2006.

[23] David JC Dennis and Francesca M Sogaro. Distinct organizational states of fully developed turbulent pipe flow. *Physical review letters*, 113(23):234501, 2014.

[24] Michael D Graham. Drag reduction in turbulent flow of polymer solutions. *Rheology reviews*, 2(2):143–170, 2004.

[25] Yohann Duguet, Chris CT Pringle, and Rich R Kerswell. Relative periodic orbits in transitional pipe flow. *Physics of fluids*, 20(11):114102, 2008.

[26] Divakar Viswanath. Recurrent motions within plane couette turbulence. *Journal of Fluid Mechanics*, 580:339–358, 2007.

[27] Hakan Wedin and RR Kerswell. Exact coherent structures in pipe flow: travelling wave solutions. *Journal of Fluid Mechanics*, 508:333–371, 2004.

[28] Holger Faisst and Bruno Eckhardt. Traveling waves in pipe flow. *Physical Review Letters*, 91(22):224502, 2003.

[29] Eberhard Hopf. A mathematical example displaying features of turbulence. *Communications on Pure and Applied Mathematics*, 1(4):303–322, 1948.

[30] Peter Constantin, Ciprian Foias, Oscar P Manley, and Roger Temam. Determining modes and fractal dimension of turbulent flows. *Journal of Fluid Mechanics*, 150:427–440, 1985.

[31] Peter Constantin, C Foias, and Roger Temam. On the dimension of the attractors in two-dimensional turbulence. *Physica D: Nonlinear Phenomena*, 30(3):284–296, 1988.

[32] Alec J Linot and Michael D Graham. Deep learning to discover and predict dynamics on an inertial manifold. *arXiv preprint arXiv:2001.04263*, 2019.

[33] Patrice Marcotte and Jean-Pierre Dussault. A note on a globally convergent newton method for solving monotone variational inequalities. *Operations Research Letters*, 6(1):35–42, 1987.

[34] M Nagata. Bifurcations in couette flow between almost corotating cylinders. *Journal of Fluid Mechanics*, 169:229–250, 1986.

[35] Holger Faisst and Bruno Eckhardt. Transition from the couette-taylor system to the plane couette system. *Physical Review E*, 61(6):7227, 2000.

[36] Tjalling J Ypma. Historical development of the newton–raphson method. *SIAM review*, 37(4):531–551, 1995.

[37] Dana A Knoll and David E Keyes. Jacobian-free newton–krylov methods: a survey of approaches and applications. *Journal of Computational Physics*, 193(2):357–397, 2004.

[38] Genta Kawahara and Shigeo Kida. Periodic motion embedded in plane couette turbulence: regeneration cycle and burst. *Journal of Fluid Mechanics*, 449:291–300, 2001.

[39] Bruce J Bayly, Steven A Orszag, and Thorwald Herbert. Instability mechanisms in shear-flow transition. *Annual review of fluid mechanics*, 20(1):359–391, 1988.

[40] Nils Tillmark and P Henrik Alfredsson. Experiments on transition in plane couette flow. *Journal of Fluid Mechanics*, 235:89–102, 1992.

[41] M Nagata. Three-dimensional finite-amplitude solutions in plane couette flow: bifurcation from infinity. *J. Fluid Mech*, 217:519–527, 1990.

[42] Simon Rosenblat and Stephen H Davis. Bifurcation from infinity. *SIAM Journal on Applied Mathematics*, 37(1):1–19, 1979.

[43] Alberto De Lozar, F Mellibovsky, M Avila, and Björn Hof. Edge state in pipe flow experiments. *Physical review letters*, 108(21):214502, 2012.

[44] Joseph D Skufca, James A Yorke, and Bruno Eckhardt. Edge of chaos in a parallel shear flow. *Physical review letters*, 96(17):174101, 2006.

[45] Tobias M Schneider, Bruno Eckhardt, and James A Yorke. Turbulence transition and the edge of chaos in pipe flow. *Physical review letters*, 99(3):034502, 2007.

[46] Chris CT Pringle, Yohann Duguet, and Rich R Kerswell. Highly symmetric travelling waves in pipe flow. *Philosophical Transactions of the Royal Society A: Mathematical, Physical and Engineering Sciences*, 367(1888):457–472, 2009.

[47] Michael D Graham. Drag reduction and the dynamics of turbulence in simple and complex fluids. *Physics of Fluids*, 26(10):625–656, 2014.

[48] Jue Wang, John Gibson, and Fabian Waleffe. Lower branch coherent states in shear flows: transition and control. *Physical review letters*, 98(20):204501, 2007.

[49] Tobias M Schneider and Bruno Eckhardt. Edge states intermediate between laminar and turbulent dynamics in pipe flow. *Philosophical Transactions of the Royal Society A: Mathematical, Physical and Engineering Sciences*, 367(1888):577–587, 2009.

[50] Grégoire Lemoult, Liang Shi, Kerstin Avila, Shreyas V Jalikop, Marc Avila, and Björn Hof. Directed percolation phase transition to sustained turbulence in couette flow. *Nature Physics*, 2016.

[51] Yves Pomeau. Front motion, metastability and subcritical bifurcations in hydrodynamics. *Physica D: Nonlinear Phenomena*, 23(1-3):3–11, 1986.

[52] Maksim Sipos and Nigel Goldenfeld. Directed percolation describes lifetime and growth of turbulent puffs and slugs. *Physical Review E*, 84(3):035304, 2011.

[53] Masaki Sano and Keiichi Tamai. A universal transition to turbulence in channel flow. *Nature Physics*, 2016.

[54] Dwight Barkley, Baofang Song, Vasudevan Mukund, Grégoire Lemoult, Marc Avila, and Björn Hof. The rise of fully turbulent flow. *Nature*, 526(7574):550–553, 2015.

[55] Sabine Bottin, Francois Daviaud, Paul Manneville, and Olivier Dauchot. Discontinuous transition to spatiotemporal intermittency in plane couette flow. *EPL (Europhysics Letters)*, 43(2):171, 1998.

[56] Liang Shi, Marc Avila, and Björn Hof. Scale invariance at the onset of turbulence in couette flow. *Physical review letters*, 110(20):204502, 2013.

[57] Olivier Dauchot and Francois Daviaud. Finite amplitude perturbation and spots growth mechanism in plane couette flow. *Physics of Fluids*, 7(2):335–343, 1995.

[58] Stephen J Kline, William C Reynolds, FA Schraub, and PW Runstadler. The structure of turbulent boundary layers. *Journal of Fluid Mechanics*, 30(4):741–773, 1967.

[59] Javier Jiménez and Parviz Moin. The minimal flow unit in near-wall turbulence. *Journal of Fluid Mechanics*, 225:213–240, 1991.

[60] James M Hamilton, John Kim, and Fabian Waleffe. Regeneration mechanisms of near-wall turbulence structures. *Journal of Fluid Mechanics*, 287:317–348, 1995.

[61] William Thomson. Xlvi. hydrokinetic solutions and observations. *The London, Edinburgh, and Dublin Philosophical Magazine and Journal of Science*, 42(281):362–377, 1871.

[62] HLF Helmholtz. Uber discontinuierlich flussigkeitsbewegungen, monatsberichte konigl. *Preu. Akad. Wiss. Berlin*, 215, 1868.

[63] Fabian Waleffe. Hydrodynamic stability and turbulence: Beyond transients to a self-sustaining process. *Studies in applied mathematics*, 95(3):319–343, 1995.

[64] Fabian Waleffe, John Kim, and James M Hamilton. On the origin of streaks in turbulent shear flows. In *Turbulent Shear Flows 8*, pages 37–49. Springer, 1993.

[65] Olivier Dauchot and F Daviaud. Streamwise vortices in plane couette flow. *Physics of Fluids*, 7(5):901–903, 1995.

[66] Sabine Bottin, Olivier Dauchot, Francois Daviaud, and Paul Manneville. Experimental evidence of streamwise vortices as finite amplitude solutions in transitional plane couette flow. *Physics of Fluids*, 10(10):2597–2607, 1998.

[67] Fabian Waleffe. On a self-sustaining process in shear flows. *Physics of Fluids*, 9(4):883–900, 1997.

[68] S Schmitz and A Tilgner. Transitions in turbulent rotating rayleigh-bénard convection. *Geophysical and Astrophysical Fluid Dynamics*, 104(5-6):481–489, 2010.

[69] Matthew Chantry, Laurette S Tuckerman, and Dwight Barkley. Turbulent–laminar patterns in shear flows without walls. *Journal of Fluid Mechanics*, 791, 2016.

[70] Philip Holmes, John L Lumley, and Gal Berkooz. *Turbulence, coherent structures, dynamical systems and symmetry*. Cambridge university press, 1998.

[71] Clive AJ Fletcher. Computational galerkin methods. In *Computational Galerkin Methods*, pages 72–85. Springer, 1984.

[72] BG Galerkin. On electrical circuits for the approximate solution of the laplace equation. *Vestnik Inzh*, 19:897–908, 1915.

[73] Fabian Waleffe. Three-dimensional coherent states in plane shear flows. *Physical Review Letters*, 81(19):4140, 1998.

[74] Jeff Moehlis, Holger Faisst, and Bruno Eckhardt. Periodic orbits and chaotic sets in a low-dimensional model for shear flows. *SIAM Journal on Applied Dynamical Systems*, 4(2):352–376, 2005.

[75] Jeff Moehlis, Holger Faisst, and Bruno Eckhardt. A low-dimensional model for turbulent shear flows. *New Journal of Physics*, 6(1):56, 2004.

[76] RM Clever and Fritz H Busse. Tertiary and quaternary solutions for plane couette flow. *Journal of Fluid Mechanics*, 344:137–153, 1997.

[77] Sabine Bottin and Hugues Chaté. Statistical analysis of the transition to turbulence in plane couette flow. *The European Physical Journal B-Condensed Matter and Complex Systems*, 6(1):143–155, 1998.

[78] Jorge Peixinho and Tom Mullin. Decay of turbulence in pipe flow. *Physical review letters*, 96(9):094501, 2006.

[79] Holger Faisst and Bruno Eckhardt. Sensitive dependence on initial conditions in transition to turbulence in pipe flow. *Journal of Fluid Mechanics*, 504:343–352, 2004.

[80] Tobias M Schneider, Filippo De Lillo, Juergen Buehrle, Bruno Eckhardt, Tim Dörnemann, Kay Dörnemann, and Bernd Freisleben. Transient turbulence in plane couette flow. *Physical review E*, 81(1):015301, 2010.

[81] Vered Rom-Kedar. Homoclinic tangles-classification and applications. *Nonlinearity*, 7(2):441, 1994.

[82] Paul Manneville. On the decay of turbulence in plane couette flow. *Fluid Dynamics Research*, 43(6):065501, 2011.

[83] Kerstin Avila, David Moxey, Alberto de Lozar, Marc Avila, Dwight Barkley, and Björn Hof. The onset of turbulence in pipe flow. *Science*, 333(6039):192–196, 2011.

[84] Nigel Goldenfeld, Nicholas Guttenberg, and Gustavo Gioia. Extreme fluctuations and the finite lifetime of the turbulent state. *Physical Review E*, 81(3):035304, 2010.

[85] EMIL J Gumbel. Statistics of extremes, columbia univ. *Press, New York*, page 201, 1958.

[86] Olivier Dauchot and Eric Bertin. Subcritical transition to turbulence: What we can learn from the physics of glasses. *Physical Review E*, 86(3):036312, 2012.

[87] J A Sorrentino. Classification of non-newtonian fluids, May 2019.

[88] Alexander Morozov and Saverio E Spagnolie. Introduction to complex fluids. In *Complex Fluids in Biological Systems*, pages 3–52. Springer, 2015.

[89] R Byron Bird and John M Wiest. Constitutive equations for polymeric liquids. *Annual review of fluid mechanics*, 27(1):169–193, 1995.

[90] Bayode E Owolabi, David JC Dennis, and Robert J Poole. Turbulent drag reduction by polymer additives in parallel-shear flows. *Journal of Fluid Mechanics*, 827, 2017.

[91] RB Bird, PJ Dotson, and NL Johnson. Polymer solution rheology based on a finitely extensible bead—spring chain model. *Journal of Non-Newtonian Fluid Mechanics*, 7(2-3):213–235, 1980.

[92] Nhan Phan Thien and Roger I Tanner. A new constitutive equation derived from network theory. *Journal of Non-Newtonian Fluid Mechanics*, 2(4):353–365, 1977.

[93] Alexei E Likhtman and Richard S Graham. Simple constitutive equation for linear polymer melts derived from molecular theory: Rolie–poly equation. *Journal of Non-Newtonian Fluid Mechanics*, 114(1):1–12, 2003.

[94] Ismail Hameduddin, Dennice F Gayme, and Tamer A Zaki. Perturbative expansions of the conformation tensor in viscoelastic flows. *Journal of Fluid Mechanics*, 858:377–406, 2019.

[95] Martien A Hulsen. A sufficient condition for a positive definite configuration tensor in differential models. *Journal of non-newtonian fluid mechanics*, 38(1):93–100, 1990.

[96] Martien A Hulsen, Raanan Fattal, and Raz Kupferman. Flow of viscoelastic fluids past a cylinder at high weissenberg number: stabilized simulations using matrix logarithms. *Journal of Non-Newtonian Fluid Mechanics*, 127(1):27–39, 2005.

[97] Brian Toms. Some observations on the flow of linear polymer solutions through straight tubes at large reynolds numbers. *Proc. of In. Cong. On Rheology, 1948*, 135, 1948.

[98] Christopher M White and M Godfrey Mungal. Mechanics and prediction of turbulent drag reduction with polymer additives. *Annu. Rev. Fluid Mech.*, 40:235–256, 2008.

[99] RJ Hansen and RC Little. Early turbulence and drag reduction phenomena in larger pipes. *Nature*, 252(5485):690, 1974.

[100] JL Zakin, CC Ni, RJ Hansen, and MM Reischman. Laser doppler velocimetry studies of early turbulence. *The Physics of Fluids*, 20(10):S85–S88, 1977.

[101] MP Escudier, F Presti, and S Smith. Drag reduction in the turbulent pipe flow of polymers. *Journal of non-newtonian fluid mechanics*, 81(3):197–213, 1999.

[102] Arthur G Kravchenko, Haecheon Choi, and Parviz Moin. On the relation of near-wall streamwise vortices to wall skin friction in turbulent boundary layers. *Physics of Fluids A: Fluid Dynamics*, 5(12):3307–3309, 1993.

[103] Kyoungyoun Kim, Chang-F Li, Radhakrishna Sureshkumar, S Balachandar, and Ronald J Adrian. Effects of polymer stresses on eddy structures in drag-reduced turbulent channel flow. *Journal of Fluid Mechanics*, 584:281–299, 2007.

[104] Andrey Nikolaevich Kolmogorov. The local structure of turbulence in incompressible viscous fluid for very large reynolds numbers. *Cr Acad. Sci. URSS*, 30:301–305, 1941.

[105] Preetinder S Virk. Drag reduction fundamentals. *AIChE Journal*, 21(4):625–656, 1975.

[106] Chang-Feng Li, Radhakrishna Sureshkumar, and Bamin Khomami. Simple framework for understanding the universality of the maximum drag reduction asymptote in turbulent flow of polymer solutions. *Physical Review E*, 92(4):043014, 2015.

[107] Li Xi and Michael D Graham. Dynamics on the laminar-turbulent boundary and the origin of the maximum drag reduction asymptote. *Physical review letters*, 108(2):028301, 2012.

[108] Sung-Ning Wang, Ashwin Shekar, and Michael D Graham. Spatiotemporal dynamics of viscoelastic turbulence in transitional channel flow. *Journal of Non-Newtonian Fluid Mechanics*, 244:104–122, 2017.

[109] Sung-Ning Wang, Michael D Graham, Friedemann J Hahn, and Li Xi. Time-series and extended karhunen–loève analysis of turbulent drag reduction in polymer solutions. *AIChE Journal*, 60(4):1460–1475, 2014.

[110] Vassilios Dallas, J Christos Vassilicos, and Geoffrey F Hewitt. Strong polymer-turbulence interactions in viscoelastic turbulent channel flow. *Physical Review E*, 82(6):066303, 2010.

[111] CF Li, VK Gupta, Radhakrishna Sureshkumar, and B Khomami. Turbulent channel flow of dilute polymeric solutions: drag reduction scaling and an eddy viscosity model. *Journal of Non-Newtonian Fluid Mechanics*, 139(3):177–189, 2006.

[112] Yves Dubief, Vincent E Terrapon, Christopher M White, Eric SG Shaqfeh, Parviz Moin, and Sanjiva K Lele. New answers on the interaction between polymers and vortices in turbulent flows. *Flow, turbulence and combustion*, 74(4):311–329, 2005.

[113] Shinji Tamano, Michael D Graham, and Yohei Morinishi. Streamwise variation of turbulent dynamics in boundary layer flow of drag-reducing fluid. *Journal of fluid mechanics*, 686:352–377, 2011.

[114] YX Hou, VSR Somandepalli, and MG Mungal. Streamwise development of turbulent boundary-layer drag reduction with polymer injection. *Journal of Fluid Mechanics*, 597:31–66, 2008.

[115] PK Ptasinski, FTM Nieuwstadt, BHAA Van Den Brule, and MA Hulsen. Experiments in turbulent pipe flow with polymer additives at maximum drag reduction. *Flow, Turbulence and Combustion*, 66(2):159–182, 2001.

[116] MP Escudier, AK Nickson, and RJ Poole. Turbulent flow of viscoelastic shear-thinning liquids through a rectangular duct: Quantification of turbulence anisotropy. *Journal of non-newtonian fluid mechanics*, 160(1):2–10, 2009.

[117] MD Warholic, H Massah, and TJ Hanratty. Influence of drag-reducing polymers on turbulence: effects of reynolds number, concentration and mixing. *Experiments in fluids*, 27(5):461–472, 1999.

[118] Devranjan Samanta, Yves Dubief, Markus Holzner, Christof Schäfer, Alexander N Morozov, Christian Wagner, and Björn Hof. Elasto-inertial turbulence. *Proceedings of the National Academy of Sciences*, 110(26):10557–10562, 2013.

[119] Yves Dubief, Vincent E Terrapon, and Julio Soria. On the mechanism of elasto-inertial turbulence. *Physics of Fluids*, 25(11):110817, 2013.

[120] Li Xi and Michael D Graham. Turbulent drag reduction and multistage transitions in viscoelastic minimal flow units. *Journal of Fluid Mechanics*, 647:421–452, 2010.

[121] Li Xi and Michael D Graham. Intermittent dynamics of turbulence hibernation in newtonian and viscoelastic minimal channel flows. *Journal of Fluid Mechanics*, 693:433–472, 2012.

[122] Wei Li and Michael D Graham. Polymer induced drag reduction in exact coherent structures of plane poiseuille flow. *Physics of Fluids*, 19(8):083101, 2007.

[123] Th Von Karman. Mechanische ahnlichkeit und turbulenz. *Math.-Phys. Klasse*, 1930.

[124] Li Xi and Michael D Graham. Active and hibernating turbulence in minimal channel flow of newtonian and polymeric fluids. *Physical review letters*, 104(21):218301, 2010.

[125] Richard D Whalley, Jae Sung Park, Anubhav Kushwaha, David JC Dennis, Michael D Graham, and Robert J Poole. Low-drag events in transitional wall-bounded turbulence. *Physical Review Fluids*, 2(3):034602, 2017.

[126] Rishav Agrawal, Henry C-H Ng, Richard D Whalley, David JC Dennis, and Robert J Poole. In search of low drag events in newtonian turbulent channel flow at low reynolds number. In *11th International Symposium on Turbulence and Shear Flow Phenomena, TSFP 2019*. Newcastle University, 2019.

[127] RD Whalley, DJC Dennis, MD Graham, and RJ Poole. An experimental investigation into spatiotemporal intermittencies in turbulent channel flow close to transition. *Experiments in Fluids*, 60(6):102, 2019.

[128] Philip J Holmes, John L Lumley, Gal Berkooz, Jonathan C Mattingly, and Ralf W Wittenberg. Low-dimensional models of coherent structures in turbulence. *Physics Reports*, 287(4):337–384, 1997.

[129] Jeffrey S Baggett and Lloyd N Trefethen. Low-dimensional models of subcritical transition to turbulence. *Physics of Fluids*, 9(4):1043–1053, 1997.

[130] Kunlun Bai, Dandan Ji, and Eric Brown. Ability of a low-dimensional model to predict geometry-dependent dynamics of large-scale coherent structures in turbulence. *Physical Review E*, 93(2):023117, 2016.

[131] Ahmet Omurtag and Larry Sirovich. On low-dimensional modeling of channel turbulence. *Theoretical and Computational Fluid Dynamics*, 13(2):115–127, 1999.

[132] H Kuhlmann. Model for taylor-couette flow. *Physical Review A*, 32(3):1703, 1985.

[133] Xia Ma and George Em Karniadakis. A low-dimensional model for simulating three-dimensional cylinder flow. *Journal of Fluid Mechanics*, 458:181–190, 2002.

[134] Bruno Eckhardt and Alois Mersmann. Transition to turbulence in a shear flow. *Physical Review E*, 60(1):509, 1999.

[135] Fabian Waleffe. Homotopy of exact coherent structures in plane shear flows. *Physics of Fluids*, 15(6):1517–1534, 2003.

[136] Siegfried Grossmann. The onset of shear flow turbulence. *Rev. Mod. Phys.*, 72:603–618, Apr 2000.

[137] Philip Holmes. *Turbulence, coherent structures, dynamical systems and symmetry*. Cambridge university press, 2012.

[138] İhsan Timuçin Dolapçi. Chebyshev collocation method for solving linear differential equations. *Mathematical and Computational Applications*, 9(1):107–115, 2004.

[139] Peter Deuflhard. *Newton methods for nonlinear problems: affine invariance and adaptive algorithms*, volume 35. Springer Science & Business Media, 2011.

[140] Tobias Kreilos, Bruno Eckhardt, and Tobias M Schneider. Increasing lifetimes and the growing saddles of shear flow turbulence. *Physical review letters*, 112(4):044503, 2014.

[141] Tobias Kreilos and Bruno Eckhardt. Periodic orbits near onset of chaos in plane couette flow. *Chaos: An Interdisciplinary Journal of Nonlinear Science*, 22(4):047505, 2012.

[142] Julian CR Hunt, Alan A Wray, and Parviz Moin. Eddies, streams, and convergence zones in turbulent flows. 1988.

[143] Stefan Zammert and Bruno Eckhardt. Transition to turbulence when the tollmien–schlichting and bypass routes coexist. *Journal of Fluid Mechanics*, 880, 2019.

[144] William H Press. *Numerical recipes 3rd edition: The art of scientific computing*. Cambridge university press, 2007.

[145] Tobias M Schneider and Bruno Eckhardt. Lifetime statistics in transitional pipe flow. *Physical Review E*, 78(4):046310, 2008.

[146] Paul Turner. xmgrace.

[147] Celso Grebogi, Edward Ott, and James A Yorke. Crises, sudden changes in chaotic attractors, and transient chaos. *Physica D: Nonlinear Phenomena*, 7(1-3):181–200, 1983.

[148] Celso Grebogi, Edward Ott, and James A Yorke. Chaos, strange attractors, and fractal basin boundaries in nonlinear dynamics. *Science*, 238(4827):632–638, 1987.

[149] Masaki Shimizu, Takahiro Kanazawa, and Genta Kawahara. Exponential growth of lifetime of localized turbulence with its extent in channel flow. *Fluid Dynamics Research*, 51(1):011404, 2019.

[150] Bruno Eckhardt and Holger Faisst. Dynamical systems and the transition to turbulence. In *IUTAM Symposium on Laminar-Turbulent Transition and Finite Amplitude Solutions*, pages 35–50. Springer, 2005.

[151] Paul Manneville. Spatiotemporal perspective on the decay of turbulence in wall-bounded flows. *Physical Review E*, 79(2):025301, 2009.

[152] Jimmy Philip and Paul Manneville. From temporal to spatiotemporal dynamics in transitional plane couette flow. *Physical Review E*, 83(3):036308, 2011.

[153] Wolfram Research, Inc. Mathematica, Version 12.1.

[154] Julius Rhoan T Lustro, Genta Kawahara, Lennaert van Veen, Masaki Shimizu, and Hiroshi Kokubu. The onset of transient turbulence in minimal plane couette flow. *Journal of Fluid Mechanics*, 862, 2019.

[155] Philip A Stone, Fabian Waleffe, and Michael D Graham. Toward a structural understanding of turbulent drag reduction: nonlinear coherent states in viscoelastic shear flows. *Physical review letters*, 89(20):208301, 2002.

[156] Wei Li, Li Xi, and Michael D Graham. Nonlinear traveling waves as a framework for understanding turbulent drag reduction. *arXiv preprint physics/0601183*, 2006.

[157] Katepalli R Sreenivasan and Christopher M White. The onset of drag reduction by dilute polymer additives, and the maximum drag reduction asymptote. *Journal of Fluid Mechanics*, 409:149–164, 2000.

[158] PK Patasinski, BJ Boersma, FTM Nieuwstadt, MA Hulsen, BHAA Van den Brule, and JCR Hunt. Turbulent channel flow near maximum drag reduction: simulations, experiments and mechanisms. *Journal of Fluid Mechanics*, 490:251–291, 2003.

[159] John L Lumley. Drag reduction in turbulent flow by polymer additives. *Journal of Polymer Science: Macromolecular Reviews*, 7(1):263–290, 1973.

[160] Victor S L'vov, Anna Pomyalov, Itamar Procaccia, and Vasil Tiberkevich. Drag reduction by polymers in wall bounded turbulence. *Physical review letters*, 92(24):244503, 2004.

[161] Yves Dubief, Christopher M White, Vincent E Terrapon, Eric SG Shaqfeh, Parviz Moin, and Sanjiva K Lele. On the coherent drag-reducing and turbulence-enhancing behaviour of polymers in wall flows. *Journal of Fluid Mechanics*, 514:271, 2004.

[162] George H Choueiri, Jose M Lopez, and Björn Hof. Exceeding the asymptotic limit of polymer drag reduction. *Physical review letters*, 120(12):124501, 2018.

[163] Ashwin Shekar, Ryan M McMullen, Beverley J McKeon, and Michael D Graham. Self-sustained elastoinertial tollmien-schlichting waves. *arXiv preprint arXiv:1910.11419*, 2019.

[164] Ashwin Shekar, Ryan M McMullen, Sung-Ning Wang, Beverley J McKeon, and Michael D Graham. Critical-layer structures and mechanisms in elastoinertial turbulence. *Physical review letters*, 122(12):124503, 2019.